DTIC
ELECTE

RL-TR-91-198
Final Technical Report
August 1991

AD-A242 038



MICROSTRIP DISCONTINUITY MODELS TO 60 GHz

Plessey Research Caswell Limited

R.G. Arnold, R.H. Jansen, L. Weimer

APPROVED FOR PUBLIC RELEASE; DISTRIBUTION UNLIMITED.

91-14239

Rome Laboratory
Air Force Systems Command
Griffiss Air Force Base, NY 13441-5700

91 10 28 061

This report has been reviewed by the Rome Laboratory Public Affairs Division (PA) and is releasable to the National Technical Information Service (NTIS). At NTIS it will be releasable to the general public, including foreign nations.

RL-TR-91-198 has been reviewed and is approved for publication.

APPROVED: Andrew J. Slobodnik, Jr.

ANDREW J. SLOBODNIK, JR.
Project Engineer

FOR THE COMMANDER: John K. Schindler

JOHN K. SCHINDLER
Director of Electromagnetics

If your address has changed or if you wish to be removed from the Rome Laboratory mailing list, or if the addressee is no longer employed by your organization, please notify Rome Laboratory (ERAC) Hanscom AFB MA 01731-5000. This will assist us in maintaining a current mailing list.

Do not return copies of this report unless contractual obligations or notices on a specific document require that it be returned.

REPORT DOCUMENTATION PAGE

Form Approved
OMB No. 0704-0188

Public reporting burden for this collection of information is estimated to average 1 hour per response, including the time for reviewing instructions, searching existing data sources gathering and maintaining the data needed, and completing and reviewing the collection of information. Send comments regarding this burden estimate or any other aspect of this collection of information, including suggestions for reducing this burden, to Washington Headquarters Services, Directorate for information Operations and Reports, 1215 Jefferson Davis Highway, Suite 1204, Arlington, VA 22202-4302, and to the Office of Management and Budget, Paperwork Reduction Project (0704-0188), Washington, DC 20503

1. AGENCY USE ONLY (Leave Blank)	2. REPORT DATE	3. REPORT TYPE AND DATES COVERED
	August 1991	Final Sep 86 - Sep 89

4. TITLE AND SUBTITLE
MICROSTRIP DISCONTINUITY MODELS TO 60 GHz

5. FUNDING NUMBERS
C - F19628-86-C-0111
PE - 61102F
PR - 2305
TA - J5
WU - 46

6. AUTHOR(S)
R.G. Arnold, R.H. Jansen, and L. Weimer

7. PERFORMING ORGANIZATION NAME(S) AND ADDRESS(ES)
Plessey Research Caswell Limited
Allen Clark Research Centre
Caswell, Towcester, Northants, England NN128EQ

8. PERFORMING ORGANIZATION REPORT NUMBER
N/A

9. SPONSORING/MONITORING AGENCY NAME(S) AND ADDRESS(ES)
Rome Laboratory (ERAC)
Hanscom AFB MA 01731-5000

10. SPONSORING/MONITORING AGENCY REPORT NUMBER
RL-TR-91-198

11. SUPPLEMENTARY NOTES
Rome Laboratory Project Engineer: Andrew J. Slobodnik, Jr./ERAC/(617) 377-3716

12a. DISTRIBUTION/AVAILABILITY STATEMENT
Approved for public release; distribution unlimited.

12b. DISTRIBUTION CODE

13. ABSTRACT (Maximum 200 words)

A new modeling concept, in which discontinuities are coupled to package modes, has been formulated. Analytical expressions describing the electrical behavior of various GaAs microstrip discontinuities for frequencies up to 60 GHz are derived. These are suitable for use in Computer Aided Design (CAD) of Monolithic Microwave and Millimeter Wave Integrated Circuits (MMICs). The discontinuities modelled are the Open End, Gap, 90 degree Bend and T-Junction. A physics related modeling approach was used to obtain equivalent circuits representing the microstrip and first package LSM mode and their interaction at the discontinuity. The main section explains the modeling approach undertaken and provides a description of the discontinuity models. An appendix provides details of a 3-D full wave analysis method based on a spectral operator expansion technique. This was used to check numerical results needed for the modeling.

14. SUBJECT TERMS
Microstrip Discontinuities, MMIC CAD, Spectral Operator Expansion

15. NUMBER OF PAGES
342

16. PRICE CODE

17. SECURITY CLASSIFICATION OF REPORT	18. SECURITY CLASSIFICATION OF THIS PAGE	19. SECURITY CLASSIFICATION OF ABSTRACT	20. LIMITATION OF ABSTRACT
UNCLASSIFIED	UNCLASSIFIED	UNCLASSIFIED	UL

NSN 7540-01-280-5500

Standard Form 298 (Rev. 2-89)
Prescribed by ANSI Std. 239-18
298-102

CONTENTS

		Page No.
1.	OBJECTIVE	6
2.	INTRODUCTION	
	2.1. Current discontinuity models	
	2.2. Brief summary of the mathematical techniques used in the discontinuity analysis	
	2.3. Discussion on unified systematic approaches to discontinuity modelling	
	2.4. References	
3.	INITIAL STUDIES INTO THE PHYSICS RELATED MODELLING APPROACH	15
	3.1. Basic model studies	
	3.2. Microstrip open end simulation including package resonance behaviour	
	3.3. Study of microstrip-LSM_0 mode coupling as a function of discontinuity position	
	3.4. Microstrip-LSM_0 coupling studies at the source and at the discontinuity	
	3.5. Study of the model de-embedding procedure	
	3.5.1. Discussion on model parameter de-embedding from the field theory data	
	3.5.2. Study of the microstrip LSM_0 coupling as a function of microstrip length	
	3.6. Improved physics related model studies	
	3.7. References	
4.	MICROSTRIP AND LSM_0 CHARACTERISTIC MODELLING FORMULAE	45
	4.1. Analytic formulae for the microstrip mode characteristics	
	4.2. Analytic formulae for the LSM_0 mode characteristics	
	4.3. References	
5.	DEVELOPMENT OF DISCONTINUITY EQUIVALENT CIRCUIT MODELS EXHIBITING DYNAMIC BEHAVIOUR	52
	5.1. Open end	
	5.1.1. An equivalent circuit model	
	5.1.2. Confirmation of the open end model	

Accession For
NTIS GRA&I
DTIC Tab
Unannounced
Justification
By
Distribution/
Availability Codes
Dist Avail and/or special
A-1

Page No.

5.2. Microstrip gap

5.2.1. Comparison of the current static analytical model with full wave results
5.2.2. An equivalent circuit model
5.2.3. Preliminary studies

5.3. Microstrip step

5.3.1. Comparison of a quasi-static analytical model with full wave results
5.3.2. An equivalent circuit model
5.3.3. Preliminary studies

5.4. 90° bend

5.4.1. A dynamic 90° bend model
5.4.2. Study of the dynamic model
5.4.3. Discussion on mode coupling in the bend model
5.4.4. An alternative equivalent circuit model

5.5. Microstrip T-junction

5.5.1. Preliminary equivalent circuit model
5.5.2. Study of the dynamic model

5.6. References

6. STUDY OF BIDIRECTIONAL MODAL EFFECTS AND DEVELOPMENT OF A CIRCUIT MODEL DESCRIPTION 86

6.1. Discussion on the current equivalent circuit models
6.2. A microstrip 90° bend model including bidirectional LSM_0-mode coupling
6.3. Description of the EM fields in the package in terms of LSM_0 mode excitation
6.4. Revised microstrip 90° bend model
6.5. Extended microstrip T-junction model

7. STUDY AND DEVELOPMENT OF THE MICROSTRIP-LSM_0 MODE COUPLING DESCRIPTION 100

7.1. Improved analytical formula for the coupling description
7.2. Verification of the transformer ratio description using the gap model

Page No.

7.2.1. Gap width variation
7.2.2. Strip width variation
7.2.3. Frequency variation
7.2.4. Variation with the microstrip position in the package
7.2.5. Small gap width study
7.2.6. Transformer ratio variation

7.3. Discussion of the frequency dependency of the transformer ratio
7.4. Frequency behaviour of the transformer ratio

8. PARAMETER EXTRACTION 126

8.1. Method
8.2. References

9. MICROSTRIP OPEN END MODEL 128

9.1. Analytic formulae for the static part of the dynamic equivalent circuit model
9.2. Analytic formulae for the transformer ratio
9.3. Open end model summary
9.4. References and tables

10. MICROSTRIP GAP MODEL 146

10.1. Analytic formulae for the static model
10.2. Description of the transformers in the dynamic model
10.3. Transformer analytic formulae for the frequency transition region
10.4. Gap model summary
10.5. References and tables

11. MICROSTRIP STEP MODEL 178

11.1. Analytic formulae for the quasi-static step model
11.2. Description of the transformers in the dynamic model
11.3. Transformer analytic formulae for the frequency transition region
11.4. Step model summary
11.5. References and tables

Page No.

12. MICROSTRIP 90° BEND MODEL 199

12.1. Expressions for the static part of the dynamic model
12.2. Study of the static model over the complete dynamic frequency range
12.3. Transformer ratio expressions for the dynamic model
12.4. Inclusion of an increased frequency dependency into the static circuit model
12.5. Bend model summary
12.6. References and tables

13. MICROSTRIP T-JUNCTION 226

13.1. Development of analytic formulae for normalised frequencies <3 GHz mm

13.1.1. Quasi-static database
13.1.2. Analytic formulae for the symmetic T-junction
13.1.3. Analytic formulae for the general T-junction

13.2. Development of analytic formulae for normalised frequencies <6 GHz mm

13.2.1. Study of T-junction package dynamic behaviour
13.2.2. Analytic formulae for the symmetric T-junction
13.2.3. Analytic formulae for the general T-junction

13.3. Development of the transformer ratio expressions
13.4. Verification of the T-junction analytic formulae
13.5. T-junction model summary
13.6. References and tables

14. COMPARISON OF THE 3-D ANALYSIS APPROACH USED BY SFPMIC AND THE SOE DISCONTINUITY ANALYSIS 265

14.1. Verification of the databases used in modelling with the SOE discontinuity analysis
14.2. The strengths and weaknesses of the SFPMIC program and the SOE based software

15. CONCLUSIONS 272

16. APPENDIX 273

1. OBJECTIVE

The aim of this work is to derive analytic model expressions describing the electrical behaviour of the GaAs microstrip open end, gap, step, 90° bend and T-junction for frequencies up to 60 GHz.

2. INTRODUCTION

2.1. CURRENT DISCONTINUITY MODELS

The MIC and MMIC discontinuity models used today in commercial CAD software are usually semi-empirical, based on narrow measured databases and quasi-static or magnetic wall approximations which are unable to describe full wave coupling effects or interaction of discontinuities with a shielding package (1), From their very definition and method of derivation, existing analytical discontinuity models cannot take into account interaction with their circuit environment, but are treated as isolated structures.

At mm-wave frequencies the discontinuity environment is integral to its electrical behaviour. For example a microstrip open end behaves quite differently when it is considered in a completely open environment as compared to one which is laterally open or as in the usual MMIC case enclosed by a package. The percentage of power radiated from the open end is a relatively strong function of the circuit cover height since the presence of a cover has a direct effect on the radiation mechanism (3,4). Moreover in the completely shielded situation the radiated field interaction is additionally dependent on the lateral shielding dimensions (2,5). The situation is even more complicated in the case of 90° bends and T-junctions, which are two directional orthogonal structures. The interaction of the microstrip discontinuity with the package field is bidirectional.

To obtain discontinuity models, however, both a method of obtaining 3-D electrical solutions for the discontinuities' physical structure as well as a systematic modelling scheme is required.

2.2. BRIEF SUMMARY OF THE MATHEMATICAL TECHNIQUES USED IN THE DISCONTINUITY ANALYSIS

In order to develop the discontinuity models, measured or numerical data generated by 3-D electromagnetic field analysis has to be available. Measured data is however not available and thus models have to rely on analytic generated data.

All reported field analysis methods are based on spectral domain techniques (6,7). The program, SFPMIC, used in this work is based on a source type solution (2), allowing radiation in one direction to be described.

SFPMIC (source formulation procedure for the analysis of elementary structures in MICs) is a computer program which uses a deterministic hybrid- mode spectral-domain approach for the numerical computation of the scattering parameters of elementary MIC and MMIC structures, this approach providing full-wave solutions. The only assumptions made are infinite conductivity (neglection of loss) and zero metal thickness of the conductors. The mathematical techniques used in its essential steps can be described as follows:

- A two-dimensional integral equation for the substrate surface of a general MIC/MMIC medium is analytically derived. This equation's validity is independent of the metallisation shapes to be treated. It is deterministic since on its right hand side it exhibits impressed current densities, these current densities acting as sources which excite the strip modes that interact with the discontinuity of interest.
- The deterministic equation is solved numerically by the application of a moment method in the spectral domain. This results in a relatively low order system of equations (low order as compared to other methods). However, the generation of the coefficients of this system of equations becomes time consuming for high spatial resolutions,

because a two-dimensional summation over all spectral contributions is involved.

- A special scheme of expansion functions, which are partially precomputed strip mode solutions, is used.

To check the results of this program an alternative analysis program based on the spectral operator expansion method (7) was developed. Instead of using precomputed modes this technique uses a finite grid of frequency independent expansion functions to describe the surface current density on the discontinuity conductor pattern. The outline of this approach can be found in more detail in the Appendix.

2.3. DISCUSSION ON UNIFIED SYSTEMATIC APPROACHES TO DISCONTINUITY MODELLING

The development of microstrip discontinuity models has been reported in the technical literature by many authors. Collections of frequently used discontinuity models have been published by Gupta et al (8) and also by Kirschning (9). The methodology of obtaining such models are not standardised and are based on the knowledge and physical insight of the developing scientists and engineers. Often trial and error procedures have been used to get the best results. This is far away from a unified systematic approach and usually requires a large amount of effort to obtain models with more than two physical variables.

In Kirschning's development of a gap discontinuity model, for example the empirical procedure followed was not capable of generating a model for the useful dielectric constant range $2<\varepsilon_r<13$. The model had to take into account dependences on the geometry ratios g/h, w_1/h, w_2/h and on the dielectric constant ε_r. However, modelling a function depending on four different variables is a problem that can hardly be solved just by empirical means. To achieve the best possible solution, a systematic and fully justifiable approach has to be applied.

As a related example, take the computer aided generation of microwave resistor, capacitor and inductor models as presented by Baden Fuller (10). In this method equivalent circuits descriptions of these passive components are used to obtain an approximation to the measured microwave scattering parameters. If necessary, an automatic procedure adds new equivalent circuit elements and new nodes into the equivalent circuit topology. The main disadvantages of this procedure are twofold. For a given set of measured data the model always represents a good approximation, however, the same microwave component with a slightly different geometry may be modelled by an equivalent circuit of different topology. This occurs due to the complete lack of a predefined physical morphology. The second disadvantage is the erroneous out of range behaviour of such models. These models can be used only in a restricted frequency range. For frequencies beyond the applied test values, the equivalent circuit models may have a completely different and unphysical behaviour. So, this type of computer-aided purely empirical search is again not a suitable solution to the microwave discontinuity modelling problem.

One of the few available systematic modelling procedures for the frequency dependent scattering parameters of microwave devices has been presented by Thiele (11) in which a polynomial description for scattering parameters as a function of frequency is used. This approach can be applied to general microwave discontinuities. The main idea is that if a distributed structure can in principle be described by an equivalent circuit, it can also be described in a very general sense by rational network functions in terms of complex frequencies (pole-zero-schematics).

At least, network representations which are based only on the common network properties of distributed passive structures seem better suited to an automatic modelling process and a systematic approach than a fixed set of arbitrarily selected special functions. An important question in this context is always, how to be sure that the chosen functions are able to give

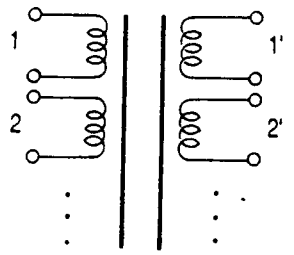
a good approximation to the discontinuity electrical characteristics. From this point of view polynomials seem a good choice. Every real function can be approximated by a rational polynomial of appropriate order.

In this approach, the basic principle used, is the successive application of one-dimensional curve fitting to multi-dimensional functions in a sequence ordered with respect to decreasing parameter sensitivities. For example take the two parameter functions for the microstrip open end effect presented by Kirschning and Jansen (12). The two dimensional end effect function $\Delta l = f(w/h, \varepsilon_r)$, where w is the strip width, h the substrate thickness and ε_r, the dielectric constant, can be treated in this manner. As a preliminary step a data base is generated by taking $n_\varepsilon \times n_w$ samples, the samples being generated from measurements or exact numerical techniques.

The first approximation step is to find the maximum number of coefficients needed for a good fit in one direction of the data grid, i.e. either n_ε curves $\Delta l = f(w/h, \varepsilon_r = \text{const.})$ or n_w curves $\Delta l = f(\varepsilon_r, w/h = \text{const.})$. The number of orthogonal polynomials or rational function coefficients, n_{c1} is then increased until a minimum predescribed deviation at all points of the grid is obtained. The associated coefficients a_i are now functions of the parameter determining the second direction of the grid. A second one-dimensional curve fitting procedure is applied obtaining n_{c2} coefficients to complete the two dimensional approximation. As a result $n_{c1} \times n_{c2}$ coefficients, necessary to establish a new description are obtained. Although this approach is systematic, the disadvantage is that a function, for example, of 5 variables will possibly result in a representation 3^5-5^5 or more polynomial coefficients depending upon the fitting accuracy required.

An alternative approach is the use of a physics related models. The concept of this approach is that a general equivalent circuit description can be developed for arbitrary junctions and discontinuities. Based on the theory of waveguides including those with non-uniform dielectric in the cross

section, these descriptions take the form of a transformer circuit with multiple windings attached to fundamental and higher modes (13).



$$U_1 = jwL_1 i_1 + jwM_{12} i_2 + \ldots jwM_{11'} i_1' + \ldots$$

$$U_2 = jwM_{12} i_2 + jwL_1 i_2 + \ldots$$

$$U_2 = -jX_2 i_2 \text{ etc.}$$

Fig. 2.1: Two port equivalent circuit

For example in Fig. 2.1, 1 and 1' might be the fundamental strip modes associated with a step in width, 2 and 2' the fundamental parasitic (package, LSM_0) modes associated with the strips and all higher order evanescent modes. All modes which are not propagating can be represented as reactances transformed to 1 and 1' and physically relate with the discontinuity or junction stored energy. In the case of the LSM_0 package modes, reactances associated with the package dimensions occur (x_2) if the package is closed (except for microstrip fundamental mode anchors), and radiation resistances (R_2) if the package is open in one-dimension (energy leakage). The coupling terms M_{12} can be generated from the modal fields by using suitable coupling integrals (scalar products) based on the mode information in the feed strip look-up tables. For the fundamental and higher order modes propagating on the feed lines of microstrip junctions and discontinuities, the modal characteristics can be easily generated for a wide range of geometries and frequencies. Look up tables of these characteristics can provide input for discontinuity modelling. In this way theory-based equivalent circuit topologies can be derived in unified form for the discontinuities.

Preliminary generated numerical data has shown that in the mm-wave range accurate modelling requires taking into account the presence of the package. Interaction effects of the discontinuity and the package thus need to be

described when modelling. Such effects can be included by properly terminating the LSM_0 mode in the models (resulting in a parallel radiation resistance).

Based on the equivalent circuit description physics-related models can be developed in which most of the necessary elements are described in terms of the mode characteristics (fundamental and parasitic). Thus it should only leave the modelling of the evanescent mode effects as parasitic reactances. Moreover these reactances can partially be obtained from quasi-static expressions existing already in the discontinuity literature.

2.4. REFERENCES

1. Hoffman, R.K., Microwave Integrated Circuits, Springer, 1983.
2. Jansen, R.H., The spectral-domain approach for microwave integrated circuits, Invited paper, IEEE Trans. MTT-33 (1985), 1043-1056.
3. Boukamp, J. and Jansen, R.H. The high-frequency behaviour of microstrip open ends in microwave integrated circuits including energy leakage, 14th European Microwave Conf., Proc., Liege, Belgium, 1984, 142-147.
4. Boukamp, J., Spectral domain techniques for the computation of radiation effects in MICs (in German), University of Aachen, W. Germany, 1984.
5. Jansen, R.H. Hybrid mode analysis of end effects of planar microwave and millimetre-wave transmission lines, IEE Proc. Vol. 128 (1981).
6. Jackson, R.W. and Pozar, D.M., Full wave analysis of microstrip open end and gap discontinuities, IEEE MTT-33 1985, p.1036-1042.
7. Jansen, R.H., Wertgen, W., A 3-D theoretical simulation tool for the CAD of mm-wave MMICs, Alta Frequenza, Italy, Vol. LVII, 1987, pp. 203-216.
8. Gupta, K.C. et al, Computer-aided design of microwave circuits, Artech House, Dedham, MA 02026, 1981, Chapters 8.3 and 8.4.

9. Kirschning, M., Development of models for the computer-aided design of hybrid and monolithic microstrip circuits (in German), Ph.D. Dissertation, University of Duisburg, W. Germany, 1984.

10. Baden Fuller, A.J. et al. Computer optimisation of circuits applied to the modelling of microwave passive IC components, IEE Proc. Vol. 133, Part H, 1986, 411-418.

11. Thiele, An analytic approach to curve fitting, AEU, 40 (1986), p.51-58.

12. Kirschning, M. and Jansen, R.H., 'Accurate model for the end effect of microstrip lines' Electronic Letters, 1981.

13. Montgomery, C.G., Dicke, R.H. and Purcell, E.M., 'Principles of microwave circuits', Dover Publications Inc., New York, published 1965.

3. INITIAL STUDIES INTO THE PHYSICS RELATED MODELLING APPROACH

In the previous section, the concept of a physics related model was introduced. To implement such an approach, studies had to be undertaken in order to obtain a systematic method for translating the discontinuity-package electromagnetic field interaction into an equivalent circuit description. The open end discontinuity, the simplest of the group to be analysed, was used to obtain the basic methodology.

3.1. BASIC MODEL STUDIES

The proposed physics related modelling approach must give correct open end results even allowing for the effects of the associated package on the discontinuity behaviour. The same applies if the shielding wall opposite to the open end is removed resulting in the radiation of energy away from the open end in the form of LSM_0 mode propagation. In order to verify this modelling approach, the simplest discontinuity, the microstrip open end was studied.

The geometry in the outlined modelling procedure is presented in Fig. 3.1.

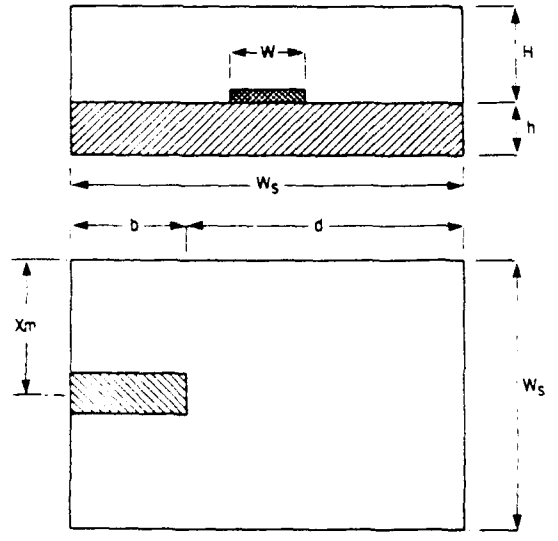


Fig. 3.1: Geometry for open end problem

In this diagram the feed strip width is w, strip length b, distance of the open end to the package wall d. The package cover height is H above a substrate thickness h and width w_s. The open end position in the package is given by x_m.

The equivalent circuit model proposed for this situation is Fig. 3.2. In this model a transformer and three reference plane shifts are the only elements.

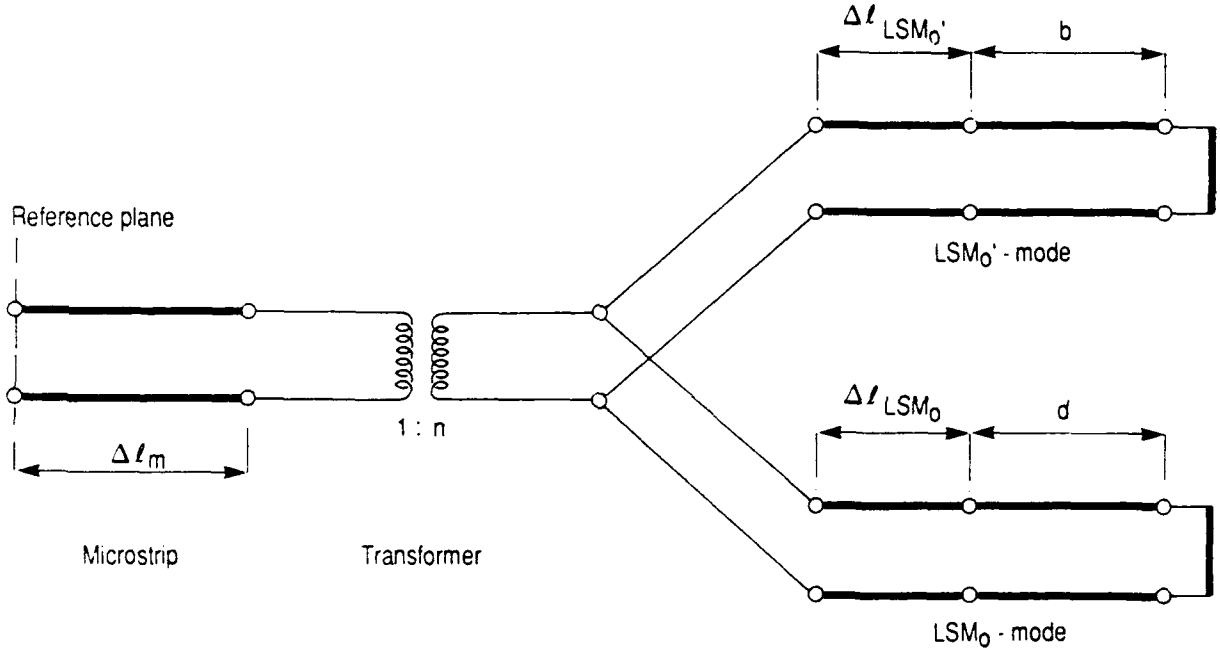


Fig. 3.2: Open end model derived from one-port data

A study on this equivalent circuit was done using the following geometric parameters: strip width 100μm, substrate thickness 100μm, package height 500μm, package width 3.1 mm, dielectric constant 12.85 and feed section length 0.8 mm. The operating frequency was 80 GHz.

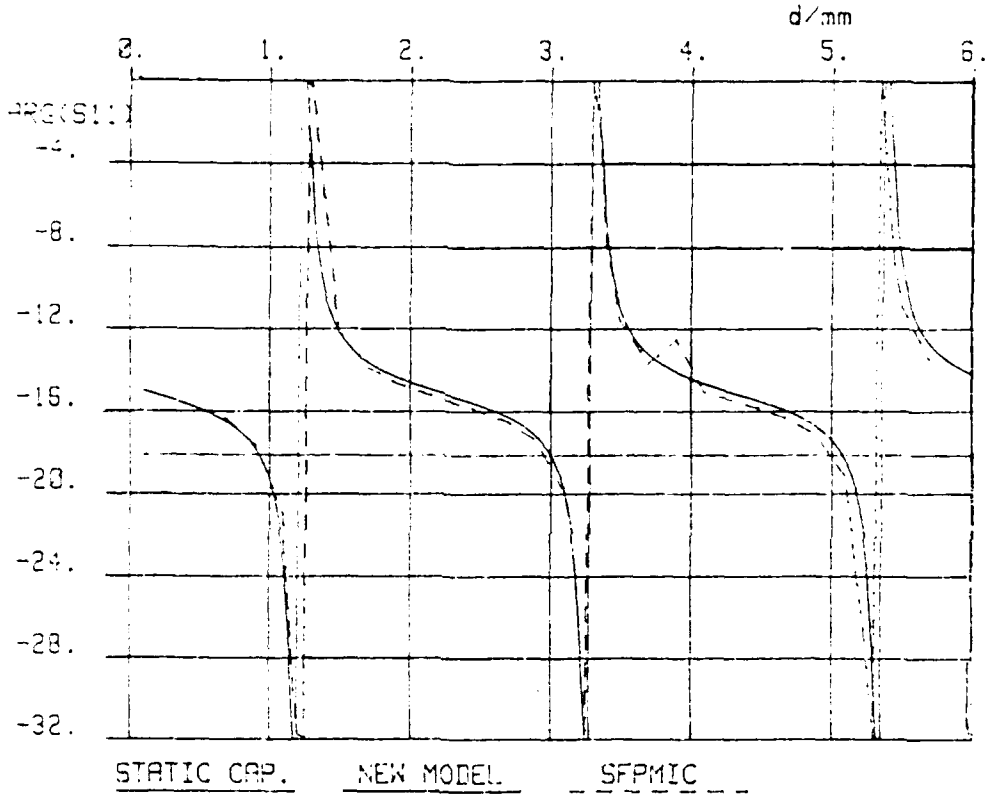


Fig. 3.3: S11 phase of open end

The model parameters generated in this case were: microstrip effective dielectric constant ε_{eff} 9.25, characteristic impedance Z_L 44.05 ohm, open end length Δl_m 0.025 mm; for the LSM_0/LSM_0' description ε_{eff} 0.816, Z_L 80.76 ohm, Δl_{LSM_0} 0.86 mm and $\Delta l_{LSM_0'}$ 0.5 mm. The transformer ratio n was 0.15.

A comparison of the open-end reflection coefficient phase computed from the model with that derived from the field-theoretial data basis, is shown in Fig. 3.3. In this figure, d, the distance between the open end and the opposite electric wall of the conducting package, was varied in the range 0.5 mm to 6 mm. The box resonances resulting for certain values of d can be clearly recognised. At such values a strong interaction between the open end leakage field and the box field occurs with the effect that the phase of S_{11} deviates strongly from its static capacitive model values. The static value model result is indicated as a straight line (~16° phase). Despite the simplicity of the model, the main physical behaviour is described accurately.

Another related model describing this situation was also studied (Fig. 3.4).

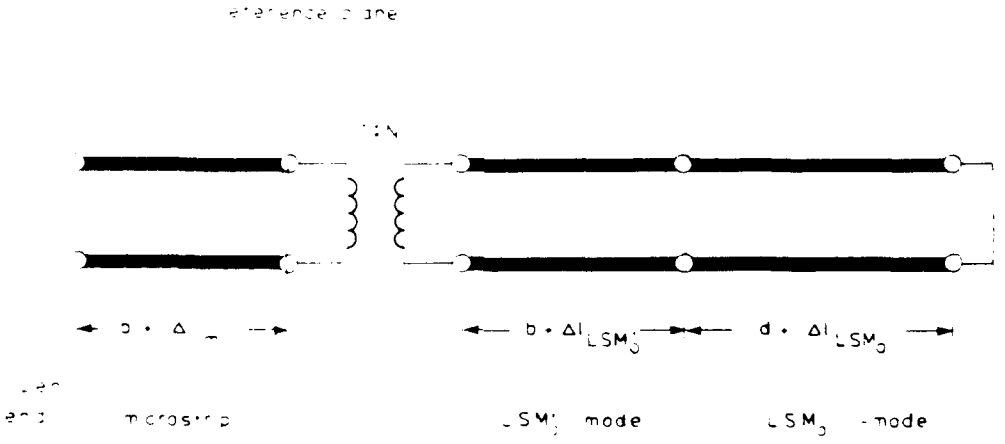


Fig. 3.4: Alternative microstrip open end model

This model still includes the different wavelengths of the LSM_0 mode and the LSM_0' mode. If the package mode characteristics are known from numerical

investigations, it was found that the package resonances can be predicted very accurately. The value of the resonance length d_{res} for a fixed length b of the microstrip feed section can be given with good accuracy by the relation

$$d_{res} = \lambda_{LSM_o} (0.5\text{-}b/\lambda_{LSM_o}')$$

where λ_{LMS_0} and λ_{LSM_0}, are the different LSM_0 wavelengths.

Further preliminary studies were carried out using the one port equivalent model. The geometric configurations analysed are those of Table 1 where the open end position, X_m in the package is given by

$$X_m = -X_A \quad \text{and the package width by} \quad W_s = X_B - X_A ,$$

the open ends having a fixed substrate thickness of 0.1 mm. The table is in two parts, the first giving the geometric values of each configuration analysed and the second the modal characteristics obtained for each configuration. ZL and EFF, and ZLSM and EFLSM are the characteristic impedance and effective dielectric constants of the microstrip and LSM_0 modes respectively.

With the reference plane of the open end one-port description situated at the microstrip end, the studies always resulted in a reference plane shift for the LSM_o mode directly related to the length b of the associated microstrip feed section. This shift, l_{LSM_0} shown in detail in Table 2 was found to be due to the special method of generating the numerical data when using a boundary value source formulation, the source used in the full-wave numerical approach being located at the beginning of the microstrip feed section. That is, at the wall of the package.

Configuration	Width	b	XA	XB	M
1	0.100	0.8	-1.50	1.60	0.5
2	0.100	1.5	-1.50	1.60	0.5
3	0.100	2.0	-1.50	1.60	0.5
4	0.100	0.8	-0.40	2.70	0.5
5	0.100	0.8	-1.50	1.60	0.2
6	0.075	0.8	-1.50	1.60	0.5
7	0.100	0.8	-0.95	0.85	0.5
8	0.100	0.8	-0.55	0.45	0.5
9	0.100	0.8	-1.00	2.10	0.5
10	0.100	0.8	-0.60	2.50	0.5
11	0.100	0.8	-1.20	1.90	0.5
12	0.050	0.8	-1.50	1.60	0.5

Configuration	Freq.	EFF	ZL	EFLSM	ZLSM
1	80	9.25	44.0	0.816	80.8
2	80	9.25	44.0	0.816	80.8
3	80	9.25	44.0	0.816	80.8
4	80	9.20	43.6	0.816	80.8
5	60	8.89	42.7	0.794	40.9
6	80	9.03	49.0	0.816	80.8
7	70	9.13	43.7	-0.234	260.0
8	80	9.21	43.7	-2.33	148.2
9	80	9.25	44.0	0.816	80.8
10	80	9.24	44.0	0.816	80.8
11	80	9.25	44.0	0.816	80.8
12	80	8.79	55.4	0.816	80.8

TABLE 1: Configuration geometry and mode characteristics

Configuration	b	l / LSM_0
1	0.8	0.860
2	1.5	1.593
3	2.0	2.109
4	0.8	0.828

Table 2

Assuming that the LSM_0 and LSM_0' characteristics are nearly equal, a unified analytical model can be presented for the two modes (Fig. 3.5).

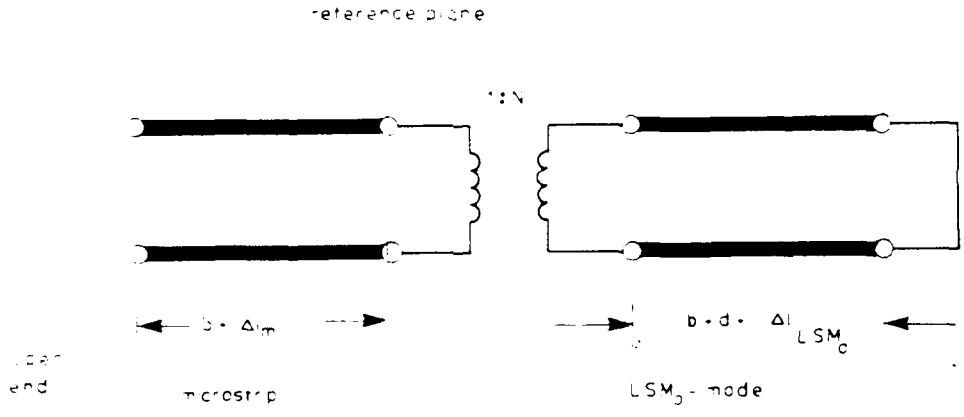


Fig. 3.5: Unified open end model

In the simplified model above this unified description is taken into account. This equivalent circuit model together with the analytical LSM_0/LSM_0' modal expressions (Section 4.2) were used to generate all the following results.

3.2. MICROSTRIP OPEN END SIMULATION INCLUDING PACKAGE RESONANCE BEHAVIOUR

The investigations clearly show that the presence of a package has a significant influence on the performance data of microstrip discontinuities at mm-wave frequencies. Therefore the package has to be considered in the modelling process. In the proposed model the coupling between the microstrip mode and the fundamental package mode is included allowing the separation of pure discontinuity effects from the effect of the package.

One method of modelling is to vary the package length by changing the distance d between the open end and the opposite package wall. A function is then obtained from which the open end data can be de-embedded. Varying the longitudinal package dimension has the advantage that all the associated mode quantities are kept at fixed values. The results of four open end configurations have been analysed in this way and are shown in Figs. 3.6-9. The numerical full-wave data are compared to those resulting from the analytical model. The parameter values for the equivalent circuit model are given in the headers (transformer ratio, microstrip open end equivalent length and LSM_0 mode reference plane shift).

Figs. 3.6 and 3.7 show the results for the discontinuity geometries in configurations 5 and 6 respectively (Table 1). In these two cases the effective dielectric constant of the LSM_0 mode is positive, i.e. the LSM_0 mode (and the LSM_0' mode with equal mode parameters) is propagating in the package. As can be seen the resonance behaviour of the coupled open end - package configuration is well described by the equivalent circuit model.

On Figs. 3.8 and 3.9 simulation results relating to the geometric configurations 7 and 8 are given (Table 1). In these two cases, the effective dielectric constant of the LSM_0 mode is negative which by definition means that the LSM_0 is below cutoff in the package. Under these

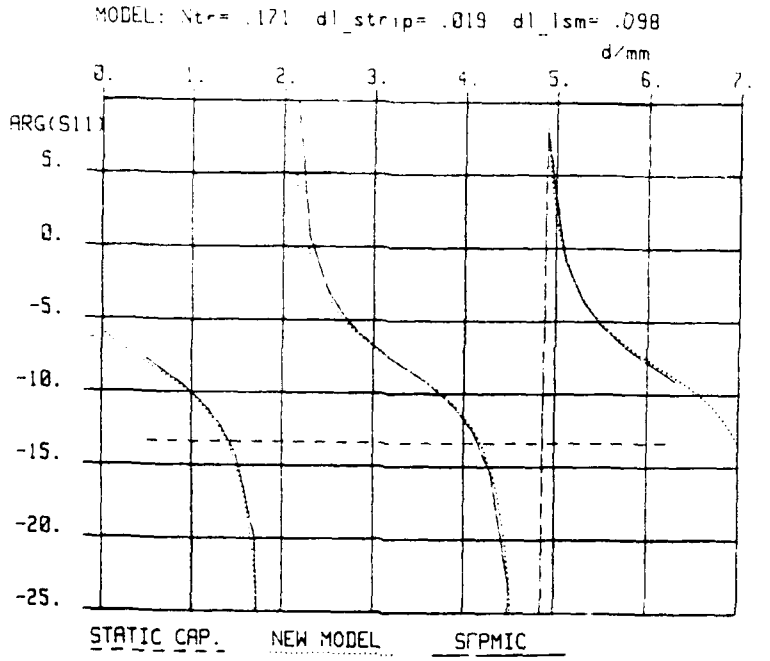


Fig. 3.6: Open end S11: configuration 5

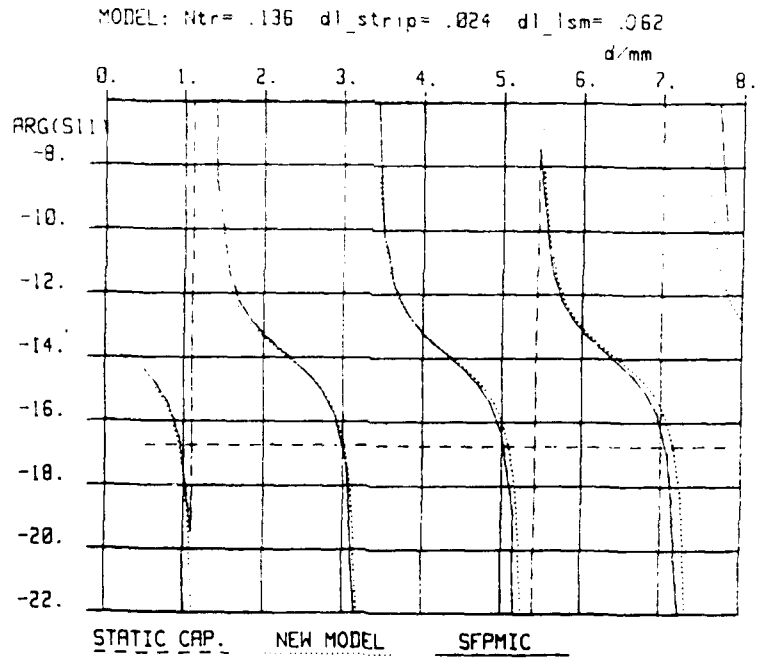


Fig. 3.7: Open end S11: configuration 6

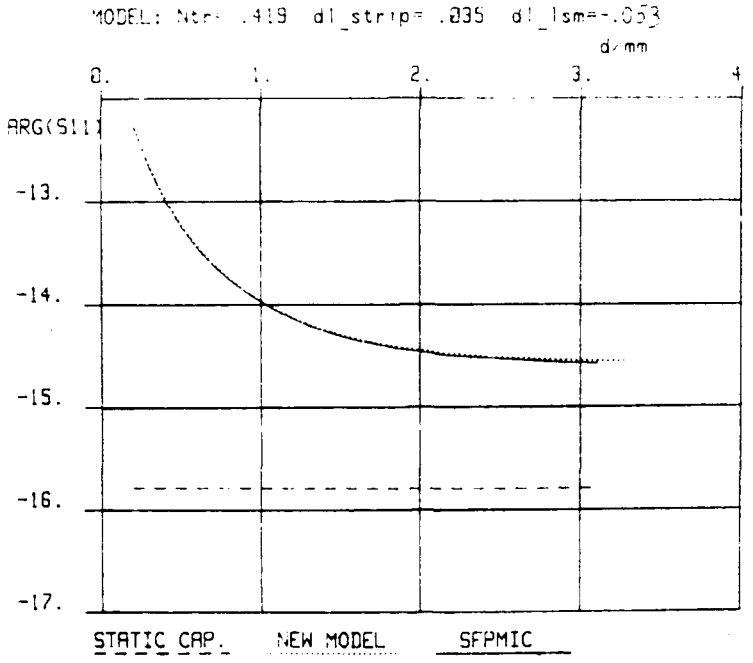


Fig. 3.8: Open end S11: configuration 7

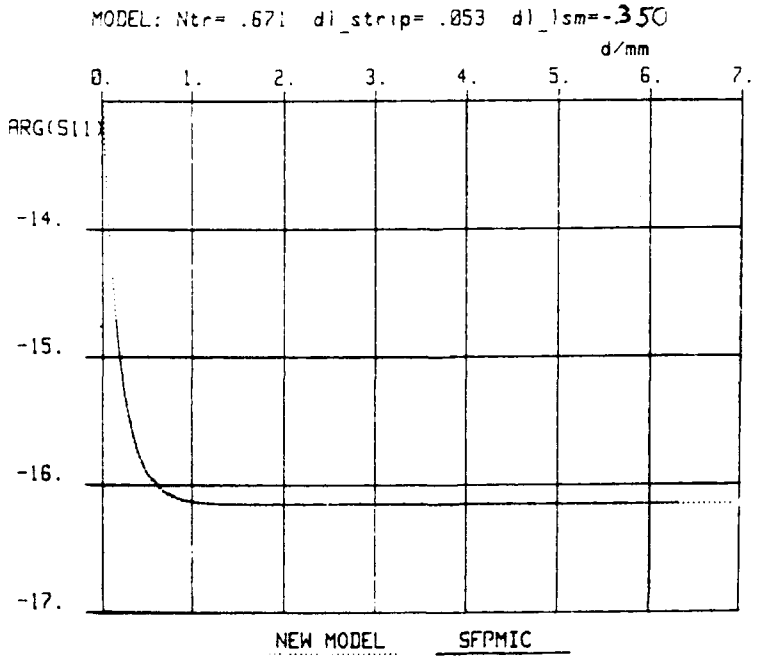


Fig. 3.9: Open end S11: configuration 8

circumstances the behaviour of the configuration is not resonant. The reflection coefficient, however, can be described by the same equivalent circuit model. Note, that in this case the characteristic impedance and the propagation constant of the package mode are no longer real but imaginary.

In the Figures 3.6-9 about 30 different package lengths were considered as the data base from which the models were generated. Since the resonance dimensions of the package can be predicted, however, to good accuracy from the LSM_0 characteristics and since the behaviour observed is that of a typical reactance function, it is possible to determine the model equivalent circuit elements from only three specific reflection coefficients, i.e. three suitably chosen package lengths. An optimum choice is to take three values near to that package length for which the effect of the package mode on the microstrip open end vanishes:

$$b/\lambda_{LSM_0'} + d/\lambda_{LSM_0} = 0.25 + 0.5n$$

where n is the number of wavelengths.

With n = 1 and three data samples chosen near to the above defined length, good model quality can be achieved using only a small numerical data basis. Due to the fact that the electric field of the LSM_0 mode is essentially directed vertical to the substrate surface and the metallisation thereon, it is expected that similar reactance behaviour will occur in the other discontinuities cases (the LSM_0 field being perturbed slightly by the presence of a metallisation and having little dependence on the conductor shape except in respect to the strength of its excitation).

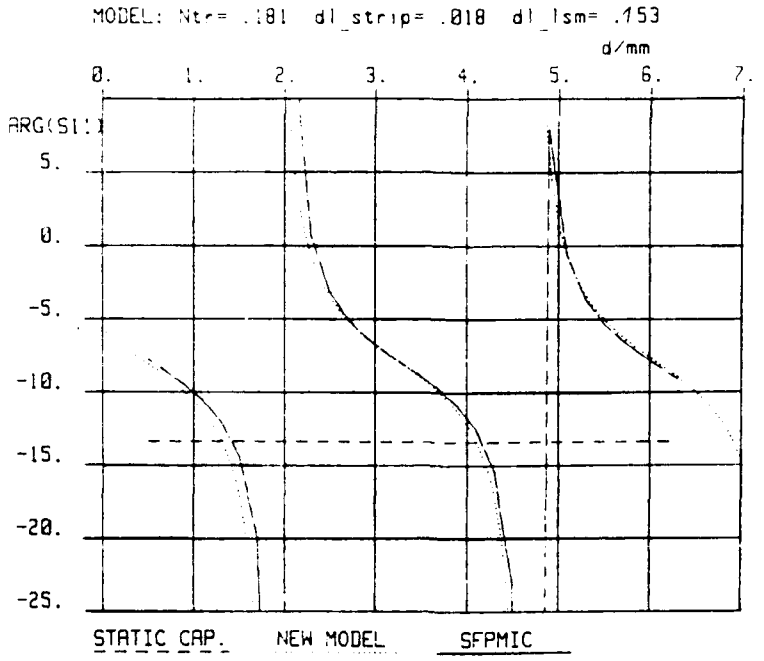


Fig. 3.10: Reanalysis of configuration 5

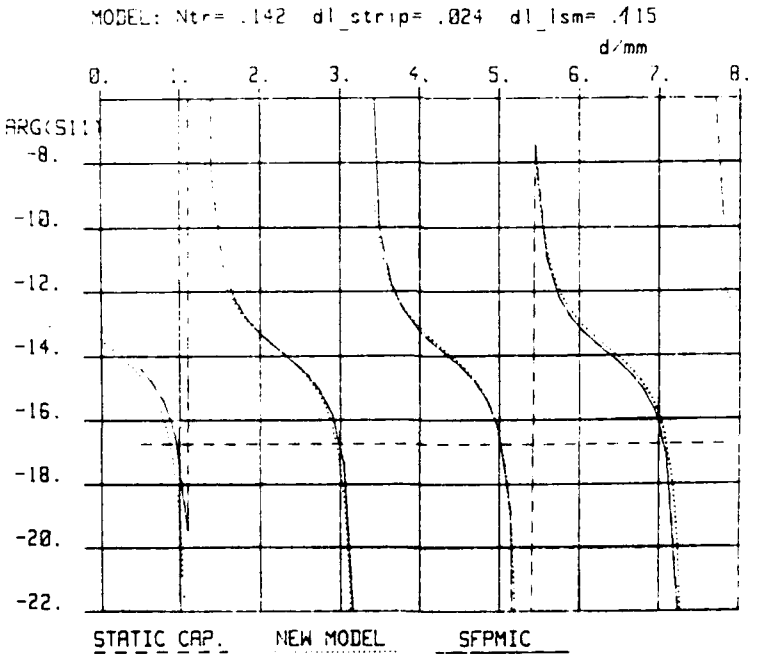


Fig. 3.11: Reanalysis of configuration 6

On Figs. 3.10 and 3.11, the microstrip open end configurations 5 and 6 were reanalysed (Table 2), but with the elements of the equivalent circuit being generated from only three data samples. As can be seen, the open end resonance behaviour is again described accurately. The open end equivalent length result is the same as that obtained from a much larger data base by curve fitting.

3.3. STUDY OF MICROSTRIP LSM_0 MODE COUPLING AS A FUNCTION OF DISCONTINUITY POSITION

While the package dimensions mainly determine the parasitic resonance frequencies associated with a shielded discontinuity, the position of that discontinuity in the package determines the strength with which package modes are excited and with which package resonance fields interact with the discontinuity. This principle provides a key to discontinuities modelling including coupled fundamental package mode coupling. To demonstrate that this physical modelling concept is capable of taking into account such effects, the microstrip open end was analysed again for five different positions of the microstrip section within the package cross section (Fig. 3.12).

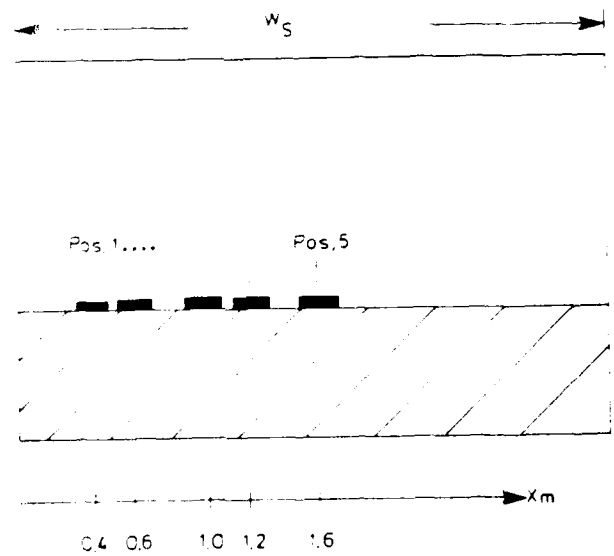


Fig. 3.12: Open end positions analysed

The strip width taken is 100μm and the width of the package, 3.1 mm. Table 2 shows the model parameters obtained for the five different strip positions, where X_m, indicates the position of the middle of the strip from the package sides for each case.

Table 3

Configuration	X_m	Δl_{LSM_o}	Δl_m	N	N/N pred
1	1.6	0.060	0.026	0.144	1.67
11	1.2	0.063	0.027	0.133	1.69
9	1.0	0.064	0.027	0.118	1.69
10	0.6	0.039	0.028	0.077	1.73
4	0.4	0.028	0.028	0.051	1.70

The positions and lengths given in Table 3 are in mm.

As can be seen, the open end length Δl_m of the microstrip does not depend noticeably on the position of the strip. This can be explained as follows. With the electric field of the LSM_o mode being similar to that of a TE_{1o} mode in a rectangular waveguide, the coupling between the LSM_o mode and the microstrip mode becomes smaller if the position of the strip is near the side wall of the package. This is reflected by the transformer ratio N of the transformer in the equivalent circuit model. Following conventional waveguide theory and introducing an effective width w_{eff} (1,2) for the prevailing microstrip, the transformer ratio and its dependence on the position of the strip in the package cross section can be predicted by the formula

$$N_{pred} \sim \iint_A \vec{E}_{Strip}(x,y)\ \vec{E}_{LSM_o}(x,y)\ dxdy$$

$$\sim \cos\left(\frac{\pi}{w_s}(x_m - 0.5w_{eff})\right) - \cos\left(\frac{\pi}{w_s}(x_m + 0.5w_{eff})\right),$$

with $$w_{eff} = 120.\pi.\frac{h}{Z}.\varepsilon_{eff}^{-0.5}.$$

The table, however, shows that the predicted transformer ratio N_{pred}, is still undetermined by a proportionality factor depending on the choice of the LSM_0 mode characteristic impedance definition. In Table 3, the constant factor was found empirically to be about 1.7. The independence of this factor on the strip position again confirms the validity of the modelling approach.

Changing the width of the microstrip for a fixed package cross section has also been considered, the results are given in Table 4.

Table 4

Configuration	w/μm	N
1	100	0.144
6	75	0.136
12	50	0.126

As expected the transformer ratio depends on the strip width.

3.4. MICROSTRIP-LSM_0 MODE COUPLING STUDIES AT THE SOURCE AND AT THE DISCONTINUITY

The transformer element in the equivalent circuit plays a basic role in the discontinuity modelling because it describes the coupling between the fundamental microstrip mode and the fundamental parasitic LSM_0 package mode. For this reason, the dependency of the transformer ratio N as a function of other geometry parameters is important in order to fully describe all physical aspects of a model. Again the elementary open end case was used to study the transformer behaviour with variation of the microstrip feed section length.

Two models A and B, (Figs. 3.13 and 3.14) equivalent to the previous model differing only by the position of the reference plane were studied. The reference plane in model A is at the microstrip open end while in model B it is at the source, i.e. at the excitation point at the beginning of the microstrip. A study showed that the parameters Δl_0 and Δl_{LSM} of both models agreed with geometry variation of strip mid and end package wall position.

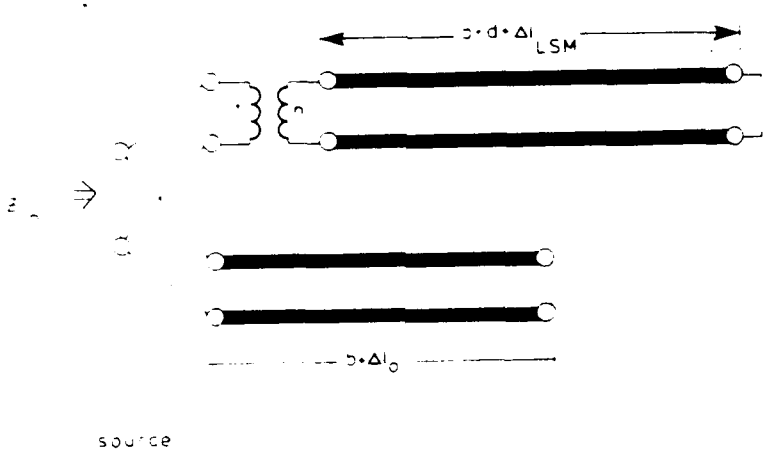


Fig. 3.13: Open end equivalent circuit A

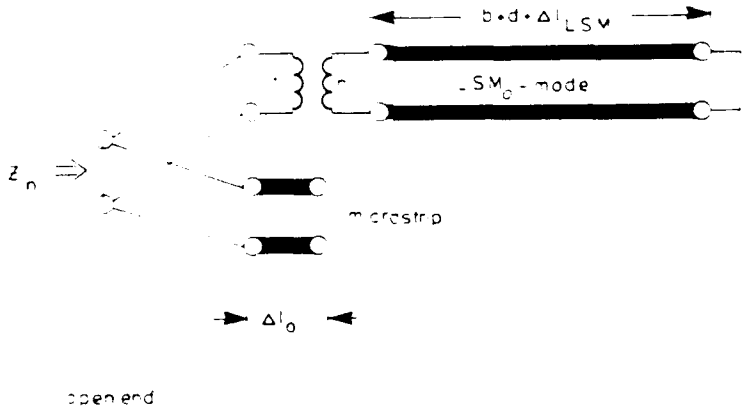


Fig. 3.14: Open end equivalent circuit B

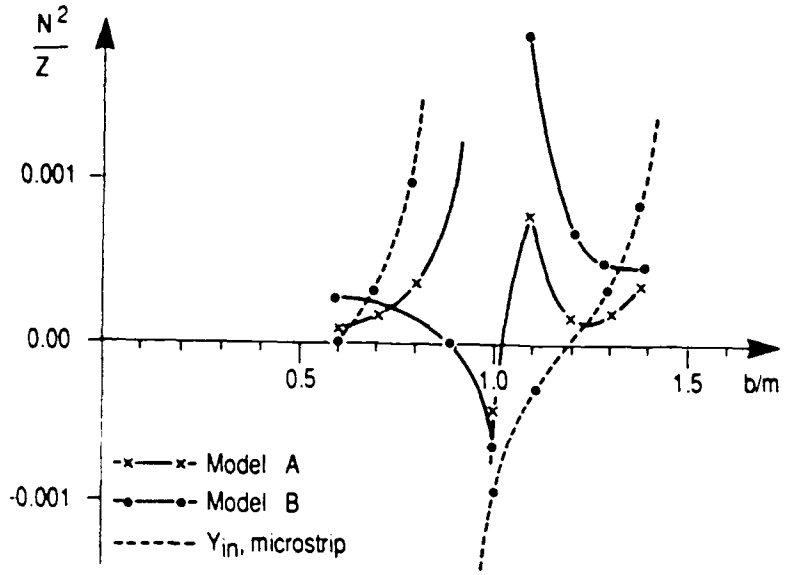


Fig. 3.15: Microstrip-LSM_0 mode coupling v. open end length

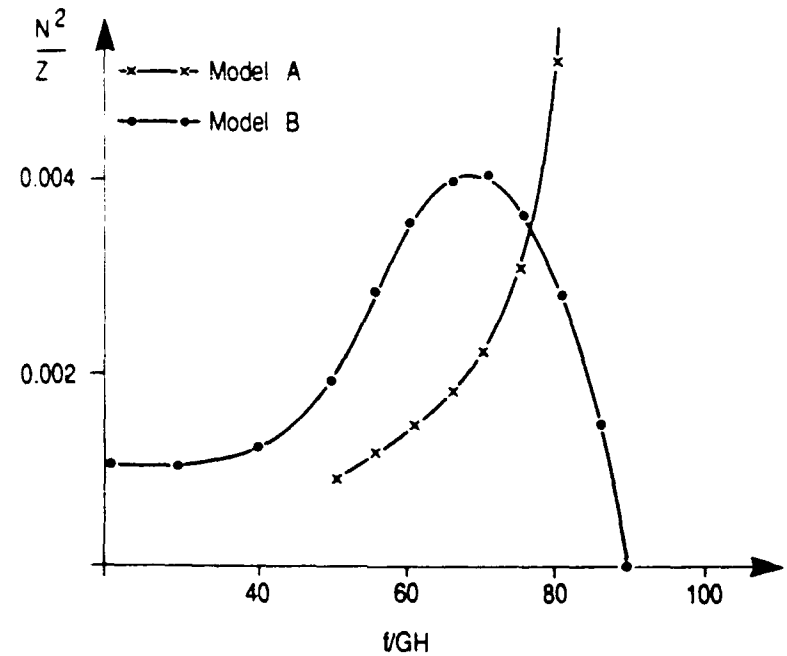


Fig. 3.16: Microstrip-LSM_0 mode coupling v. frequency

Previous investigations have shown that the simple one-port equivalent circuit used for modelling has to be extended to fully describe all effects represented by the numerical data. This can be clearly shown if the transformer ratio is investigated as a function of the microstrip feed length and of the associated variation of the reference plane. The coupling between the microstrip mode and the LSM_0 mode, represented by the value N^2/Z_{LSM}, is given as a function of the microstrip length b in Fig. 3.15. In Fig. 3.16 the value of N^2/Z_{LSM} is plotted as a function of frequency. Frequency variation is equivalent to changing the electrical length of the microstrip section. The configuration investigated was

ε_r = 12.85, w = 100μm, h = 100μm, H = 500μm,
w_s = 3.1 mm, f = 80 GHz, b = 0.8 mm

From these results a dependency of N on the microstrip feed section length is indicated. However a physical model describing the microstrip open end should be able to match the numerically generated full wave data with parameters that do not depend on the length of the microstrip feed section.

There are only two possibilities for the occurrence of such a length dependency, either the approach used in extracting the model parameters from the numerical data needs modifying or a more detailed physical model is required.

3.5. STUDY OF THE MODEL DE-EMBEDDING PROCEDURE

3.5.1. Discussion on model parameter de-embedding from the field theory data

The investigations so far have shown that numerical simulations of the open end as a simple one-port (which means looking only at the fundamental

microstrip wave amplitudes) again reveal a dependency of the transformer ratio, n as a function of the microstrip feed section length, b.

This dependency should not exist and as such means that the de-embedding of the model from the computed S-parameters must be studied in more detail.

At present the discontinuity strip sections are partitioned into three regions A, B and C; A = impressed source current density region and the transition region between the source and undisturbed mode propagation (Appendix: Section 2.3), B = feed section of nearly undisturbed mode propagation, C = discontinuity expansion region (Fig. 3.17).

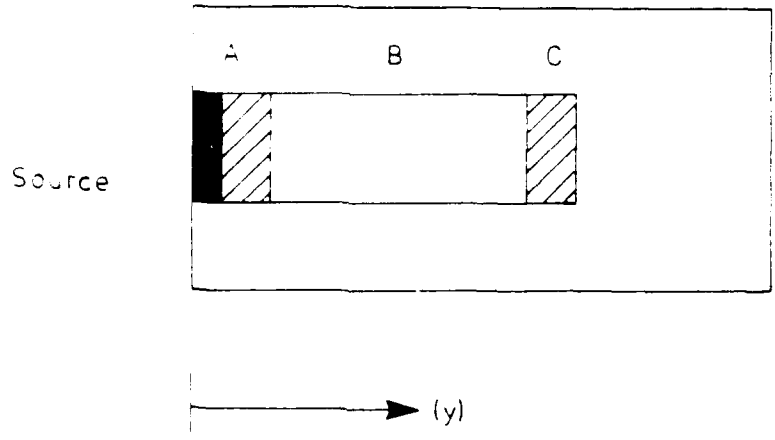


Fig. 3.17: Analysis sections of open end configuration

In section B, the current distribution is described by expansion functions generated from a priori computed transmission line solutions. Depending on which mode amplitudes have to be de-embedded from the numerical analysis, the precomputed distributions are used for the respective modes. For other modes (here the LSM_0' mode) any other kind of representation of sufficiently complete form can be used. Region C has suitable functions describing the open end disturbance, while region A is used to establish the continuity of the source distribution into the microstrip feed section, B.

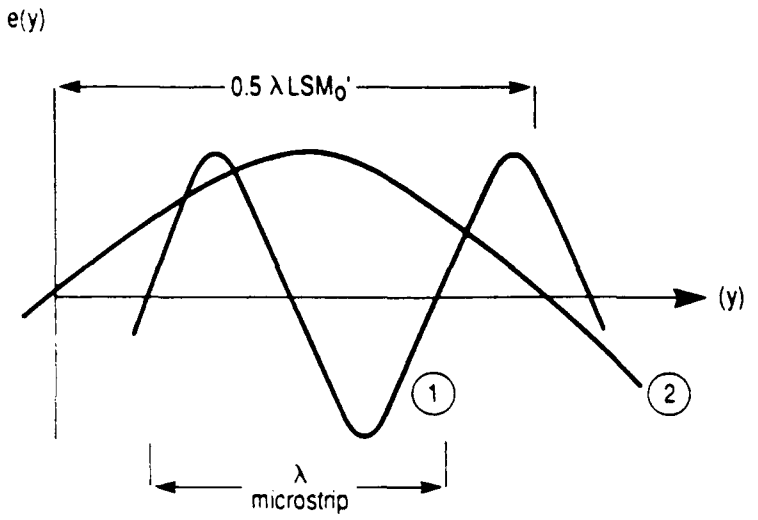


Fig. 3.18: Transverse current distribution: precomputed modal form

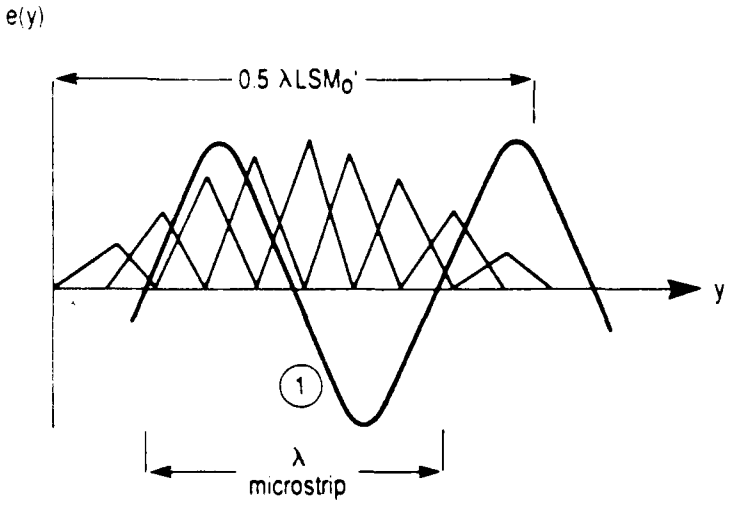


Fig. 3.19: Transverse current distribution: triangular function form

One of the problems of de-embedding correctly is the fact that the LSM_0' mode strip current is usually small compared to the microstrip fundamental mode current if the package dimensions are not in a resonance condition. Nevertheless, to de-embed in detail the LSM_0' mode behaviour, either its current distribution has to be taken into account by a precomputed expansion (direct de-embedding) or in a general but sufficiently complete form (indirect de-embedding), deriving the model parameters from the microstrip behaviour as a function of the structural data. One possible representation of the LSM_0' current is shown in Fig. 3.18, i.e. the precomputed form. Though the transverse distributions of the LSM_0' and the microstrip fundamental mode current density are neary equal, with respect to the dependency on the co-ordinate y they differ considerably due to the fact that they have different guided wavelengths λ_{LSM_0}, and $\lambda_{microstrip}$. For indirect de-embedding, a general (not precomputed) expansion for the LSM_0, for example in the form of triangle functions as shown in Fig. 3.19, is a second possibility.

3.5.2. Study of microstrip-LSM_0 mode coupling as a function of microstrip length

In Figs. 3.20-22 the reflection coefficient phase for an open-end discontinuity is shown for three different microstrip lengths, b (0.8 mm, 1.1 mm, 1.3 mm). The microstrip width was 0.1 mm, substrate thickness 0.1 mm and cover height 0.5 mm. The package width was 3.1 mm and the frequency of analysis 80 GHz. In all three cases the resonance behaviour is similar in principle depending only on the total package length. If the overall length of the package is $\lambda_{LSM}/2$ the coupling between microstrip mode and LSM_0 mode becomes significant.

The length of the applied source distribution (region A) is only 0.1 mm. To be sure that the resonance behaviour is effected by the overall package

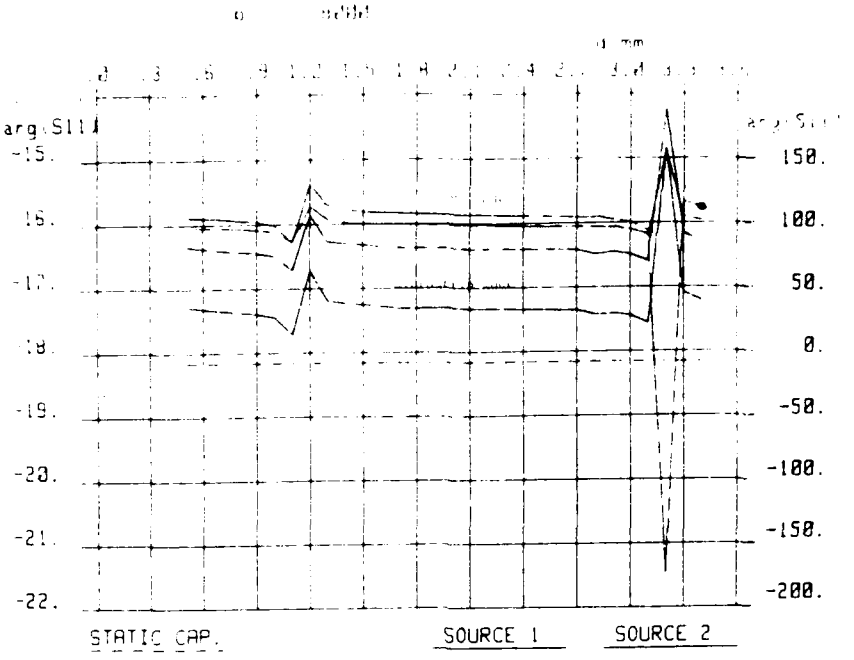


Fig. 3.20: S11 for open end: length 0.8μm

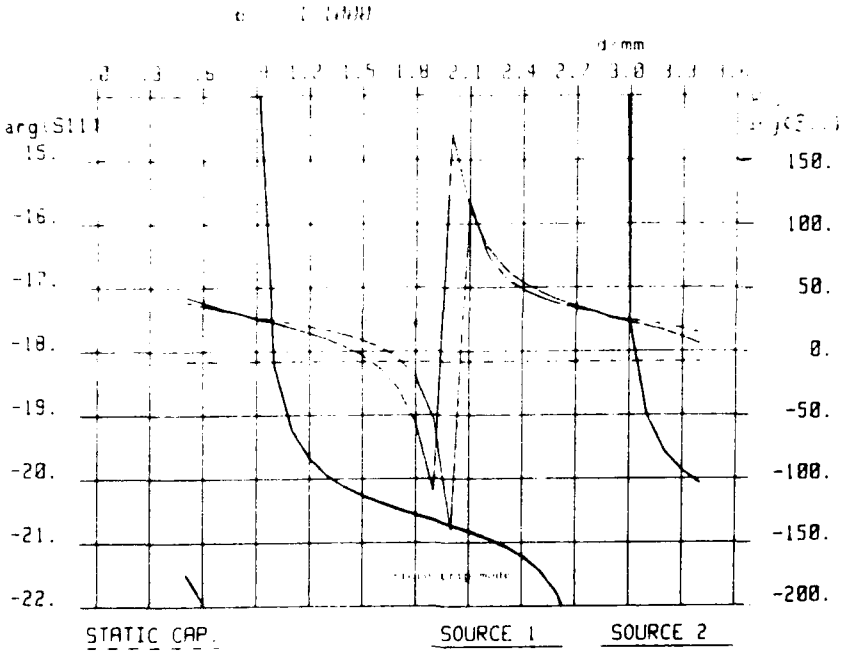


Fig. 3.21: S11 for open end: length 1.1μm

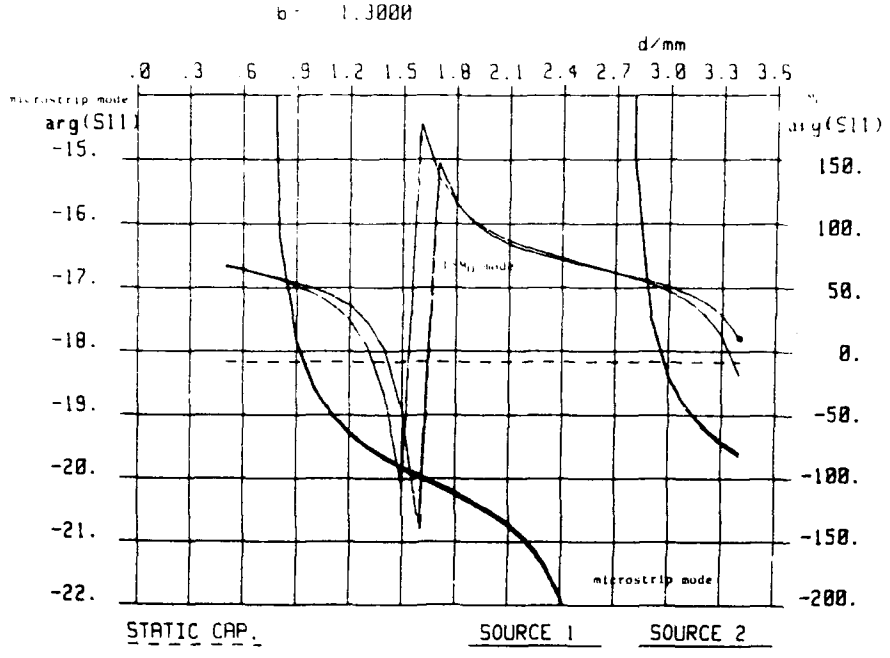


Fig. 3.22: S11 for open end: length 1.3μm

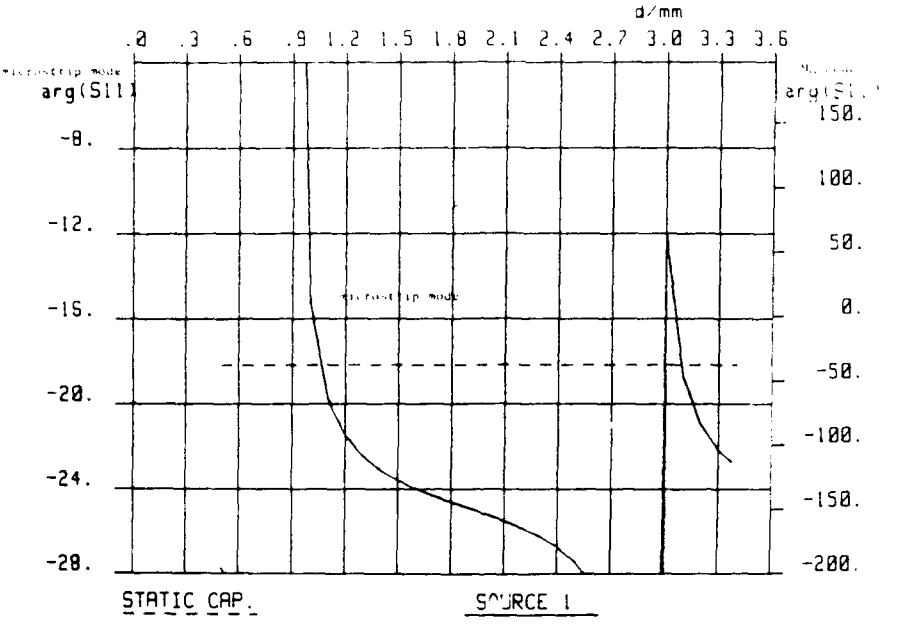


Fig. 3.23: S11 open end: source length 0.3 mm

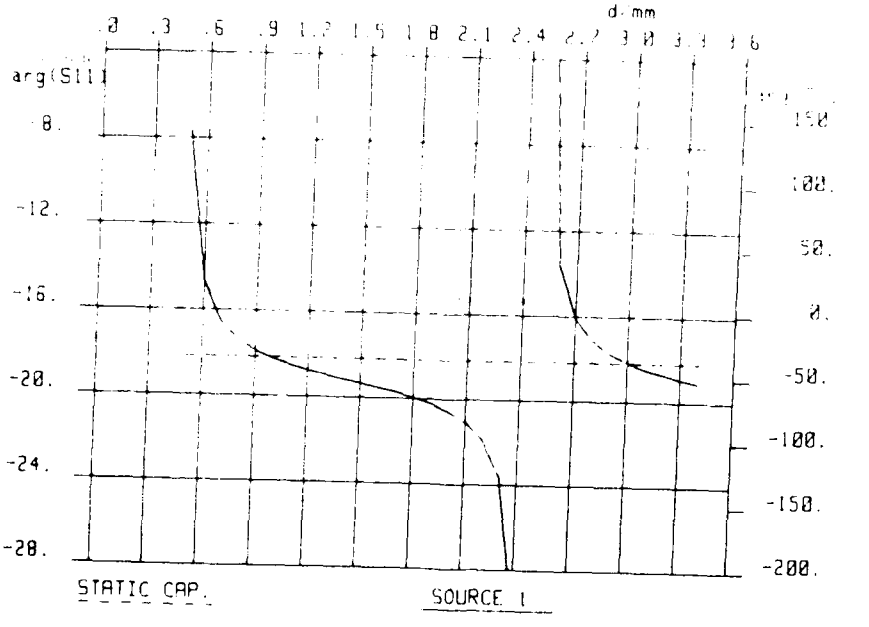


Fig. 3.24: S11 open end: source length 0.7 mm

length an additional investigation was done. The length of region A was changed from 0.1 mm to 0.7 mm (plots Figs. 3.23 and 3.24), the data in these figures showing that the package length is indeed the key factor in behaviour of the resonance, where the resonant length

$$l_{res} = b + d + l_s,$$

where l_s is the source length.

The two curve sets in Figs. 3.20-22 are the result from an analysis with two different source types. One set is the data generated with a microstrip source (source 1), the other is data for a LSM_0 source (source 2). The results which are nearly equal, indicate the stability of the applied algorithm.

3.6. IMPROVED PHYSICS RELATED MODEL STUDIES

Since the de-embedding approach has been proved, a more detailed model is therefore required with microstrip/LSM_0 coupling at the open end and at the source. This is based on the fact that the microstrip mode and the parasitic LSM_0' mode are mutually orthogonal across any microstrip cross-section and, accordingly, should couple at the ends where the feed strip terminates discontinuously.

The arguments for the extended model concept are as follows:

- On the microstrip line feed section the microstrip mode and the LSM_0' mode propagate independently (mode orthogonality). There is no direct coupling between the modes. The amplitudes of the modes will be determined by coupling mechanisms at the beginning and at the end of the microstrip section.

- At the microstrip end, the fundamental microstrip mode will be reflected and only a small portion of its energy will be transmitted into the LSM_0 mode (transformer ratio 1:n).
- At the end of the microstrip only a small portion of the fundamental mode energy will be transferred into the parasitic LSM_0' mode. Due to the close similarity between the fields of the LSM_0 mode and the LSM_0' mode, it is therefore reasonable to assume a transformer ratio of 1:1.
- At the beginning of the microstrip line feed section the source excites both modes in parallel. The source current is the sum of the conductor currents of the microstrip and LSM_0' mode (transformer ratios 1:m, 1:m'.

Various equivalent circuits were tested, the model giving the best fit is shown in Fig. 3.25.

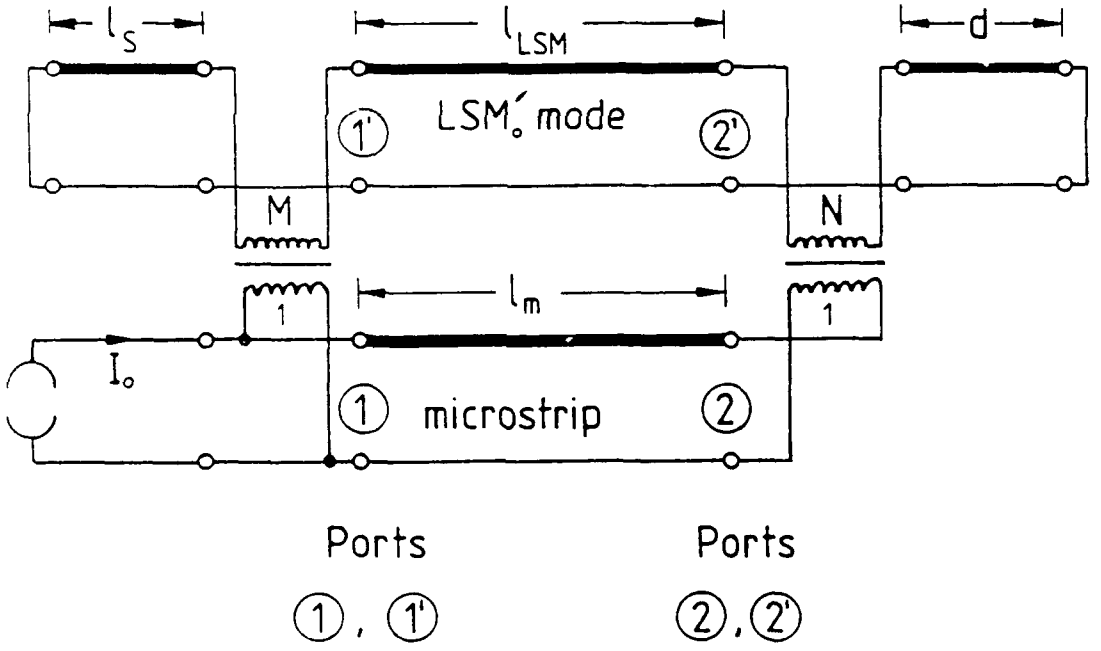


Fig. 3.25: Enhanced open end model

In this model the microstrip mode behaviour was found to be well described. A new model feature, a LSM_0 mode line section length, l_s, (length of region A) has been introduced. The LSM_0 mode description of this model now includes short stubs at both sides of the microstrip line section. This inclusion is necessary in order to represent the correct resonance dimensions of the package even for different lengths l_s of the source region. In Figs. 3.26-28 the results of fitting this model to the numerically generated data are plotted. All three curves have been generated with similar model parameters:

$$M = -1,\ N = 0.04,\ l_s = 0.1\ \text{mm},\ l_{LSM} = b,\ l_m = b + \Delta l_0.$$

open end length Δl_0: 0.031 mm as from static analytical model; and microstrip characteristic impedance, ZL = 80.8 ohms.

As can be seen, the new model gives a good fit to the microstrip mode behaviour.

From theory, the coupling between microstrip mode and LSM_0 mode is expected to be small except for package dimensions near LSM_0 mode resonance. These expectations indeed are described by the new model. The transformer ratio N turns out to be small (N = 0.04 in our examples). With the coupling between microstrip mode and LSM_0 mode being small, the LSM_0 mode behaviour is mainly determined by the electric walls of the package with no significant influence from the microstrip mode (except resonance cases). This expected behaviour is actually represented by the new model (linear phase shift as a function of parameter d). In contrast to this, the numerically generated LSM_0 mode data in Fig. 3.28 shows the phase of the reflection coefficient at ports (2) and (2') with a relatively strong resonance contribution from the microstrip mode. However as can be seen this contribution can not yet fully be described by the new model. One of possible reasons for this discrepancy may be that the numerically generated LSM_0 mode behaviour is effected by coupling to higher package modes.

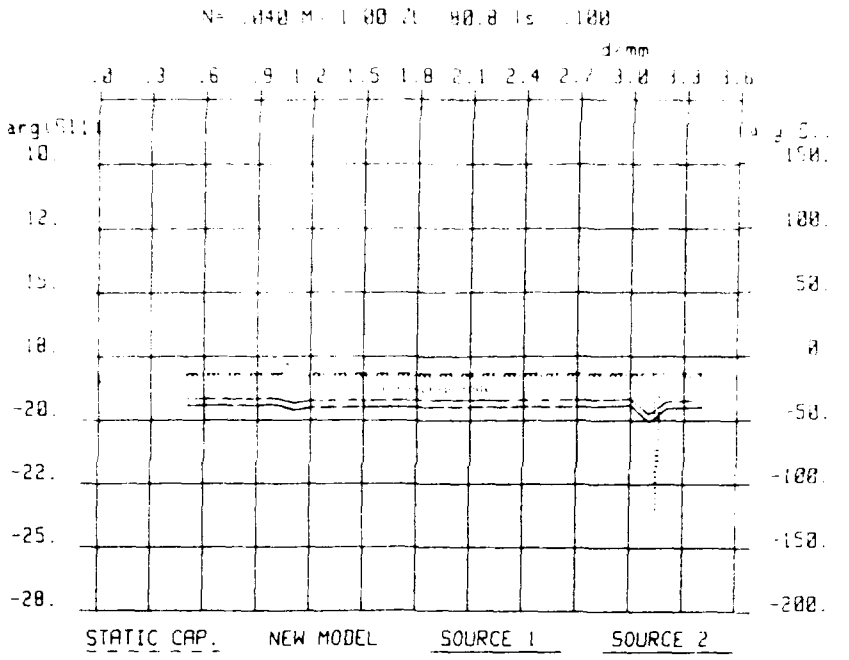


Fig. 3.26: Open end configuration 1: S11

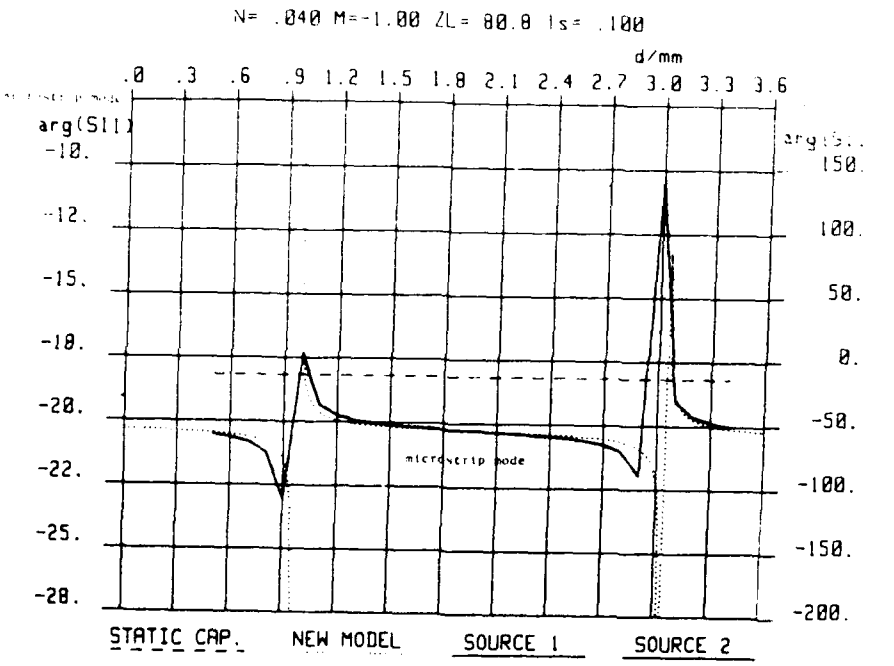


Fig. 3.27: Open end configuration 2: S11

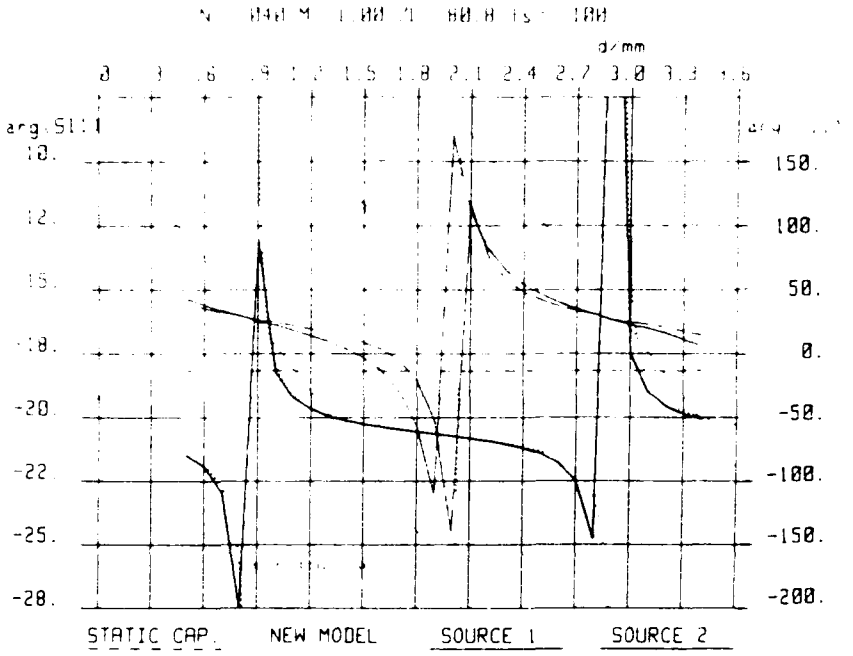


Fig. 3.28: Open end configuration 3: S11

3.7. REFERENCES

1. Wheeler, H.A., Transmission-line properties of parallel wide strips by a conformal mapping approximation, IEEE Trans. 1964, MTT-12, pp.280-289.

2. Wheeler, H.A., Transmission-line properties of parallel wide strips separated by a dielectric sheet, IEEE Trans. 1965 MTT-13, pp.172-185.

4. MICROSTRIP AND LSM_0 MODE CHARACTERISTIC MODELLING FORMULAE

As the proposed modelling approach relies on an analytical prediction based on a physical description, it requires as input the microstrip and LSM_0 mode characteristics. The effective dielectric constant and the characteristic impedance of microstrip are well-known parameters. Such characteristics have only a second order dependence on the package dimensions for walls that are not extremely close to the strip. For the derivation of the LSM_0 mode characteristics waveguide theory is used.

4.1. ANALYTIC FORMULAE FOR THE MICROSTRIP MODE CHARACTERISTICS

In the discontinuity models the characteristic impedance and the effective dielectric constnt of microstrip are important parameters. As such analytic formulae are needed which must be dependent on strip width, the substrate height, the package height and frequency. Formulae for the characteristic impedance and effective dielectric constant have already been published (1,2). These formulae, however, are not dependent upon the package height. The implementation of the package height into the published analytic formulae can be achieved by the introduction of correction factors f(w,f,h,H) such that the strip characteristic impedance and the effective dielectric constant are expressed by,

$$\varepsilon_{eff},\ Z_L(w,h,H,f) = \varepsilon_{eff},\ Z_L\ (w,h,f,)\ *(1-f(w,f,h,H),$$

where $\varepsilon_{eff},\ Z_L\ (w,h,f)$ are the published equations.

The influence of the package height on microstrip transmission line parameters is expected to be a second order effect as long as the package height is much larger than the substrate thickness, also applying to discontinuities enclosed in a package with a height so low that LSE type modes are sufficiently far below cutoff.

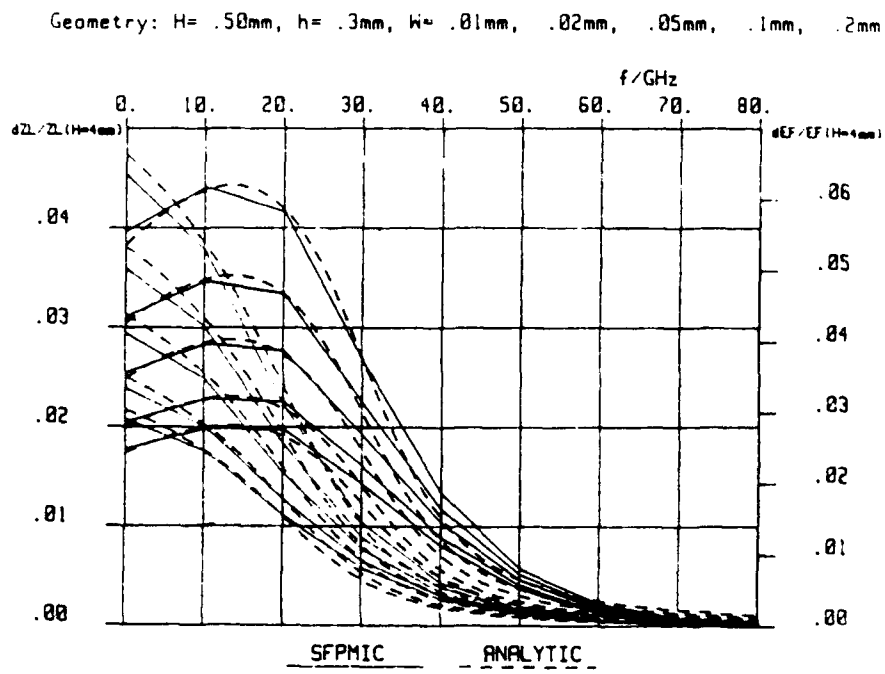


Fig. 4.1: Characteristic impedance and effective dielectric constant errors for a 0.5 mm cover height

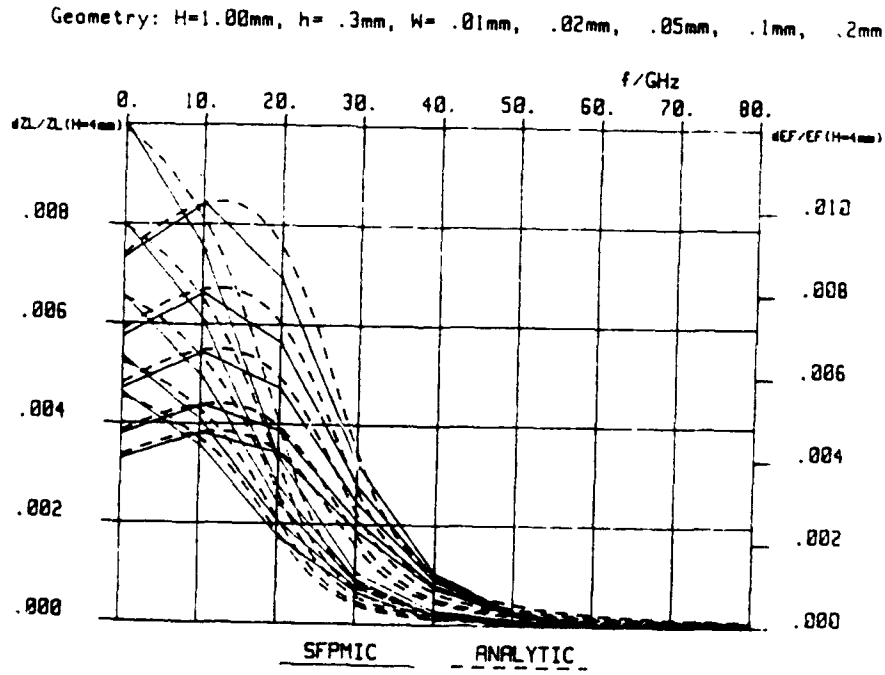


Fig. 4.2: Characteristic impedance and effective dielectric constant errors for a 1.0 mm cover height

As a first step a data base of characteristic impedance and the effective dielectric constant were generated by the field-theory based computer program SFPMIC for the following ranges:

Strip width w:	10μm, 20μm, 50μm, 100μm, 200μm
Substrate height h:	100μm, 200μm, 300μm
Cover height H:	250μm, 500μm, 1mm, 2mm, 3mm, 4mm
Frequency f:	0.80 GHz in steps of 5 GHz

From this data base constant correction factors f_{ZL} (w,f,h,H) and f_{eff} (w,f,h,H) were computed. Analytic formulae were then developed to approximate the field-theory based correction factors. These formulae were tested against the numerical results across the geometry and frequency ranges. The results (Figs. 4.1 and 4.2) show the frequency and microstrip width dependency of these analytic correction factors for fixed substrate and package heights in comparison to the field-theory based computations.

The basic formulae developed describe a class of functions of shape:

$$f_{ZL} = A_{ZL} \left(1+ \frac{w/h}{w_o}\right)^{p1} * \left(\frac{H/h}{H_o}\right)^{-p2} * \left(1- \frac{\pi}{2} \arctan \frac{f*h-f_1}{f_2}\right)^2 * (f*h+f_3)$$

$$f_{eff} = A_{eff} \left(1+ \frac{w/h}{w_o}\right)^{p1} * \left(\frac{H/h}{H_o}\right)^{-p2} * \left(1- \frac{\pi}{2} \arctan \frac{f*h-f_1}{f_2}\right)^2$$

The analytic formulae for the strip characteristics' correction factors are after fitting:

Characteristic impedance

$$f_{ZL} = A_{ZL} \left(1 + \frac{w/h}{w_o}\right)^{p1} * \left(\frac{H/h}{H_o}\right)^{-p2} * \left(1- \frac{\pi}{2} \arctan \frac{f/GHz*h/mm-f_1}{f_2}\right)^2 * (f*h+f_3)$$

with

$f_1 = 4.211 * (1-0.0484*H/h)^{1.215} * (10h/mm)^{0.837}$

$f_2 = 3.177 + (5.881*h/H-2.068) * (10h/mm)^{-0.549}$

$f_3 = 4.255 * (10h/mm)^{0.837}$

$p3 = 1.821 * (1-1.18*h/mm)$

$A_{ZL} = 0.0005539 / ((0.325*H/h)^{p3} + (0.21*h/H)^{p3})$

$w_o = 0.11$, $p1 = 0.49$, $H_o = 0.102$, $p2 = 1.823$

Effective dielectric constant

$$f_{\varepsilon eff} = A_{\varepsilon eff} \left(1 + \frac{w/h}{w_o}\right)^{p1} * \left(\frac{H/h}{H_o}\right)^{-p2} * \left(1 - \frac{\pi}{2} \arctan \frac{f/GHz*h/mm - f_1}{f_2}\right)^2$$

with

$f_1 = 3.532 * (1-0.0594*H/h) * (10h/mm)^{0.754}$

$f_2 = 1.139 + (4.839*h/H)^{1.116}$

$p3 = 0.682 * (1 + 4.337*h/mm)$

$p4 = (12.9+h/H)/(12.9+0.25*h/mm) - 1$

$A_{\varepsilon eff} = 0.269* p4 /((2.209*H/h)^{p3} + (0.3247*h/H)^{p3})$

$w_o = 0.0711$, $p1 = 0.450$, $H_o = 0.1$, $p2 = 0.7684$

Fitting these formulae to the full-wave data base results shows that the mean deviation

$$E = \sum_{W_i} \sum_{h_i} \sum_{H_i} \sum_{f_i} 1 - \frac{(f_{ZL}/\varepsilon_{ff})^{analytic}}{(f_{ZL}/\varepsilon_{ff})^{data\ base}}$$

For the characteristic impedance analytic formula is 6% and for the effective dielectric constant is 3%. The error is about 1% for package heights of 1mm and of about 4%-10% for lower package heights.

4.2. ANALYTICAL FORMULAE FOR THE LSM_0 MODE CHARACTERISTICS

As outlined in the development of the physics related modelling approach, the LSM package mode is represented by transmission line sections. Analytical approximate expressions for the appropriate transmission characteristics can be derived from waveguide theory.

Simple analytic expressions were investigated as a function of the respective geometry and substrate parameters, including the package dimensions which have an important influence on the latter mode. Expressions derived for the effective dielectric constant of the LSM_0 mode and its characteristic impedance are given below. The LSM_0 mode impedance is defined as $U^2/(2P)$ where U is generated by integration over the electric field in the symmetry plane of the microstrip from the ground plane to the cover plane. The equations for the modal effective dielectric constant and impedance are:

$$\varepsilon_{eff}\ (LSM_0) \;=\; \varepsilon_{stat}\cdot\left(1 - (f_c/f)^2\right)$$

with $$f_c \;=\; \frac{c_0}{2W_s\cdot\sqrt{\varepsilon_{stat}}}$$

and $$\varepsilon_{stat} \;=\; \frac{\varepsilon_r\cdot(H+h)}{\varepsilon_r\cdot H+h}\ ,$$

$$Z_L\ (LSM_0) \;=\; \frac{H+h}{W_s}\cdot\frac{Z_0}{\sqrt{\varepsilon_{stat}}}\cdot\frac{1}{\sqrt{1 - (f_c/f)^2}}$$

$$(Z_0 = 120\pi\Omega,\ c_0 = 2.9979\ 10^8\ \text{m/s})$$

where H is the height of the air layer, h the substrate thickness within the box and W_s is the box width.

The LSM_0 mode characteristics derived from the analytic expressions and full-wave hybrid mode analyses for three different geometry configurations (variable package height H) over the frequency range 50-80 GHz are shown below. A comparison shows that the analytic formula represent the actual LSM_0 mode behaviour accurately.

FILE:1sm1, H = 200μm

F/GHz,EFc,EFm,ZLc,ZLm	50.0000	.4990	.5086	50.3160	51.1571
F/GHz,EFc,EFm,ZLc,ZLm	55.0000	.6550	.6709	43.7820	44.5411
F/GHz,EFc,EFm,ZLc,ZLm	60.0000	.7750	.7944	40.1160	40.9339
F/GHz,EFc,EFm,ZLc,ZLm	65.0000	.8700	.8904	37.7130	38.6626
F/GHz,EFc,EFm,ZLc,ZLm	70.0000	.9460	.9667	35.9670	37.1068
F/GHz,EFc,EFm,ZLc,ZLm	75.0000	1.0090	1.0282	34.5890	35.9799
F/GHz,EFc,EFm,ZLc,ZLm	80.0000	1.0630	1.0785	33.4230	35.1303

FILE:1sm1, H = 500μm

F/GHz,EFc,EFm,ZLc,ZLm	50.0000	.2500	.2464	145.5800	147.0002
F/GHz,EFc,EFm,ZLc,ZLm	55.0000	.4100	.4087	113.7100	114.1359
F/GHz,EFc,EFm,ZLc,ZLm	60.0000	.5320	.5321	99.8000	100.0244
F/GHz,EFc,EFm,ZLc,ZLm	65.0000	.6270	.6282	91.8500	92.0588
F/GHz,EFc,EFm,ZLc,ZLm	70.0000	.7040	.7045	86.6800	86.9351
F/GHz,EFc,EFm,ZLc,ZLm	75.0000	.7650	.7660	83.0200	83.3719
F/GHz,EFc,EFm,ZLc,ZLm	80.0000	.8180	.8183	80.2700	80.7606

FILE:1sm1, H = 350μm

F/GHz,EFc,EFm,ZLc,ZLm	50.0000	.3240	.3225	95.3100	96.3615
F/GHz,EFc,EFm,ZLc,ZLm	55.0000	.4820	.4848	78.0200	78.5934
F/GHz,EFc,EFm,ZLc,ZLm	60.0000	.6040	.6083	69.6800	70.1663
F/GHz,EFc,EFm,ZLc,ZLm	65.0000	.6990	.7044	64.6900	65.2056
F/GHz,EFc,EFm,ZLc,ZLm	70.0000	.7750	.7806	61.3500	61.9398
F/GHz,EFc,EFm,ZLc,ZLm	75.0000	.8380	.8421	58.8900	59.6352
F/GHz,EFc,EFm,ZLc,ZLm	80.0000	.8900	.8924	56.9900	57.8290

where EFc, ZLc are numerical hybrid mode data for the effective dielectric constant and characteristic impedance while EFm, ZLm represent the analytic descriptions derived here.

4.3. REFERENCES

1. Kirschning, M., Jansen, R.H., 'Accurate model for the effective dielectric constant of microstrip with validity up to millimetre-wave frequencies' Electronics Letters, 1982, p.272-273.
2. Kirschning, M., Jansen, R.H., 'Arguments and an accurate model for the power-current formulation of microstrip characteristic impedance' AEU, Vol. 37, 1983, p.108-112.

5. CONCEPT APPLICATION AND DEVELOPMENT OF DISCONTINUITY EQUIVALENT CIRCUIT MODELS EXHIBITING DYNAMIC BEHAVIOUR

5.1. OPEN END

5.1.1. An Equivalent Circuit Model

Preliminary studies made for the microstrip open end model in Section 3.6, indicated that it gave the type of dynamic description required to implement the physics related modelling approach. This circuit model has been found to be valid if the fundamental mode and the LSM_0-mode on the microstrip and the LSM_0 package mode are the important modes present in the circuit environment.

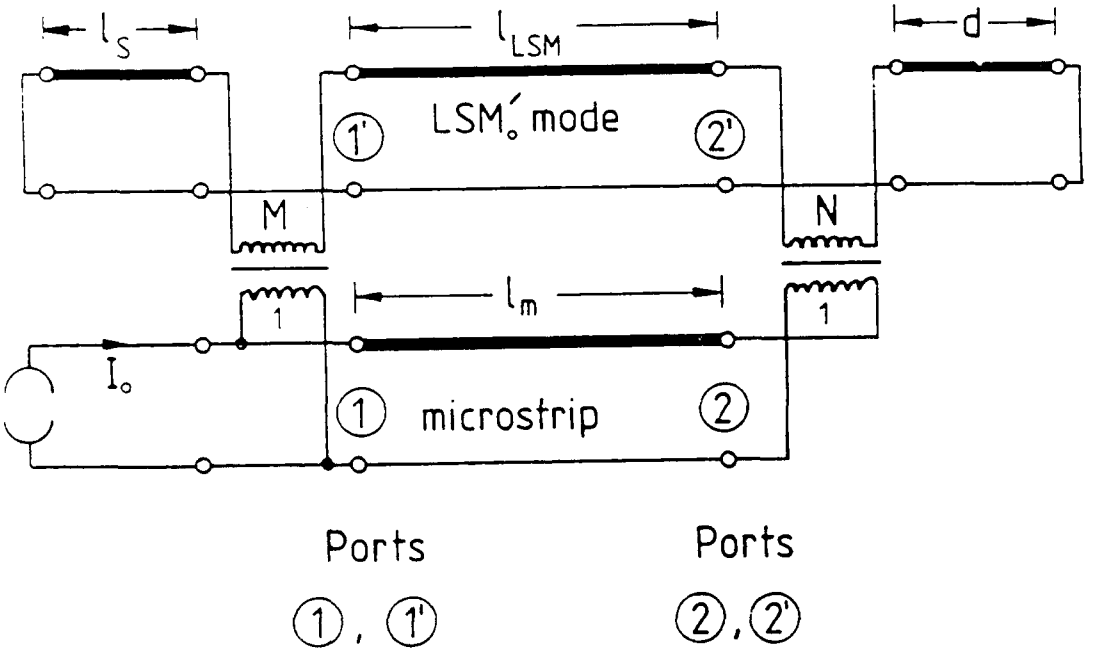


Fig. 5.1: Physics related equivalent circuit model for the microstrip open end discontinuity

The model Fig. 5.1 consists of transmission lines for the microstrip and package modes. The lengths of these transmission lines (l_s,d) are directly either related to the given structural geometry or to the physics related dimensions:

$$l_m = b + dl_0$$

$$l_{LSM} = b + dl_{LSM}$$

where dl_0 is the microstrip open end length, nearly identical to that value predicted by a static open end analytical formula. l_s is the source and the source disturbed propagation region.

The transmission line parameters of the LSM_0 package mode are expressed by simple analytical formulae defined in Section 4.2 with the LSM_0'-mode characteristics assumed to be nearly identical to those of the LSM_0-mode.

In the model the serially connected transformers describe the coupling between the microstrip and the package were found to provide the best fit results. The scattering matrix of the transformer describing the coupling between the modes has the form

$$\begin{bmatrix} 0 & s & s' \\ s & 0 & t \\ s' & t & 0 \end{bmatrix}$$

port 1 : microstrip mode
port 2 : LSM_0 mode
port 3 : LSM_0' mode

(with s, s' small and t = 1)

where the power flow from the LSM_0 mode into the LSM_0' mode is represented by the scattering parameter $S_{23} = S_{32} = t$, the microstrip mode being loosely coupled to the LSM_0 and the LSM_0' modes ($S_{12} = S_{21} = s$, $S_{13} = S_{31} = s'$).

This scattering matrix can be approximated by a 3-port including a transformer in series connection.

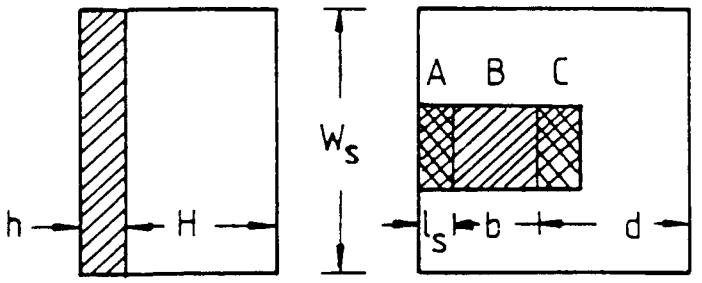
In this transformer coupling situation, the variation of parameter d causes a linear decrease of the phase of the reflection coefficient. The linear decrease can only be predicted by an equivalent circuit model, if the transformers are connected as outlined (see the reflection coefficient of the LSM_0' mode at port 2 shown in Fig. 5.2 as a function of parameter d (package dimension), the length $l_s + l_{LSM}$ being equal to $\lambda_{LSM_0'}/4$), where the predicted model LSM_0 and LSM_0' mode characteristic impedances are given by Z and Z_s and the source length l_s by d_s in the caption.

In modelling, the transformer ratio can be determined by testing the transverse electric field of the LSM_0/LSM_0' mode with the electric field of the microstrip mode, which results in a scalar product (integral) that can be evaluated approximately by simple analytical expressions.

5.1.2. Confirmation of the Open End Model

As a case study for establishing the modelling concept, the following microstrip open end discontinuity was analysed using the field theory based program and then modelled. The geometric structure of the discontinuity analysed was:

ε_r = 12.85, w = 100μm
h = 100μm, H = 500μm
W_s = 3.1mm, f = 55GHz
b = 2.8mm, 2.7, 2.5 mm.



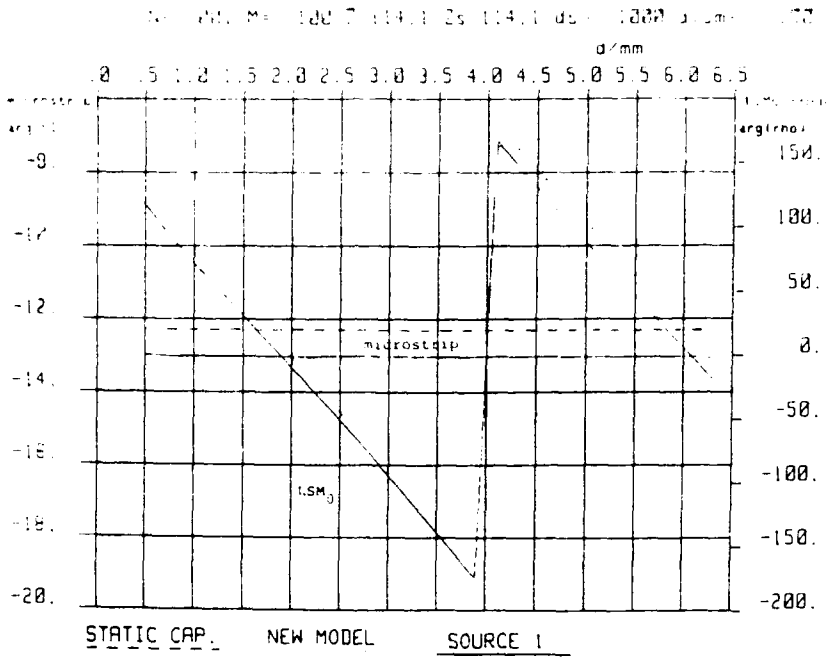


Fig. 5.2: S11 of microstrip and LSM mode for the open end

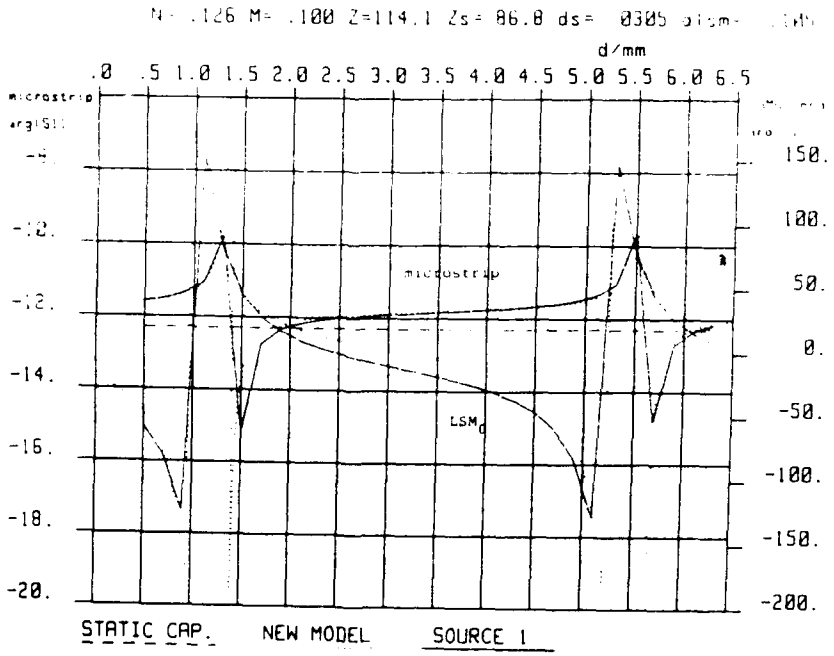


Fig. 5.3: Microstrip and LSM mode S11: length 1.8 mm

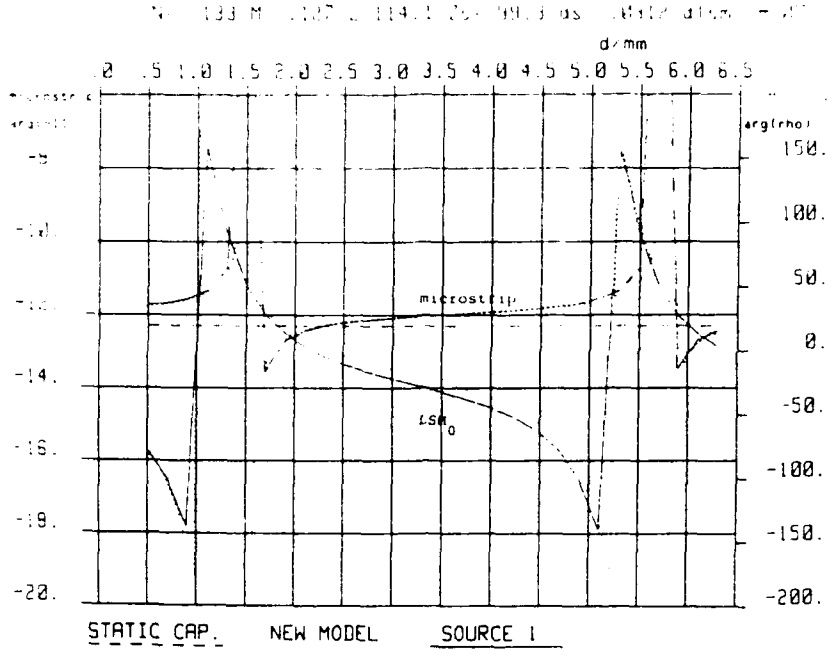


Fig. 5.4: Microstrip and LSM mode S11: length 2.7 mm

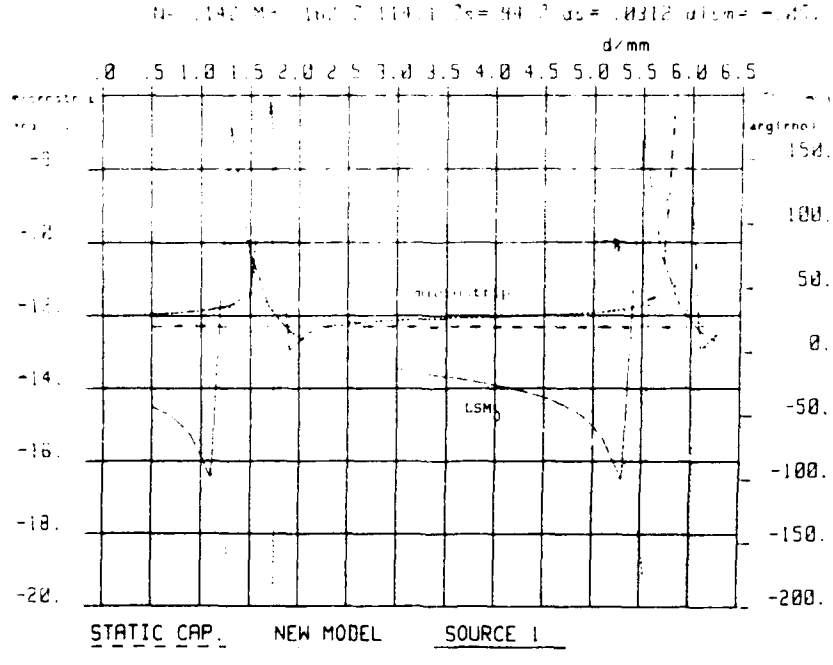


Fig. 5.5: Microstrip and LSM mode S11: length 2.5 mm

The reflection coefficients of the microstrip mode and the LSM_0' mode, extracted at port 1 and port 2', are presented on Figs. 5.3-5 as a function of parameter d (package dimension). The numerically generated data was fitted using the equivalent circuit model. Not only the reflection coefficient of the fundamental microstrip mode but also the reflection coefficient of the LSM_0' mode agrees with the numerically generated data. The given equivalent circuit obviously shows a good physical basis for a new microstrip open end model which includes the coupling to package modes.

As well as a study of the open end model, the computed and predicted LSM_0 mode characteristics were investigated. The values of the parameters of the equivalent circuit model obtained by prediction and fitting are listed in Table 1. The second data sets of Table 1 are the values estimated by simple analytical formulae or are direct geometry related values. The model transmission line parameters $\varepsilon_{eff\ LSM_0}$, $\varepsilon_{eff\ LSM_0'}$, ε_m, Z_{Lm}, l_s, d and b are fixed parameters.

Table 1: Parameter values of the equivalent circuit model for the microstrip open end discontinuity

	b = 2.8 mm		b = 2.7 mm		b = 2.5 mm	
	fitted	predicted	fitted	predicted	fitted	predicted
dl_0 (static microstrip open end length)	0.0305	0.0311	0.0312	0.0311	0.0312	0.0311
dl_{LSM}	-0.105	0.0	-0.051	0.0	-0.051	0.0
N	0.126	0.093	0.133	0.093	0.142	0.093
M	0.100	0.093	0.127	0.093	0.162	0.093
$Z_{L\ LSM_0}$	114.1	114.1	114.1	114.1	114.1	114.1
$Z_{L\ LSM_0'}$	86.8	114.1	99.3	114.1	94.7	114.1

Although the predictions are good, there is still some uncertainty in the definition of characteristic impedance for the LSM_0 mode and the LSM_0' mode which could be the reason for the slightly higher numerical fitted values of the transformer ratios M,N. This uncertainty is because the LSM_0'-mode is guided partially by the microstrip metallisation, the characteristic impedance of this mode turns out to be lower than the characteristic impedance of the LSM_0 mode. This difference in the model parameters could be a reflection on the de-embedding method used to extract the parameters of the equivalent circuit model from full wave numerical data.

5.2. MICROSTRIP GAP

The gap structure to be investigated consists of two microstrip lines and a gap with two current sources I_{01} and I_{02} as described in Fig. 5.6. The structure is situated in a package of width w_s, height h + H and total length d, where h is the GaAs substrate thickness.

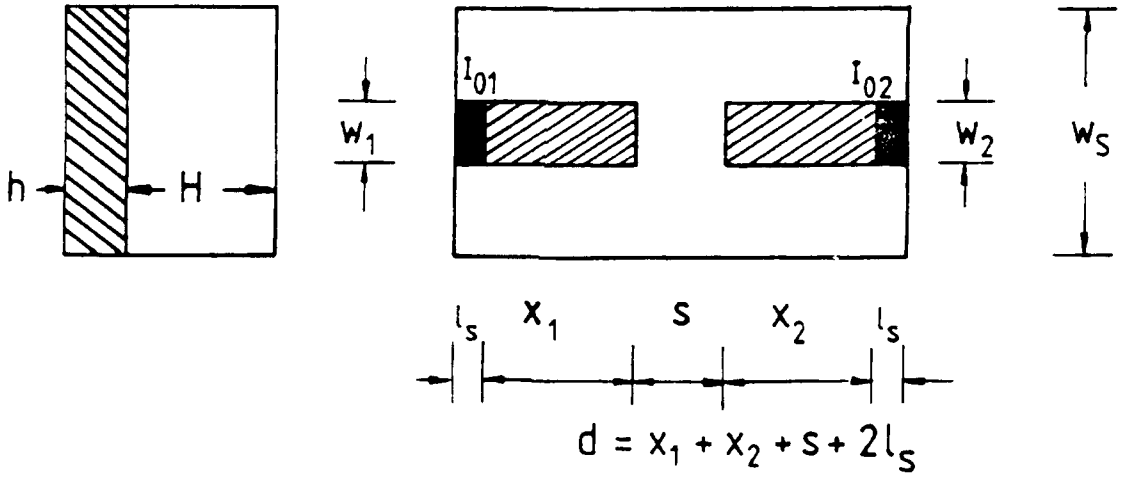


Fig. 5.6: Microstrip gap discontinuity with microstrip feed lines and current sources.

5.2.1. Comparison of the Current Static Analytical Model with Full-Wave Results

At present the microstrip gap discontinuity is a standard library component in microwave CAD simulators as far as its quasi-static behaviour is considered. An equivalent circuit with three capacitances and analytic formulae for the description of these capacitances are available from the literature (1).

In a preliminary study the quasi-static analysis was compared with full wave generated results for a range of gap widths.

The configurations studied had the following geometric parameters:

$h = 100\mu m$, $H = 500\mu m$, $w = 100\mu m$, $W_s = 3.1mm$, $f = 55GHz$, $I_{01} = 1$, $I_{02} = 0$, $s = (1mm, 100\mu m, 100\mu m)$, $x_1 = x_2 = (1.3mm - 3.2mm)$.

The quasi-static analysis took into account only the fundamental modes on the microstrip lines, package modes being neglected. These results were obtained applying the commercial CAD program LINMIC+ (2). For the full wave analysis the package dimensions were set such that the LSM_0 package mode is above cut-off at the operating frequency of 55 GHz. Reflection coefficients phases, $\rho 1$ and $\rho 2$, of the fundamental modes on the microstrip lines 1 and 2 were analysed with the reference planes defined at the ends of the microstrip lines. The results obtained were for gap values $100\mu m$ (Fig. 5.7), $200\mu m$ (Fig. 5.8) and 1 mm (Fig. 5.9).

The $100\mu m$ gap results (Fig. 5.7) reveals that there is still some correlation between the quasi-static simulation (using an analytical LINMIC+ model) and the full-wave results including package effects. The reason for this is that the gap behaviour is mainly determined by the quasi-static capacitive coupling effect between the open microstrip ends. Nevertheless there is

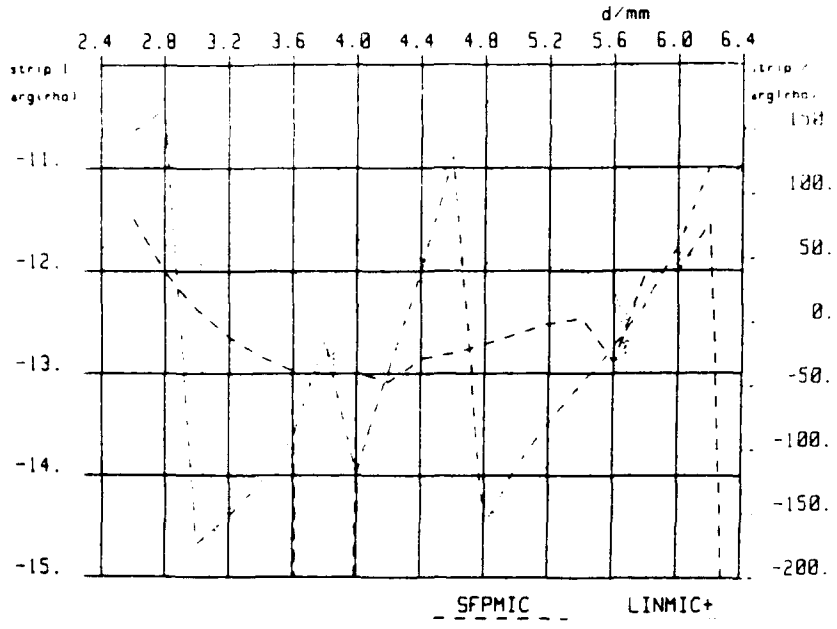


Fig. 5.7: S11 and S22 for gap model: gap 0.1 mm

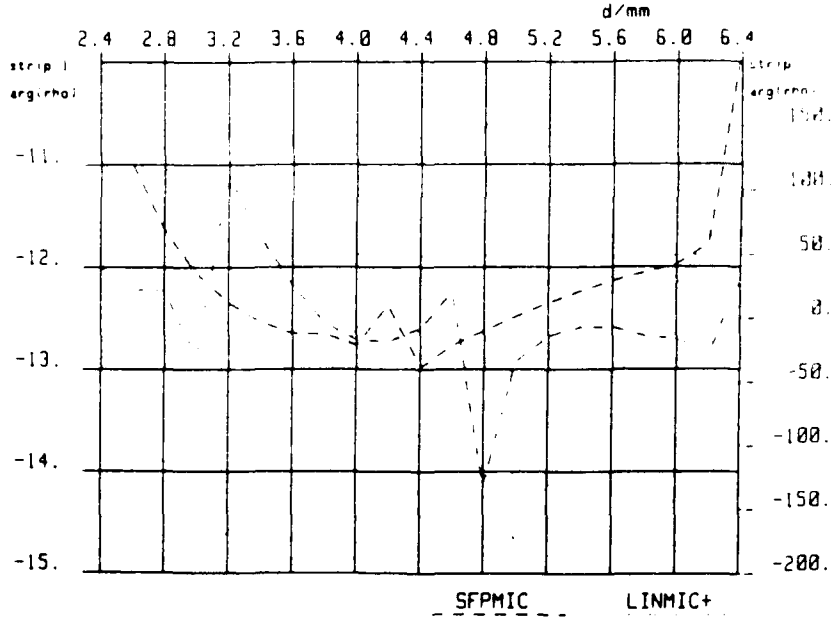


Fig. 5.8: S11 and S22 for gap model: gap 0.2 mm

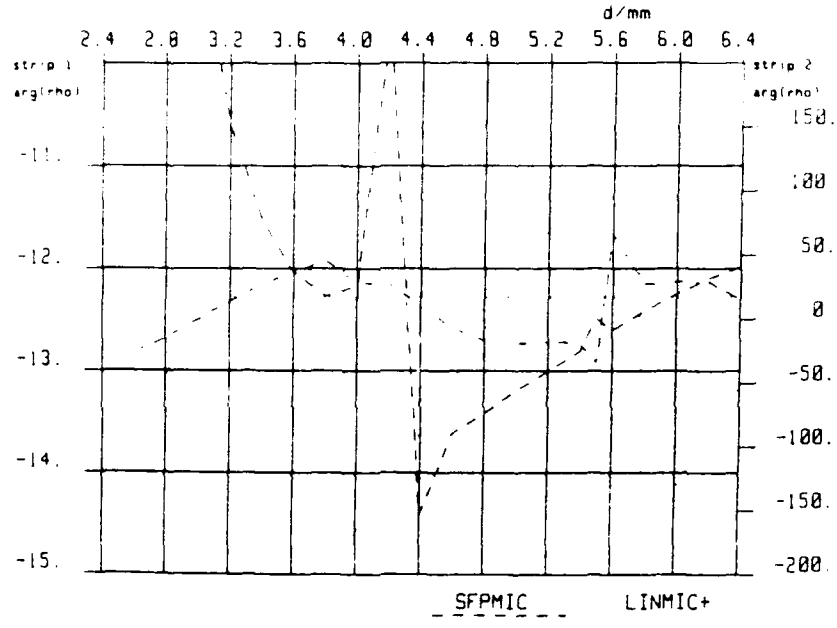


Fig. 5.9: S11 and S22 for gap model: gap 1.0 mm

already a significant difference between the conventional CAD circuit analysis and the numerical analysis which takes the package coupling mode into account. The situation is similar for the 200μm gap (Fig. 5.8). However, in this case the dominance of the quasi-static coupling is reduced and the discrepancy with the full wave results increases. The linear/constant phases (LINMIC+) shown in Fig. 5.8 essentially represent the end effects of the two open ended microstrips in the considered configuration. In contrast to this, the full-wave package mode effects show a more complicated behaviour. Note, however, that the discrepancy for the values obtained for the phase of ρ1, the reflection coefficient on the excited strip, is not very large, arg(rho1) being approximately -12 degrees.

The analysis results for a gap width 1.0 mm are given in Fig. 5.9. In this example the distance between the microstrip lines is now large compared to the strip width of 100μm and the substrate height of 100μm. Therefore the microstrip lines are nearly uncoupled capacitively for the fundamental microstrip modes. The conventional package analysis shows a reflection coefficient on strip 1 identical to the reflection coefficient of the microstrip open end discontinuity. If the full wave results are considered, the behaviour of the gap discontinuity is quite different due to interaction with package modes/resonances. The fundamental modes of both microstrip lines are coupled to the package modes and by this coupling effect both microstrip lines are dynamically coupled in an indirect way. The LSM_0 and LSM_0' package modes are above cut-off and therefore the large distance between the microstrip lines (s = 1.0 mm) does not prevent coupling. The reflection coefficient of strip 1 depends on the length of strip 2 and shows a behaviour different from the results of the quasi-static CAD analysis.

5.2.2. An Equivalent Circuit Model

Having substantiated in some detail the modelling approach for the open end, the concept has been applied in deriving an enhanced (dynamic) gap model. An

equivalent circuit for an improved description of the microstrip gap discontinuity is shown in Fig. 5.10.

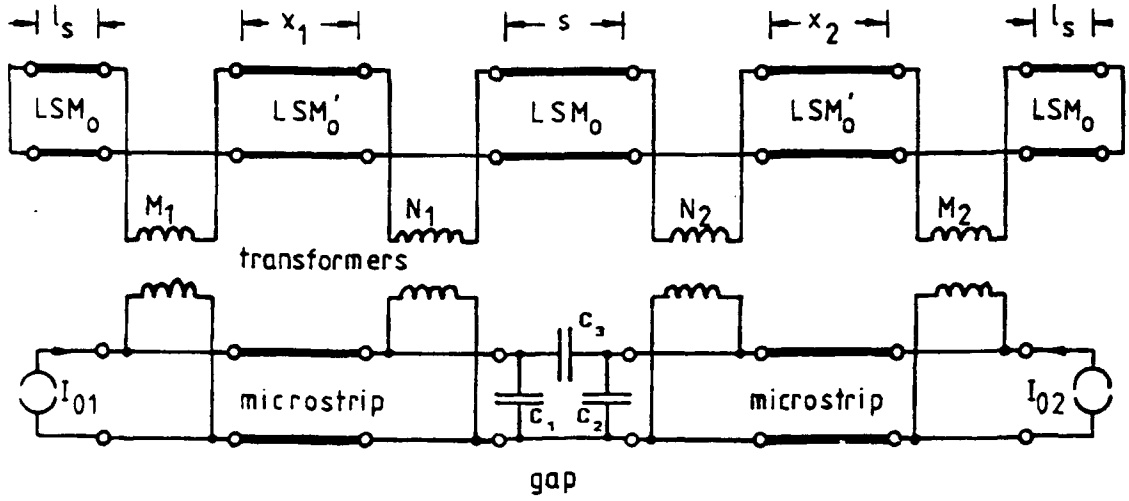


Fig. 5.10: Equivalent circuit for the microstrip gap discontinuity including dynamic parasitic effects

The equivalent circuit of Fig. 5.10 contains the same circuit elements as the open end equivalent circuit. The package mode is descibed by LSM_0 and LSM_0' modes which are dependent on the presence of the microstrip metallisation. At the ends of the microstrip lines and also at the sources at the beginning of the microstrip lines, transformers describe the coupling to the package modes. The effective dielectric constants, the strip characteristic impedances of the fundamental modes (strip 1 and strip 2 can have different strip widths) and the effective dielectric constants of the package modes (LSM_0, LSM_0') are as obtained from a full wave analysis or from equivalent analytical expressions. The strip characteristic impedance of the LSM_0 mode has been determined by the analytic formula described in Section 4. The characteristic impedances of the LSM_0' modes have been determined from the characteristic impedance of the LSM_0 mode multiplied by a correction factor not much different from 1. Assuming a symmetric gap between equal width feed strips, the capacitances $C'_1 = C'_2$ and C'_3 from the standard microstrip gap equivalent circuit are modified by suitable correction factors. These

factors again do not differ much from the numerical value of 1 and have been added to make the original quasi-static expressions more adjustable to the dynamic case.

The mathematical form in which the correction factors F_{ZL}, F_{C1} and F_{C3} are applied is:

$$Z_L(LSM_0') = Z_L(LSM_0) * F_{ZL}$$
$$C_1 = C'_1 * F_{C1}$$
$$C_3 = C'_3 * F_{C3}$$

These three correction factors and the four transfomer ratios N_1, N_2, M_1, M_2 can be determined by curve fitting techniques, i.e. by optimising the equivalent dynamic circuit model to the available full-wave numerical results.

5.2.3. Preliminary Studies

Three microstrip circuits containing a gap discontinuity and two microstrip feed lines each, were analysed as a function of total package length using the field-theory based computer program. The quasi-static circuit analysis neglecting coupling between the fundamental microstrip modes and the package modes gives results disagreeing with the field-theory based analysis. However the improved circuit description is capable of fitting the full wave generated data. The reference planes for the reflection coefficients of the fundamental microstrip modes on both feed lines are set to the ends of the microstrip lines. The reflection coefficients were determined as a function of the length d of the package; the transformer ratios N_1, N_2, M_1, M_2 and the correction factors F_{ZL}, F_{C1} and F_{C3} by fitting the reflection coefficients, calculated by the equivalent circuit description to the field-theory based data. Both wide and narrow gaps examples were studied.

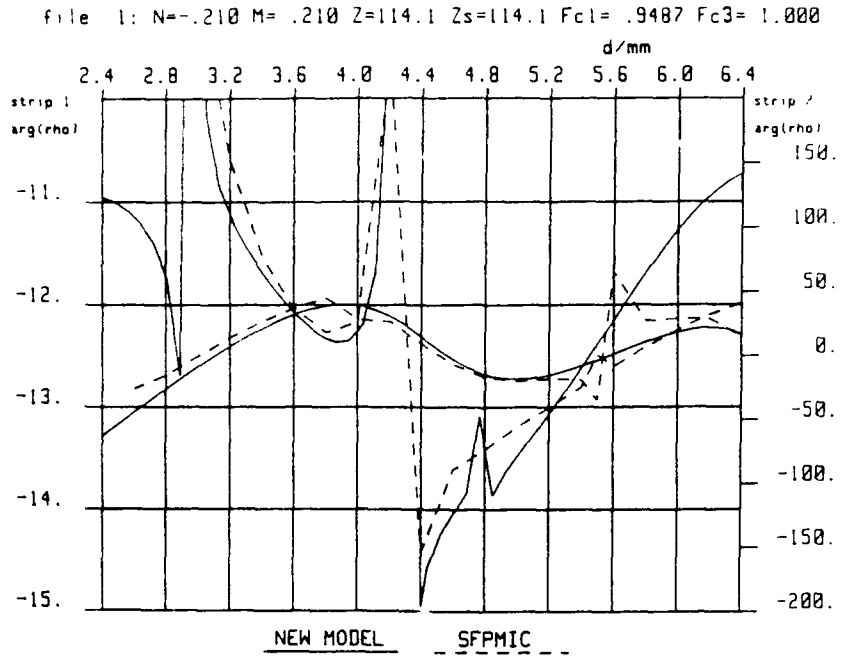


Fig. 5.11: S11 and S22 for 1 mm gap and varying package length

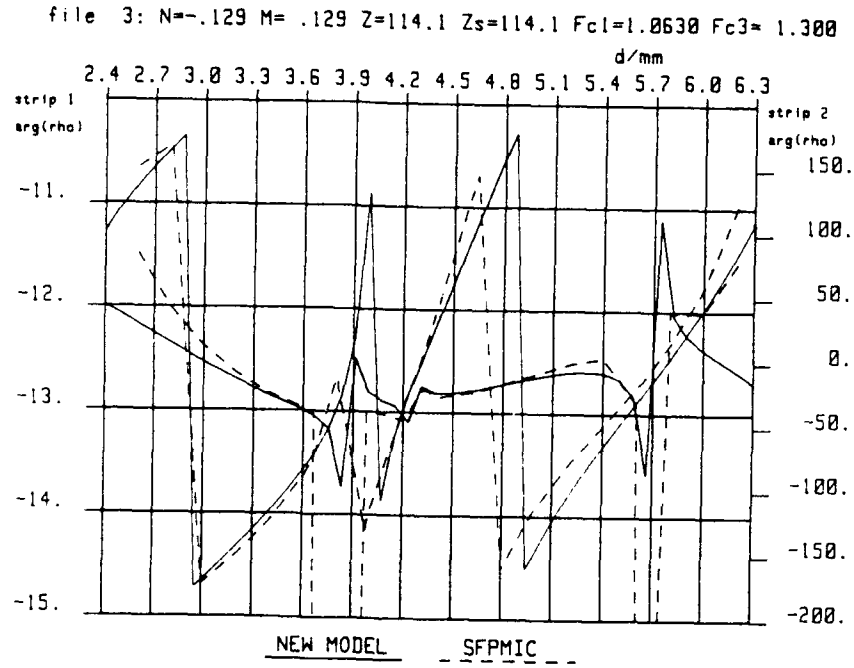


Fig. 5.12: S11 and S22 for 0.1 mm gap and varying package length

The reflection coefficients shown in Fig. 5.11 describe the same configuration as discussed in section 5.2.1 (Fig. 5.9) but for a wide gap width. The gap width is 1.0 mm, much larger than the strip width of 100μm. The correction factors F_{ZL} and F_{C3} have been set equal to 1. Again Z and Z_s in the caption are the LSM_0 and LSM_0' mode characteristic impedances.

The dynamic capacitance C_1 of the new circuit model is found to be about 5% smaller than the value of the quasi-static gap equivalent circuit model used (F_{C1} = 0.9487). This may partially be due to the prevailing numerical accuracy (number of expansion functions, spectral density) in the field theory based analysis. The transformer ratios $N = N_1 = N_2$ and $M = M_1 = M_2$ are nearly identical (N = -0.21, M = 0.21), where the negative sign of the transformer ratio N results from the way in which the transformer windings are connected to the circuit.

In Fig. 5.12 the results of the analysis with a smaller gap width of s = 100μm are shown. In this example the reflection coefficients on strip 1 and strip 2 are well described.

5.3. MICROSTRIP STEP

The microstrip structure to be modelled contains a microstrip step discontinuity with additional feed lines and two current sources I_{01} and I_{02}. The structure is shown in Fig. 5.13 situated in a package of width w_s, height h+H, where h is the GaAs substrate thickness and box length d.

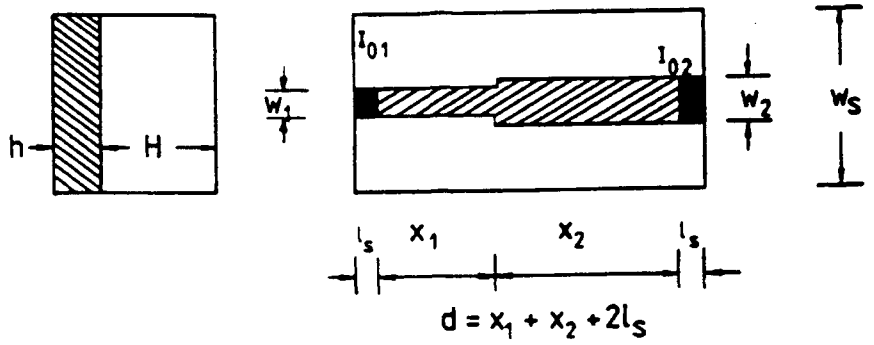


Fig. 5.13: Microstrip step discontinuity with microstrip feel lines and current sources

5.3.1. Comparison of a Quasistatic Analytical Model with Full-Wave Results

A common quasi-static equivalent circuit for the microstrip step discontinuity contains two serial inductances and a parallel capacitance to ground. For a comparison between a quasi-static analysis and full wave analysis, the program LINMIC+ was used to perform the former.

The field-theory based computations were carried out on the structure of Fig. 5.13. The structure was investigated first in a state of excitation with I_{02} = 0, using the following geometric configurations:

h = 100μm, H = 200μm, w_1 = 60μm, w_2 = 100μm, W_s = 2.1 mm, f = 70 GHz
I_{01} = 1, I_{02} = 0, l_s = 100μm, x_1 = x_2 = 1.2 mm - 2.1 mm.

With the package dimensions chosen such that the LSM_0 mode is above cut-off at the frequency of 70 GHz. The reference planes are at the ends of the microstrip lines (at the step plane) where the strip width decreases from 100μm to 60μm.

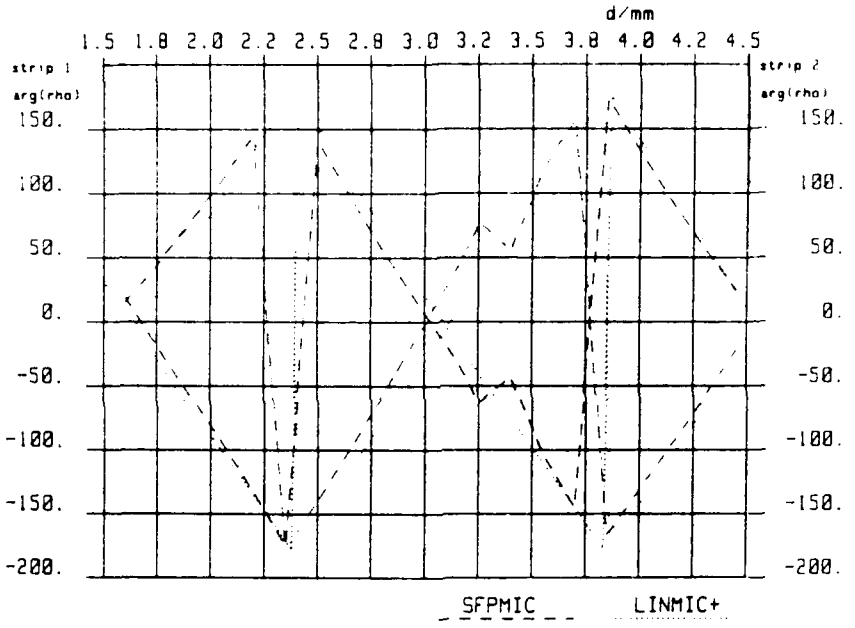


Fig. 5.14: Step model S11 and S22

The comparison (Fig. 5.14) shows the phase of the reflection coefficients ρ_1 and ρ_2 of the fundamental modes on the microstrip lines 1 and 2. The quasi-static analysis shown takes into account only the fundamental modes on the microstrip lines, whereas the full wave analysis includes the coupling between these fundamental modes and the dominant parasitic package modes.

The electrical behaviour of the structure in Fig. 5.13 reflects the presence of the open ended microstrip line 2 (current source $I_{02} = 0$), the reflection coefficients $\rho 1$ and $\rho 2$ showing the typical behaviour of linear phase increase. The negative phase of the reflection coefficient $\rho 1$ is plotted in Fig. 5.14. The full-wave results show a resonance behaviour for both of the reflection coefficients for a total box length of about 3.3 mm. These resonances cannot be described by the standard quasi-static approach.

5.3.2. An Equivalent Circuit Model

An equivalent circuit model for the microstrip step discontinuity can be derived from the gap equivalent circuit model in a straight forward manner. The three capacitor quasi-static gap model is replaced by a commonly used step model containing two serial inductances and a parallel capacitance to ground. The microstrip gap length, s has to be reduced to zero for the step model. The respective LSM_0 mode transmission line in the gap equivalent circuit model has to be neglected for the step. Taking all these features into account the equivalent circuit in Fig. 5.15 results.

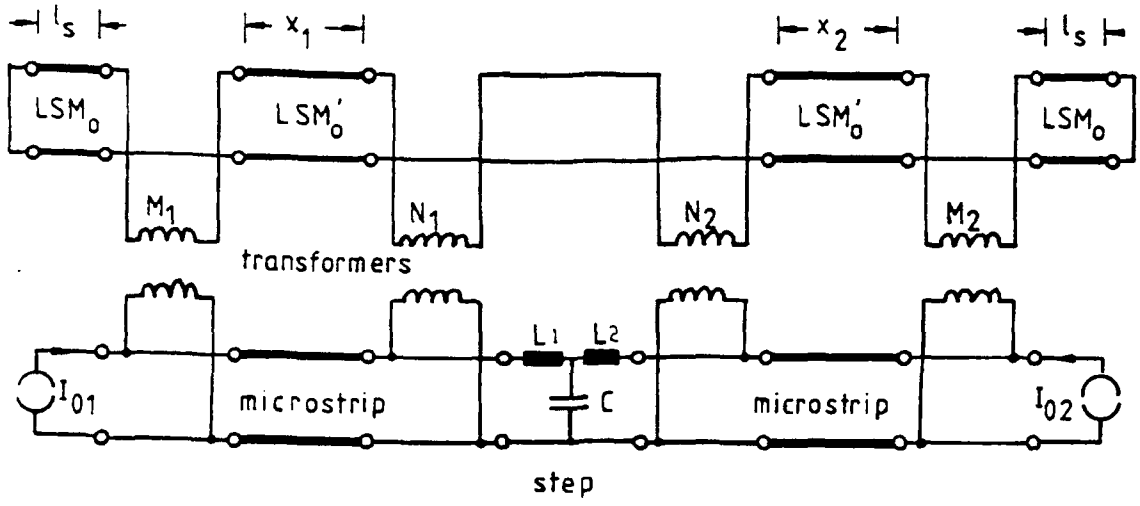


Fig. 5.15: Equivalent circuit for the microstrip step discontinuity including dynamic parasitic effects.

This dynamic microstrip step model contains two feed lines with different characteristic transmission line data (different strip widths) for the fundamental modes and for the LSM_0' package modes. The coupling between the fundamental modes and the LSM_0' modes is described by four transformers N_1, N_2, M_1, M_2. As for the dynamic gap modelling, the effective dielectric constants of the modes are taken from the field-theory based data generation. The LSM_0 mode characteristic impedance is determined by the analytical formula in Section 4.2. In the studies the LSM_0' mode characteristic impedances are calculated from this LSM_0 impedance by multiplication with correction factors not much different from 1. The admittance matrix of the quasi-static step model is also modified by suitable correction factors F_{y1} (for Y_{11} and Y_{22}) and F_{y2} (for Y_{12} and Y_{21}).

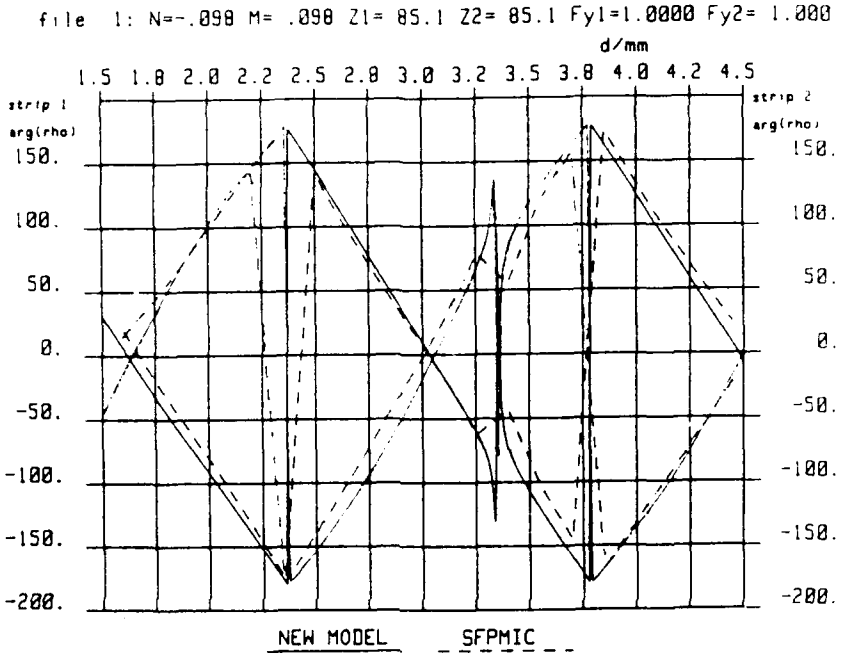


Fig. 5.16: Improved step model S11 and S22

5.3.3. Preliminary Studies

The microstrip structure was simulated using the improved dynamic step model of Fig. 5.15. These results together with full-wave results are shown in Fig. 5.16. The equivalent circuit elements have been predicted by simple expressions as outlined from box dimensions, pre-calculated transmission line data and correction factors equal to 1. The transformer ratios were predicted from the previously given analytic formula Section 3.3. The LSM_0' mode characteristic impedances (Z_1 and Z_2) for the different width feedstrips were approximated to that of the LSM_0 package mode. No curve fitting was applied to modify the predicted equivalent circuit elements. The enhanced equivalent circuit was able to predict the circuit behaviour including the effects of parasitic package modes. The resonance length of the box is well predicted.

5.4. 90° BEND

The microstrip bend structure to be modelled (Fig. 5.17) is situated on GaAs within a package. The package dimensions are width w_s, height h+H and a total box length $d + l_s + x_1 + w_2$.

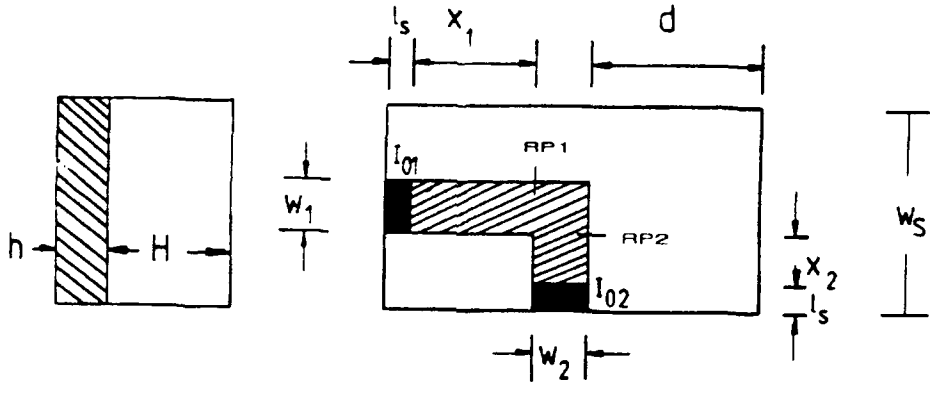


Fig. 5.17: Microstrip 90° bend discontinuity with microstrip feed lines and current sources

5.4.1. A Dynamic 90° Bend Model

A complication for the bend model, which does not occur in the open end, gap and step models is that there are two directions of propagation involved for both the fundamental microstrip modes and the parasitic LSM_0 modes. In the model these are considered as two separate parasitic transmission line structures being correlated only by their dependence on the same package dimensions.

Applying physics related modelling to the microstrip bend discontinuity results in a preliminary equivalent circuit model. The equivalent circuit model consists of two microstrip feed lines of lengths x_1 and x_2, two current sources I_{01} and I_{02} and a quasi-static equivalent circuit model for the 90°-bend. The quasi-static equivalent circuit model for the 90°-bend consists of two lumped inductances and a capacitance to ground as shown in Fig. 5.18.

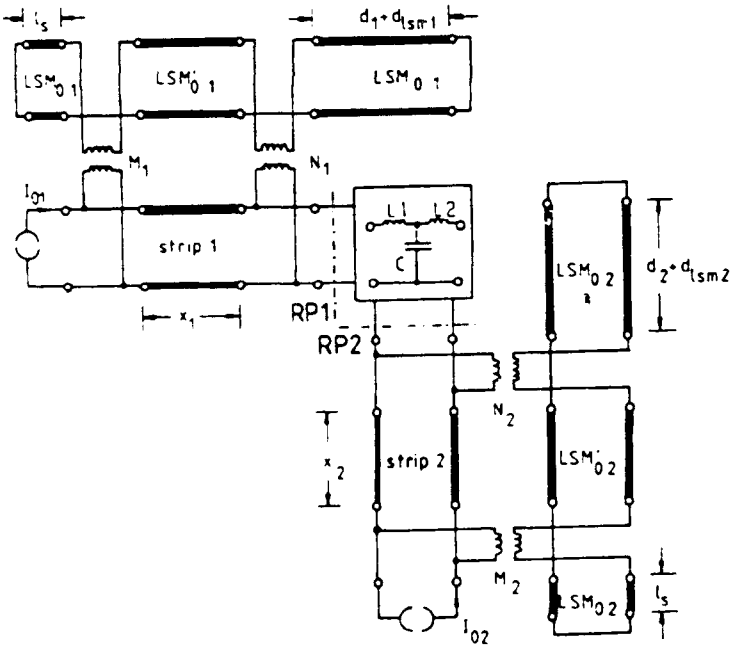


Fig. 5.18: A preliminary dynamic equivalent circuit model for the microstrip 90°-bend discontinuity

In the model d_1 and d_2 are LSM_0 transmission line lengths given by $d_1 = d$ and $d_2 = w_s - w_1 - x_2 - l_s$, d_{lsm1} and d_{lsm2} are additional line lengths for tuning the dynamic equivalent circuit model, being added to the physical line lengths d_1 and d_2 of the LSM_0-mode transmission lines.

To take dynamic effects into account, the coupling between the microstrip modes and the package modes is included in the model. The parasitic effects of the bend are described by two LSM_0/LSM_0'-modes coupled to the microstrip modes by lumped transformers N_1, N_2, M_1 and M_2.

5.4.2. Study of the Dynamic Model

The microstrip structure was studied using the field-theory based computer program, a quasi-static analysis (running the CAD package LINMIC+ in the quasi-static mode of operation) and using the dynamic equivalent circuit model presented in Fig. 5.18.

The geometric parameter values with $I_{02} = 0$ for investigation convenience are described below.

$h = 100\mu m$, $H = 200\mu m$, $w_1 = 100\mu m$, $w_2 = 100\mu m$, $w_s = 1.9$ mm
$f = 80$ GHz, $I_{01} = 1$, $I_{02} = 0$, $l_s = 100\mu m$, $x_1 = 0.75$ mm, $x_2 = 0.95$ mm, $d =$ 0.9 mm - 2.1 mm.

The characteristic impedance for the LSM_0 modes are precalculated by an analytic formula (Section 4.). Fz1 and Fz2 are correction factors that have been used to modify the LSM_0-mode characteristic impedances to get the LSM_0'-mode characteristic impedances.

The results giving the reflection coefficients $\rho 1$ and $\rho 2$ on the microstrip lines the reference planes RP1 and RP2 are plotted in Fig. 5.19 as a function of d. The figure shows good agreement between the field-theory based

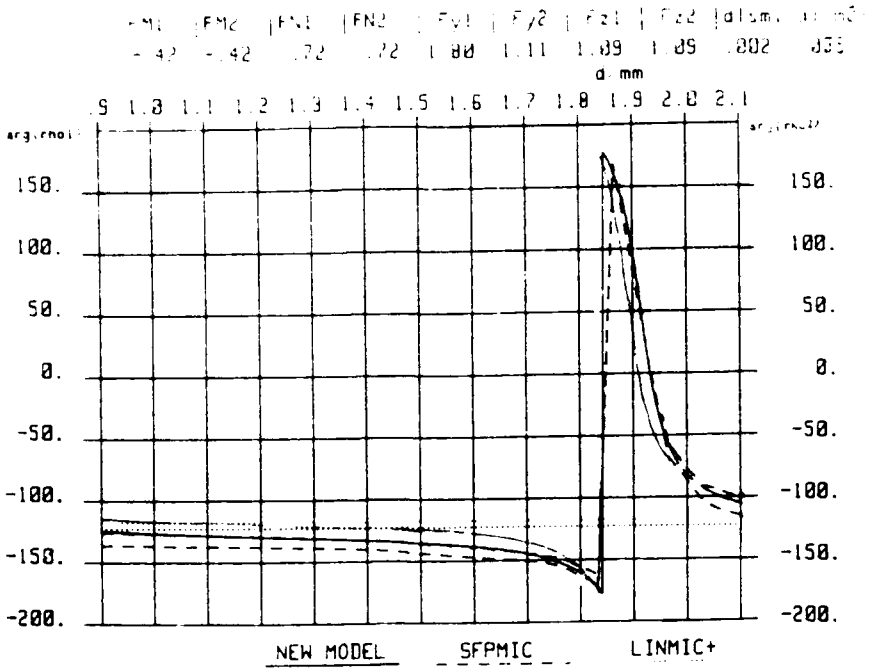


Fig. 5.19: 90° bend model S11 and S22

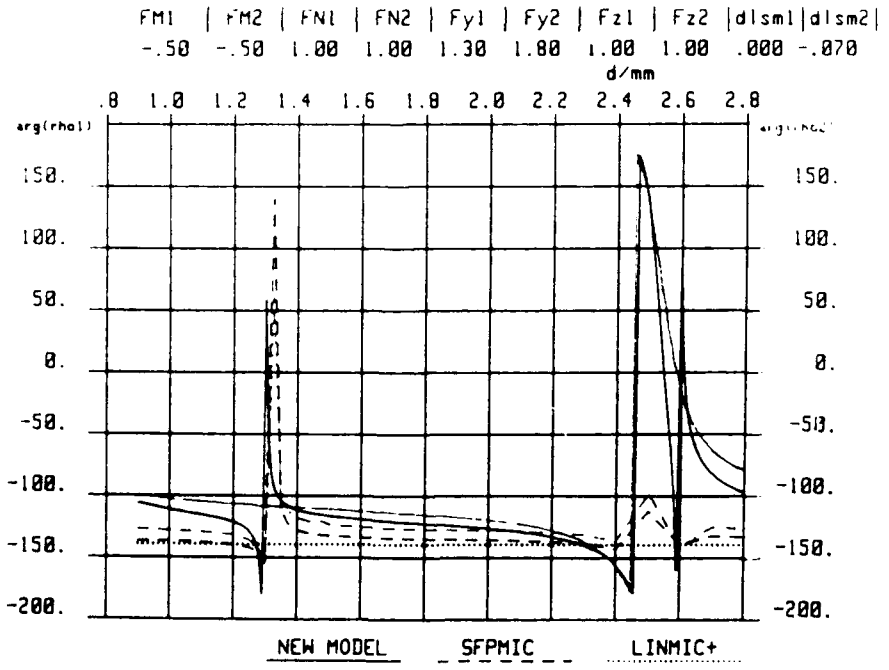


Fig. 5.20: S11 and S22 of 90° bend model with increasing package length

data and the reflection coefficients generated for the dynamic circuit model.

The element values of the equivalent circuit model are given in the heading of the figure. In this study The values FM1, FM2, FN1 and FN2 are the correction factors with which the precalculated transformer ratios have been multiplied to obtain the transformer ratios applied in the equivalent circuit model ($M1 = FM1*M1_{precalculated}$). Fy1 and Fy2 are the correction factors for the admittance matrix elements of the quasi-static bend model.

The field-theory based reflection coefficients show a constant phase difference between the quasi-static and the dynamic equivalent circuit model results of about 10° for nearly all package widths d. This indicates that an additional equivalent circuit element must be introduced. The microstrip circuit of Fig. 5.17 contains two current sources I_{01} and I_{02}. If one of these current sources is set to zero the microstrip line appears terminated with an open end. Therefore, the quasi-static equivalent circuit model for an open microstrip end has to be introduced into the dynamic microstrip bend model of Fig. 5.18.

A second microstrip configuration was also investigated as a function of d. This configuration is nearly identical to the circuit example described above. The difference is that the lengths $d_1 = d$ and $d_2 = w_s-w_1-x_2-l_s$ have been increased simultaneously. The results (Fig. 5.20) show that the resonance dimensions derived by the field-theory based calculations can be predicted by the dynamic equivalent circuit model. However, there is still a significant quantitative difference between the full-wave numerical results and the data generated by the equivalent circuit model.

The box dimensions d = 1.3 mm and d = 2.6 mm are resonance dimensions for the reflection coefficients $\rho 1$ and $\rho 2$ at the reference planes RP1 and RP2. The full wave data show resonance behaviour for both reflection coefficients. The equivalent circuit model predicts only the resonant behaviour for the reflection coefficient $\rho 1$ of strip 1. It seems that the reason for these discrepancies is due to 2D parasitic coupling mechanisms prevailing in the bend structure in contrast to the 1D LSM_0/LSM_0' mode propagation valid for the previously discussed models. A modification of the dynamic equivalent circuit model appears necessary.

5.4.3. Discussion on Mode Coupling in the Bend Model

For the microstrip open end, the microstrip gap and the microstrip step, the dynamic coupling effects of these discontinuities have been described successfully by dynamic equivalent circuit models which contain in addition to the quasi-static description, parasitic LSM_0/LSM_0'-mode transmission lines. The field distribution of the dominant package mode is described by a chain connection of these LSM_0/LSM_0'-mode lines. In contrast to this the dynamic equivalent circuit model for the microstrip 90°-bend contains two sets of LSM_0/LSM_0'-mode transmission lines (subscripts 1 and 2).

This equivalent circuit model is formulated with two package modes operating independently. The $LSM_{01}/LSM_0'_1$ and the $LSM_{02}/LSM_0'_2$ modes are reasonable approximations of the field distribution of the package mode. However, both mode sets have to describe the same field distribution since there is only one unique physical field distribution in a given configuration. In reality the microstrip modes are physically coupled to one common set of package modes, while the description of this common field distribution can be achieved in different ways. Thus an equivalent circuit model with two independent descriptions (except for the dependency on the same dimensions) of the package mode cannot describe the dynamic coupling effects accurately.

5.4.4. An Alternative Equivalent Circuit Model

Fig. 5.21 shows an alternative equivalent circuit model for the microstrip 90°-bend which takes the mentioned coupling into account. It contains the same circuit elements as the preliminary equivalent circuit model with the package effects being described by two LSM_0/LSM_0' package modes (LSM_{01}/LSM_{01}', LSM_{02}/LSM_{02}') and both modes being coupled to the fundamental microstrip modes by transformers. The transformers N_1 and N_2 are connected parallel to the centre of the microstrip bend. Due to this parallel connection the reflection coefficient phases of the fundamental microstrip modes at reference planes RP1 and RP2 are expected to show similar resonance behaviour.

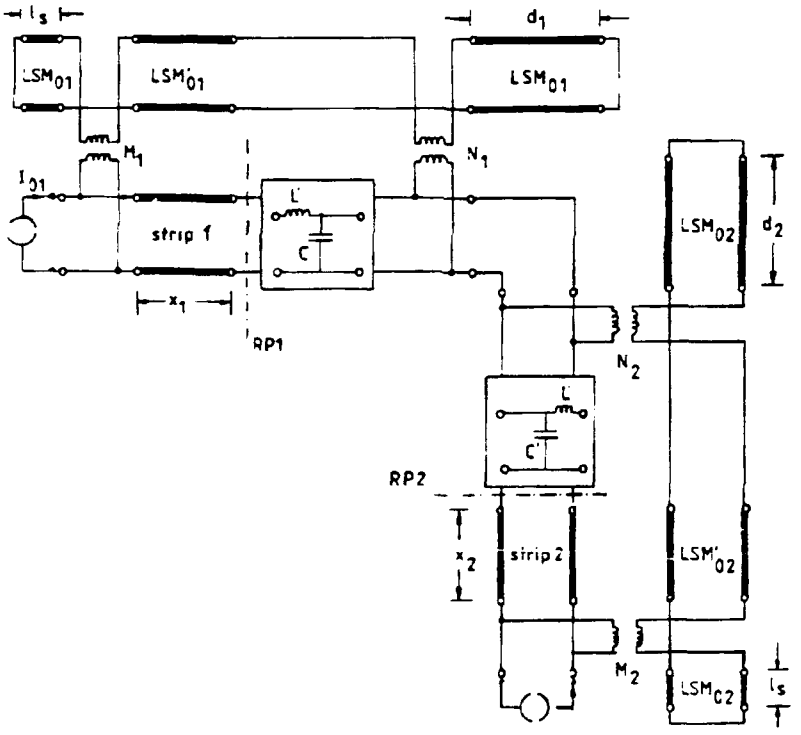


Fig. 5.21: An alternative equivalent circuit model for the microstrip 90°-bend

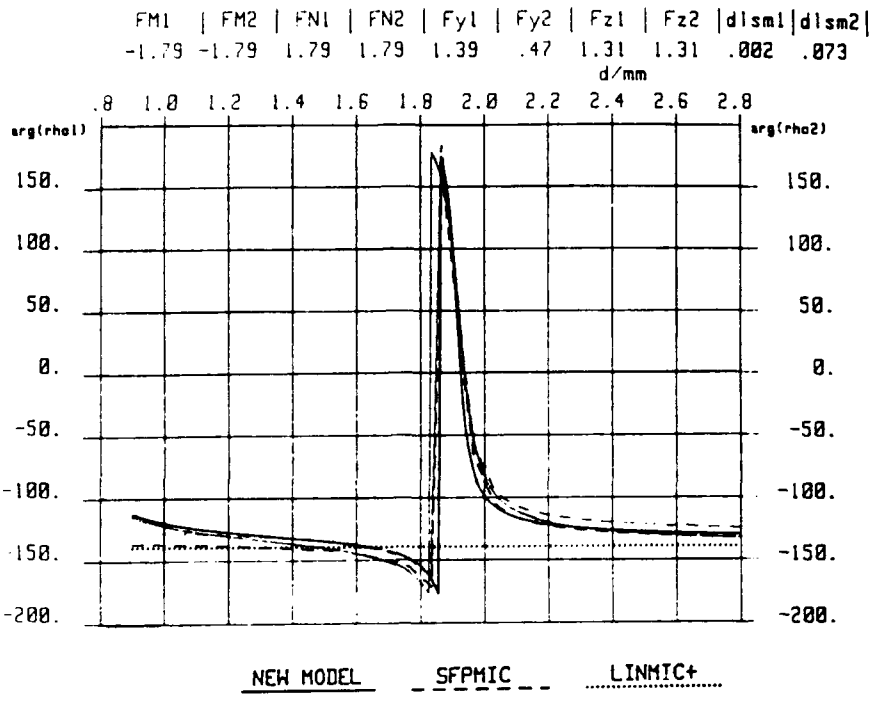


Fig. 5.22: Alternative 90° bend model S11 and S22

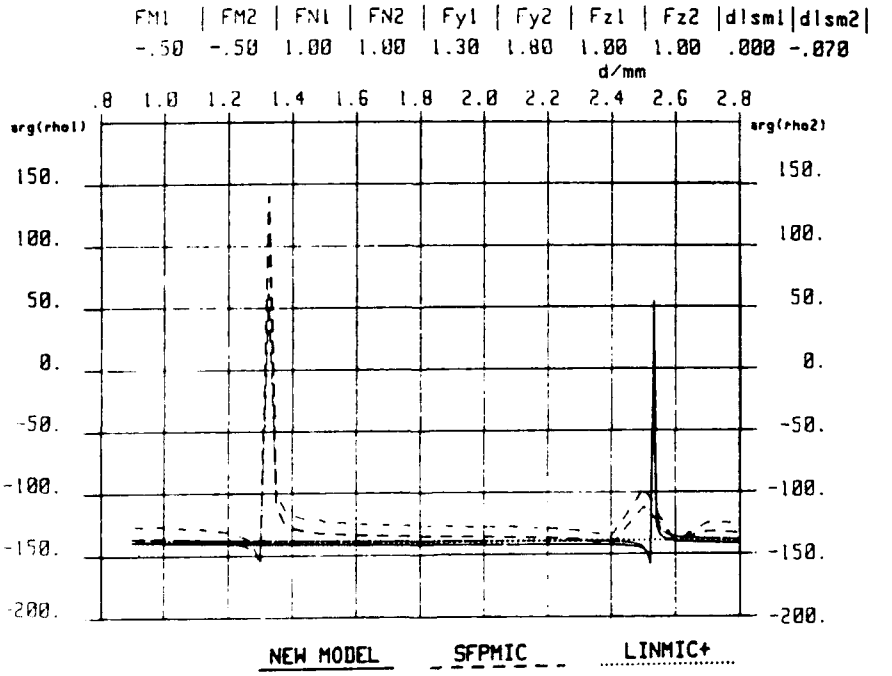


Fig. 5.23: Alternative 90° bend model S11 and S22

In the previously equivalent circuit model the circuit elements L and C describe the quasi-static behaviour of the 90°-bend. In the above equivalent circuit these elements have been replaced by two T equivalent circuits (elements L' and C') which when connected in series describe the quasi-static behaviour of the 90°-bend. As an approximation, the elements L' and C' are related to L and C by

$$L' = L \qquad C' = 0.5C$$

The two studies of Section 5.4.2. were redone for the alternative circuit model.

Figs. 5.22 and 5.23 show for the respective studies the reflection coefficient phases ρ1 and ρ2 on the microstrip lines at the reference planes RP1 and RP2. Fig. 5.22 now shows good agreement between the field-theory based data and the reflection coefficients generated for the dynamic equivalent circuit model. Fig. 5.23 however again shows that the resonance behaviour for the box dimension d = 1.3 mm is not represented by the equivalent circuit model. This indicates that the preliminary circuit models with two independent modes for the description of the package effects has a fundamental deficiency. The bidirectional, common excitation of the parasitic package fields still requires further study.

5.5. MICROSTRIP T-JUNCTION

5.5.1. Preliminary Equivalent Circuit Model

The microstrip T-junction in a package (Fig. 5.24) consists of 3 microstrip lines of length x1, x2, x3, three current sources and the T-junction. The discontinuity considered is deposited on GaAs in a package of width w_s, height h + H and a total box width $d + l_s + x_3 + w_2$.

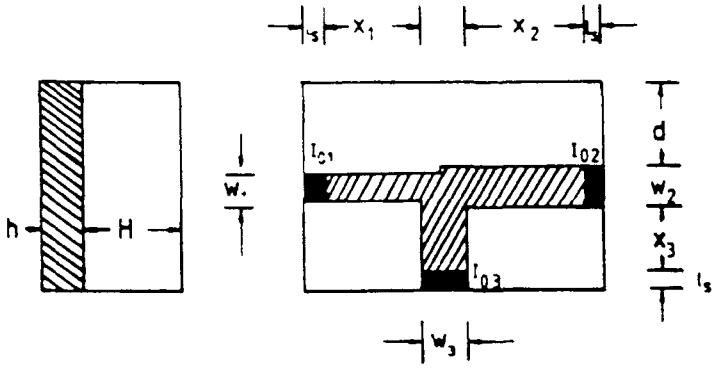


Fig. 5.24: Microstrip T-junction discontinuity with microstrip feed lines and current sources

The physics modelling approach, applied to the microstrip 90°-bend discontinuity, was extended to the T-junction discontinuity, the equivalent circuit model of Fig. 5.25 taking dynamic coupling effects into account.

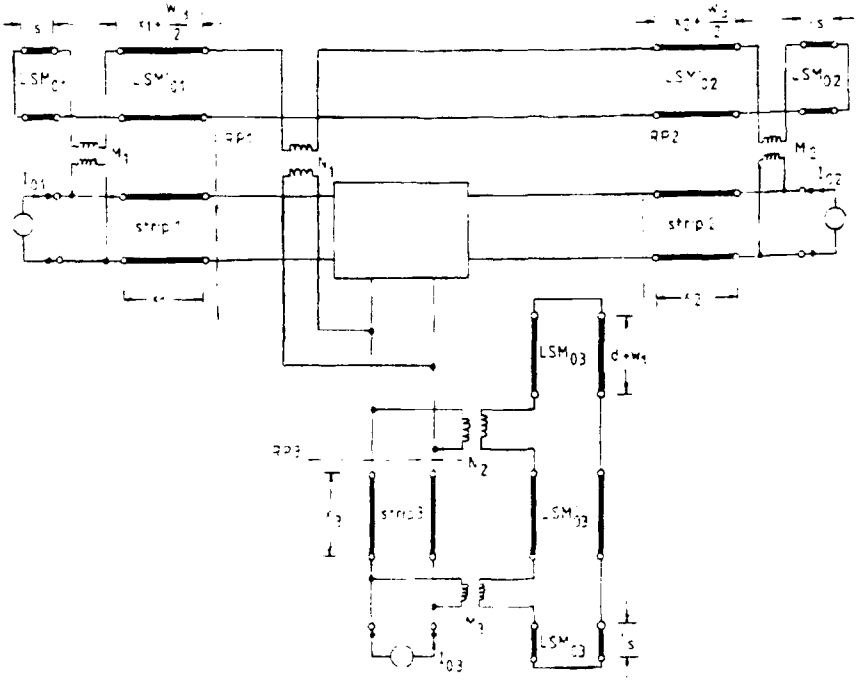


Fig. 5.25: A preliminary dynamic equivalent circuit model for the microstrip T-junction discontinuity

The equivalent circuit consists of three microstrip feed lines of lengths x_1, x_2 and x_3, three current sources I_{01}, I_{02} and I_{03} and a quasi-static description for the T-junction discontinuity. The quasi-static equivalent circuit model for the T-junction discontinuity has been extracted from the CAD program LINMIC+ and is represented by the T type black box in Fig. 5.25. The dynamic effects are included, by describing the coupling of microstrip modes and package modes with lumped transformers. As in the dynamic gap, step and bend modelling, the mode effective dielectric constants and the characteristic impedances were taken from the numerically generated field-theory based data set.

As has been stated for the 90° bend model investigation, a complication is that there are two directions of propagation for the fundamental microstrip modes and the LSM_0/LSM_0' package modes. This is also true for the T-junction. Until now these modes have been considered by two separate parasitic transmission line structures. In reality however, they are correlated by their dependence on the package dimensions. Their correlated influence on the reflection coefficient of the fundamental microstrip modes can be enforced to some degree in the model by a parallel connection of transformers.

5.5.2. Study of the Dynamic Model

The T-junction structure was analysed using the field-theory based computer program, a quasi-static analysis (using the CAD package LINMIC+) and the dynamic equivalent circuit model.

The structure under investigation was described by the parameters given below with $I_{02} = 0$ for convenience:

GaAs: $h = 100\mu m$, $H = 200\mu m$, $w_1 = 100\mu m$, $w_2 = 100\mu m$, $w_3 = 100\mu m$
$f = 80$ GHz, $t_s = 100\mu m$, $x_1 = x_2 = x_3 = 0.9$ mm, $d = 0.7$ mm - 2.9 mm (variable).

As in the bend model, an additional line length d_{lsm3} for tuning the dynamic equivalent circuit model was added to the physical line length d of the LSM_{03}-mode transmission line.

In the following plot headings are the element values of the equivalent circuit model and the values, FM1, FM3, FN1 and FN2 which are the correction factors by which the precalculated transformer ratios have been multiplied to get the transformer ratios shown in the equivalent circuit model (M1 = $FM1*M1_{precalculated}$). Fy1 and Fy2 are the correction factors for the admittance matrix elements of the quasi-static T-junction model. The characteristic impedance for the LSM_0 modes is precalculated by an analytic formula as given in Section 4. Fz1 and Fz2 are correction factors that have been used to modify the LSM_0'-mode characteristic impedances.

The results (Fig. 5.26) show the phases of the reflection coefficients $\rho 1$ and $\rho 2$ on the microstrip lines at the reference planes RP1 and RP2. The resonance behaviour of the reflection coefficient $\rho 2$ at d = 1.8 mm is well predicted by the equivalent circuit model. Furthermore there are additional resonances at d = 0.8 mm, d = 1.5 m and d = 2.7 mm. These resonances are not predicted by the curve generated from the equivalent circuit model. The reflection coefficient of the microstrip mode at reference plane RP1 shows a double resonance at d = 0.9 mm and a weak resonance behaviour at d = 1.9 mm. This small resonance effect and even the one of the two double resonances at d = 0.9 mm can be predicted by the dynamic circuit model. Nevertheless there is still a significant quantitative deviation between the full-wave results and the data obtained from the equivalent circuit model.

One reason for the considerable deviation between the full-wave results and the equivalent circuit data may be that the package height is very small (h + H = 0.3 mm). A small package height was chosen mainly to reduce computer time for generating the full-wave results. However the quasi-static equivalent circuit models used as part of the dynamic circuit models, work well for packages with infinite or large package heights. The ratio h/H =

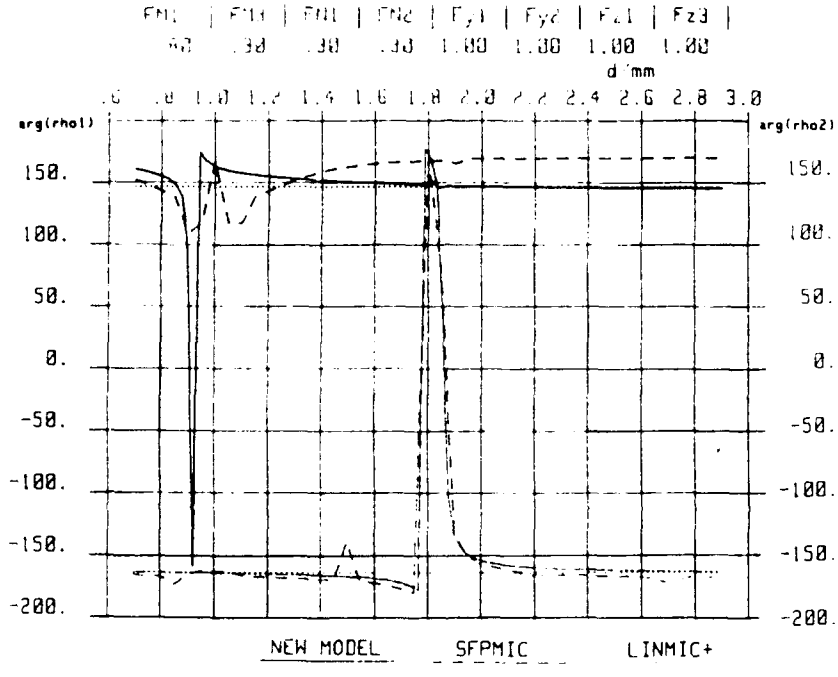


Fig. 5.26: T-junction model S11 and S22

0.5 as applied in the investigation is very small. It can be assumed that in these cases the static behaviour of the structures under investigation can not be described accurately by the quasi-static circuit models.

Nevertheless there is still the problem of the unexplained additional resonances. As discussed the description of the package mode by two separate LSM_0/LSM_0' modes may be one of the major disadvantages of the presented dynamic equivalent circuit model.

5.6. REFERENCES

1. Benedik, P., Silvester, P., Equivalent capacitances for microstrip gaps and steps, IEEE MTT-20, 1972, pp.792-733.

2. Jansen, R.H., LINMIC a CAD package for the layout-oriented design of single and multi-layer MICs/MMICs up to mm-wave frequencies, Microwave Journal, Feb. 1986, pp.151.

6. STUDY OF BIDIRECTIONAL MODAL EFFECTS AND THE DEVELOPMENT OF A CIRCUIT DESCRIPTION

6.1. DISCUSSION ON THE CURRENT EQUIVALENT CIRCUIT MODELS

At present in the microstrip open end, gap and step the interaction with the package field has been described by LSM_0/LSM_0' mode excitation. This excitation is described by a unidirectional coupling mechanism. In contrast to these cases, the microstrip 90°-bend and T-junction discontinuities are associated with orthogonal feed lines. The wave propagation on these feed lines implies excitation in two directions. In the preliminary models for the 90°-bend and T-junctions bidirectional parasitic mode excitation was neglected. The current models only include a quasi-static equivalent circuit for the low frequency junction effects and lumped transformers for the LSM_0/LSM_0' mode coupling. These equivalent circuit models consist of two separate uncoupled parasitic transmission line stuctures LSM_{01}/LSM_{02}' for the two othogonal directions, each parasitic structure being described by wave propagation in one direction only.

As has been shown these simplified circuit models are able to fit the numerically generated full-wave data to some extent. The reflection coefficients phases at the reference planes for both fundamental modes show nearly the same resonance behaviour expected by the numerically generated full-wave data. The significant deviation between the results of the simplified circuit models and the numerically generated full-wave data can be seen in Section 5.4.2, Fig. 5.20 for the bend discontinuity example. The resonance at d = 1.3 mm occurs at a total box length of half the wavelength of the LSM_{01} mode. The resonance behaviour of the reflection coefficients phases on microstrip 1 is well predicted by the dynamic equivalent circuit model of Section 5.4.1. However, the numerically generated full wave data also show resonance behaviour for the reflection coefficient phase on microstrip 2.

The reason for the expected but missing resonance peak in the description based on the simplified (piecewise unidirectional) circuit model is due to the fact that the employed LSM_{01}/LSM_{01}' and LSM_{02}/LSM_{02}' transmission lines represent only a partial description of the total package field. A resonance description for the total package field has to be reflected in both partial field descriptions LSM_{01}/LSM_{01}' and LSM_{02}/LSM_{02}' simultaneously.

6.2. A MICROSTRIP 90°-BEND MODEL INCLUDING BIDIRECTIONAL LSM_0-MODE COUPLING

From the discussion of the dynamic equivalent circuit models for the microstrip 90°-bend and the T-junction, it is obvious that these models have to be extended by introducing a coupling mechanism between the LSM_{01}/LSM_{01}' and LSM_{02}/LSM_{02}' mode transmission lines. To demonstrate the effect of introducing such a coupling mechanism into the equivalent circuit for the 90°-bend, Fig. 6.1 shows an improved circuit representation containing an additional transformer.

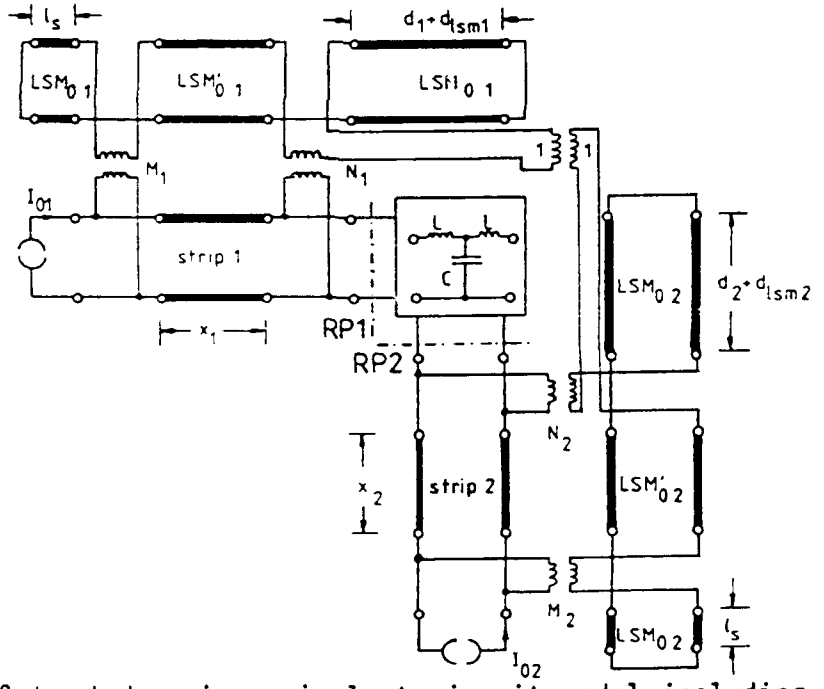


Fig. 6.1: A 90° bend dynamic equivalent circuit model including LSM_0/LSM_0' coupling

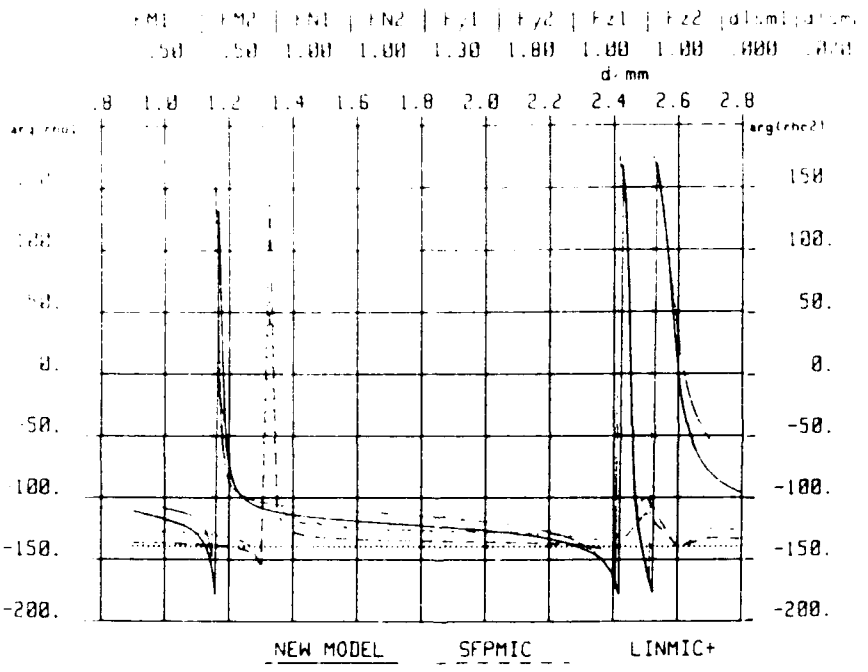


Fig. 6.2: S11 and S22 of 90° bend model

This equivalent circuit model is a simple extension of the previous bend model of Section 5.4.1, Fig. 5.18. The transformer ratio has not been determined or optimised. A ratio 1:1 was assumed and used to generate the results in Fig. 6.2 which is based on the second study of Section 5.4.2. The reflection coefficient phases $\rho 1$ and $\rho 2$ on both microstrip lines now show the same expected resonance behaviour. Resonances for packages of any dimension can now be predicted by this extended equivalent circuit model.

Nevertheless, further consistent quantitative investigations are required to achieve a good fit between the numerically generated full-wave data and the results produced by the circuit model.

6.3. DESCRIPTION OF THE EM FIELDS IN THE PACKAGE IN TERMS OF LSM_0-MODE EXCITATION

A general description of the electric and magnetic LSM_0 field in a rectangular box can be achieved by considering the electric wave potential $\psi(x,y)$. If the electromagnetic field has negligible component H_z, as is assumed for the propagation of the partial parasitic fields in the package, the electric and magnetic fields can be determined from $\psi(x,y)$ by applying the equations

$$E_x = \frac{1}{j\omega\varepsilon} \frac{\partial^2\psi}{\partial x \partial x} \qquad H_x = \frac{\partial\psi}{\partial y}$$

$$E_y = \frac{1}{j\omega\varepsilon} \frac{\partial^2\psi}{\partial x \partial x} \qquad H_y = \frac{\partial\psi}{\partial y}$$

$$E_z = \frac{1}{j\omega\varepsilon} \left(\frac{\partial^2}{\partial z^2} + k^2\right)\psi \qquad H_z = 0$$

The LSM_0 package mode field is not disturbed significantly by the metallisation pattern of a microstrip circuit as can be concluded from full wave computations. The field distribution of package modes is similar to the field in a rectangular box homogeneously filled with a material of dielectric

constant ε_{eff}. In the case of a general excitation mechanism the total potential $\phi^t(x,y)$ of a rectangular box (see geometry of Fig. 6.3) can be expressed by a summation over a set of orthogonal eigenfunctions $t_{ik}(x,y)$.

$$\varphi^t(x,y) = \sum_i \sum_k A_{ik} \sin\left\{\frac{i\pi}{y_b - y_a}(y - y_a)\right\} \sin\left\{\frac{k\pi}{x_b - x_a}(x - x_a)\right\}$$

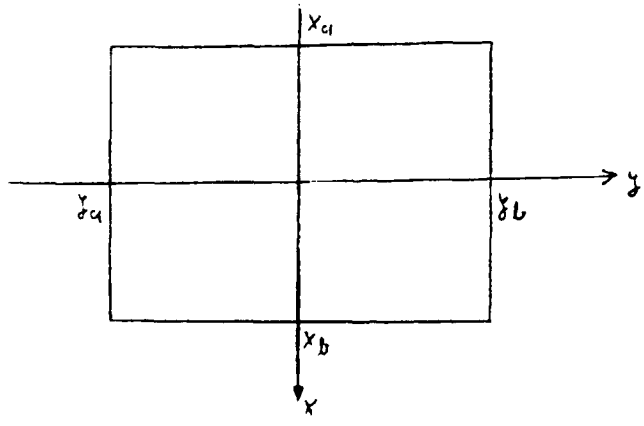


Fig. 6.3: Package co-ordinates for the configuration under investigation

In this way, the electric and magnetic field in the package are described through the potential $\phi^t(x,y)$ dependent on the co-ordinates x and y and on the amplitudes A_{ik} of the rectangular box eigenfunctions t_{ik}. Only the electrical field E_z and the magnetic fields H_x and H_y are of interest for further study. These components can be written thus,

$$E_z^t(x,y,A_{ik}) = -j\omega \sum_i \sum_k A_{ik} \sin\left\{\frac{i\pi}{y_b - y_a}(y - y_a)\right\} \sin\left\{\frac{k\pi}{x_b - x_a}(x - x_a)\right\}$$

$$H_x^i\,(x,y,A_{ik}) = \sum_i \sum_k A_{ik}\, cos\left\{\frac{i\pi}{y_b - y_a}\,(y-y_a)\right\} sin\left\{\frac{k\pi}{x_b - x_a}\,(x-x_a)\right\}$$

$$H_y^i\,(x,y,A_{ik}) = \sum_i \sum_k A_{ik}\, sin\left\{\frac{i\pi}{x_b - x_a}\,(y-y_a)\right\} cos\left\{\frac{k\pi}{x_b - x_a}\,(x-x_a)\right\}$$

The partial LSM_{01}/LSM_{01}' and LSM_{02}/LSM_{02}' parasitic fields in the package can be described by potentials $\phi^{LSM_{01}}(x,y)$ and $\phi^{LSM_{02}}(x,y)$. These potentials can be obtained if the electric field components $E_z^{LSM_{01}}(x,y)$ and $E_z^{LSM_{02}}(x,y)$ are known. The components E_z of the electric fields can be determined from the voltage and/or current distribution on the parasitic transmission lines in the equivalent circuit model.

They have the form:

$$E_z^{LSM_{o1}}\,(x,y,P_1 \ldots P_N) = E_z^{LSM_{o1}}\,(y_1 P_1 \ldots P_N)\, sin\left\{\frac{\pi}{x_b - x_a}\,(x-x_a)\right\},$$

$$E_z^{LSM_{o2}}\,(x,y,P_1 \ldots P_N) = E_z^{LSM_{o2}}\,(x_1 P_1 \ldots P_N)\, sin\left\{\frac{\pi}{y_b - y_a}\,(y-y_a)\right\}.$$

where the parameters $P_1 \ldots P_n$ denote voltages or currents on the LSM_{02}/LSM_{02}' transmission line. From these voltages or currents the distribution of the

electric field component $E_z^{LSM_{02}}(x,y)$ can be determined. With the knowledge of the distribution of the potentials $\psi^{LSM_{01}}(x,y)$ and $\psi^{LSM_{02}}(x,y)$ the magnetic field components $H_x^{LSM_{01}}(x,y)$ and $H_y^{LSM_{02}}(x,y)$ can be derived.

$$\varphi^{LSM_{o1}} = \frac{1}{-j\omega} E_z^{LSM_{o1}}(x,y,P_1 \ldots P_N) \quad \varphi^{LSM_{o2}} = \frac{1}{-j\omega} E_z^{LSM_{o2}}\left(x,y,P_1^1 \ldots P_N^1\right)$$

$$H_x^{LSM_{o1}} = \frac{1}{-j\omega} \frac{\partial}{\partial y} E_z^{LSM_{o1}}(y,P_1 \ldots P_N) \sin\left\{\frac{\pi}{x_b - x_a}(x - x_a)\right\}$$

$$H_y^{LSM_{o2}} = \frac{1}{-j\omega} \frac{\partial}{\partial x} E_z^{LSM_{o2}}(x,P_1 \ldots P_N) \sin\left\{\frac{\pi}{y_b - y_a}(y - y_a)\right\}$$

The method of obtaining the partial parasitic fields from the total package field is as follows:

The electric field component $E_z^{LSM_{01}}(x,y)$ and $E_z^{LSM_{02}}(x,y)$ of the LSM_{01} and LSM_{02} field distributions have to be set equal to the total electric field function $E_z^t(x,y)$ describing the total field by summation over the eigenfunctions of the rectangular box. Also the magnetic field components $H_x^{LSM_{01}}(xm,y)$ and $H_y^{LSM_{02}}(x,y)$ have to be set equal to the total magnetic field components $H_x^t(x,y)$ and $H_y^t(x,y)$ in a similar manner. This leads to the following four equations for bidirectional excitation.

Their general form is:

$$E_z^{LSM_{o1}}(x,y,P_1 \ldots P_N) = E_z^t(x,y,A_{ik})$$

$$E_z^{LSM_{o2}}\left(x,y,P_1^1 \ldots P_N^1\right) = E_z^t(x,y,A_{ik})$$

$$H_x^{LSM_{01}}(x,y,P_1 \ldots P_N) = H_x^t\ (x,y,A_{ik})$$

$$H_y^{LSM_{01}}\left(x,y,P_1^1 \ldots P_N^1\right) = H_y^t\ (x,y,A_{ik})$$

By testing equation (a) with the M eigenfunctions $t_{i1\ i=1\ldots M}$ the amplitudes $A_{i1}(P_1 \ldots P_N)$ are determined and equation (b) with M eigenfunctions $t_{1k\ K=1..M}$ the amplitudes $A_{1k}(P'_1 \ldots P'_N)$. By testing the respective magnetic fields, a second set of equations is obtained. Thus:

$$A_{i1}\ (P_1 \ldots P_N) = \frac{1}{y_b - y_a}\ \frac{1}{-j\omega}\ \int_{y_a}^{y_b} E_z^{LSM_{01}}\ (y, P_1 \ldots P_N)\ sin\left\{\frac{i\pi}{y_b - y_a}\ (y - y_a)\right\} dy$$

$$A_{1k}\ \left(P_1^1 \ldots P_N^1\right) = \frac{1}{y_b - y_a}\ \frac{1}{-j\omega}\ \int_{x_a}^{x_b} E_z^{LSM_{02}}\ \left(x, P_1^1 \ldots P_N^1\right)\ sin\left\{\frac{k\pi}{x_b - x_a}\ (x - x_a)\right\} dx$$

$$A_{i1}\ (P_1 \ldots P_N) = \frac{y_b - y_a}{i\pi}\ \frac{-j\omega}{y_b - y_a}\ \int_{y_a}^{y_b} \frac{\partial}{\partial y}\ E_z^{LSM_{02}}\ (x, P_1 \ldots P_N)\ cos\left\{\frac{i\pi}{y_b - y_a}\ (y - y_a)\right\} dy$$

$$A_{1k}\ \left(P_1^1 \ldots P_N^1\right) = \frac{x_b - x_a}{-k\pi}\ \frac{j\omega}{x_b - x_a}\ \int_{x_a}^{x_b} \frac{\partial}{\partial x}\ E_z^{LSM_{02}}\ \left(x, P_1^1 \ldots P_N^1\right)\ sin\left\{\frac{k\pi}{y_b - y_a}\ (x - x_a)\right\} dx$$

From these linear equations, the amplitudes A_{ik} can be eliminated and a new set of equations which gives a relationship between the N values of the parameters $P_1 \ldots P_N$ and the N values of the parameters $P'_1 \ldots P'_N$ results.

Since $P_1 \ldots P_N$ and $P'_1 \ldots P'_N$ denote voltages and/or currents of the equivalent circuit model this establishes a relation from which the coupling between the LSM_{01}/LSM_{01}' and the LSM_{02}/LSM_{02}' can be determined. Depending on the number of unknowns, the total package field expansion can be truncated after a few terms and a complete system of equations for the relation between the parameters $P_1 \ldots P_N$ and the parameters $P'_1 \ldots P'_N$ results. The simple extension of the bend model of Section 5.4.1, Fig. 5.18, corresponds to the first term of the total field expansion (A_{11} only).

6.4. REVISED MICROSTRIP 90° BEND MODEL

In the previous section the description of the electric and magnetic field in the package for bidirectional LSM_0 mode excitation was discussed for 90°-bends and T-junctions. It was concluded that the distributions of the partial electric and magnetic field of the LSM_0 modes of orthogonal directions are related by a coupling description to the common electric and magnetic field in the package. These relations have been studied in more detail and applied in a variety of microstrip 90°-bend equivalent circuit models. The application of the respective coupling equations to the equivalent circuit models results in much more complex circuit topologies. A simple equivalent circuit model including the bidirectional LSM_0 mode excitation was reported, the equivalent circuit model for the 90°-bend, using a lumped transformer to demonstrate the effects of coupling between the orthogonal LSM_0 modes.

As the application of extended coupling relations between the electric and magnetic fields of orthogonal LSM_0 packages modes showed no significant improvements during the investigation of more sophisticated dynamic equivalent circuit models for the 90°-bend, this simple equivalent circuit model has been reinvestigated and adopted in a slightly improved version (Fig. 6.4).

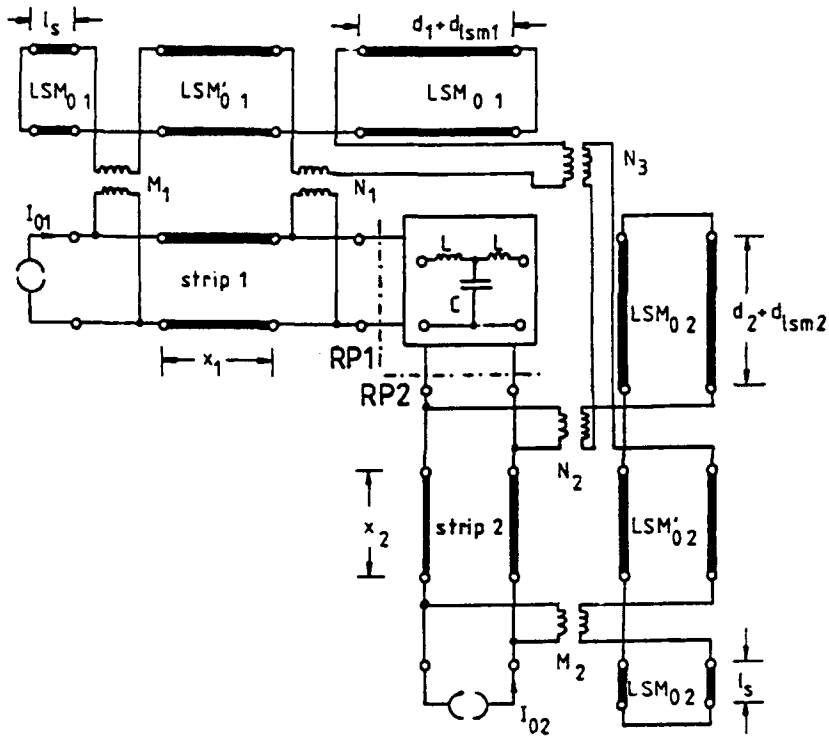


Fig. 6.4: A dynamic equivalent circuit model for the microstrip 90°-bend including the coupling between the partial parasitic LSM_{01}/LSM'_{01} and LSM_{02}/LSM'_{02} mode structures

The fixed transformer ratio of 1:1 used in the previous investigations was modified to achieve a better fit between the field-theory based data of the structure analysed in Section 5.4.2. and the results of the equivalent circuit model. The transformer ratio N3 (previously 1:1) was optimised together with the other elements of the equivalent circuit model. As an example the reflection coefficient phases p1 and p2 of a 90°-bend of strip width 100μm on a 100μm GaAs substrate was calculated. The transformer ratios M1, N1 and N2 are as predicted by the simple formula given in Section 3. The correction factors FM1, FN1 and FN2 are all equal to one. The correction factors FY1, FY2 and FZ1 have also been set to 1 for simplicity. Further, the additional shift d_{LSM1} of the length of the transmission line representing the LSM_{01} mode was set to 0 and the equivalent circuit elements M2, N3 and d_{LSM2} optimised. In this example both package dimensions (d_1, d_2)

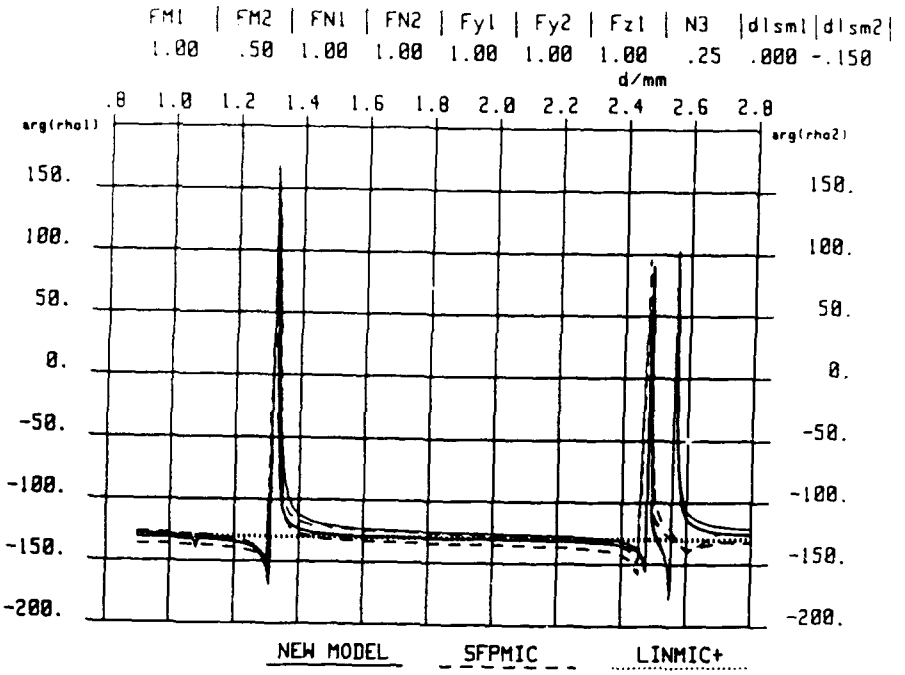


Fig. 6.5: S11 and S22 of 90° bend model including bidirectional coupling

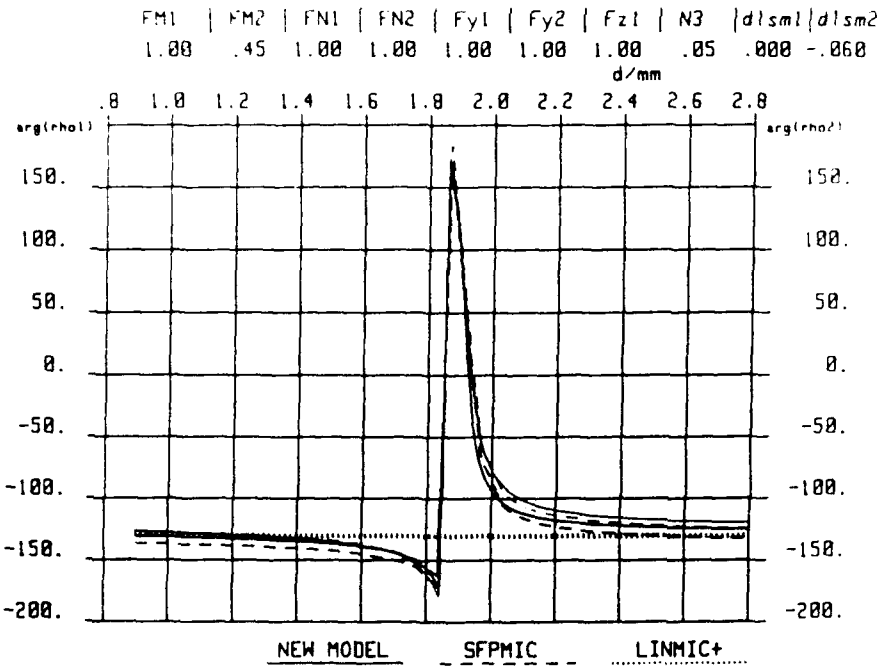


Fig. 6.6: Model comparison with 90° bend of section 5.4.2.

were changed simultaneously. The equivalent circuit model with optimised circuit element values given in the headline in Fig. 6.5, is able to predict all the reflections coefficients p1 and p2 resonances.

The new equivalent circuit model was also applied to the first bend configuration whose set of data has been generated in Section 5.4.2. The results are shown in Fig. 6.6. Again a good fit between the field-theory based data and the results of the equivalent circuit model was obtained by tuning only the equivalent circuit elements M2, M3 and d_{1sm2}.

6.5. EXTENDED MICROSTRIP T-JUNCTION MODEL

For the T-junction two orthogonal parasitic LSM_0 mode transmission lines have been considered in representing the bidirectional LSM_0 mode excitation in the package.

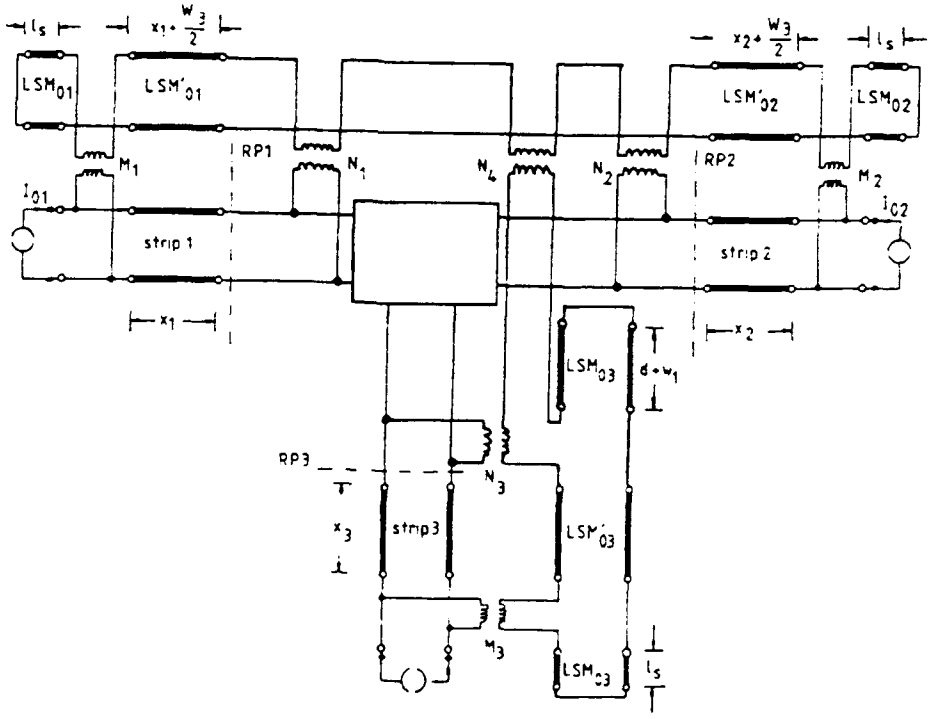


Fig. 6.7: A dynamic equivalent circuit model for the microstrip T-junction discontinuity, first revision.

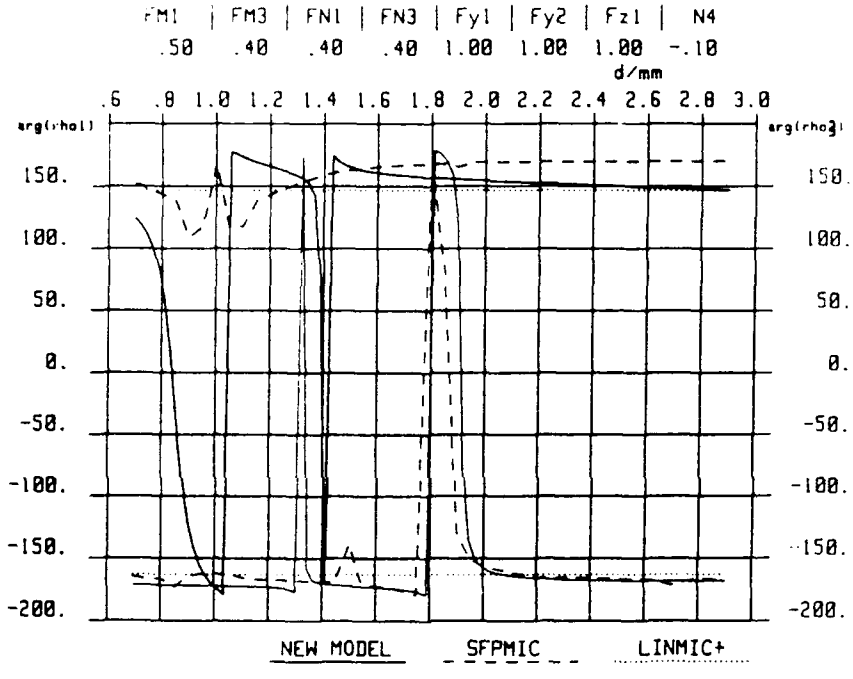


Fig. 6.8: S11 and S22 of T-junction model including bidirectional coupling

A revised equivalent circuit model is given in Fig. 6.7. This model contains 6 transformers to represent the coupling between the fundamental microstrip modes on the three feed lines and the three parasitic LSM_0' modes. In addition transformer N4 has been introduced to include the coupling between the parasitic LSM_0 modes of orthogonal directions (bidirectional excitation).

Fig. 6.8 shows the reflection coefficient phases of the fundamental microstrip modes at the reference planes RP1 and RP3 as a function of the package width, d + w2 + x3 + 1s for the structure analysed in Section 5.5.2. The field-theory based data (dashed curves) show resonance behaviour of the reflection coefficient p1 at box dimensions d = 0.9mm and d = 1.1mm. The phase of the reflection coefficient p3 shows resonance behaviour at box dimensions d = 1.5mm and d = 1.8mm. The previously used equivalent circuit model was able to predict only one box dimension of resonance behaviour for each reflection coefficient. The new circuit model of Fig. 6.7 predicts the resonance behaviour of all 4 package dimensions. The resonances at box dimensions d = 0.9mm and d = 1.8mm are predicted accurately but the two other resonances appear still shifted with the box dimension d. Moreover tuning of the circuit elements does not result in the fitting of these resonances. The resonances at d = 1.1mm and d = 1.5mm are predicted by the equivalent circuit model to be close together. However the full wave data does not show resonances of the same strength and location.

7. STUDY AND DEVELOPMENT OF THE MICROSTRIP-LSM_0 MODE COUPLING DESCRIPTION

7.1. IMPROVED ANALYTIC FORMULA FOR THE COUPLING DESCRIPTION

The coupling between the fundamental microstrip mode and the parasitic LSM_0 mode is described by transformers in the physics related equivalent circuit models . Up to now the prediction of the transformer ratios have been based on a first order analytic approximation (Section 3.3). Therefore, in order to obtain more refined equivalent circuit models a more detailed investigation into the transformer ratio description was done.

The fundamental microstrip mode and the LSM_0 package mode are coupled by their common electric field in the package. Therefore, the coupling between the fundamental microstrip mode and the package mode can be determined by the scalar product of the electric fields of both modes in the package cross-section A:

$$n_E = 1/A \int_A \int E_{strip} \cdot E_{LSM_0} \, dA \qquad (1)$$

The electric field of the parasitic LSM_0 mode is only weakly disturbed by the presence of the metallisation of a microstrip line. The electric field of the parasitic LSM_0 mode can be described to a good approximation by:

$$E_{LSM_0}(x,y) = E_{LSM_0} \sin(\pi x/W_s) \qquad (2)$$

Fig. 1 shows the cross section of the package and the geometry and electrical data used in the following calculations. The electric field of the fundamental microstrip mode can be approximated by:

$$E_{strip}(x,y) = E_{strip}, \; -W_{eff}/2 < x < W_{eff}/2 \qquad (3)$$

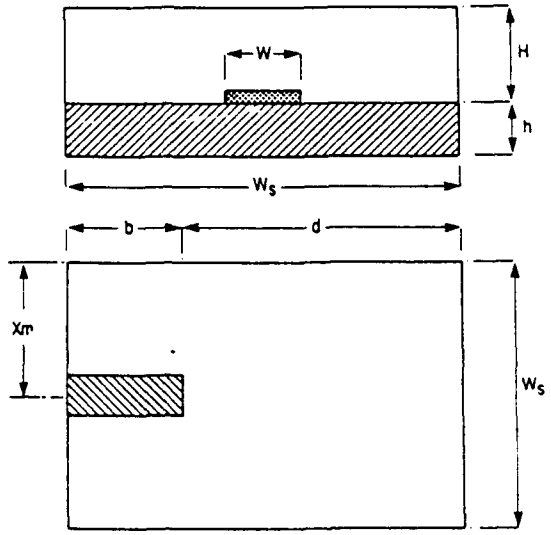


Fig. 7.1: Cross-section of the package under investigation

where W_{eff} is the effective width of the microstrip line. The value of the effective microstrip width can be determined using an equivalent magnetic wall model. With this approximation, the coupling between the electric field of the fundamental microstrip mode and the LSM_0 package mode is determined by:

$$E_{LSM_0}/E_{strip} = \frac{1}{\pi}\left[\cos\left(\frac{\pi}{W_s}\cdot\left(x_m - \frac{W_{eff}}{2}\right)\right) - \cos\left(\frac{\pi}{W_s}\cdot\left(x_m + \frac{W_{eff}}{2}\right)\right)\right]$$

However, the transformer ratios n and m are defined in the equivalent circuit models as:

$$n_u, m_u = U_{LSM_0}/U_{strip} \qquad (5)$$

Therefore, the voltages at the transformers in the equivalent circuits have to be determined as a function of the models' electric field in the package. The voltage between the ground plane and the microstrip can be found approximately from the electric field of the fundamental microstrip mode using

$$U_{strip} = h \cdot E_{strip}$$

For the parasitic LSM_0 mode, evaluation of the power flux of the parasitic mode in the package and its representation by a transmission line in the equivalent circuit models gives a relationship between the voltage at the transformers and the electric field in the package. The power flux of the LSM_0 mode can be calculated from:

$$P = 0.5(E_y.H_x).(h+H).W_s = E_y^2\,(h+H).W_s/2Z_f$$

$$\text{with } Z_f = (Z_0/\sqrt{\varepsilon r})/\sqrt{1-(f_c/f)^2}$$

The power flux in the transmission line in the equivalent circuit models can also be described by:

$$P = 0.5 \cdot U^2_{LSM_0}/Z_L \tag{8}$$

$$\text{with } Z_L = \frac{Z_o}{\sqrt{\varepsilon r}} \cdot \frac{(h+H)}{W_s} \cdot \frac{1}{\sqrt{1-(f_c/f)^2}}$$

Since both descriptions of the power flux are equivalent then

$$U_{LSM_0} = W_s \cdot E_{LSM_0} \tag{9}$$

With the application of this relationship the transformer ratios are determined by

$$n_u, m_u = \frac{W_s}{h\pi} \cdot \left[\cos\left(\frac{\pi}{W_s} \cdot \left(x_m - \frac{W_{eff}}{2}\right)\right) - \cos\left(\frac{\pi}{W_s} \cdot \left(x_m + \frac{W_{eff}}{2}\right)\right)\right] \tag{10}$$

The investigation of the transformer ratio uses the characteristic impedance

Z_L of the LSM_0 package mode. However, the definition of characteristic package mode impedances is ambiguous with respect to its absolute value. Therefore, a correction factor must be introduced to fit the equivalent circuit models to the numerically generated full-wave data. The transformer ratios n_u,m_u of equation (10) have to be modified by a factor 0.25 to account for the LSM_0 standing wave situation in the package in regard to the above transported power considerations. The additional correction factors mentioned are the quantities N,M listed in the header of each result figure. Their nominal (uncorrected) values are +1/-1 depending on the transformer orientation.

7.2. VERIFICATION OF THE TRANSFORMER RATIO DESCRIPTION USING THE GAP MODEL

Because the coupling between the fundamental microstrip mode and the LSM_0 package mode is significant, the microstrip gap discontinuity is a good test case for applying the new transformer ratio formula.

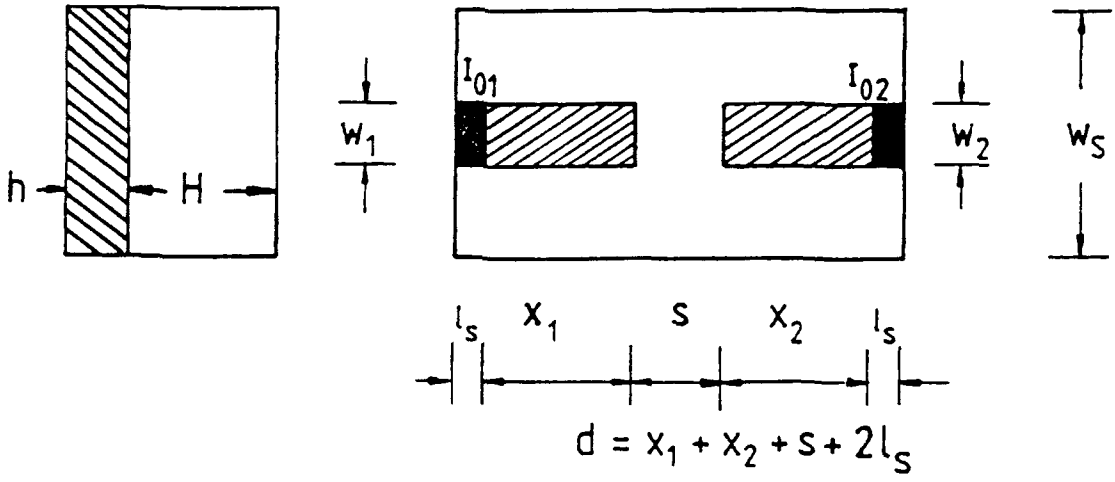


Fig. 7.2: Microstrip gap discontinuity with feed lines and current sources

7.2.1. Gap Width Variation

First the coupling between the fundamental microstrip mode and the LSM_0 package mode as a function of the microstrip gap width was investigated, for the gap discontinuity structure of Fig. 7.2.

Numerical full-wave data was used for comparison with the circuit models. The configurations studied had the following geometric parameters:

$h = 100\mu m$, $H = 500\mu m$, $w = 100\mu m$, $w_s = 3.1mm$, $X_m = 1.5mm$, $\varepsilon_r = 12.9$ with the following gap variations, $g = 1000\mu m$, $200\mu m$ and $100\mu m$. The analysis frequency was 55 GHz.

The results (Figs. 7.3-5) show the phase of reflection coefficients on the microstrips at both ports of the discontinuity. The correction factors M and and N for the transformer ratios were set to -1 or 1. M = -1 indicating that the transformer should be connected in the equivalent circuit with ports of one winding interchanged. Z and Z_s, are the LSM_0 and LSM_0' mode characteristic impedances.

As can be seen the physics related gap model including the coupling between the fundamental microstrip mode and the LSM_0 package mode gives a comparatively accurate agreement between the numerically generated full-wave data and the results of the equivalent circuit model. The transformer ratio is well described by the improved analytical formula for large gap widths (g = 1mm) up to small gap widths ($g = 100\mu m$).

7.2.2. Strip Width Variation

The microstrip strip width $w = 100\mu m$ was changed to further verify the new transformer ratio. Two cases, $w = 50\mu m$ and $w = 200\mu m$ were studied. The geometric parameters for this second study were:

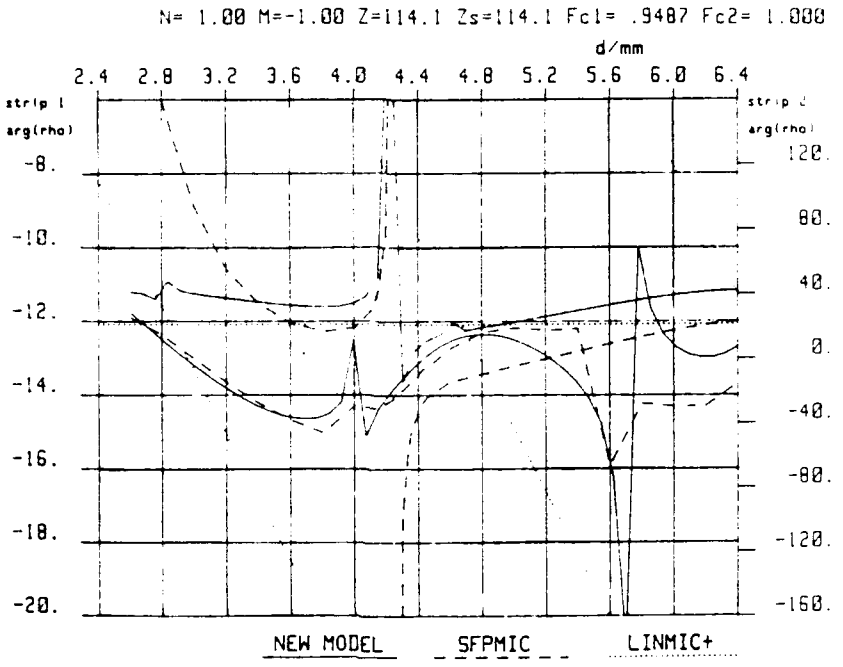


Fig. 7.3: Gap model S11 and S22: gap 1.0 mm

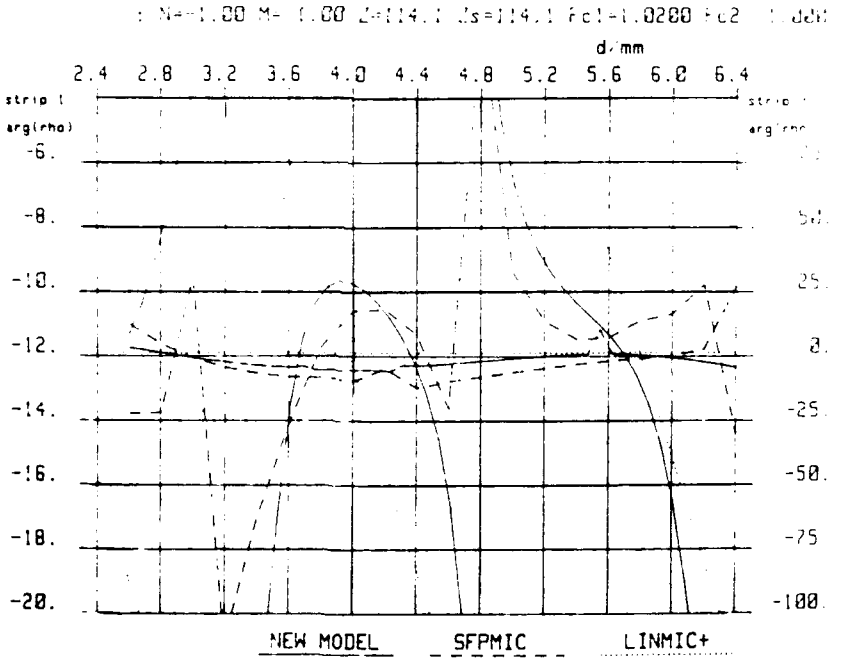


Fig. 7.4: Gap model S11 and S22: gap 0.2 mm

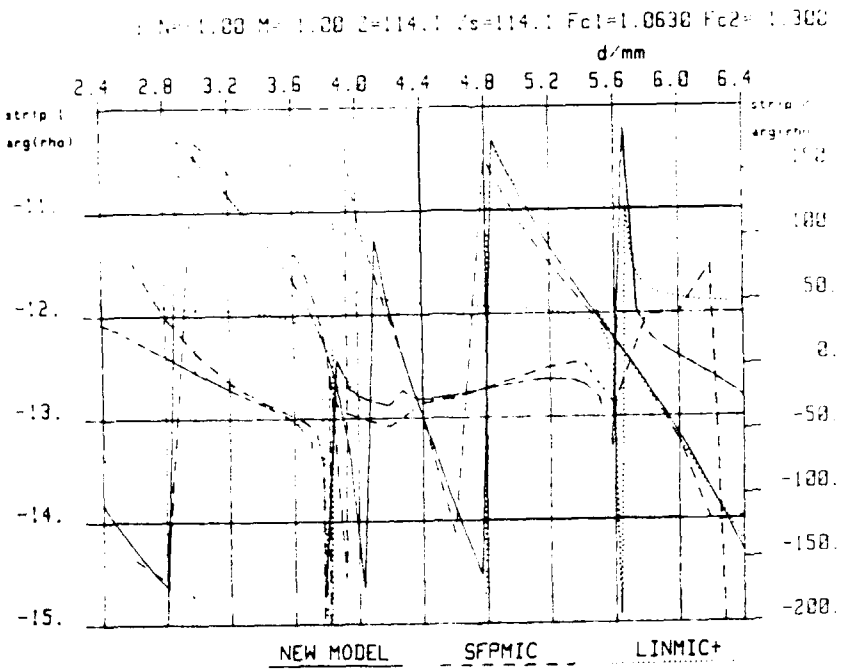


Fig. 7.5: Gap model S11 and S22: gap 0.1 mm

f = 55GHz, h = 100μm, H = 500μm, g = 100μm, W_s = 3.1mm, X_m = 1.5mm, ε_r = 12.9

The results of the analysis using the physics related equivalent circuit model with ideal correction factors for the transformer ratios n = -1 and m = 1 are shown in Figs. 7.6 and 7.7. The agreement between the numerically generated full-wave data and the results of the equivalent circuit model is excellent for the w = 200μm example. The predicted resonance due to the coupling between the fundamental microstrip mode and LSM_0 package mode (d = 4.0mm) for the w = 50μm example shows good agreement.

7.2.3. Frequency Variation

For further verification of the calculated transformer ratios, the frequency of f = 55GHz investigated before was extended to f = 50GHz and f = 80GHz.

In this study the geometric parameters were set to:

w = 100μm, h = 100μm, H = 500μm, g = 100μm, W_s = 3.1mm, X_m = 1.5mm, ε_r = 12.9.

The decrease of frequency 55GHz to 50GHz results in a significant decrease of the effective dielectric constant of the LSM_0 package mode (ε_{eff} (55GHz) = 0.422, ε_{eff} (50GHz) = 0.258). The phase of the reflection coefficient of the fundamental microstrip mode at both ports of the discontinuity is given in Figs. 7.8 and 7.9. Both examples show a good agreement between the numerically generated full-wave data and the results of the equivalent circuit model.

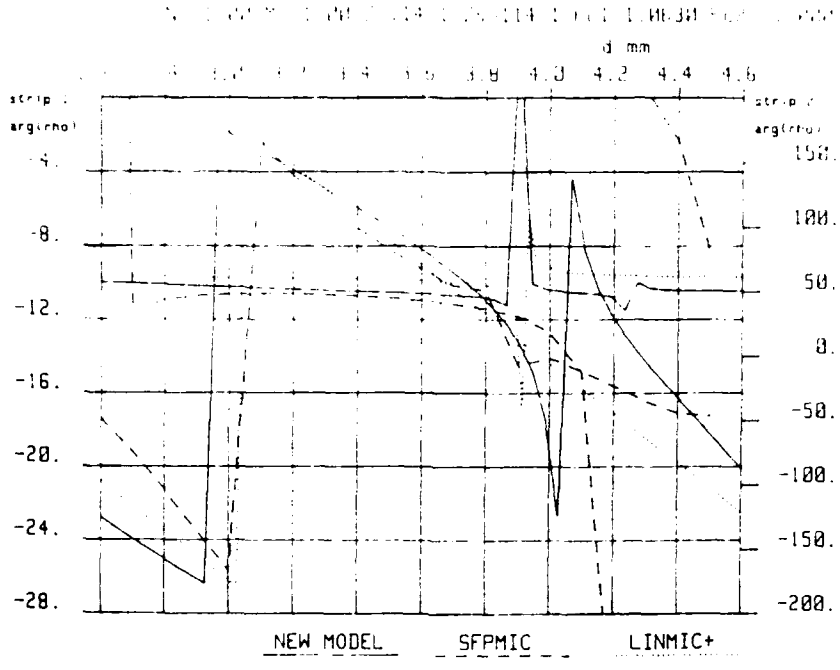


Fig. 7.6: Gap model S11 and S22: width 0.05 mm

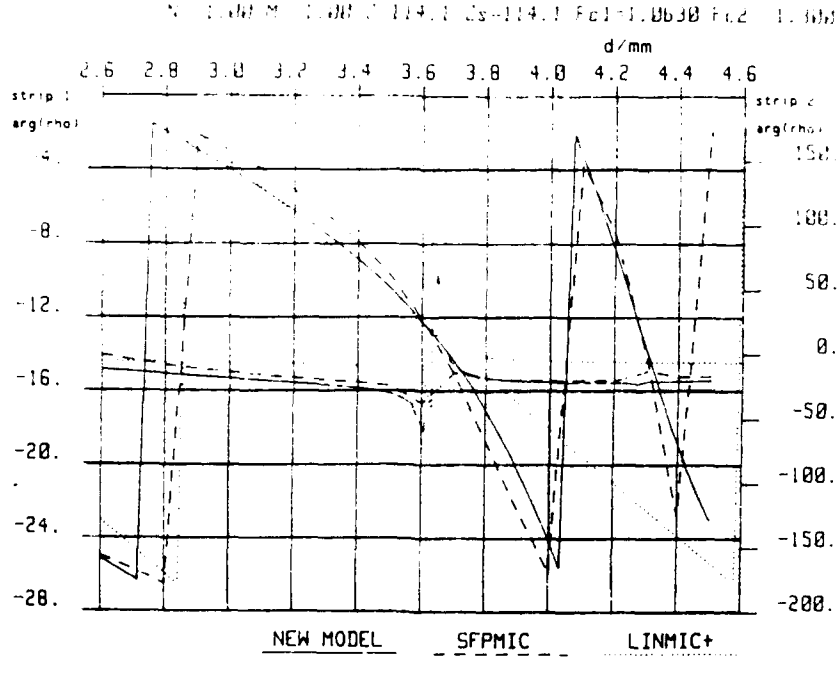


Fig. 7.7: Gap model S11 and S22: width 0.20 mm

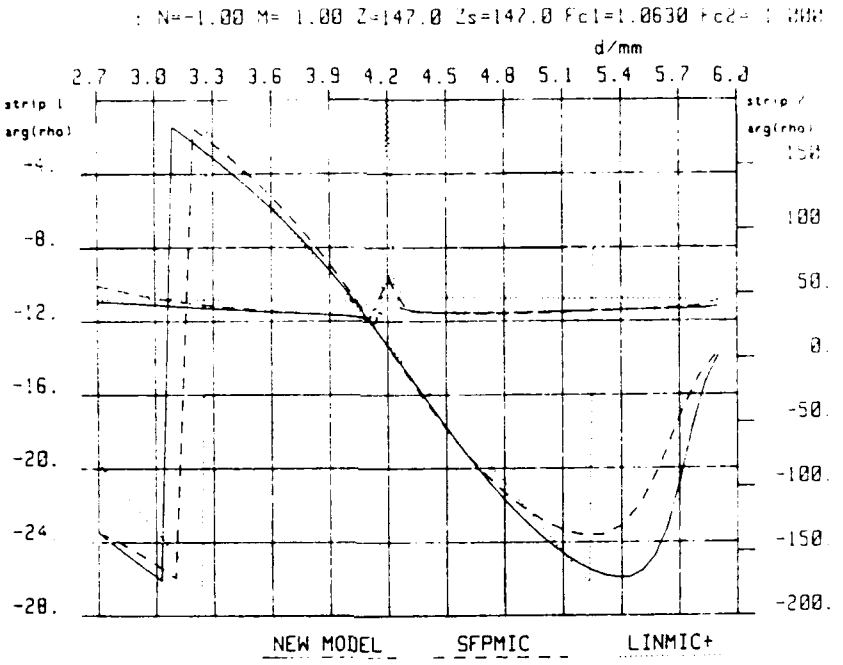


Fig. 7.8: Gap model S11 and S22: frequency 50 GHz

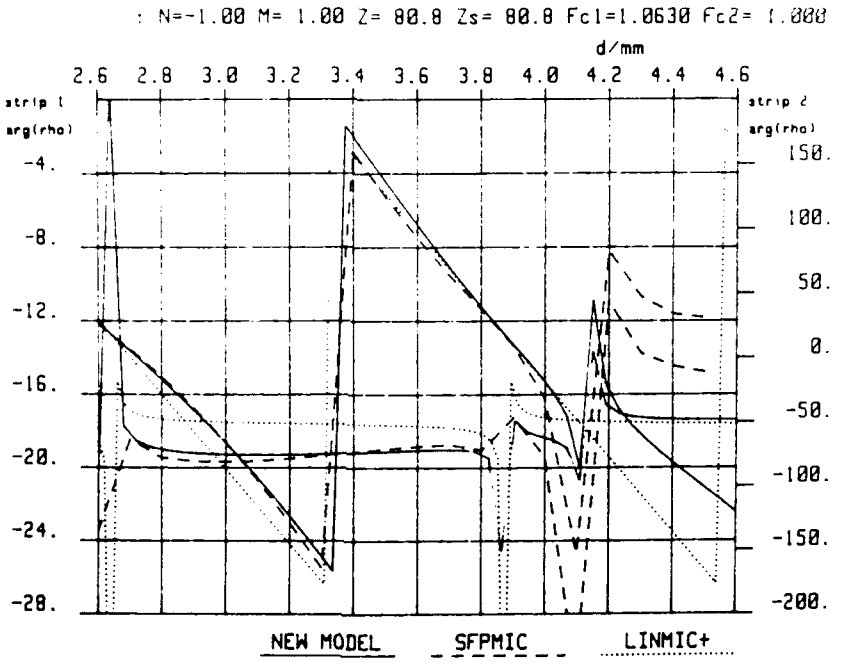


Fig. 7.9: Gap model S11 and S22: frequency 80 GHz

7.2.4. Variation with the microstrip position in the package

In the previous studies the microstrip position was set in the middle of the package (package width W_s = 3.1mm, position X_m of the strip X_m = 1.5mm). The following three gap configurations show the transformer ratio dependency on the position of the microstrip in the package. The structural paramters in this study were set to:

w = 100μm, h = 100μm, H = 500μm, g = 100μm, W_s = 3.1mm, f = 60GHz, ε_r = 12.9, for the following positions, X_m = 1.5, X_m = 1mm, and X_m = 0.5mm

The predicted transformer ratios for these microstrips are 0.12, 0.1 and 0.06 respectively. On using these predicted transformer ratios in the microstrip gap model, good correlation between the numerically generated full-wave data and the results of the equivalent circuit model is obtained (Figs. 7.10-12).

7.2.5. Small gap width study

Up to now the microstrip gap discontinuity has been analysed for relatively large gap widths (s = 1mm, 200μm, 100μm) as compared to a strip width of 100μm and a substrate height of 100μm. In the previous examples it has been shown that for various gap configurations (all of relatively large gap width) the field-theory based full-wave data show essentially the same behaviour of the phase of the reflection coefficient at the discontinuity ports as the results of the equivalent circuit model. For a smaller gap width the phase of the reflection coefficient of the microstrip mode decreases and therefore the strength of the excitation of the package mode decreases (destructive interaction of the two open end effects). A gap discontinuity of width s = 20μm (w = 100μm, h = 100μm) was analysed for additional verification of the

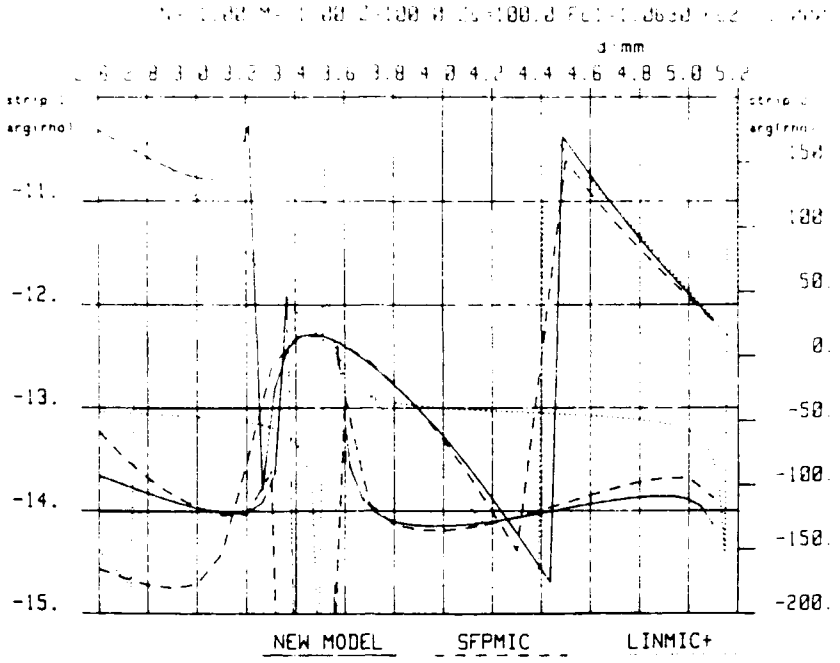


Fig. 7.10: Gap model S11 and S22: position 1.5 mm

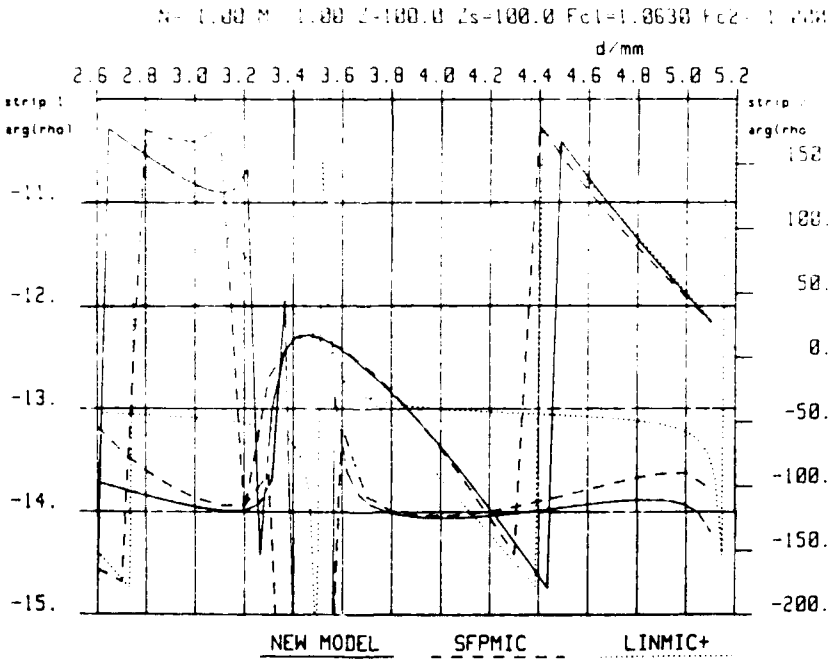


Fig. 7.11: Gap model S11 and S22: position 1.0 mm

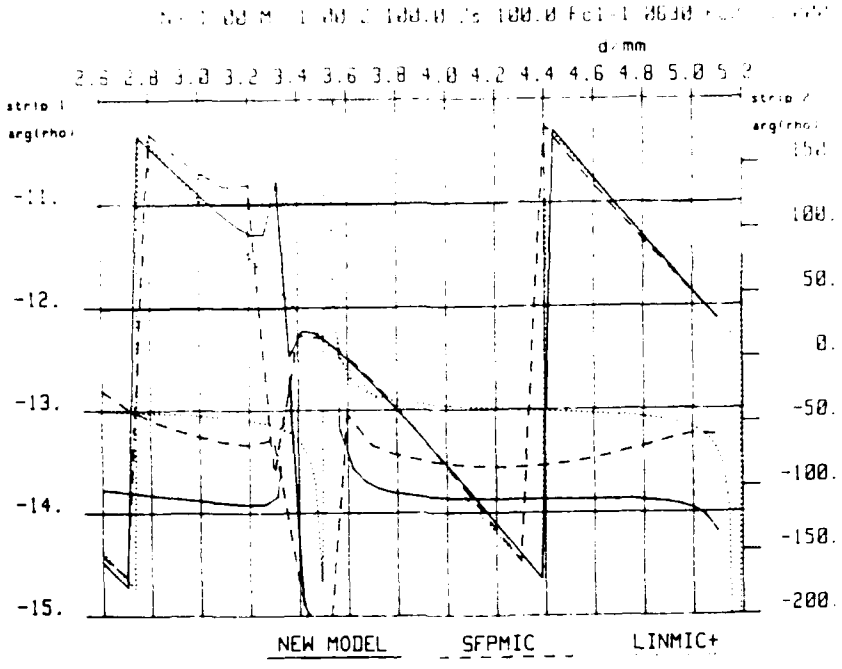


Fig. 7.12: Gap model S11 and S22: position 0.5 mm

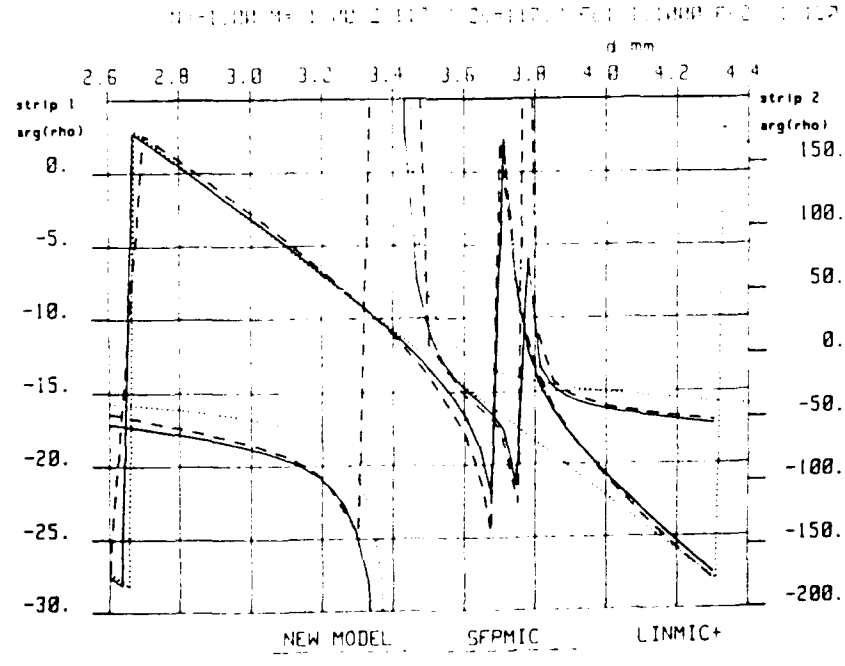


Fig. 7.13: S11 and S22 for small gap 0.02 mm

dynamic gap discontinuity model. The full-wave data and the results of the equivalent circuit model are plotted in Fig. 7.13. The resonance behaviour of d = 3.7mm is predicted quite accurately using the predicted transformer ratios. The correction factors N and M are set to -1 and 1.

7.2.6. Transformer Ratio Variation

To test the new transformer formula further, the effect of changing the predicted ratios set in the previous examples on the model performance was studied. The cases investigated are given below.

The gap discontinuity described by the case, f = 50GHz in Section 7.2.3. was studied again. The correction factors M and N, which have been set to -1 and 1 in the previous analysis of the transformer ratios were set at N = -1.2 and M = 1.2. This increase of 20% of the transformer ratios gives a significant change in the behaviour of the phase of fundamental microstrip mode reflection coefficient (Fig. 7.14), from that obtained for the ideal correction factors.

Another case re-examined was the gap discontinuity described by f = 60GHz, w = 100μm, g = 100μm, X_m = 1.5mm is the second example for sensitivity considerations. The correction factors M and N, which have been set to -1 and 1 in the previous verification of the transformer ratios were set at N = -0.8 and M = 0.8. This decrease of 20% in the transformer ratios does not show significant influence on the behaviour of the phase of the reflection coefficient of the fundamental microstrip mode (Fig. 7.15).

The last case analysed was that of Section 7.2.1. g = 100μm. The correction factors M and N, which have been set to -1 and 1 in the previous verification of the transformer ratios were increased significantly to N = -1.5 and M = 1.5. This increase of 50% of the transformer ratios shows its influence on the behaviour of the phase of the reflection coefficient of the fundamental microstrip mode (Fig. 7.16), resulting in less agreement with the model.

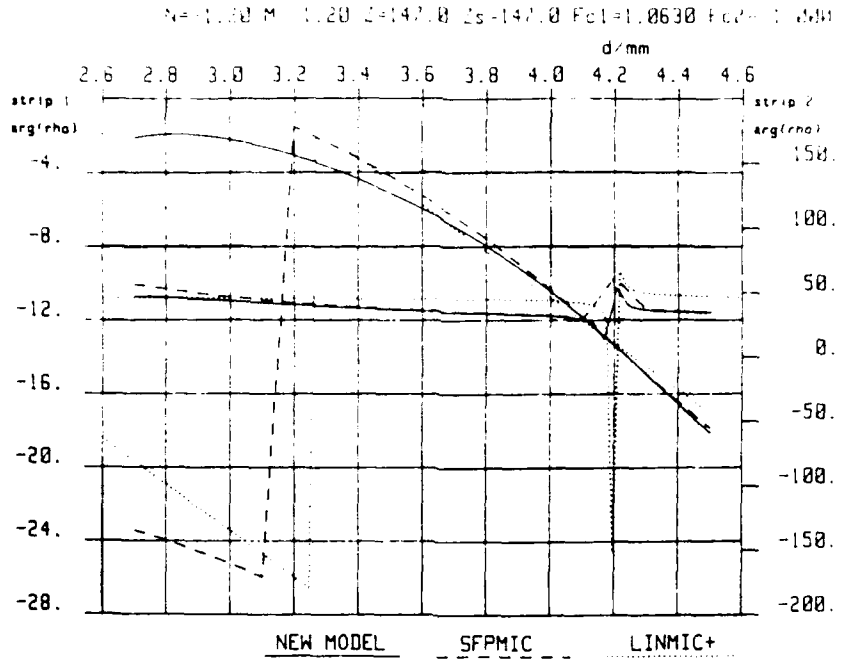


Fig. 7.14: Transformer ratio increase of 20%

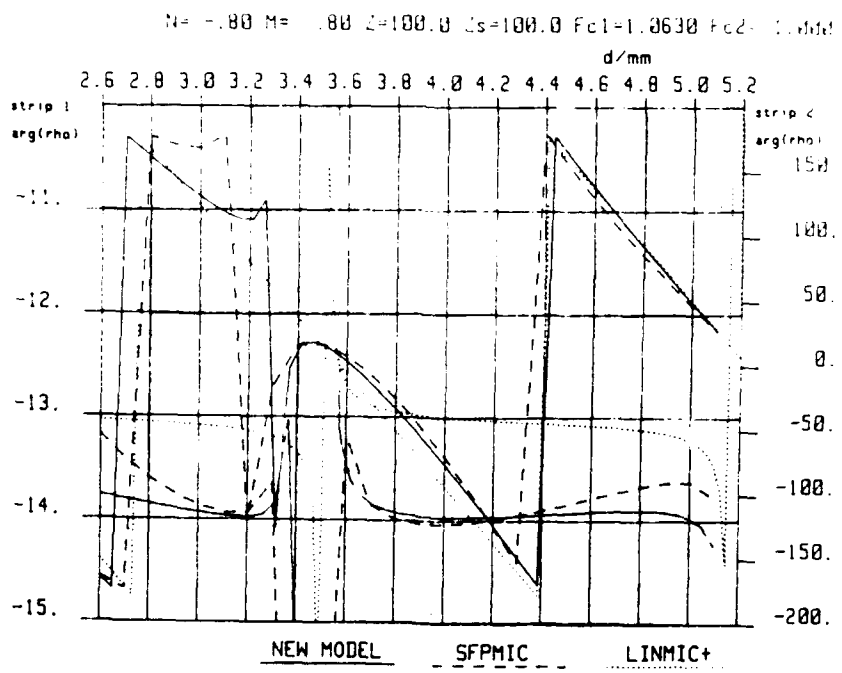


Fig. 7.15: Transformer ratio decrease of 20%

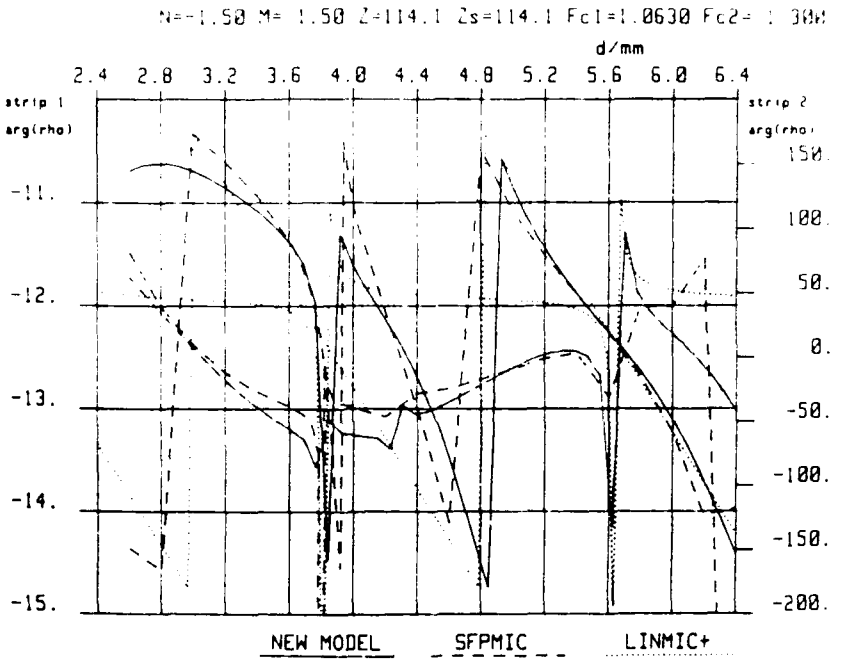


Fig. 7.16: Transformer ratio increase of 50%

These simple sensitivity studies show that the new transformer ratio formula basically describes the fundamental microstrip mode and the LSM_0 package mode coupling for the microstrip gap discontinuity.

7.3. DISCUSSION OF THE FREQUENCY DEPENDENCY OF THE TRANSFORMER RATIO

In order to study the frequency dependency of the transformer ratio, the model given in Fig. 5.1 was replaced by that shown in Fig. 7.17.

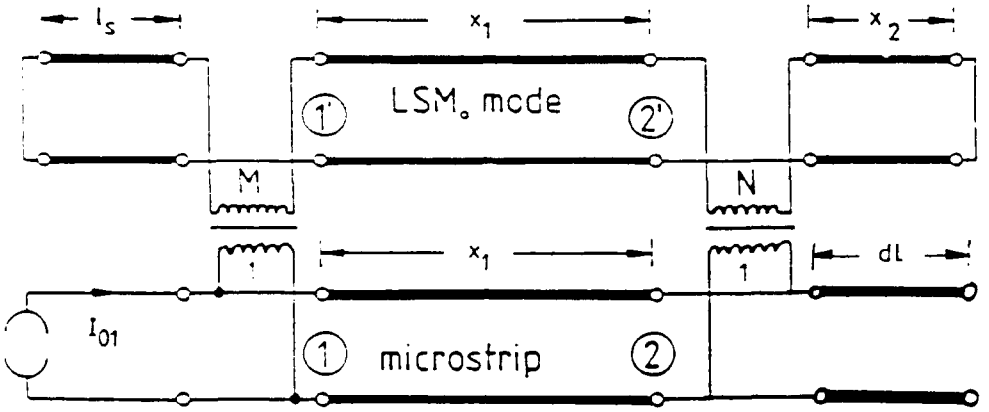


Fig. 7.17: Modified open-end circuit model in a package

This equivalent circuit was found to be more accurate where l_s is the source length, x_1 the microstrip length, dl the microstrip end effect and x_2 the distance from the microstrip end to the package end.

The equivalent circuit model for the open end discontinuity is given in Figure 7.17 by the equivalent circuit to the right of the ports 2 and 2' with the LSM_0 mode length x_2 removed.

This circuit model was applied to example open end configurations over a large frequency range. One of the structures modelled had the following open end geometry parameters:

$h = 100\mu m$, $H = 0.500mm$, $w_s = 3.000mm$, $x_m = 0.500\ w_s$
$w = 50\mu m$, $x_s = 1.179mm$, $x_p = 2.886mm$, $l_s = 1.20w$

where x_s is the feed length, x_m the strip position along the package width, x_p the package length and l_s the source length.

The following correction factors were also applied to the elements of the equivalent circuit model. FC_DL is the correction factor that modifies the the open end equivalent length dl. FC_N is the correction factor that modifies the predicted transformer ratio N. FC_P is the correction factor that modifies the approximated propagation constant β_{LSM}. The dashed curve (Fig. 7.18) shows the phase of the scattering parameter S_{11}, if the approximate propagation constant is used together with the correction factor FC_P. The dotted curve in Fig. 7.18 shows the phase of S_{11} if the correct values for the propagation constants β_{LSM_0} and β_{LSM_0}' (derived from full wave analysis) are used giving a very small further improvement.

The above results show a discrepancy between the numerical full-wave results and the scattering parameter S_{11} determined from the circuit model when low frequencies are approached. The reasons for this discrepancy can be determined as follows. At low frequencies the LSM_0 mode is below cut-off (below 46 GHz) for the above structure. The input impedance of the LSM_0 transmission line loaded with the short circuit representing the electric end wall is:

$$Z_{in} = j \left|Z_{LSM}\right| \tanh\left(-\left|\beta_{LSM}\right| l\right)$$

$$Z_{in}(f<f_c) \sim 1/\sqrt{1-(f_c/f)^2} \sim f$$

where l is the line length.

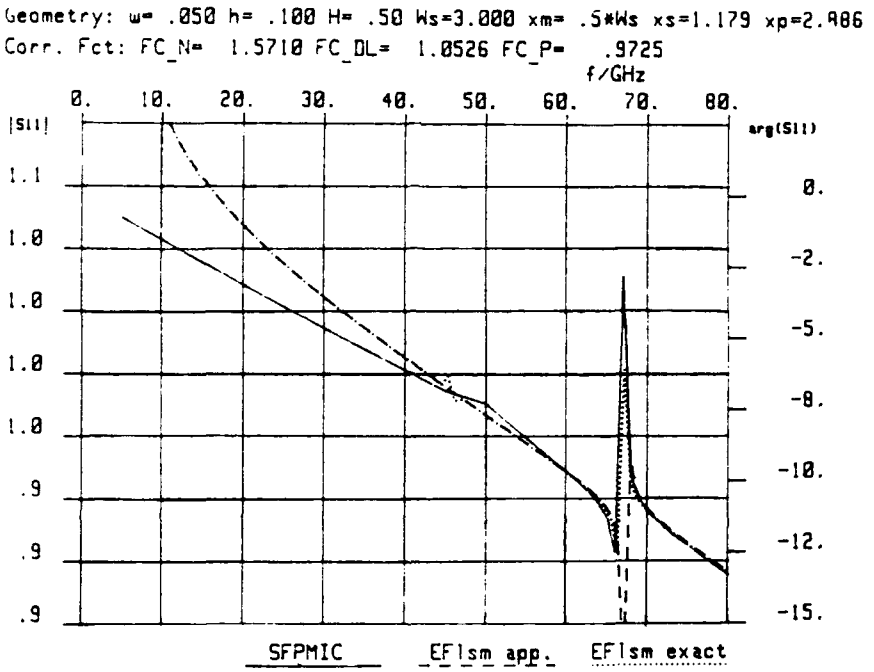


Fig. 7.18: Open end S11 with correction factor

the microstrip open end transformer being loaded with impedances relating to the LSM_0 and LSM_0' modes. If these impedances vanish for frequencies approaching zero and the transformer ratio N is considered independent of frequency, the equivalent circuit model will show the incorrect low frequency behaviour . Since the transmission line characteristics $Z_{f\ LSM}$ and β_{LSM} of the package mode are sufficiently justifiable, the reason is found to be in the factor $1-(f_c/f)^2$ which is only weakly dependent on frequencies sufficiently high above cut-off. A theoretical study therefore was made which shows how the voltage and associated parasitic mode current behaves in the asymptotic low frequency limit. From this study it was concluded that the transformer ratio description had to be frequency dependent.

7.4. FREQUENCY BEHAVIOUR OF THE TRANSFORMER RATIO

The major problem in the open end model was the frequency dependent behaviour of the transformer ratio N describing the coupling between the microstrip node and the LSM_0 package mode. Up to now the transfer ratio N has been considered successfully independent of frequency. However, an inconsistency occurs because the frequency behaviour of the transformer mode in conjunction with the frequency dependent LSM_0 characteristic impedance results in a short circuit of the LSM_0 mode transmission line in the static circuit model. This behaviour is considered as not being physical and has to be reconsidered. To overcome this inconsistency a theoretical study similar to those already performed on ideal wave-guide discontinuities was undertaken in order to get a more detailed look on the frequency dependency of the transformer behaviour above cut-off.

In this study for frequencies above cut-off the following assumptions have been made. Two waves are propagating on the microstrip transmission line on the left port of the discontinuity (Fig. 7.19). One wave is travelling in the positive and the other in the negative z-direction. At the other discontinuity port there is only one LSM_0 mode travelling in a positive

z-direction. All other modes are assumed to be sufficiently cut-off and as such are lumped into the quasi-static model parameters.

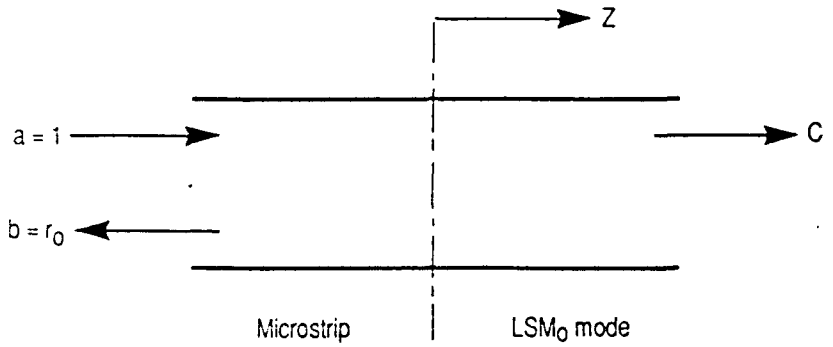


Fig. 7.19: Schematic of the discontinuity microstrip - LSM_0 mode

From the boundary condition for the electric field in the transverse plane of the discontinuity, the equation

$$(1 + r_0) * T = E_{LSM0}/E_{microstrip}$$

can be estimated, where T is the scalar product between the electric field distribution of the fundamental microstrip mode and the electric field distribution of the LSM_0 package mode. Previously this scalar product has been used to predict analytically the transformer ratio N. The boundary condition for the magnetic field in the transverse plane of the discontinuity gives a second equation

$$(1 + r_0) * (1/Z_{L\ microstrip} - 1/Z_{LLSM0}T^2) = 2/Z_{L\ microstrip}$$

where $Z_{Lmicrostrip}$ and Z_{LLSM0} are the characteristic impedances of the fundamental microstrip mode and the LSM_0 package mode. From these two equations the reflection coefficient r_0 can be calculated.

$$r_o = \frac{Z_{LLSMO} - T^2 * Z_{Lmicrostrip}}{Z_{LLSMO} + T^2 * Z_{Lmicrostrip}}$$

The next step is to compare this reflection coefficient to the reflection coefficient of the ideal transformer shown in Fig. 7.20.

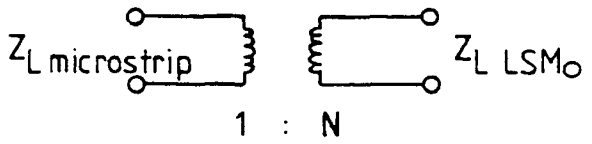


Fig. 7.20: Mode coupling transformer

The scattering matrix of this transformer is

$$[S] = \begin{bmatrix} \frac{Z_{LLSMO} - N^2 * Z_{Lmicrostrip}}{Z_{LLSMO} + N^2 * Z_{Lmicrostrip}} & \frac{2*N*\sqrt{Z_{LLSMO}\ Z_{Lmicrostrip}}}{Z_{LLSMO} + N^2 * Z_{Lmicrostrip}} \\ \frac{2*N*\sqrt{Z_{LLSMO}\ Z_{Lmicrostrip}}}{Z_{LLSMO} + N^2 * Z_{Lmicrostrip}} & \frac{Z_{LLSMO} - N^2 * Z_{Lmicrostrip}}{Z_{LLSMO} + N^2 * Z_{Lmicrostrip}} \end{bmatrix}$$

A comparison between the reflection coefficient of the ideal transformer and the ideal discontinuity (microstrip - LSM_O mode) shows that for N=T the

ideal transformer reduces to the equivalent circuit model for the junction microstrip mode - LSM_0 mode, indicating again that the transformer ratio for frequencies above LSM_0 cut-off is frequency independent.

At the same time this result shows that two different frequency regions are needed for the transformer ratio description, one applying above LSM_0 cut-off with no frequency dependency (used up to now) and the other for frequencies below cut-off having a frequency dependence. The frequency dependent description of the LSM_0 mode for use in the low frequency part of the spectrum below cut-off is already included into the discontinuity quasi-static portion.

Within the quasi-static range the package field can be described for every frequency by a superposition of LSM and LSE modes. The stray field of the open end is mainly determined by a superposition of LSE modes only, but contains implicitly a small LSM_0 portion. The LSE modes are dominant and represent a capacitive load on the microstrip, this effect being considered in the equivalent circuit model by the quasi-static open end length. In this case all higher modes are far below cut-off and as such this quasi-static description is valid for increasing frequency.

As the LSM_0 mode approaches cut-off or is above cut-off, the LSM_0 package field content becomes important. LSE mode effects now can be described by the quasi-static effective open end length, because the LSE modes are far below cut-off. Since the LSM_0 mode is dominant in the package field, the coupling between the fundamental microstrip mode and the LSM_0 package mode has to be considered, as in the dynamic circuit model description.

The following illustration shows the range of validity for the quasi static part and the LSM_0 part of the dynamic model, Fig. 7.21. The two ranges overlap showing the unified description of the dynamic model.

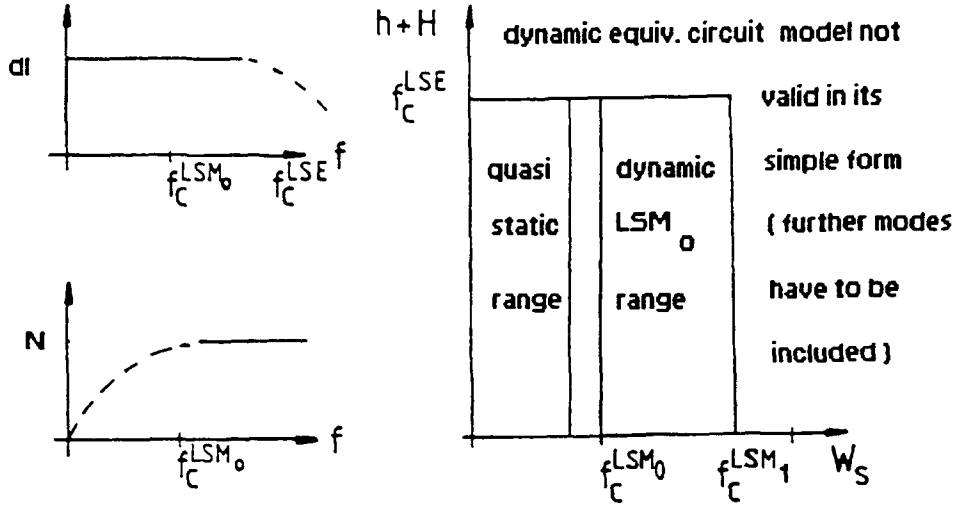


Fig. 7.21: Validity of the dynamic, open end discontinuity model

The superposition of LSM and LSE modes in the form (dl,N) shows the correct quasi-static and dynamic mode behaviour, the equivalent circuit representation of the LSM and LSE mode parts of the dynamic model having to reflect this superposition.

As can be deduced the range of validity of the quasi static model part is restricted to frequencies below the first cut-off frequency of LSE modes, where

$$f \ll f_c^{LSE} = 2c_0/(h+H)\sqrt{\varepsilon_{reff}}$$

In this range the quasi static open end length can be considered essentially constant, nearly independent of frequency.

The LSM_0 mode behaviour, represented by a transformer and transmission lines has to reflect that the LSM_0 mode is frequency dependent below cut-off and that the LSM_0 energy content is lumped into the value of dl in

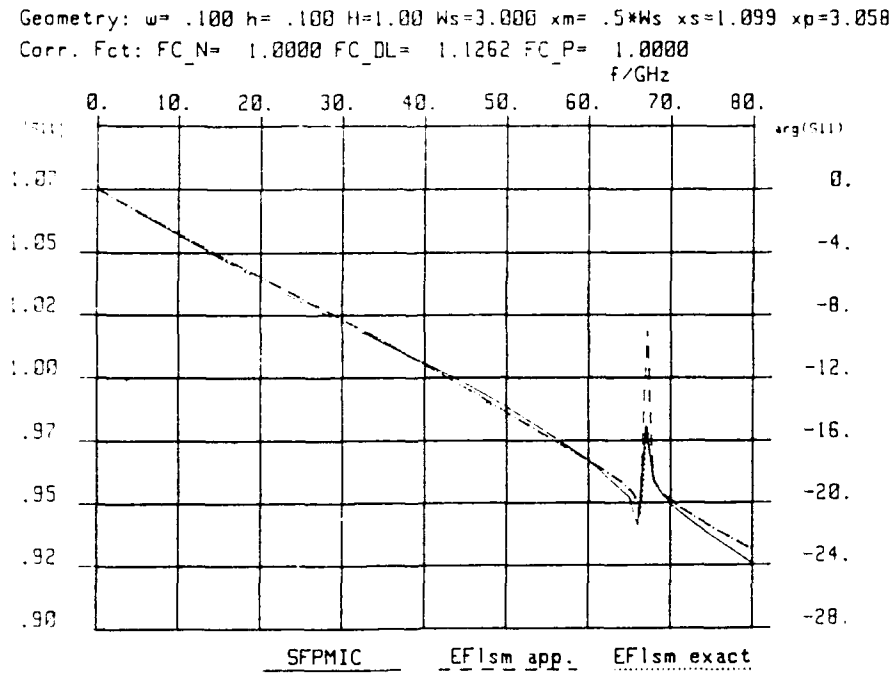


Fig. 7.22: Open end 1 S11 with empirical correction

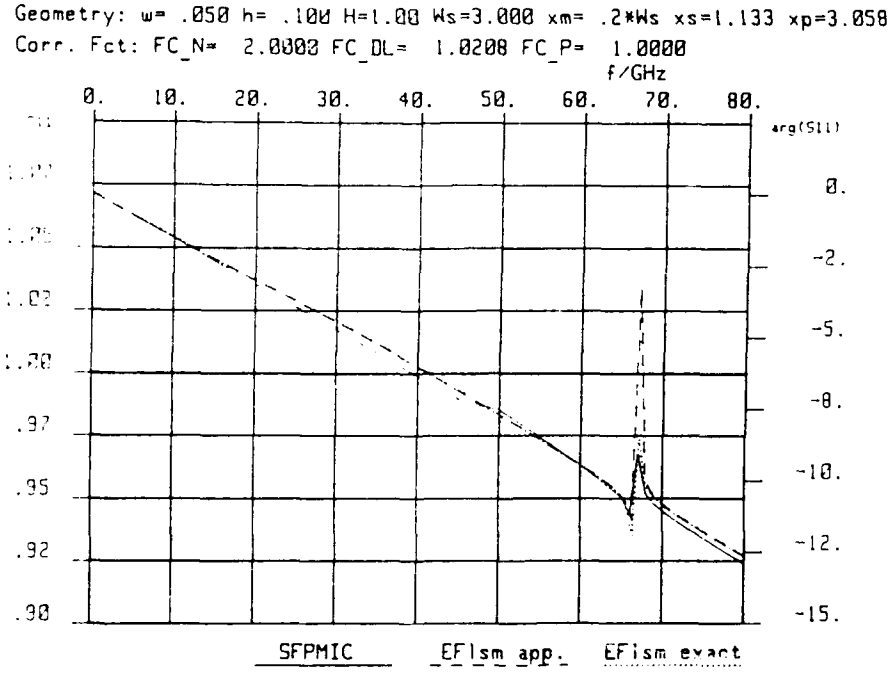


Fig. 7.23: Open end 2 S11 with empirical correction

the asymptotic limit. This LSM_0 behaviour below cut-off is taken into account by the introduction of the empirical function.

$$N = N_0 \cdot \cos^2 \left(\frac{\pi.(f-f_c LSM_0)}{2\, f_c LSM_0}\right)$$

where N_0 is the transformer ratio that has been used for frequencies above cut-off. The results in Figs. 7.22 and 7.23 use this empirical correction for the transformer ratio and as can be seen show good agreement with the numerical data.

8. PARAMETER EXTRACTION METHOD

8.1. METHOD

In the modelling procedure two numerical full-wave S-parameter databases are generated for each discontinuity. These databases are dependent on the geometric dimensions of the discontinuity structure in the package and upon frequency. The first database is based on a low frequency analysis with package dimensions such that LSM_0 mode effects are at a minimum. This database is used to obtain the quasi-static elements of the model. For the second database, package lengths are chosen so that the length is larger than λ_{LSM_0} at the maximum frequency under consideration and the LSM_0 package mode goes resonant within the frequency range of analysis. In such a situation the coupling between the microstrip and package mode has considerable influence on the discontinuity behaviour and the transformer ratios can be determined with good accuracy.

The curve fitting procedure based on such data is organised in automated form with the additional possibility of manual tuning. This procedure is based on a computer assisted search for the minimum of the function

$$\sum_{n=1}^{N} \sum_{m=1}^{M} \left| S^{D}m\,(f_n) - S^{M}m\,(f_m, p_i) \right|^{q}$$

where $S^{D}m\,(f_n)$ is the scattering parameter m of the data base for frequency f_n, $S^{M}m\,(f_n, p_i)$ is that of the equivalent circuit model and parameter set p_i and q is a variable in the optimisation procedure. The algorithm used is based on the method of conjugate directions (1), the value of q being increased to obtain an error minimum.

The equivalent circuit models previously studied are able to predict the discontinuity behaviour with reasonable accuracy. The elements in these models are described by geometrical dimensions, electric characteristics of

the transmission lines and the LSM_0/LSM_0' package modes and analytical formula for the transformer ratios. In addition quasi-static analytical formulae descriptions of the discontinuity are used to build up the dynamic equivalent circuit models.

For example in the open end discontinuity case, the reflection coefficient on the feed line is calculated from the equivalent circuit model as a function of the geometric variables and frequency.

$$\rho = a(w, h, H, f, w_s, x_p, \varepsilon_{LSM_0}, \varepsilon_{LSM_0'})$$

The quasi-static effective line length and the transformer ratios for the open end will be evaluated as a function of the input parameters

$$dl_{static} = b(w, h, H, f, w_s)$$

where the start function for dl_{static} can be published analytic formula. If a refinement to the dynamic model is required the current formulae will be used in conjuction with correction factors FC_DL and a new function derived from curve fitting. Such a method is also used in deriving the transformer ratio.

$$n_{fitted} = n_{predicted} \cdot f^{n}_{c}.d(w, h, H, f, w_s)$$

where the correction factor f^{n}_{c}, (FC_N) will have a value of about 1 for most geometric configurations, d being a function depending upon frequency and the discontinuity configuration dimension parameters in the package.

8.2. REFERENCES

(1) Bandler, J.W., Chen, S.H., Circuit Optimisation: The state of the art, IEEE MTT-36, Feb. 1988, p.424.

9. MICROSTRIP OPEN END MODEL

The physical environment used in the full wave analysis of the open end discontinuity in a package is shown in Fig. 9.1.

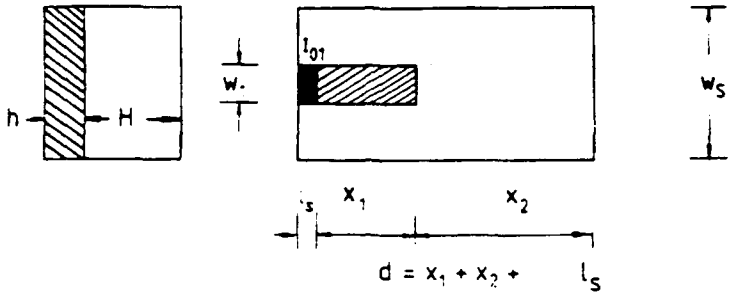


Fig. 9.1: Microstrip open end discontinuity in a package

where d is the package length and w_s the package width, l_s is the length of the source, x_1 the feed strip length and w_1 the strip width. The equivalent circuit model of this situation is shown in Fig. 9.2.

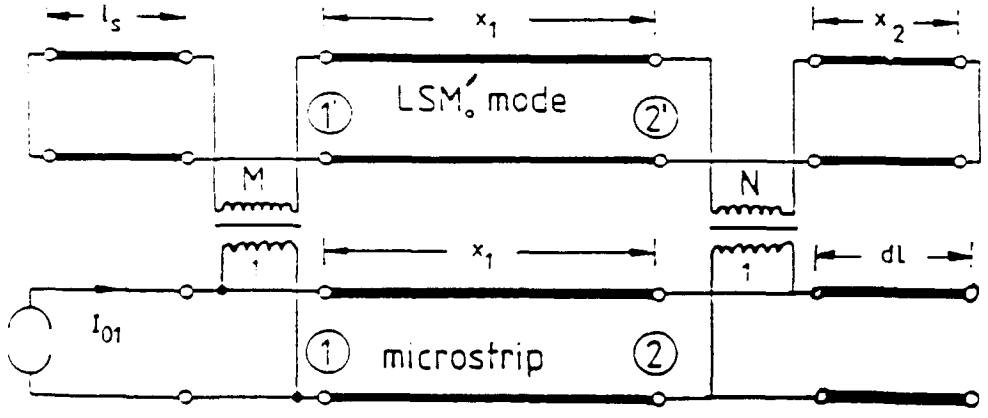


Fig. 9.2: Dynamic circuit for the open end discontinuity in a package

The model takes into account the excitation of the LSM_0 package mode at the open end discontinuity and at the current source through the transformers N and M respectively. The discontinuity model is a 3-port circuit shown in Fig. 9.3.

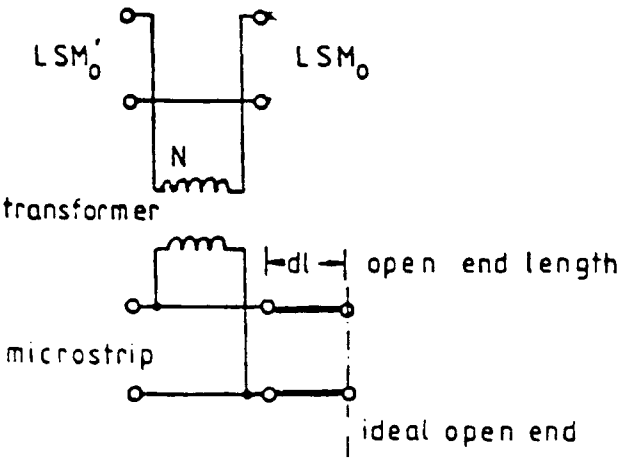


Fig. 9.3: Open discontinuity model

where dl is the extra static open end length.

9.1. ANALYTIC FORMULA FOR THE STATIC PART OF THE DYNAMIC EQUIVALENT CIRCUIT MODEL

The dynamic equivalent circuit model consists of a quasi-static part (the effective equivalent open end length dl) and a dynamic part describing the coupling between the fundamental microstrip mode and the parasitic LSM_0 package mode. The quasi-static part of the equivalent circuit model needs refining for the effective equivalent open end length dl. The analytic description of dl was based on published formulae. However, the published analytic open end formula does not consider the effects of package width. The smallest package width under consideration in this project is W_S=0.5mm that is 5 times the substrate thickness. The behaviour of such open end configurations is influenced considerably by the lateral side walls.

Therefore, the new analytic formula for the quasi static effective open end length must take the effects of package width into account.

In order to obtain the refined analytic formula a database of S-prameters for a wide range of open end-package structures were generated. For the database normalised parameters for the open end configurations: strip width w/h, cover height H/h, substrate width W_s/h and frequency f*h, were used.

The dielectric constant of the substrate was 12.9 (GaAs).

The position of the strips was fixed to the center of the package ($X_m=0.5*W_s$). To cover the geometry range from 1mm to 3mm for both package lateral dimensions, a minimum substrate height of h=0.05mm and a maximum substrate height of 0.2mm, the range of normalised package parameters W_s/h and H/h for the data base was set for $5 \leq W_s/h$, $H/h \leq 60$. However since high H/h ratios cause LSE modes in the package and high W_s/h ratios cause the second LSM mode to be excited in the frequency range of interest, the upper limit was not used. Therefore, considering a 0.1mm substrate, the physical parameter range for the data base generation was fixed to $0.5 \leq W_s, H \leq 3$.

The normalised frequency range used was $0 \leq f*h \leq 12$ GHz*mm (frequency range 0-120 GHz on a 0.1 mm substrate).

For some of the open end configurations investigated, convergence was checked with respect to the number of expansion functions and spectral density used in generating the numerical data base. The CPU time spent for the numerical analysis of the open end configurations was small for wide strips in narrow packages, increasing considerably for the analysis of narrow strips in wide packages. The computation accuracy of the effective open end length dl in the final data base generation was estimated to be less than 5% for narrow strips and much better for wide strips.

The second step in the generation of final quasi-static analytical formulae for the discontinuity was to fit the numerical data base results, that is the phase of the reflection coefficient of the fundamental microstrip mode, to the equivalent circuit model by computer matching. The correction factors,

$$f_{c_dl} = \frac{dl_{\text{data base}}}{dl_{\text{state-of-the-art}}}$$

were generated for final model tuning and are listed in Table 1 (Section 9.4) together with the geometrical parameters describing the open end configuration (HH is the height from package cover to substrate, x_p the package length and XFEED the microstrip length). The analytic formula for the open end length, $dl_{\text{state-of-the-art}}$ was taken from M. Kirschning (1,2). The correction factors f_{c_dl} have a value near 1. The maximum relative deviation between data base and published formula found for $\left| 1-f_{c_dl} \right|$ is 9.2% and the average error is 2.2%. The maximum relative error appears for small package widths.

Starting from the published analytic open end formula and taking into account a correction factor for the substrate width, the final analytic formula for the quasi-static effective open end length is

$$dl/h = f_1 \cdot f_2 \cdot f_3$$

$$f_1 = 0.4372 \cdot \left(1 + \frac{0.449}{\varepsilon eff^{0.81} - 0.1890}\right) \left(1 - \frac{0.634}{(w/h)^{0.8544} - 0.87}\right)$$

$$f_2 = 1 - 0.1248 \cdot \exp\left(-3.7259 \cdot w/h\right)$$

$$f_3 = 1 - 0.0385 \cdot \frac{h}{w} \left(1 - \frac{2}{\pi} \cdot \operatorname{atan}\left(\frac{W_s}{h}\right)\right)$$

The maximum relative deviation between data base and these formulae is 3.92%

and the mean deviation is 0.75%. The range of validity is determined by the outlined parameter range of the data base.

9.2. ANALYTIC FORMULAE FOR THE TRANSFORMER RATIO

Although in the dynamic part of the equivalent circuit model a preliminary analytic description of the transformer ratio has been developed (Section 7), up to now the coupling between the microstrip and the LSM_0 package mode has not been studied in detail for frequencies near package resonance. For such a study a full wave database was generated for a set of open end discontinuity structures.

As previously, normalised parameters were introduced for the data base generation. The physical reference substrate height for the numerical computations was again h=100μm. The denormalised frequencies used were 50...120 GHz.

The database package height values were restricted to H=0.5mm and H=1mm, because for larger package height the first LSE cut-off frequency would be lower than 120 GHz, i.e. within the frequency range of interest, the dynamic equivalent circuit model being invalid for frequencies beyond LSE mode cut-off.

The package widths considered were W_s=2mm (W_s/h=20) and W_s=3mm (W_s/h=30). For smaller package widths the cut-off frequency of the LSM_0 mode is higher than the maximum frequency of interest and for larger package widths the second LSM mode becomes significant in the frequency range of interest beyond cut-off. In this case the validity of the dynamic equivalent circuit model would be exceeded.

Open end strip widths between w=0.4mm (w/h=40) and w=10μm (w/h = 0.1) were used in the database generation.

Investigation of the package resonances for various open end discontinuity configurations highlighted that computer matching for fine tuning of the analytic formula of the transformer ratio required a very high numerical effort and the reflection phase coefficient needs the computation of a large number of frequencies near package resonance to obtain accurate behaviour.

From the study of all these open end configurations the final analytic formula

$$N' = a_o \left[\cos\left(\frac{\pi}{2W_s} \cdot (W_s - W_{eff})\right) - \cos\left(\frac{\pi}{2W_s} \cdot (W_s + W_{eff})\right)\right]$$

$$W_{eff} = Z_o \cdot h/Z_L \sqrt{\varepsilon eff}, \qquad \text{where } (Z_o = 120\pi \text{ ohms})$$

was developed for strips positioned in the middle of the package where the parameter a_o is a fine tuning parameter. In Figs. 9.4-7 representative results demonstrate the degree of accuracy achieved with this final analytic formula with $a_o=1$. In the figures x_m is the feedstrip position along the package width, x_s the feed length and x_p the package length.

Due to the CPU time limitations outlined it was not possible to quantify the relative maximum deviation or a mean deviation for the above analytic formula. A deviation in the resonance frequency of about 1% is large enough to cause a high maximum deviation in the reflection coefficient phase for frequencies near package resonance. The deviation of the predicted resonance frequency is a more suitable measure of accuracy and is estimated to be less than about 2%.

A whole variety of open end configurations for strip widths of w=0.4mm to w=10μm, for package widths of 2mm and 3mm and for package heights of 0.5mm and 1mm were analysed by setting the remaining fine tuning parameter to $a_o=1$,

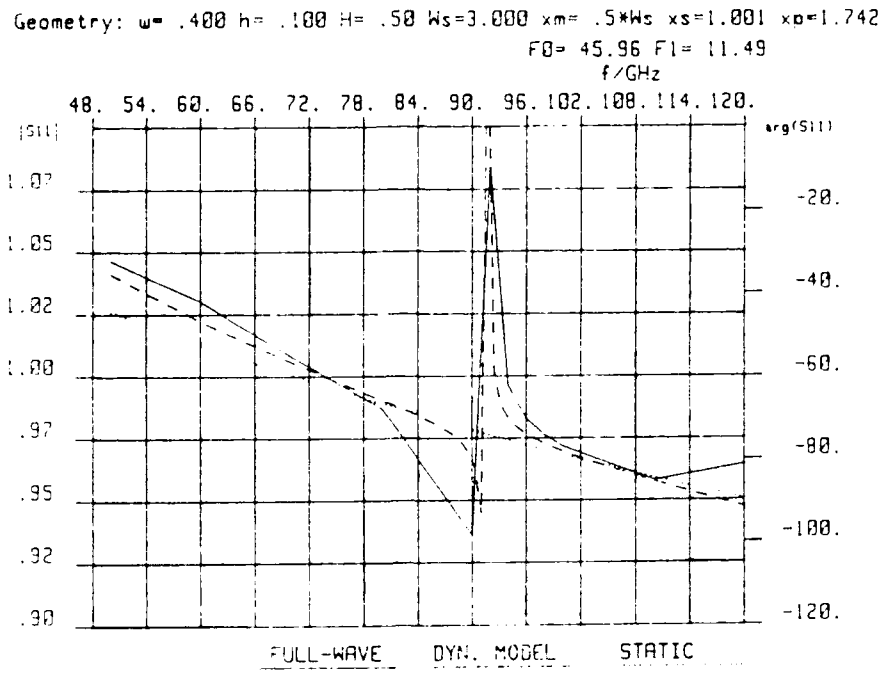


Fig. 9.4: S11 open end transformer ratio verification, first configuration

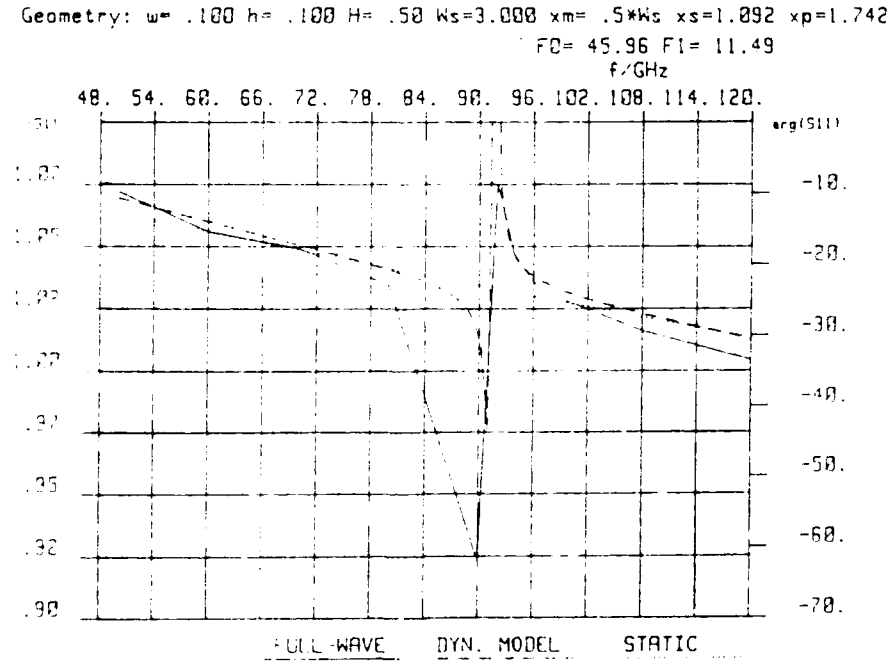


Fig. 9.5: S11 open end transformer ratio verification, second configuration

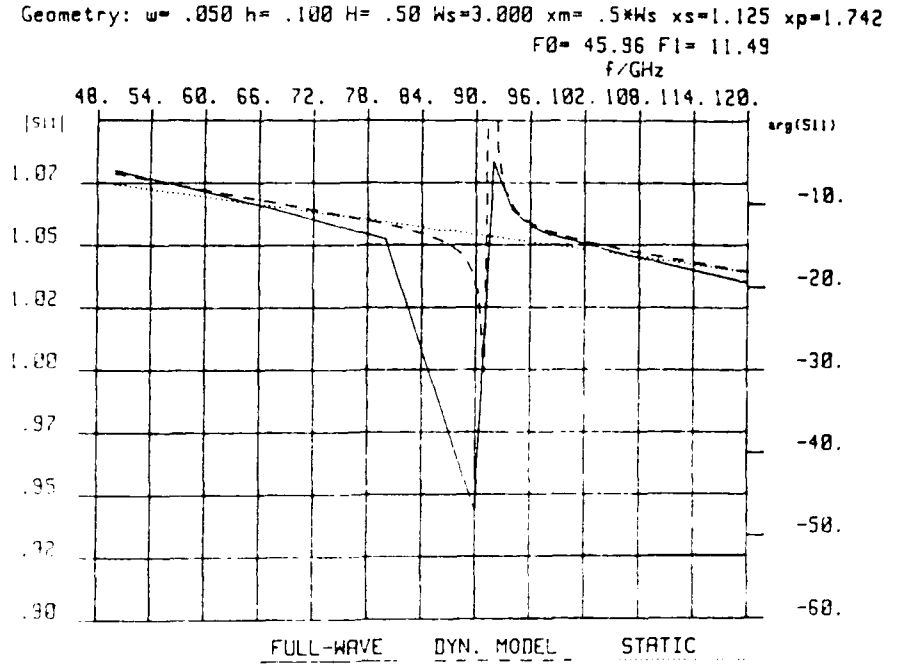


Fig. 9.6: S11 open end transformer ratio verification, third configuration

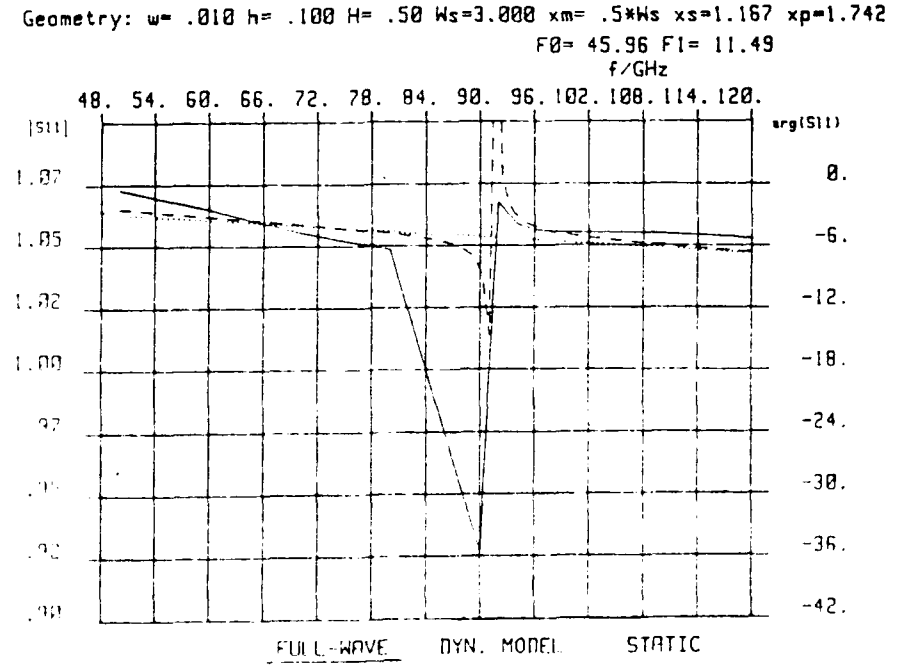


Fig. 9.7: S11 open end transformer ratio verification, fourth configuration

independent of strip width, package width or package height. To avoid very high CPU times for data base generation, strip widths less than 10 μm were not reconsidered in this final data base. Moreover, it was found that the behaviour of the LSM_0 mode excitation (transformer ratio) is nearly independent of width w for very small widths, thus eliminating the necessity of such additional data.

As outlined in Section 7, the transformer ratio provides the correct description of the coupling between the fundamental microstrip mode and the LSM_0 package mode for frequencies beyond LSM_0 mode cut-off, f_0. In that section the transformer ratio has been made dynamic for frequencies below the LSM_0 mode cut-off by the introduction of a correction factor

$$N_{dyn} = N' \cdot \cos^{f1}(0.5\,\pi.(f-f_0)/f_0), \qquad f<f_0.$$

where the fine tuning parameter f_1 can be fixed to the value of 2 for most open end cases in order to reduce the model complexity.

For each open end configuration under investigation the optimum value of the parameter, f_0 was determined as the parameter $f_0' = f_0/f_c^{LSM_0}$, where $f_c^{LSM_0}$ is the LSM_0 mode cut-off frequency, by computer fitting the frequency dependent scattering parameters. The mean deviation Fmean, the maximum deviation Fmax (in degrees) and the maximum deviation Fmaxr (in %) between the phase of the reflection coefficients taken from the data base and the equivalent circuit model, were determined and are given in Table 2 (Section 9.4) for each open end configuration. The individually fitted parameters f_0 are dependent on the geometry of the open end configurations. The maximum deviation is less than 2°. The computer based fitted values and the deviation are based on a frequency range $0<f<0.85\ f_{res}$. This restriction was introduced during optimisation because a small deviation in the predicted package resonance frequency causes significant deviations in the reflection coefficient phases for frequencies close to package resonance. This sensitiv range had to be avoided. The results in Figs. 9.8-10 show the

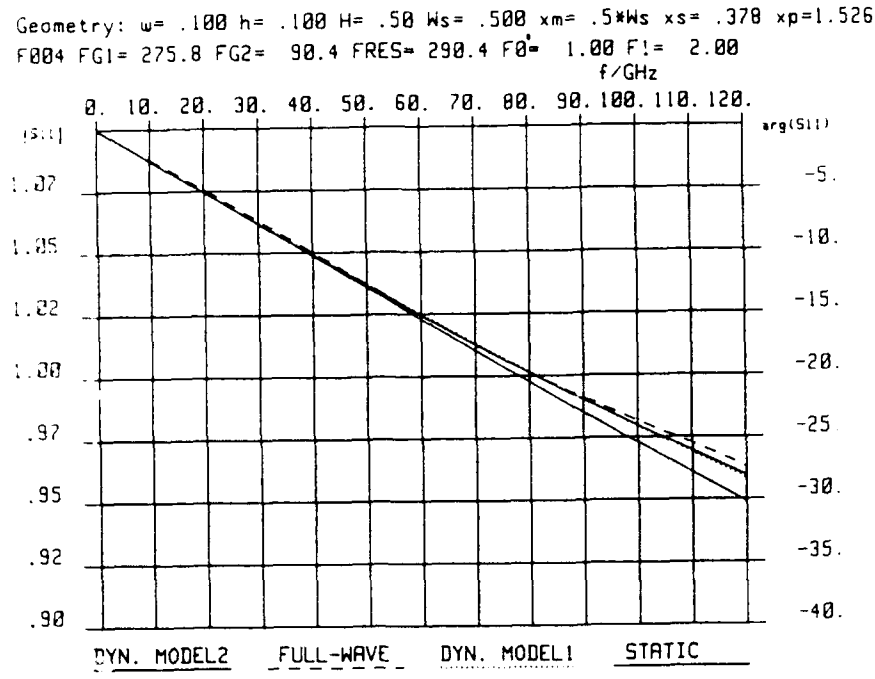


Fig. 9.8: S11 open end model verification, first configuration

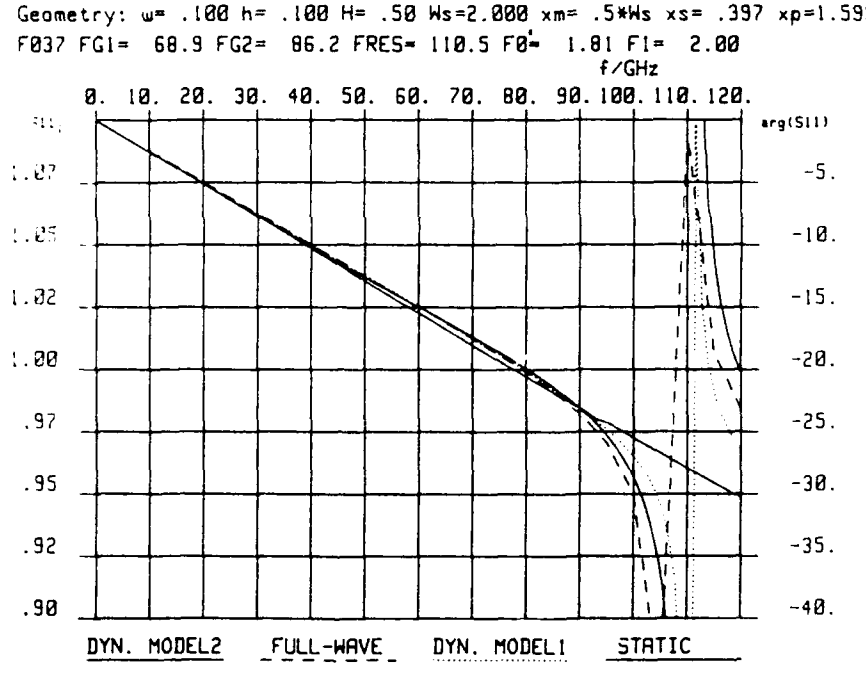


Fig. 9.9: S11 open end model verification, second configuration

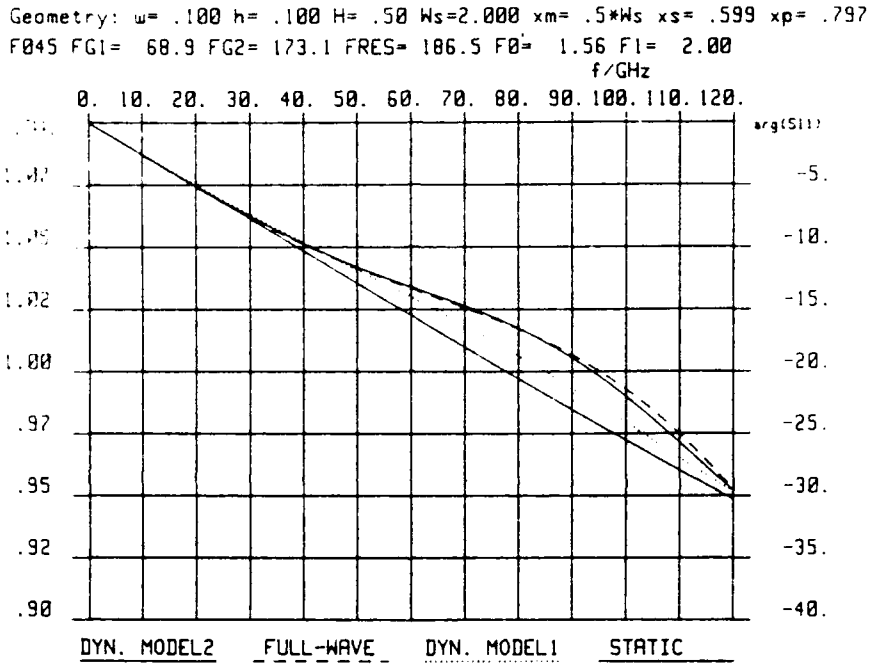


Fig. 9.10: S11 open end model verification, third configuration

reflection coefficients calculated from the equivalent circuit model together with full-wave results. The optimised parameter f_0' was found in most cases to be greater than 1 except for configurations with a substrate width Ws=0.5mm.

The analytic formula for f_0 would have to include a dependence on package length and the discontinuity position in the package. From modelling, a simple analytic formula for the parameter f_0 was obtained. This formula is

$$f_0 = 1.4\, f_c^{LSM_0} \cdot (1 + \exp(-0.0638 \cdot (W_s/h) \cdot H/h)) \cdot (1 - 2.33 \cdot \exp(-0.33 \cdot W_s/h))$$

In order to verify the final analytic formulae additional discontinuity configurations with strip width 200μm, 50μm, 20μm and 10μm were analysed. In Table 3 (Section 9.4) the mean deviation Fmean and the maximum deviations Fmax and Fmaxr are listed for all investigated open end configurations. The maximum deviation is less than 2.5%. A comparison of the reflection, coefficient phase of the fundamental microstrip mode and the data base results demonstrate the accuracy of the analytic formulae.

9.3. OPEN END MODEL SUMMARY

A summary of the analytic formulae for the open end discontinuity is given in this section where $Z_L^{microstrip}$ and $\varepsilon_{eff}^{microstrip}$ are computed according to procedures in Section 4. Units are MKS unless indicated otherwise.

Quasi-static open end length

$$dl/h = f_1 * f_2 * f_3$$

$$f_1 = 0.4372 * \left(1 + \frac{0.449}{\varepsilon_{eff}^{0.81} - 0.1890}\right)\left(1 - \frac{0.634}{(w/h)^{0.8544} - 0.87}\right)$$

$$f_2 = 1 - 0.1248 * \exp(-3.7259 * w/h)$$

$$f_3 = 1 - 0.0385 * h/w * \left(1 - \frac{2}{\pi} * \operatorname{atan}(W_s/h)\right)$$

Transformer Ratio

$$N = N_{dyn}$$

$$M = -N_{dyn}$$

$$N_{dyn} = \begin{cases} N' * \cos^2\left(0.5 * \pi * (f - f_0)/f_0\right) & f < f_0 \\ N' & f > f_0 \end{cases}$$

$$N' = 2/\pi * \left(\cos\left(\frac{\pi}{2W_s} * (W_s - W_{eff}) \right) - \cos\left(\frac{\pi}{2W_s} * (W_s + W_{eff}) \right) \right)$$

$$W_{eff} = Z_0 * h / Z_L^{microstrip} / \sqrt{\varepsilon_{eff}^{microstrip}}$$

$$f_0 = f_c * 1.4 * \left(1 + \exp(-0.0638 * W_s/h * H/h) \right) * (1 - 2.33 * \exp(-0.33 * W_s/h))$$

$$\varepsilon_{eff}(LSM_0) = \varepsilon_{stat}\left(1 - \left(\frac{f_c}{f}\right)^2\right)$$

with $$f_c = \frac{c_0}{2W_s \cdot \sqrt{\varepsilon_{stat}}}$$

and $$\varepsilon_{stat} = \frac{\varepsilon_r (H+h)}{\varepsilon_r H + h},$$

$$Z_L(LSM_0) = \frac{H+h}{W_s} \cdot \frac{Z_0}{\sqrt{\varepsilon_{stat}}} \cdot \frac{1}{\sqrt{1 - (f_c/f)^2}}$$

$(Z_0 = 120\pi\Omega,\ c_0 = 2.9979\ 10^8\ m/s)$

Range of Model Validity

The above models are valid for $\varepsilon_r = 12.9$ and the following geometric ranges:

quasi-static model:	50µm	< h	<	200µm
	0.025	< w/h	<	4
	5	< Ws/h	<	30
	5	< H/h	<	20

dynamic model: $0.2 \leq w/h \leq 1$

$5 \leq Ws/h \leq 30$

$5 \leq H/h \leq 20$

where the quasi-static model is the open end length and the dynamic model is that of Fig. 9.3.

The dynamic model range is valid for $0 \leq f*h \leq 12$ GHz mm. Package mode coupling has little influence for $0 \leq f*h \leq 3$ GHz mm and the quasi-static formulae can be used on their own.

9.4. REFERENCES AND TABLES

1. Kirschning, M. Jansen, R.H. and Koster, N.H.L.: Accurate model for open end effect of microstrip lines, Electronics Letters, Vol. 17 (1981), No. 3, 123-125.
2. Kirschning, M.: Development of models for the computer-aided design of hybrid and monolithic microstrip circuits (in German). University of Duisburg, W. Germany 1984.

Table 1

OPEN END GEOMETRY

	H	W	WS	HH	XP	XFEED	FC_DL
1	.10	.1000	.48	.50	1.075	.533	.994
2	.10	.0500	.50	.50	1.106	.550	.984
3	.10	.0200	.50	.50	1.130	.565	.975
4	.10	.0100	.50	.50	1.140	.570	.961
5	.10	.0050	.50	.50	1.147	.573	.965
6	.10	.0025	.50	.50	1.155	.575	.908
7	.10	.1000	.48	1.00	1.075	.533	1.000
8	.10	.0500	.50	1.00	1.100	.550	.982
9	.10	.0200	.50	1.00	1.130	.565	.976
10	.10	.0100	.50	1.00	1.140	.570	.963
11	.10	.0050	.50	1.00	1.147	.573	.966
12	.10	.0025	.50	1.00	1.155	.575	.909
13	.10	.1000	.48	3.00	1.075	.533	1.000
14	.10	.0500	.50	3.00	1.100	.550	.981
15	.10	.0200	.50	3.00	1.130	.565	.977
16	.10	.0100	.50	3.00	1.140	.570	.963
17	.10	.0050	.50	3.00	1.147	.573	.966
18	.10	.0025	.50	3.00	1.155	.575	.909
19	.10	.2000	.97	.50	1.033	.517	1.007
20	.10	.1000	.98	.50	1.075	.533	1.000
21	.10	.0500	1.00	.50	1.106	.550	.986
22	.10	.0200	1.00	.50	1.130	.565	.979
23	.10	.0100	1.00	.50	1.140	.567	1.000
24	.10	.0050	1.00	.50	1.150	.575	1.026
25	.10	.2000	.97	1.00	1.033	.517	1.010
26	.10	.1000	.98	1.00	1.075	.533	1.000
27	.10	.0500	1.00	1.00	1.100	.550	.982
28	.10	.0200	1.00	1.00	1.130	.565	.979
29	.10	.0100	1.00	1.00	1.140	.567	1.000
30	.10	.0050	1.00	1.00	1.150	.575	1.027
31	.10	.2000	.97	3.00	1.033	.517	1.010
32	.10	.1000	.98	3.00	1.075	.533	1.000
33	.10	.0500	1.00	3.00	1.100	.550	.983
34	.10	.0200	1.00	3.00	1.130	.565	.979
35	.10	.0100	1.00	3.00	1.140	.567	1.000
36	.10	.0050	1.00	3.00	1.150	.575	1.017
37	.10	.4000	3.00	.50	.988	.494	1.000
38	.10	.2000	2.97	.50	1.033	.517	1.000
39	.10	.1000	2.98	.50	1.075	.533	.990
40	.10	.0500	3.00	.50	1.106	.550	.980
41	.10	.0200	3.00	.50	1.130	.560	1.010
42	.10	.0100	3.00	.50	1.140	.570	1.017
43	.10	.4000	3.00	1.00	.988	.494	1.005
44	.10	.2000	2.97	1.00	1.033	.517	1.000
45	.10	.1000	2.98	1.00	1.075	.533	.995
46	.10	.0500	3.00	1.00	1.100	.550	.979
47	.10	.0200	3.00	1.00	1.130	.560	1.017
48	.10	.0100	3.00	1.00	1.140	.570	1.018
49	.10	.4000	3.00	3.00	.988	.494	1.009
50	.10	.2000	2.97	3.00	1.033	.517	1.005
51	.10	.1000	2.98	3.00	1.075	.533	1.000
52	.10	.0500	3.00	3.00	1.100	.550	.982
53	.10	.0200	3.00	3.00	1.130	.560	1.015
54	.10	.0100	3.00	3.00	1.140	.570	1.025
55	.10	.1000	.73	.50	1.075	.533	1.000
56	.10	.0500	.75	.50	1.106	.550	.986
57	.10	.0200	.75	.50	1.130	.565	.977
58	.10	.0100	.75	.50	1.140	.570	.961
59	.10	.0050	.75	.50	1.150	.575	1.016

60	.10	.0025	.75	.50	1.155	.575	.910
61	.10	.1000	.73	1.00	1.075	.533	1.000
62	.10	.0500	.75	1.00	1.100	.550	.983
63	.10	.0200	.75	1.00	1.130	.565	.979
64	.10	.0100	.75	1.00	1.140	.570	.967
65	.10	.0050	.75	1.00	1.150	.575	1.017
66	.10	.0025	.75	1.00	1.155	.575	.911
67	.10	.1000	.73	3.00	1.075	.533	1.000
68	.10	.0500	.75	3.00	1.100	.550	.982
69	.10	.0200	.75	3.00	1.130	.565	.979
70	.10	.0100	.75	3.00	1.140	.570	.963
71	.10	.0050	.75	3.00	1.150	.575	1.017
72	.10	.0025	.75	3.00	1.155	.575	.911

Table 2

	OPEN END GEOMETRY					OPTIMIZED CORRECTION FACTORS			
	W	WS	HH	XP	XFEED	FO'	Fmean	Fmax	Fmaxr
1	.100	.50	.50	2.030	.502	.785	.014	.380	.026
2	.100	.50	.50	1.018	.509	.803	.017	.448	.032
3	.100	.50	.50	.678	.509	.773	.019	.477	.034
4	.100	.50	.50	1.526	.378	.934	.010	.246	.044
5	.100	.50	.50	.763	.380	.931	.011	.246	.044
6	.100	.50	.50	.509	.380	.922	.013	.491	.024
10	.100	.50	1.00	2.030	.502	.633	.017	.432	.030
11	.100	.50	1.00	1.018	.509	.650	.021	.501	.036
12	.100	.50	1.00	.678	.509	.626	.024	.653	.039
13	.100	.50	1.00	1.526	.378	.758	.011	.326	.042
14	.100	.50	1.00	.763	.380	.764	.011	.386	.042
15	.100	.50	1.00	.509	.380	.750	.014	.595	.025
19	.100	1.00	.50	2.030	.502	1.186	.008	.325	.016
20	.100	1.00	.50	1.018	.509	1.172	.010	.263	.025
21	.100	1.00	.50	.678	.509	1.133	.010	.252	.024
22	.100	1.00	.50	1.526	.378	1.484	.013	.416	.051
23	.100	1.00	.50	.763	.380	1.412	.011	.272	.051
24	.100	1.00	.50	.509	.380	1.397	.004	.116	.029
28	.100	1.00	1.00	2.030	.502	1.012	.007	.214	.017
29	.100	1.00	1.00	1.018	.509	1.008	.010	.279	.025
30	.100	1.00	1.00	.678	.509	.967	.012	.299	.026
31	.100	1.00	1.00	1.526	.378	1.332	.013	.419	.050
32	.100	1.00	1.00	.763	.380	1.261	.011	.290	.050
33	.100	1.00	1.00	.509	.380	1.253	.004	.131	.028
37	.100	2.00	.50	1.599	.397	1.803	.014	.665	.035
38	.100	2.00	.50	1.599	.795	1.286	.022	1.168	.052
41	.100	2.00	.50	1.198	.599	1.562	.009	.192	.026
42	.100	1.97	.50	1.195	.898	1.210	.022	.827	.040
44	.100	2.00	.50	.799	.400	2.147	.012	.355	.031
45	.100	2.00	.50	.797	.599	1.536	.019	.941	.041
46	.100	2.00	1.00	1.599	.397	1.615	.024	1.726	.062
47	.100	2.00	1.00	1.599	.795	1.173	.017	.593	.032
48	.100	2.00	1.00	1.591	1.194	.937	.032	.986	.041
50	.100	2.00	1.00	1.198	.599	1.538	.011	.740	.028
51	.100	1.97	1.00	1.195	.898	1.112	.015	.827	.033
53	.100	2.00	1.00	.799	.400	2.883	.018	.753	.034
54	.100	2.00	1.00	.797	.599	1.480	.007	.506	.021
55	.100	3.00	.50	1.599	.397	2.815	.019	.293	.036
56	.100	3.00	.50	1.599	.795	1.618	.030	1.124	.057
58	.100	3.00	.50	1.199	.299	.428	.017	.498	.043
59	.100	3.00	.50	1.198	.599	1.962	.020	.766	.035
60	.100	2.97	.50	1.195	.898	1.533	.050	1.695	.092
62	.100	3.00	.50	.799	.400	2.662	.010	.229	.032
63	.100	3.00	.50	.797	.599	1.954	.042	1.954	.091
64	.100	3.00	1.00	1.599	.397	1.632	.007	.171	.038
65	.100	3.00	1.00	1.599	.795	1.510	.024	.733	.035
66	.100	3.00	1.00	1.591	1.194	1.191	.054	1.547	.077
67	.100	3.00	1.00	1.199	.299	.273	.030	1.301	.054
68	.100	3.00	1.00	1.198	.599	1.919	.010	.733	.027
69	.100	2.97	1.00	1.195	.898	1.441	.024	.876	.050
71	.100	3.00	1.00	.799	.400	4.670	.021	.861	.035
72	.100	3.00	1.00	.797	.599	1.881	.011	.397	.020

Table 3

	OPEN END GEOMETRY					OPTIMIZED CORRECTION FACTORS			
	W	WS	HH	XP	XFEED	FO'	Fmeam	Fmax	Fmaxr
1	.100	.50	.50	2.030	.502	.930	.021	1.499	.064
2	.100	.50	.50	1.018	.509	.930	.024	1.413	.060
3	.100	.50	.50	.678	.509	.930	.031	2.044	.090
4	.100	.50	.50	1.526	.378	.930	.016	.228	.044
5	.100	.50	.50	.763	.380	.930	.016	.241	.044
6	.100	.50	.50	.509	.380	.930	.013	.562	.024
10	.100	.50	1.00	2.030	.502	.805	.025	1.814	.077
11	.100	.50	1.00	1.018	.509	.805	.028	1.746	.074
12	.100	.50	1.00	.678	.509	.805	.036	2.405	.105
13	.100	.50	1.00	1.526	.378	.805	.016	.642	.043
14	.100	.50	1.00	.763	.380	.805	.016	.673	.043
15	.100	.50	1.00	.509	.380	.805	.014	1.054	.044
19	.100	1.00	.50	2.030	.502	1.332	.018	.837	.042
20	.100	1.00	.50	1.018	.509	1.332	.025	1.034	.051
21	.100	1.00	.50	.678	.509	1.332	.040	1.754	.088
22	.100	1.00	.50	1.526	.378	1.332	.021	1.018	.051
23	.100	1.00	.50	.763	.380	1.332	.019	.702	.051
24	.100	1.00	.50	.509	.380	1.332	.013	.623	.029
28	.100	1.00	1.00	2.030	.502	1.282	.021	1.021	.048
29	.100	1.00	1.00	1.018	.509	1.282	.026	1.164	.055
30	.100	1.00	1.00	.678	.509	1.282	.040	1.873	.089
31	.100	1.00	1.00	1.526	.378	1.282	.019	.543	.050
32	.100	1.00	1.00	.763	.380	1.282	.018	.226	.050
33	.100	1.00	1.00	.509	.380	1.282	.009	.173	.028
37	.100	2.00	.50	1.599	.397	1.398	.026	.778	.044
38	.100	2.00	.50	1.599	.795	1.398	.028	1.169	.052
41	.100	2.00	.50	1.198	.599	1.398	.028	.665	.045
42	.100	1.97	.50	1.195	.898	1.398	.046	1.024	.086
44	.100	2.00	.50	.799	.400	1.398	.058	2.109	.108
45	.100	2.00	.50	.797	.599	1.398	.039	.982	.069
46	.100	2.00	1.00	1.599	.397	1.396	.025	1.648	.059
47	.100	2.00	1.00	1.599	.795	1.396	.025	.638	.040
48	.100	2.00	1.00	1.591	1.194	1.396	.058	1.292	.116
50	.100	2.00	1.00	1.198	.599	1.396	.018	.750	.028
51	.100	1.97	1.00	1.195	.898	1.395	.034	.948	.070
53	.100	2.00	1.00	.799	.400	1.396	.038	2.087	.077
54	.100	2.00	1.00	.797	.599	1.396	.015	.507	.022
55	.100	3.00	.50	1.599	.397	1.400	.024	1.192	.052
56	.100	3.00	.50	1.599	.795	1.400	.045	1.124	.067
58	.100	3.00	.50	1.199	.299	1.400	.051	.654	.127
59	.100	3.00	.50	1.198	.599	1.400	.053	1.405	.114
60	.100	2.97	.50	1.195	.898	1.400	.055	1.695	.092
62	.100	3.00	.50	.799	.400	1.400	.055	1.666	.113
63	.100	3.00	.50	.797	.599	1.400	.085	2.104	.172
64	.100	3.00	1.00	1.599	.397	1.400	.013	.187	.038
65	.100	3.00	1.00	1.599	.795	1.400	.026	.733	.035
66	.100	3.00	1.00	1.591	1.194	1.400	.051	1.547	.077
67	.100	3.00	1.00	1.199	.299	1.400	.060	1.301	.131
68	.100	3.00	1.00	1.198	.599	1.400	.028	.733	.058
69	.100	2.97	1.00	1.195	.898	1.400	.025	.876	.050
71	.100	3.00	1.00	.799	.400	1.400	.039	1.798	.066
72	.100	3.00	1.00	.797	.599	1.400	.037	1.036	.081
76	.050	.50	1.00	1.754	.525	.805	.020	.874	.065
77	.020	.50	1.00	1.812	.540	.805	.022	.248	.034
78	.010	.50	1.00	1.841	.547	.805	.025	.117	.041
79	.200	.97	.50	1.620	.481	1.325	.020	1.554	.046

80	.050	1.00	.50	1.754	.525	1.332	.016	.450	.037
81	.020	1.00	.50	1.812	.540	1.332	.010	.084	.019
82	.010	1.00	.50	1.843	.553	1.332	.014	.064	.029
83	.200	.97	1.00	1.620	.481	1.270	.022	1.801	.049
84	.050	1.00	1.00	1.754	.525	1.282	.019	.561	.044
85	.020	1.00	1.00	1.812	.540	1.282	.012	.165	.024
86	.010	1.00	1.00	1.843	.553	1.282	.014	.078	.023
89	.050	2.00	.50	1.597	.477	1.398	.026	.504	.049
90	.020	2.00	.50	1.600	.478	1.398	.034	.356	.062
91	.010	2.00	.50	1.596	.477	1.398	.050	.400	.093
94	.050	2.00	1.00	1.597	.477	1.396	.023	1.029	.062
95	.020	2.00	1.00	1.600	.478	1.396	.031	.723	.079
96	.010	2.00	1.00	1.596	.477	1.396	.046	.718	.111
98	.200	2.97	.50	1.597	.473	1.400	.032	1.501	.069
99	.050	3.00	.50	1.597	.477	1.400	.025	.401	.054
100	.020	3.00	.50	1.595	.479	1.400	.058	.456	.098
101	.010	3.00	.50	1.596	.477	1.400	.035	.210	.075
103	.200	2.97	1.00	1.597	.473	1.400	.019	1.322	.037
104	.050	3.00	1.00	1.597	.477	1.400	.014	.241	.025
105	.020	3.00	1.00	1.595	.479	1.400	.049	.623	.073

10. MICROSTRIP GAP MODEL

The physical structure of the gap discontinuity in a package showing the two current source areas used in the full wave analysis is shown in Fig. 10.1.

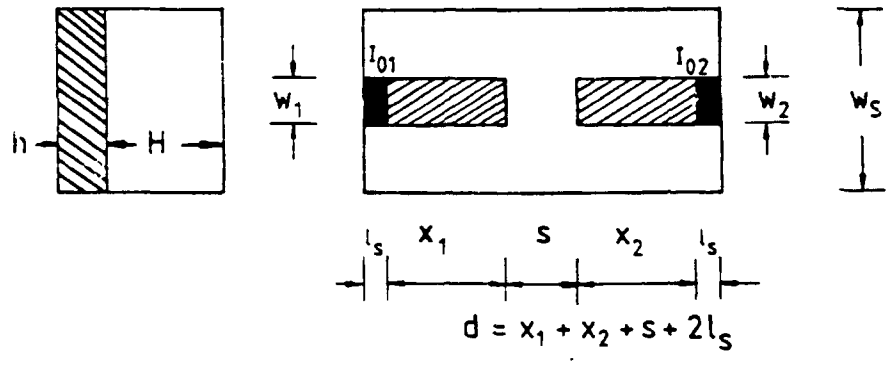


Fig. 10.1: Microstrip gap discontinuity

The structure represents two microstrip lines of width w_1, w_2 and lengths x_1, x_2 and source length l_s respectively, separated by a gap s. The microstrip structure is positioned centrally in a package of width w_s, cover height, H and situated on a substrate of thickness h.

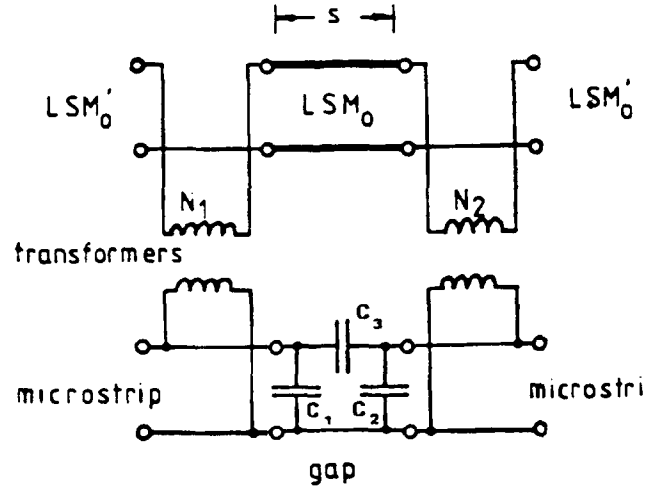


Fig. 10.2: Equivalent circuit for the gap discontinuity

Fig. 10.2 shows the 4-port equivalent circuit for the gap discontinuity. This model contains a quasi-static equivalent circuit for the discontinuity description of the fundamental microstrip mode and a transmission line between the reference planes which describes the behaviour of the parasitic LSM_0' mode. The transformers N1 and N2 represent the coupling between the fundamental microstrip modes and the parasitic LSM_0' modes and the LSM_0' mode ports are loaded with transmission lines. These transmission lines are terminated by a short circuit to represent the electric end walls of the package (see Fig. 10.3).

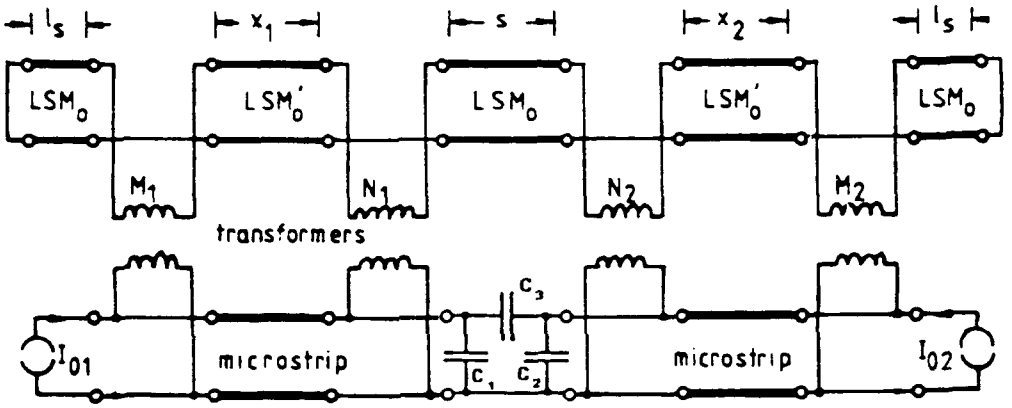


Fig. 10.3: Dynamic equivalent circuit of the microstrip gap in a package

In this circuit the transformers M_1 and M_2 represent the excitation of the LSM_0 mode at the current sources.

10.1. ANALYTIC FORMULA FOR THE STATIC MODEL

The first step in obtaining a suitable gap model is the development of analytic formulae for the quasi-static circuit part. In the case of the microstrip gap discontinuity this means the determination of analytic formulae for the three capacitances of the π-equivalent circuit, Fig. 10.4.

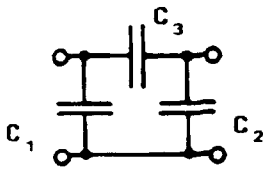


Fig. 10.4: π-equivalent circuit model for the quasi-static microstrip gap discontinuity.

In order to determine these formulae a quasi-static S-parameter data base was generated over the geometric range of interest. A total of 960 different gap configurations were analysed. However this number of different gap configurations was reduced by omitting certain possible combinations because of higher mode excitation.

The dielectric constant was fixed to ε_r= 12.9 (GaAs).

The position of the strips was fixed to the centre of the package (X_m= 0.5*w_s). To cover the geometry range from 1mm to 3mm for both package lateral dimensions for substrate thicknesses of h=0.05mm to 0.2mm, the range of normalized package parameters w_s/h and H/h for the data base generation was set $5 \leq w_s/h$, $H/h \leq 60$. Upper limit configurations were eliminated because high H/h ratios caused excitation of LSE modes in the package and high w_s/h ratios the excitation of the second LSM mode with in the frequency range of interest. Therefore, considering a 0.1mm substrate, the physical parameter range for the data base generation was fixed to $0.5 \leq w_s \leq$ 3mm and $1 \leq H \leq$ 3mm.

The data base was generated for the following normalized strip and gap widths. $0.025 \leq w_1/h \leq 4$, $1 \leq w_2/w_1 \leq 3$ and $0.1 \leq g/h \leq 1.5$. With respect to a 0.1mm substrate, this means denormalized parameter ranges of $2.5\mu m \leq w_1 \leq 400\mu m$, $1 \leq w_2/w_1 \leq 3$ and $10\mu m \leq g \leq 150\mu m$.

For the 0.1 mm substrate, the configurations were analysed over the frequency range 0-120 GHz, equivalent to 0-60 GHz for a 0.2 mm substrate. The normalised frequency range is in both cases $0 \leq f*h \leq 12\text{GHz}*\text{mm}$. For the quasi-static modelling the S-parameter database was used for frequencies up to 30 GHz.

Convergence investigations were done for some configurations with respect to the number of expansion functions and spectral density. It was found that the computation accuracy increased with the number of expansion functions and spectral density. Furthermore the analysis of discontinuity configurations with narrow strips required a higher spectral density than the analysis of wide strip configurations. As a result the accuracy of the data base generation for narrow strips is less than the accuracy achieved for wide strips. The accuracy of the scattering parameter phase is expected to be better than 5%.

The generation of final quasi-static formulae was completed by fitting the scattering parameters of the gap database configurations to the equivalent circuit model by computer matching. As with the open end discontinuity correction factors of the form.

$$f_{c\text{-}Ci} = \frac{Ci \text{ data base}}{Ci \text{ state-of-the-art}} \qquad i=1,2,3$$

were generated for final model tuning, the state-of-the-art analytic formulae $Ci_{\text{ state-of-the-art}}$ having been taken from published literature (1). The correction factors $f_{c\ Ci}$ were found to have a value near 1 except for very small strips of width 5μm and 2.5μm. The maximum relative deviation between the data base and the previous formulae for

$$\left| 1\text{-}S_{ij}{}_{\text{state-of-the-art}} \Big/ S_{ij}{}_{\text{ data base}} \right|$$

1.82% for S11, 4.12% for S22 and 48.5% for S12. The average errors are 0.177% for S11, 0.181% for S22 and 15.2% for S12.

Using as a base the state-of-the-art analytic formulae, the final analytic formula for the quasi-static gap capacitances are

$$2*\pi*f * C_3 / mS = Q1 * \pi *(f/GHz) * (h/mm) * \exp(-2.011*g/h*(1.-0.111*w_1/h)^{0.2935})$$
$$* (1+4.12 * (1-\exp(-0.6688*(h/w_1)^{0.5} * (w_2/w_1)))$$
$$* (1.+0.966*\exp(-14.47*g/h + 0.6645*w_1/h))$$

$$Q1 = 0.0594 * (0.0428 * (1-0.5895 * (w_1/h)) + (w_1/h)^{1.213/(1+0.0985*(w_2/w_1-1)^{1.1}})$$

$$2*\pi*f * C_1 / mS = 2\pi * (f/GHz) * (C_{1\ open\ end}/pF) * (Q2+Q3) / (1+Q2)$$
$$2*\pi*f * C_2 / mS = 2\pi * (f/GHz) * (C_{2\ open\ end}/pF) * (Q2+Q4) / (1+Q2)$$

$$Q2 = 0.1381 * (w_1/h+9.0) * (g/h)^{3.64} + 2.25 * (g/h)^{1.14} * (1.52+0.389 * w_1/h) / (1+0.792 * w_1/h)$$
$$Q3 = \exp(-0.9545*(w_2/w_1)^{1.23}) - 0.37$$
$$Q4 = \exp(-0.9545*(w_1/w_2)^{1.23}) - 0.37$$

where the abbreviations $C_{1\ open\ end}$ and $C_{2\ open\ end}$ denote the static open end capacitances of the microstrips of width w_1 and w_2, respectively, and

$$C_{open\ end} = \frac{\tan(\beta.dl_{open\ end})}{2\pi f.Z_L^{microstrip}}$$

where g is the gap, $Z_L^{microstrip}$ is the microstrip characteristic impedance and β the microstrip propagation constant.

The maximum relative deviation, between the data base and the new formula is 1.14% for S11, 1.68% for S22 and 7.44% for S12. The average errors based on all discontinuity configurations investigated are 0.142% for S11, 0.140% for S22 and 2.8% for S12. The mean deviation and maximum deviations for scattering parameters S11 and S22 are obviously very small. The maximum relative deviations for parameter S12 are found for large gap widths, where the absolute values of elements C3 of the π-equivalent circuits are very small. In Table 1 (Section 10.5) the geometry parameters, the mean deviation from the data base scattering parameters (in dBs) and the deviation of the

susceptance (in mS) of the elements of the π-equivalent circuit to the data base values are listed for f*h=2.54. This normalised frequency was chosen to show the accuracy of the state-of-the-art analytic formulae. The accuracy, originally given as a susceptance absolute error, is better than 0.1mS. Such a degree of accuracy is also obtained by the new analytic formulae for the static part of the discontinuity model, but at the same time it is valid for an increased parameter range for very large and very narrow strips.

10.2. DESCRIPTIONS OF THE TRANSFORMERS IN THE DYNAMIC MODEL

Preliminary analyses (Figs. 10.5-8, where G is the gap parameter s and xp the package length), show that the coupling between the fundamental microstrip mode and the parasitic LSM_0 mode is well described by the dynamic circuit model using an approximate value for the LSM effective dielectric constant. The good agreement between the full-wave results and those predicted by the gap model was achieved by making use of the transformer ratio formulae developed in the open end discontinuity model. In order to refine the transformer ratios formulae for the general case the coupling between the fundamental microstrip mode and the LSM_0 package mode was further studied.

In preparation for a more in depth study a full wave data base was generated for the following geometric parameters:

strip width w_1: 400μm, 100μm, 20μm, 10μm
strip width ratio w_1/w_2: 1, 2, 3
gap widths: 100μm, 50μm, 20μm, 10μm
substrate width W_s:2mm, 3mm
cover height H:05mm, 1mm

This combination of geometric parameters represented a total of 192 configurations of which a subset of 117 configurations was selected.

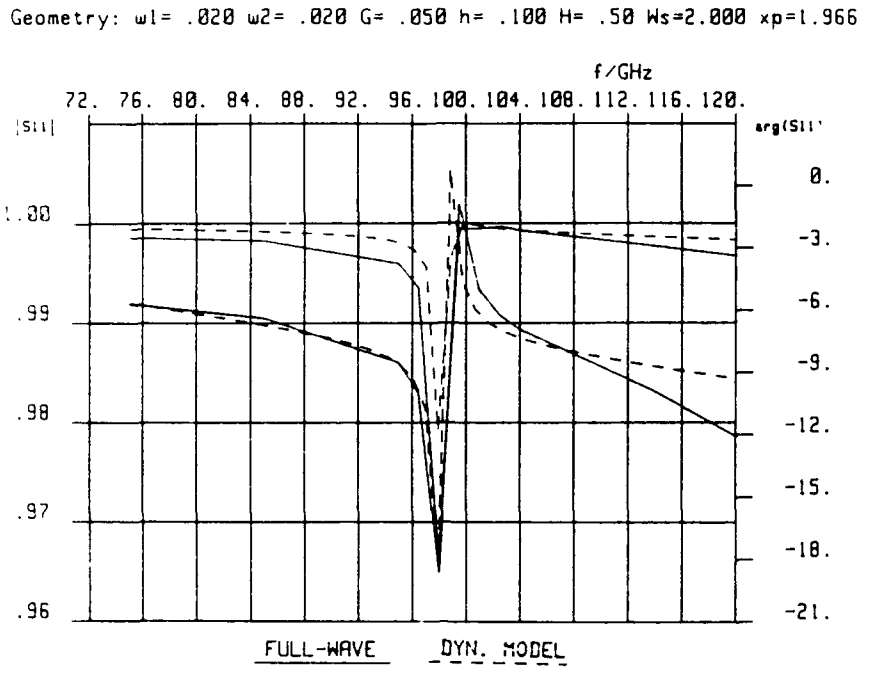


Fig. 10.5: S11 of microstrip gap: gap 0.05 mm

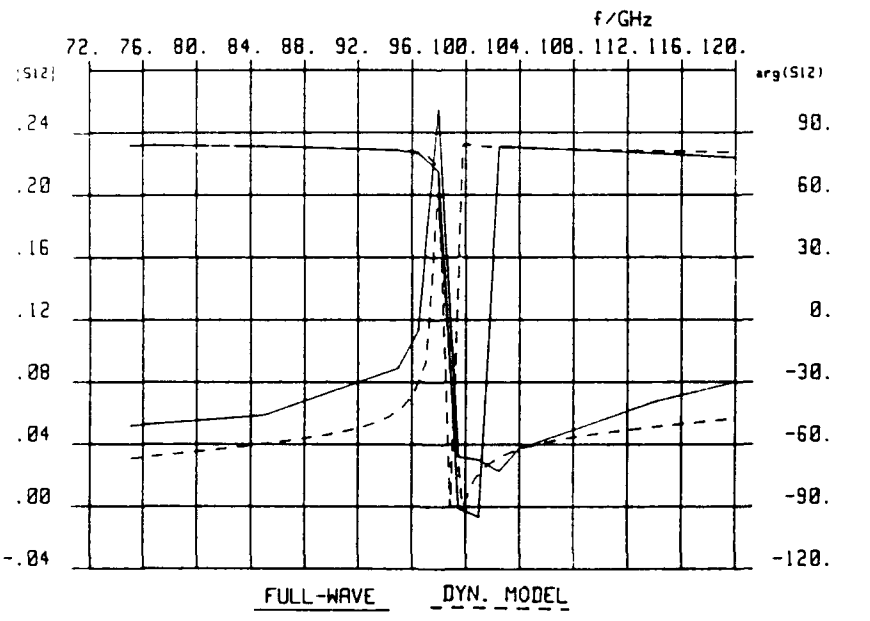


Fig. 10.6: S12 of microstrip gap: gap 0.05 mm

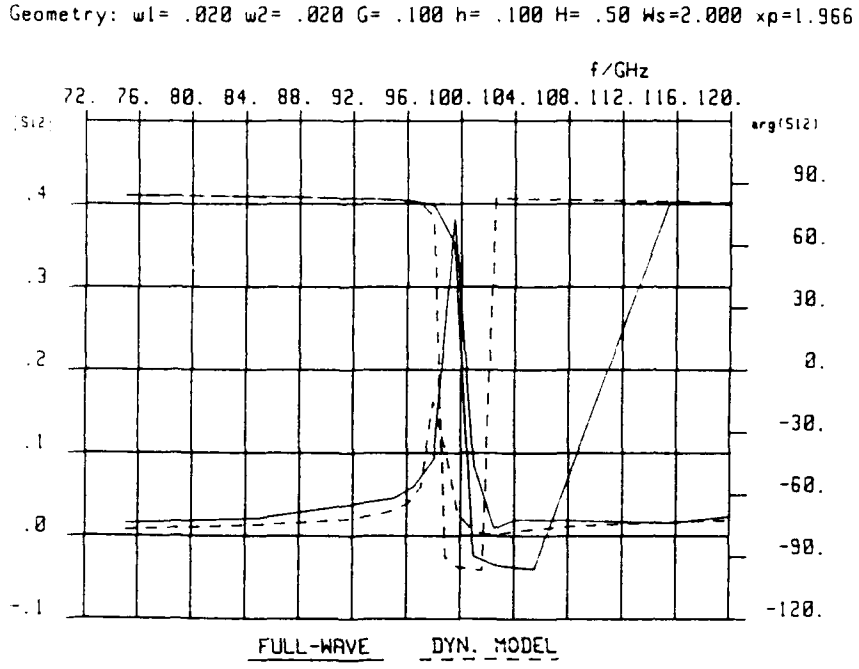


Fig. 10.7: S11 of microstrip gap: gap 0.10 mm

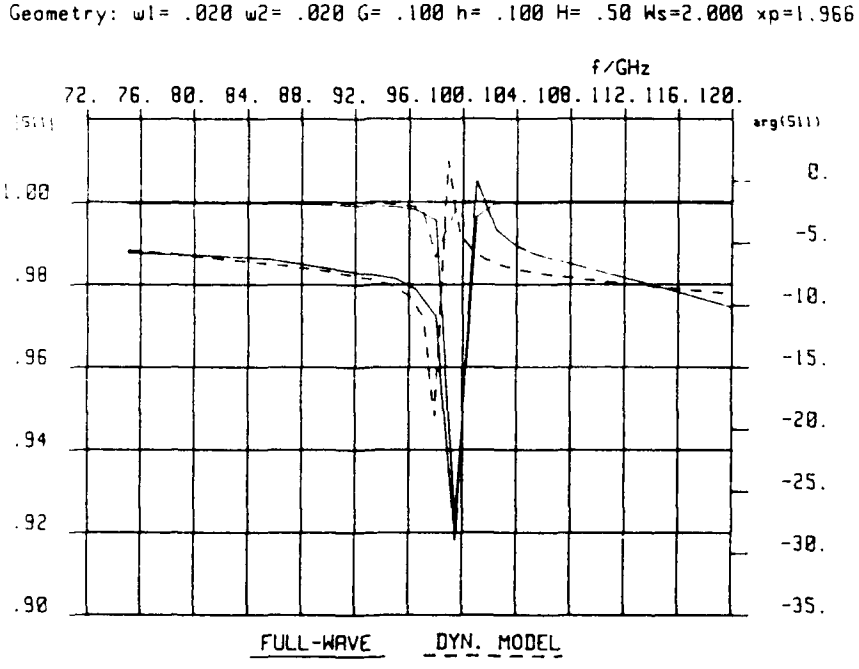


Fig. 10.8: S12 of microstrip gap: gap 0.10 mm

In model element de-embedding procedure the dynamic equivalent circuit of Fig. 10.3 was used. During the de-embedding the following assumptions were made:

- the transformer ratios N1 and N2 to be calculated using the same analytic formulae, introducing the respective strip width of the feed lines and
- the transformer ratios M1 and M2 to be determined by setting: M1=-N1 and and M2=-N2

The negative signs of the transformer ratios M1 and M2 are related to the way of connecting the ports of the transformer ports to the equivalent circuit. This also considers that for zero current sources the parasitic wave excitation at the source ends has the same mechanism as at the gap ends.

The optimum values of the transformer ratios N_{opt} for every single gap configuration were determined by fitting the equivalent circuit model to the full-wave data base sets. It was found that the analytic formulae for the transformer ratios developed for the open end discontinuity have to be modified by a multiplication factor of about 0.6 to obtain an optimum fit in the data base. With this modification, the final analytic formula for the transformer ratios N1...M2 is:

$$N_i, -M_i = \frac{1.2}{\pi} \cdot \left[\cos\left(\frac{\pi}{2W_s} \cdot (w_s - w_{eff,i})\right) - \cos\left(\frac{\pi}{2W_s} \cdot (w_s + w_{eff,i})\right)\right]$$

$$w_{eff,i} = Z_o \cdot h / Z_{L,i}^{microstrip} / \sqrt{\varepsilon_{eff,i}^{microstrip}}$$

where $Z_o = 120\pi$ ohms.

A parallel investigation showed that for narrow gap widths in which the strip to strip interaction is quite strong, the open end transformer value does not fit the formulae. The optimum transformer ratios N_{opt} computed by fitting

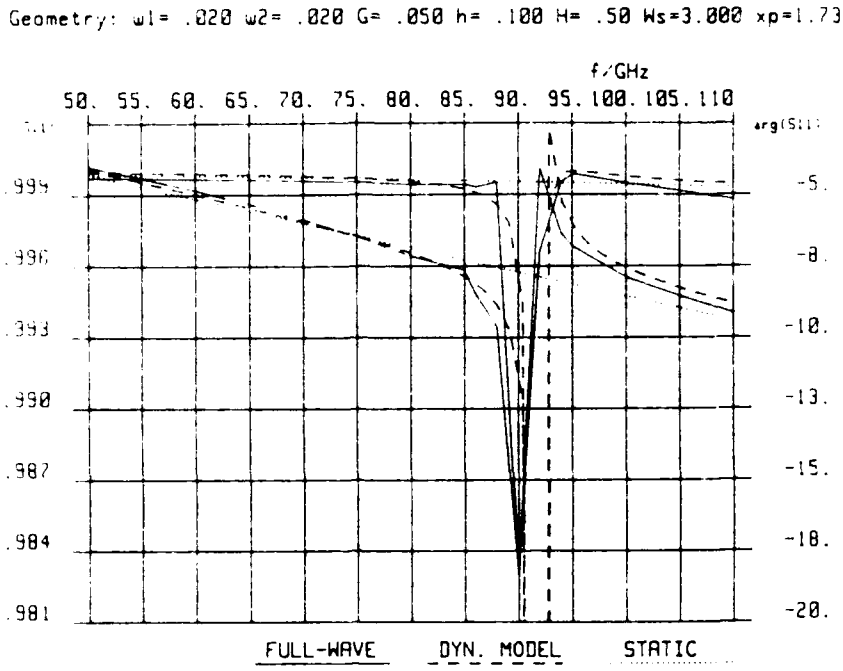


Fig. 10.9: S11 for gap with same feed strip widths: gap 50μm

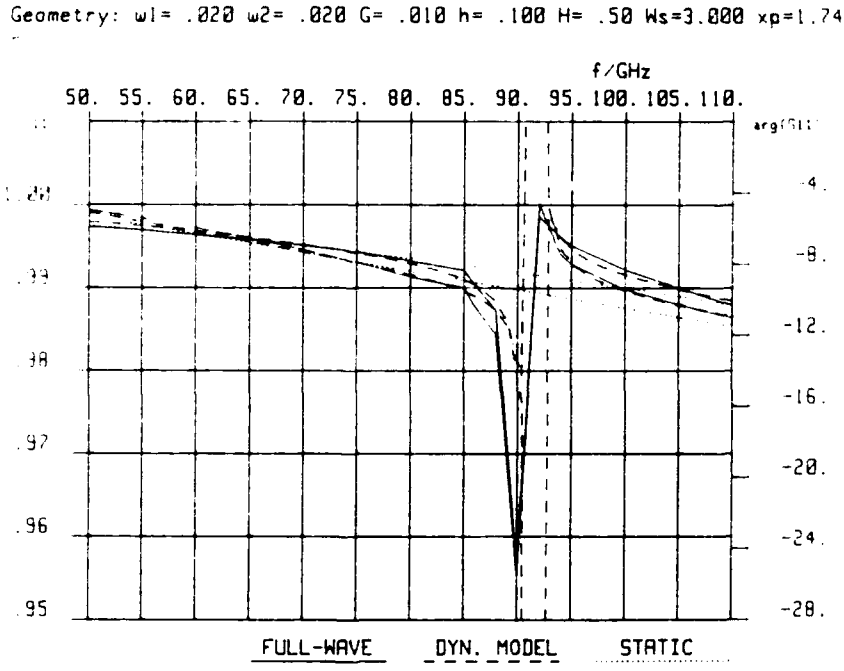


Fig. 10.10: S11 for gap with same feed strip widths: gap 10μm

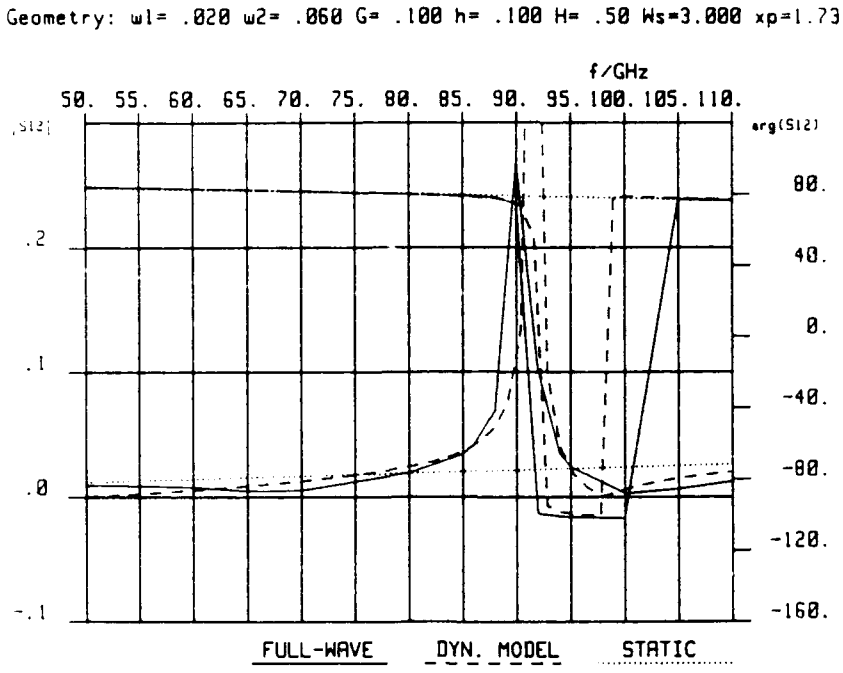


Fig. 10.11: S12 for gap with different feed strip widths: gap 100μm

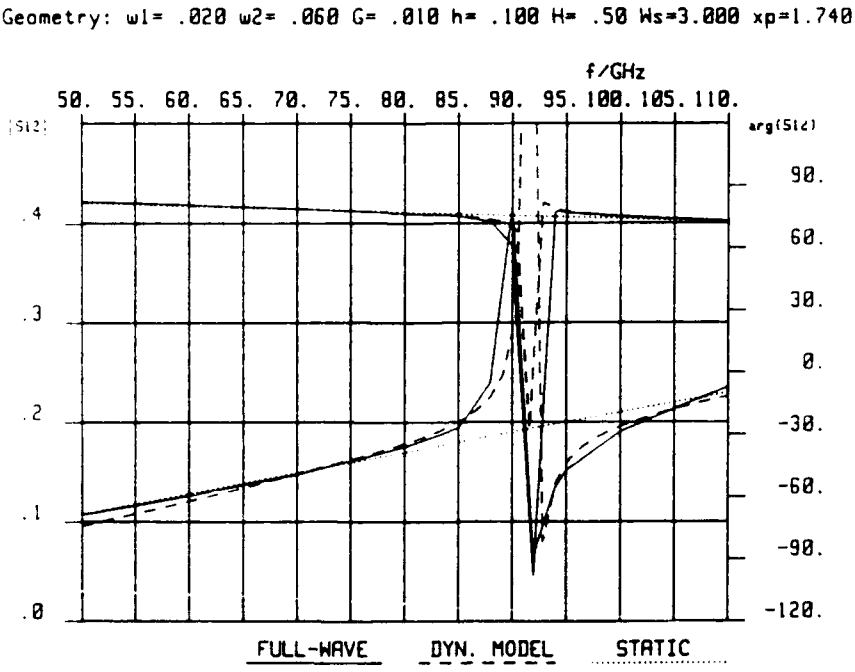


Fig. 10.12: S12 for gap with different feed strip widths: gap 10μm

Geometry: w1= .100 w2= .100 G= .050 h= .100 H=1.00 Ws=2.967 xp=1.825

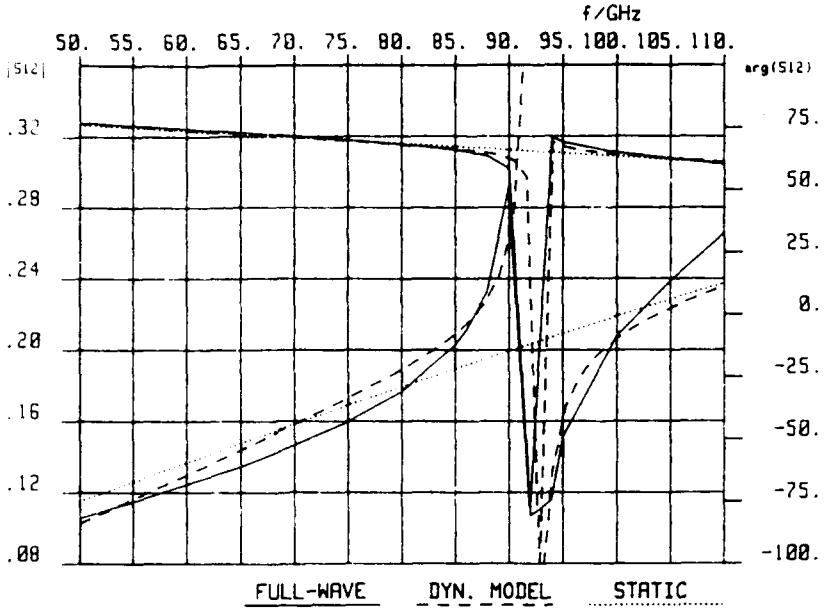


Fig. 10.13: S12 for gap of strip width ratio 1

Geometry: w1= .100 w2= .300 G= .050 h= .100 H=1.00 Ws=3.000 xp=1.825

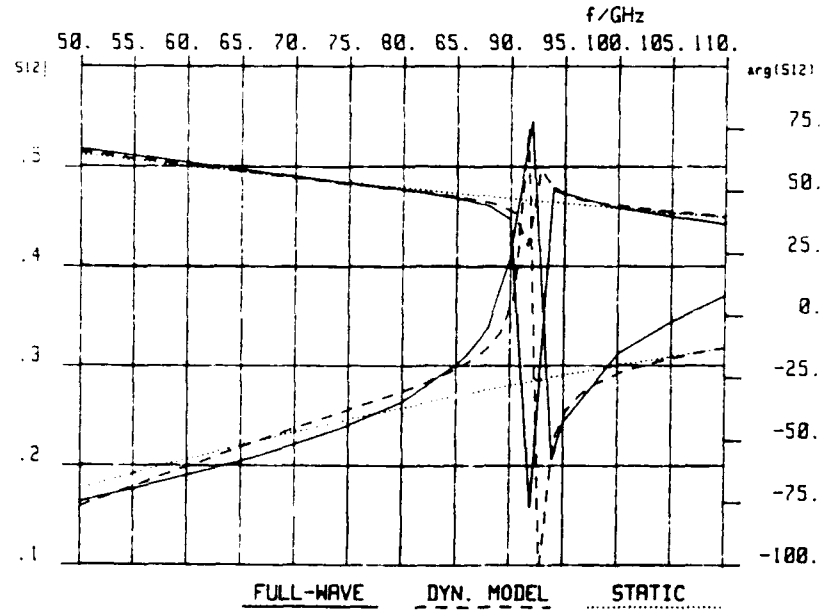


Fig. 10.14: S12 for gap of strip width ratio 3

the equivalent circuit model S-parameters to the data base sets have been related to the analytical predictions and are given in Table 2 (Section 10.5) in the indirect form

$FC_N = N_{opt}/N_{analytic}$.

As can be seen for most of the discontinuity configurations the factor FC_N has a value near 1, deviations of up to 44% occurring. These larger deviations however do not indicate an incorrectly predicted transformer ratio. It was found that if the predicted resonance frequency in the equivalent circuit model differs slightly from the numerically computed resonance frequency, the model fitting became sensitive. To overcome these difficulties, the frequency range $0.9*f_{res} < f_{res} < 1.1*f_{res}$ was not considered in a computer refitting for most of the configurations with the result that the above formulae were found to be correct.

The Figs. 10.9-10 show the magnitude and the S11 phase of a symmetrical gap configuration of 20μm strip width; gap widths of 50μm, and 10μm. A second set of S12 results for strip width w_1=20μm and w_2=60μm; gap widths of 100μm and 10μm is given in Figs. 10.11-12. In the third set of gap configurations, the strip width ratio has been changed from a value of 1 to 3 for fixed strip widths of 100μm and a gap width of 50μm. These results are given in Figs. 10.13-14 for S12.

These results and others show that the strength of the coupling between the fundamental microstrip mode and the parasitic LSM_0 mode can be predicted by applying the above analytic formulae for the transformer ratios in the gap equivalent circuit model with good agreement.

10.3. TRANSFORMER ANALYTIC FORMUALE FOR THE FREQUENCY, TRANSITION REGION

Having developed formulae for the quasi-static model and the transformer ratios, fundamental microstrip mode and the parasitic LSM_0 mode near the package, the equivalent circuit model was refined for the whole frequency range (0-120GHz) including frequencies in the transition region. Investigations on the open end discontinuity have revealed that this fine tuning can be achieved by choosing of a suitable frequency dependent analytic formula for the transformer ratios.

In order to refine the model a data base was generated for frequencies 10GHz up to 120GHz for different gap configurations on a 100μm GaAs substrate. The data base covers the following geometrical parameters of the gap discontinuity:

strip width w_1:	400μm, 100μm, 20μm, 10μm
strip width w_1/w_2:	1, 1.5, 3
gap width s:	100μm, 50μm, 20μm
substrate width W_s:	1mm, 1.5mm, 3mm
cover height H:	0.5mm, 0.8mm, 1mm

This combination of geometric parameters results in a total of 324 different gap configurations. For the data base generation this high number was reduced by selecting 88 of the possible combinations. The simulation of structures with small strip and gap widths was avoided to reduce the necessary computer time. As outlined already for the open end discontinuity this does not limit the range of validity of the final circuit model, the coupling between the fundamental microstrip mode and the parasitic LSM_0 mode being only a weak function of strip width and gap width for narrow feed lines. Cover heights of more than H=10*h were not considered to ensure that LSE mode cut-off frequencies were beyond the maximum frequency of interest.

The dynamic transformer ratio for the open end discontinuity

$$N_{dyn} = N * \cos^{f1}(0.5*\pi*(f-fo)/fo), \quad f<fo$$
$$N_{dyn} = N \quad f>fo$$

and

$$f_0 = f_c * 1.4 * f_0' (1 + \exp(-0.0638 * w_s/h * H/h))* (1 - 2.33 * \exp(-0.33 * W /h))$$

was used, where f_0' and f_1 were found by fitting the S-parameters of the equivalent circuit model to the numerical data sets.

Table 3 (Section 10.5) shows the optimised fine tuning parameters for the 88 different gap configurations. The mean devations F_{mean}, maximum deviations F_{max} and relative maximum deviations F_{maxr} are listed in Table 4 (Section 10.5) where

$$F_{mean} = \sum_{i=1}^{2}\sum_{j=1}^{2} \left(\sum_{n=1}^{N_f} \left| S_{ij}^{\text{data base}}(f_n) - S_{ij}^{\text{analytic}}(f_n) \right| \right) / \left(\sum_{n=1}^{N_f} \left| S_{ij}^{\text{data base}}(f_n) \right| \right)$$

$$F_{max} = \max \left| S_{ij}^{\text{data base}}(f_n) / S_{ij}^{\text{data base}}(f_n) \right|$$

$$F_{maxr} = \max \left| 1 - S_{ij}^{\text{analytic}}(f_n) / S_{ij}^{\text{data base}}(f_n) \right|$$

The deviations are calculated for the frequency range $0 < f < 0.85*f_{res}$. The mean deviation is less than 5% for all the gap configurations. The relative maximum error shows deviations of up to 46% for some of the data sets. These large deviations are calculated for the S12 large gap width configurations.

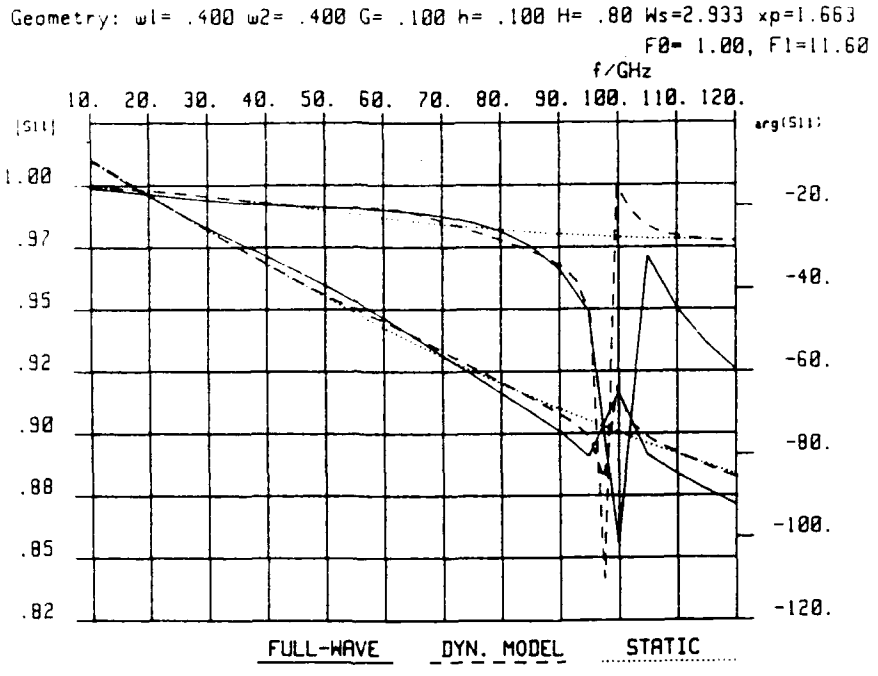


Fig. 10.15: Gap model verification S11 of first configuration

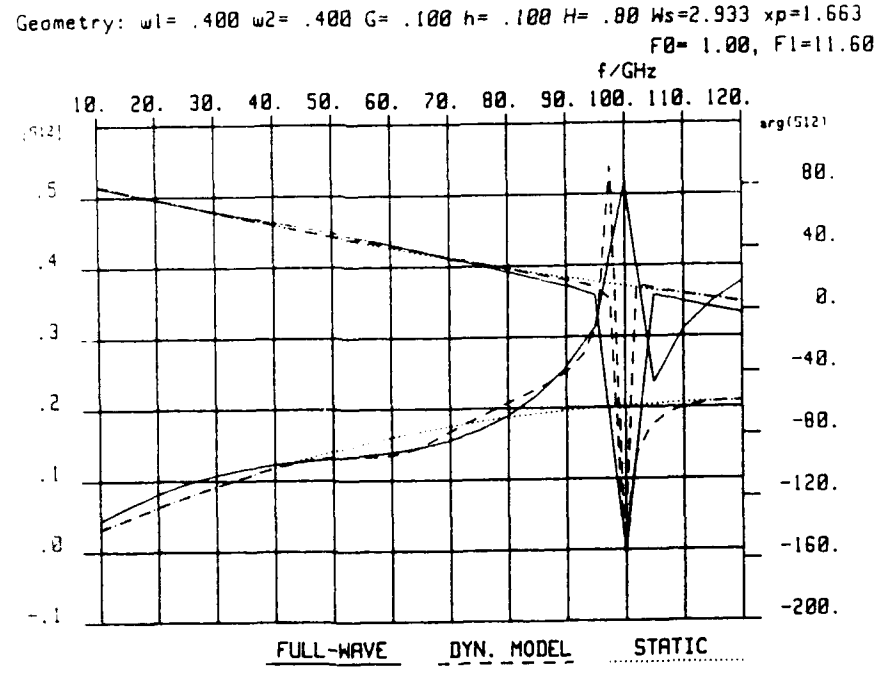


Fig. 10.16: Gap model verification S12 of first configuration

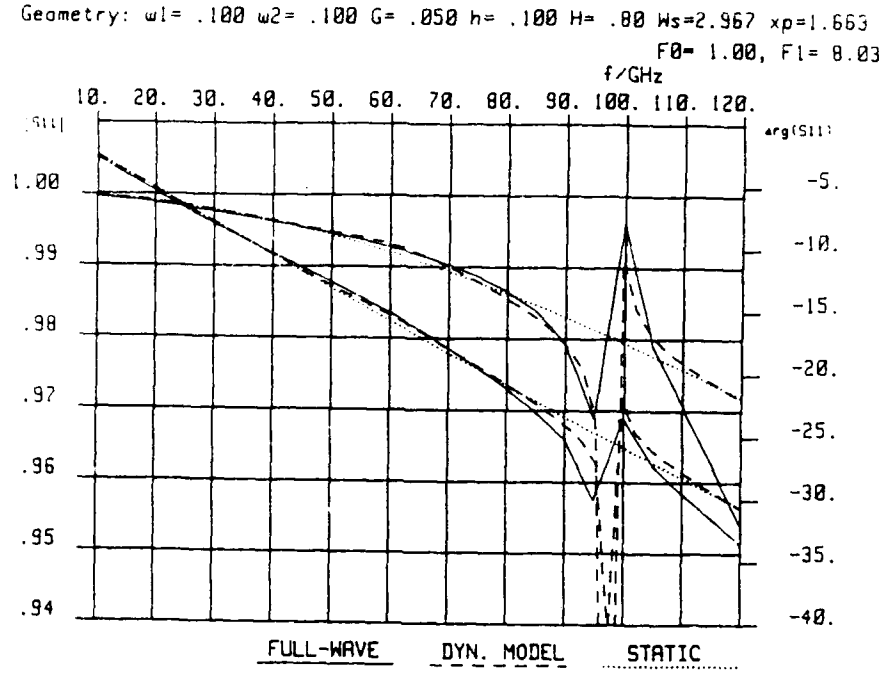


Fig. 10.17: Gap model verification S11 of second configuration

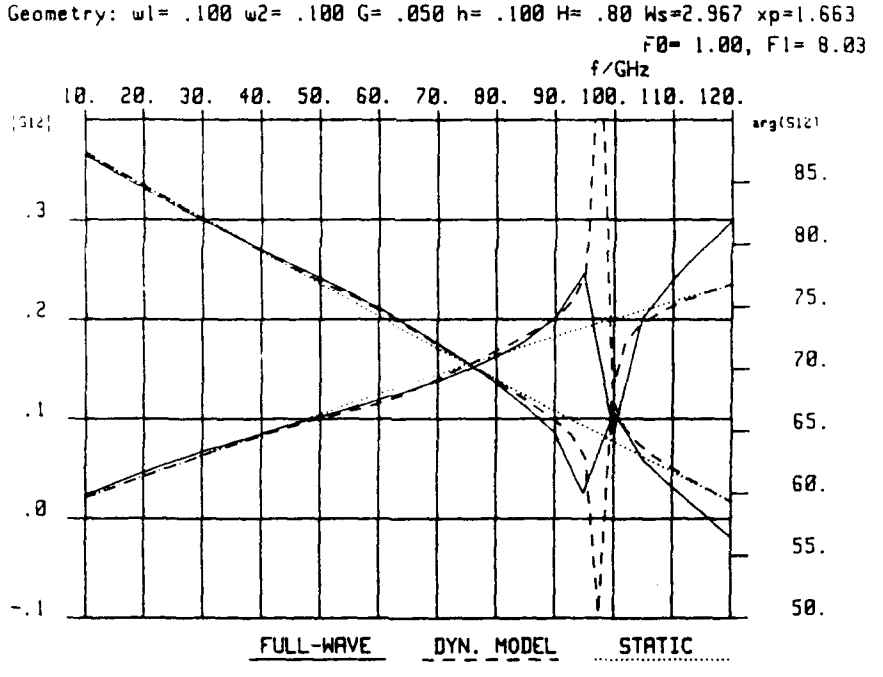


Fig. 10.18: Gap model verification S12 of second configuration

In these cases the magnitude of S12 is quite small. If the respective absolute maximum deviations are considered, it can be seen that they are comparatively small (see e.g. data set 19. F_{maxr}=0.46, F_{max}=0.09) and it can be concluded that the accuracy of the equivalent circuit model is reasonable.

It was found that parameter f_0' can be fixed to a value of 1. This means that the formula for parameter f_0 is the same as that for the open end discontinuity. However, for the gap discontinuity, the parameter f_1 was found to have a considerable influence on the magnitude of the scattering parameters. Its value cannot be kept constant and must be defined by:

$$f_1 = 1.32 * (1 + 0.7311 * (s/h)^{1.08}) * (1 + 0.0094 *(w_s/h)^{1.89})$$

This formula considers only optimum dependencies of the fine tuning parameter f_1 on the geometrical parameters. Nevertheless, the achieved degree of accuracy is good. In Table 5 (Section 10.5) the deviation factors F_{mean}, F_{max} and F_{maxr} are listed for each gap configurations. On using the developed analytic formula for the parameter f_1 instead of the fitted discrete values a slight decrease in accuracy was observed. In order to show the formulae's accuracy some verification results are presented in Figs. 10.15-18.

10.4. GAP MODEL SUMMARY

A summary of the analytic formulae for the microstrip gap discontinuity is given in this section, where $Z_L^{microstrip}$ and $\varepsilon_{eff}^{microstrip}$ are computed according to Section 4 and g is the model gap parameter s. All units are MKS unless stated otherwise.

Quasi-static capacitances C1, C2 and C3

$$2*\pi*f * C_3 / mS = Q1 * \pi *(f/GHz) * (h/mm) * \exp\left(-2.011*g/h*(1.-0.111*w_1/h)^{0.2935}\right)$$

$$* (1+4.12 * (1-\exp(-0.6688*(h/w_1)^{0.5} * (w_2/w_1)))$$

$$* (1.+0.966*\exp(-14.47*g/h + 0.6645*w_1/h))$$

$$Q1 = 0.0594 * (0.0428 * (1-0.5895 * (w_1/h)) + (w_1/h)^{1.213/(1+0.0985*(w_2/w_1-1)^{1.1}})$$

$$2*\pi*f * C_1 / mS = 2\pi * (f/GHz) * (C_{1\ \text{open end}}/pF) * (Q2+Q3) / (1+Q2)$$

$$2*\pi*f * C_2 / mS = 2\pi * (f/GHz) * (C_{2\ \text{open end}}/pF) * (Q2+Q4) / (1+Q2)$$

$$Q2 = 0.1381 * (w_1/h+9.0) * (g/h)^{3.64} + 2.25 * (g/h)^{1.14} * (1.52+0.389 * w_1/h) / (1+0.792 * w_1/h)$$

$$Q3 = \exp(-0.9545*(w_2/w_1)^{1.23}) - 0.37$$

$$Q4 = \exp(-0.9545*(w_1/w_2)^{1.23}) - 0.37$$

The abbreviations $C_{1\ \text{open end}}$ and $C_{2\ \text{open end}}$ denote the static open end capacitances of the discontinuity feed lines, width w_1 and w_2 respectively, where

$$C_{\text{open end}} = \frac{\tan(\beta * dl_{\text{open end}})}{2*\pi*f * Z_L^{\text{microstrip}}}$$

$$\beta = 2*\pi*f * \sqrt{\varepsilon_{\text{eff}}^{\text{microstrip}}} / c$$

Transformer ratios N1, N2, M1, M2

$N1 = N_{dyn}(w_1)$

$N2 = N_{dyn}(w_2)$

$M1 = -N1, \quad M2 = -N2$

$$N_{dyn}(w_i) = \begin{cases} N(w_i) * \cos^{f1}\left(0.5*\pi*(f-f_0)/f_0 \right) & f<f_0 \\ N(w_i) & f>f_0 \end{cases}$$

$$N(w_i) = 1.2/\pi * \left(\cos\left(\frac{\pi}{2w_s} * (w_s - w_{eff}(w_i)) \right) - \cos\left(\frac{\pi}{2w_s} * (w_s + w_{eff}(w_i)) \right) \right)$$

$$w_{eff}(w_i) = Z_0 * h / Z_L^{microstrip}(w_i) / \sqrt{\varepsilon_{eff}^{microstrip}(w_i)}$$

$$f_0 = f_c * 1.4 * \left(1 + \exp(-0.0638 * W_s/h * H/h) \right) * (1 - 2.33 * \exp(-0.33 * W_s/h))$$

$$f_1 = 1.32 * \left(1 + 0.7311 * (s/h)^{1.08} \right) * \left(1 + 0.0094 * (W_s/h)^{1.89} \right)$$

$$\varepsilon_{eff}(LSM_0) = \varepsilon_{stat}\left(1 - \left(\frac{f_c}{f}\right)^2\right)$$

with $$f_c = \frac{c_0}{2W_s \cdot \sqrt{\varepsilon_{stat}}}$$

and $$\varepsilon_{stat} = \frac{\varepsilon_r (H+h)}{\varepsilon_r H + h},$$

$$Z_L(LSM_0) = \frac{H+h}{W_s} \cdot \frac{Z_0}{\sqrt{\varepsilon_{stat}}} \cdot \frac{1}{\sqrt{1 - (f_c/f)^2}}$$

($Z_0 = 120\pi\Omega$, $c_0 = 2.9979\ 10^8$ m/s)

Range of Model Validity

The above gap models are valid for ε_r = 12.9 and the following geometric ranges:

quasi-static model:	50μm	≤	h	≤	200μm
	0.025	≤	w/h	≤	4
	1	≤	w2/w1	≤	3
	0.1	≤	s/h	≤	1.5
	5	≤	Ws/h	≤	30
	5	≤	H/h	≤	20
dynamic model:	0.1	≤	w/h	≤	4
	1	≤	w2/w1	≤	3
	0.1	≤	s/h	≤	1
	5	≤	Ws/h	≤	30
	5	≤	H/h	≤	20

where the quasi-static model is that of Fig. 10.4 and the dynamic model that of Fig. 10.2.

The dynamic model range is valid for 0 ≤ f*h ≤ 12 GHz mm. Package mode coupling has little influence for 0 ≤f*h ≤ 3 GHz mm and the quasi-static formulae can be used on their own.

10.5. REFERENCES AND TABLES

1. Kirschning M.: Development of models for the computer-aided design of hybrid and monolithic microstrip circuits (in German). University of Duisburg, W. Germany, 1984.

Table 1

W1	W2	G	Ws	H	xp	Fmean dB			mS		
						S11	S12	S22	C1	C3	C2
.4000	.4000	.0444	2.93	1.00	1.51	.0012	.0050	.0012	-.0152	.0128	-.0152
.4000	.4000	.0889	2.93	1.00	1.58	.0067	.0192	.0067	.0875	.0226	.0875
.4000	.6000	.0889	3.00	1.00	1.56	.0042	.0402	.0038	-.0530	.0527	-.0485
.4000	.4000	.0444	2.93	3.00	1.51	.0016	.0097	.0016	-.0201	-.0266	-.0201
.4000	.4000	.0889	2.93	3.00	1.58	.0061	.0093	.0061	.0796	-.0076	.0796
.4000	.6000	.0889	3.00	3.00	1.56	.0009	.0036	.0052	-.0119	.0019	-.0684
.2000	.2000	.0444	2.97	1.00	1.60	.0020	.0074	.0020	.0261	-.0091	.0261
.2000	.2000	.0889	2.97	1.00	1.64	.0021	.0250	.0021	.0270	.0146	.0270
.2000	.3000	.0444	3.00	1.00	1.58	.0011	.0164	.0003	.0130	-.0255	.0010
.2000	.3000	.0889	3.00	1.00	1.62	.0032	.0113	.0026	.0416	-.0075	.0334
.2000	.4000	.0444	2.93	1.00	1.56	.0002	.0093	.0081	-.0016	.0130	-.1045
.2000	.4000	.0889	2.93	1.00	1.60	.0016	.0058	.0009	.0202	-.0044	-.0112
.2000	.2000	.0444	2.97	3.00	1.60	.0012	.0145	.0012	.0155	-.0191	.0155
.2000	.2000	.0889	2.97	3.00	1.64	.0020	.0020	.0020	.0255	-.0002	.0255
.2000	.3000	.0444	3.00	3.00	1.58	.0017	.0289	.0014	.0199	-.0456	-.0167
.2000	.3000	.0889	3.00	3.00	1.62	.0033	.0410	.0038	.0416	-.0295	.0487
.2000	.4000	.0444	2.93	3.00	1.56	.0002	.0095	.0081	.0009	-.0151	-.1044
.2000	.4000	.0889	2.93	3.00	1.60	.0018	.0325	.0003	.0227	-.0256	.0035
.1000	.1000	.0200	3.00	1.00	1.62	.0013	.0133	.0012	-.0163	.0148	.0152
.1000	.1000	.0444	3.00	1.00	1.64	.0010	.0156	.0010	.0127	.0101	.0127
.1000	.1000	.0889	3.00	1.00	1.71	.0007	.0571	.0007	-.0084	.0160	-.0084
.1000	.1500	.0200	3.00	1.00	1.60	.0010	.0532	.0006	-.0084	.0682	.0006
.1000	.1500	.0444	3.00	1.00	1.64	.0004	.0405	.0009	.0051	.0308	.0112
.1000	.1500	.0889	3.00	1.00	1.69	.0004	.0692	.0014	-.0045	.0230	.0181
.1000	.2000	.0444	2.97	1.00	1.62	.0041	.0123	.0025	.0521	.0104	.0327
.1000	.2000	.0889	2.97	1.00	1.67	.0013	.0251	.0026	.0161	.0097	.0336
.1000	.3000	.0889	3.00	1.00	1.64	.0039	.0030	.0012	.0496	.0007	.0155
.1000	.1000	.0200	3.00	3.00	1.62	.0010	.0097	.0010	.0131	.0108	.0131
.1000	.1000	.0444	3.00	3.00	1.64	.0003	.0086	.0003	.0039	.0056	.0039
.1000	.1000	.0889	3.00	3.00	1.71	.0002	.0355	.0002	.0025	.0101	.0025
.1000	.1500	.0444	3.00	3.00	1.64	.0011	.0282	.0010	.0143	.0217	.0121
.1000	.1500	.0889	3.00	3.00	1.69	.0002	.0514	.0013	.0025	.0174	.0169
.1000	.2000	.0444	2.97	3.00	1.62	.0043	.0034	.0022	.0550	-.0005	.0288
.1000	.2000	.0889	2.97	3.00	1.67	.0018	.0083	.0029	.0227	-.0031	.0368
.1000	.3000	.0889	3.00	3.00	1.64	.0038	.0321	.0023	.0481	-.0148	.0296
.0500	.0500	.0067	.50	1.00	1.67	.0006	.0327	.0007	-.0070	-.0349	.0086
.0500	.0500	.0200	.50	1.00	1.66	.0010	.0018	.0001	-.0121	-.0010	.0014
.0500	.0500	.0444	.50	1.00	1.69	.0007	.0238	.0007	-.0091	.0079	-.0091
.0500	.0500	.0889	.50	1.00	1.76	.0015	.0546	.0015	-.0195	.0078	-.0195
.0500	.0500	.0056	.50	1.00	1.66	.0005	.0231	.0004	-.0055	.0252	.0049
.0500	.0750	.0200	.50	1.00	1.66	.0004	.0028	.0019	-.0056	.0019	.0246
.0500	.0750	.0444	.50	1.00	1.69	.0004	.0327	.0010	-.0052	.0132	.0133
.0500	.0750	.0889	.50	1.00	1.73	.0012	.0628	.0003	-.0150	.0109	.0032
.0500	.1000	.0444	.50	1.00	1.67	.0013	.0239	.0027	.0169	.0109	.0350
.0500	.1000	.0889	.50	1.00	1.73	.0006	.0471	.0013	-.0079	.0093	.0161
.0500	.0500	.0067	.50	3.00	1.67	.0006	.0327	.0007	-.0070	-.0349	.0085
.0500	.0500	.0200	.50	3.00	1.66	.0010	.0018	.0001	-.0121	-.0010	.0014
.0500	.0500	.0444	.50	3.00	1.69	.0007	.0238	.0007	-.0091	.0079	-.0091
.0500	.0500	.0889	.50	3.00	1.76	.0015	.0546	.0015	-.0195	.0078	-.0195
.0500	.0500	.0056	.50	3.00	1.66	.0005	.0231	.0004	-.0055	.0252	.0048
.0500	.0750	.0200	.50	3.00	1.66	.0004	.0028	.0019	-.0056	.0019	.0242
.0500	.0750	.0444	.50	3.00	1.69	.0002	.0327	.0010	-.0030	.0132	.0127
.0500	.0750	.0889	.50	3.00	1.73	.0012	.0628	.0003	-.0155	.0109	.0032
.0500	.1000	.0444	.50	3.00	1.67	.0013	.0239	.0027	.0169	.0109	.0342
.0500	.1000	.0889	.50	3.00	1.73	.0007	.0471	.0013	-.0083	.0093	.0161
.0500	.0500	.0067	1.00	1.00	1.67	.0007	.0475	.0010	-.0065	-.0514	.0117
.0500	.0500	.0200	1.00	1.00	1.66	.0009	.0020	.0009	-.0111	-.0010	-.0111

W1	W2	G	Ws	H	xp	Fmean S11	S12	S22	C1	C3	C2
.0500	.0500	.0444	1.00	1.00	1.69	.0005	.0188	.0005	-.0070	.0063	-.0070
.0500	.0500	.0056	1.00	1.00	1.66	.0004	.0063	.0007	-.0051	.0070	.0092
.0500	.0750	.0200	1.00	1.00	1.66	.0004	.0028	.0021	-.0049	.0019	.0270
.0500	.0750	.0444	1.00	1.00	1.69	.0001	.0327	.0013	.0010	.0132	.0168
.0500	.0750	.0889	1.00	1.00	1.73	.0010	.0628	.0004	-.0122	.0109	.0056
.0500	.1000	.0444	.98	1.00	1.67	.0016	.0122	.0023	.0209	.0056	.0294
.0500	.1000	.0889	.98	1.00	1.73	.0005	.0471	.0016	-.0066	.0093	.0202
.0500	.1500	.0889	1.00	1.00	1.71	.0013	.0242	.0019	.0169	.0057	.0245
.0500	.0500	.0067	1.00	3.00	1.67	.0007	.0475	.0010	-.0065	-.0514	.0110
.0500	.0500	.0200	1.00	3.00	1.66	.0009	.0028	.0009	-.0111	-.0015	-.0111
.0500	.0500	.0444	1.00	3.00	1.69	.0005	.0188	.0005	-.0066	.0063	-.0066
.0500	.0500	.0889	1.00	3.00	1.76	.0011	.0684	.0011	-.0144	.0097	-.0144
.0500	.0500	.0056	1.00	3.00	1.66	.0004	.0045	.0009	-.0051	.0050	.0108
.0500	.0750	.0200	1.00	3.00	1.66	.0004	.0028	.0021	-.0049	.0019	.0266
.0500	.0750	.0444	1.00	3.00	1.69	.0001	.0327	.0013	.0010	.0132	.0168
.0500	.0750	.0889	1.00	3.00	1.73	.0010	.0628	.0004	-.0127	.0109	.0056
.0500	.1000	.0444	.98	3.00	1.67	.0017	.0122	.0023	.0222	.0056	.0293
.0500	.1000	.0889	.98	3.00	1.73	.0005	.0471	.0016	-.0066	.0093	.0202
.0500	.1500	.0889	1.00	3.00	1.71	.0022	.0024	.0022	.0277	.0002	.0284
.0200	.0200	.0200	.50	1.00	1.70	.0005	.0374	.0005	-.0067	-.0101	-.0067
.0200	.0200	.0444	.50	1.00	1.73	.0004	.0357	.0015	-.0049	-.0058	-.0192
.0200	.0200	.0889	.50	1.00	1.78	.0020	.0074	.0020	-.0250	.0005	-.0250
.0200	.0200	.0067	.50	1.00	1.69	.0003	.0124	.0003	-.0042	-.0056	-.0042
.0200	.0300	.0200	.50	1.00	1.70	.0002	.0146	.0001	-.0025	-.0046	.0016
.0200	.0300	.0444	.50	1.00	1.73	.0001	.0142	.0003	-.0015	-.0027	-.0032
.0200	.0300	.0889	.50	1.00	1.78	.0023	.0598	.0013	-.0295	.0046	-.0167
.0200	.0400	.0200	.50	1.00	1.70	.0009	.0137	.0015	-.0115	-.0049	.0196
.0200	.0400	.0444	.50	1.00	1.71	.0017	.0147	.0005	-.0211	.0030	.0059
.0200	.0400	.0889	.50	1.00	1.78	.0023	.0455	.0007	-.0296	.0040	-.0089
.0200	.0600	.0100	.50	1.00	1.68	.0039	.0040	.0025	.0493	-.0014	.0321
.0200	.0600	.0200	.50	1.00	1.68	.0017	.0061	.0026	.0219	-.0023	.0337
.0200	.0600	.0444	.50	1.00	1.71	.0007	.0018	.0021	.0094	-.0002	.0268
.0200	.0600	.0889	.50	1.00	1.76	.0011	.0614	.0003	-.0146	.0062	.0039
.0200	.0200	.0200	.50	3.00	1.70	.0005	.0374	.0005	-.0067	-.0101	-.0067
.0200	.0200	.0444	.50	3.00	1.73	.0004	.0357	.0015	-.0049	-.0058	-.0194
.0200	.0200	.0889	.50	3.00	1.78	.0020	.0065	.0020	-.0250	.0004	-.0250
.0200	.0200	.0067	.50	3.00	1.69	.0003	.0124	.0003	-.0042	-.0056	-.0042
.0200	.0300	.0200	.50	3.00	1.70	.0002	.0146	.0001	-.0025	-.0046	.0009
.0200	.0300	.0444	.50	3.00	1.73	.0001	.0142	.0003	-.0015	-.0027	-.0032
.0200	.0300	.0889	.50	3.00	1.78	.0023	.0598	.0013	-.0297	.0046	-.0167
.0200	.0400	.0200	.50	3.00	1.70	.0010	.0137	.0015	-.0126	-.0049	.0196
.0200	.0400	.0444	.50	3.00	1.71	.0017	.0147	.0005	-.0211	.0030	.0059
.0200	.0400	.0889	.50	3.00	1.78	.0023	.0455	.0007	-.0296	.0040	-.0089
.0200	.0600	.0100	.50	3.00	1.68	.0039	.0040	.0025	.0494	-.0014	.0317
.0200	.0600	.0200	.50	3.00	1.68	.0017	.0061	.0026	.0219	-.0023	.0333
.0200	.0600	.0444	.50	3.00	1.71	.0007	.0018	.0021	.0093	-.0002	.0267
.0200	.0600	.0889	.50	3.00	1.76	.0013	.0614	.0004	-.0168	.0062	.0052
.0200	.0200	.0200	1.00	1.00	1.70	.0004	.0374	.0004	-.0052	-.0101	-.0052
.0200	.0200	.0444	1.00	1.00	1.73	.0002	.0457	.0002	-.0024	-.0075	-.0024
.0200	.0200	.0889	1.00	1.00	1.78	.0021	.0074	.0021	-.0266	.0005	-.0266
.0200	.0200	.0067	1.00	1.00	1.69	.0003	.0124	.0003	-.0035	-.0056	-.0035
.0200	.0300	.0200	1.00	1.00	1.70	.0001	.0146	.0003	-.0015	-.0046	.0035
.0200	.0300	.0444	1.00	1.00	1.73	.0001	.0142	.0001	.0007	-.0027	-.0008
.0200	.0300	.0889	1.00	1.00	1.78	.0021	.0598	.0010	-.0267	.0046	-.0132
.0200	.0400	.0200	1.00	1.00	1.70	.0009	.0137	.0018	-.0117	-.0049	.0227
.0200	.0400	.0444	1.00	1.00	1.71	.0016	.0147	.0004	-.0204	.0030	.0055
.0200	.0400	.0889	1.00	1.00	1.78	.0020	.0455	.0004	-.0259	.0040	-.0045
.0200	.0600	.0100	1.00	1.00	1.68	.0023	.0028	.0021	.0290	-.0010	.0268
.0200	.0600	.0200	1.00	1.00	1.68	.0018	.0053	.0025	.0224	-.0020	.0317
.0200	.0600	.0444	1.00	1.00	1.71	.0010	.0017	.0024	.0126	.0000	.0301
.0200	.0600	.0889	1.00	1.00	1.76	.0011	.0614	.0008	-.0136	.0062	.0105
.0200	.0200	.0200	1.00	3.00	1.70	.0004	.0374	.0004	-.0052	-.0101	-.0052

W1	W2	G	Ws	H	xp	Fmean dB S11	S12	S22	mS C1	C3	C2
.0200	.0200	.0444	1.00	3.00	1.73	.0002	.0457	.0002	-.0024	-.0075	-.0024
.0200	.0200	.0889	1.00	3.00	1.78	.0021	.0074	.0021	-.0266	.0005	-.0266
.0200	.0200	.0067	1.00	3.00	1.69	.0003	.0124	.0003	-.0035	-.0056	-.0035
.0200	.0300	.0200	1.00	3.00	1.70	.0001	.0146	.0003	-.0015	-.0046	.0033
.0200	.0300	.0444	1.00	3.00	1.73	.0001	.0142	.0001	.0007	-.0027	-.0008
.0200	.0300	.0889	1.00	3.00	1.78	.0021	.0598	.0011	-.0270	.0046	-.0136
.0200	.0400	.0200	1.00	3.00	1.70	.0010	.0137	.0018	-.0131	-.0049	.0224
.0200	.0400	.0444	1.00	3.00	1.71	.0016	.0147	.0004	-.0206	.0030	.0055
.0200	.0400	.0889	1.00	3.00	1.78	.0021	.0455	.0005	-.0262	.0040	-.0060
.0200	.0600	.0100	1.00	3.00	1.68	.0023	.0028	.0021	.0290	-.0010	.0268
.0200	.0600	.0200	1.00	3.00	1.68	.0018	.0061	.0028	.0224	-.0023	.0352
.0200	.0600	.0444	1.00	3.00	1.71	.0009	.0016	.0023	.0118	.0000	.0296
.0200	.0600	.0889	1.00	3.00	1.76	.0011	.0614	.0008	-.0139	.0062	.0098
.0100	.0100	.0200	.50	1.00	1.72	.0019	.0159	.0019	-.0248	-.0026	-.0248
.0100	.0100	.0444	.50	1.00	1.76	.0017	.0567	.0017	-.0219	-.0058	-.0219
.0100	.0100	.0889	.50	1.00	1.80	.0020	.0148	.0020	-.0255	-.0006	-.0255
.0100	.0150	.0200	.50	1.00	1.72	.0025	.0175	.0007	-.0318	-.0033	-.0084
.0100	.0150	.0444	.50	1.00	1.76	.0021	.0625	.0008	-.0268	-.0074	-.0104
.0100	.0150	.0889	.50	1.00	1.80	.0024	.0466	.0017	-.0309	.0021	-.0222
.0100	.0200	.0444	.50	1.00	1.76	.0021	.0325	.0001	-.0262	-.0041	-.0017
.0100	.0200	.0889	.50	1.00	1.80	.0023	.0383	.0012	-.0297	.0019	-.0157
.0100	.0300	.0100	.50	1.00	1.70	.0015	.0071	.0022	.0196	-.0024	.0277
.0100	.0300	.0444	.50	1.00	1.73	.0010	.0063	.0006	-.0124	-.0009	.0079
.0100	.0300	.0889	.50	1.00	1.78	.0019	.0159	.0005	-.0239	.0010	-.0070
.0100	.0100	.0200	.50	3.00	1.72	.0020	.0159	.0020	-.0249	-.0026	-.0249
.0100	.0100	.0444	.50	3.00	1.76	.0017	.0567	.0017	-.0218	-.0058	-.0218
.0100	.0100	.0889	.50	3.00	1.80	.0020	.0148	.0020	-.0255	-.0006	-.0255
.0100	.0150	.0200	.50	3.00	1.72	.0025	.0175	.0007	-.0318	-.0033	-.0086
.0100	.0150	.0444	.50	3.00	1.76	.0021	.0625	.0008	-.0269	-.0074	-.0104
.0100	.0150	.0889	.50	3.00	1.80	.0024	.0466	.0017	-.0311	.0021	-.0222
.0100	.0200	.0200	.50	3.00	1.72	.0022	.0292	.0003	-.0282	-.0062	.0039
.0100	.0200	.0444	.50	3.00	1.76	.0021	.0325	.0002	-.0262	-.0041	-.0020
.0100	.0200	.0889	.50	3.00	1.80	.0023	.0383	.0013	-.0299	.0019	-.0160
.0100	.0300	.0100	.50	3.00	1.70	.0015	.0071	.0022	.0196	-.0024	.0275
.0100	.0300	.0444	.50	3.00	1.73	.0010	.0063	.0006	-.0124	-.0009	.0076
.0100	.0300	.0889	.50	3.00	1.78	.0019	.0159	.0006	-.0239	.0010	-.0074
.0100	.0100	.0167	1.00	1.00	1.73	.0001	.0262	.0016	-.0019	-.0047	-.0203
.0100	.0133	.0200	1.00	1.00	1.72	.0022	.0205	.0000	-.0278	-.0037	-.0004
.0100	.0133	.0444	1.00	1.00	1.76	.0016	.0578	.0001	-.0204	-.0065	.0015
.0100	.0133	.0889	1.00	1.00	1.80	.0018	.0032	.0013	-.0235	.0001	-.0168
.0100	.0200	.0200	1.00	1.00	1.72	.0017	.0384	.0008	-.0222	-.0082	.0103
.0100	.0200	.0444	1.00	1.00	1.76	.0019	.0325	.0001	-.0243	-.0041	.0011
.0100	.0200	.0889	1.00	1.00	1.80	.0020	.0383	.0010	-.0255	.0019	-.0126
.0100	.0300	.0100	1.00	1.00	1.70	.0015	.0071	.0022	.0191	-.0024	.0286
.0100	.0300	.0200	1.00	1.00	1.70	.0012	.0153	.0020	.0158	-.0038	.0250
.0100	.0300	.0444	1.00	1.00	1.73	.0007	.0063	.0010	-.0091	-.0009	.0121
.0100	.0300	.0889	1.00	1.00	1.78	.0015	.0158	.0003	-.0187	.0010	-.0033
.0100	.0100	.0167	1.00	3.00	1.73	.0001	.0262	.0016	-.0019	-.0047	-.0203
.0100	.0133	.0200	1.00	3.00	1.72	.0022	.0205	.0000	-.0278	-.0037	-.0004
.0100	.0133	.0444	1.00	3.00	1.76	.0016	.0578	.0001	-.0207	-.0065	.0014
.0100	.0133	.0889	1.00	3.00	1.80	.0018	.0032	.0015	-.0235	.0001	-.0186
.0100	.0200	.0200	1.00	3.00	1.72	.0019	.0376	.0008	-.0239	-.0081	.0097
.0100	.0200	.0444	1.00	3.00	1.76	.0019	.0325	.0001	-.0243	-.0041	.0011
.0100	.0200	.0889	1.00	3.00	1.80	.0020	.0383	.0010	-.0256	.0019	-.0126
.0100	.0300	.0100	1.00	3.00	1.70	.0015	.0071	.0023	.0191	-.0024	.0290
.0100	.0300	.0200	1.00	3.00	1.70	.0012	.0153	.0019	.0156	-.0038	.0247
.0100	.0300	.0444	1.00	3.00	1.73	.0008	.0063	.0008	-.0098	-.0009	.0104
.0100	.0300	.0889	1.00	3.00	1.78	.0014	.0158	.0003	-.0178	.0010	-.0033

W1	W2	G	Ws	H	xp	Fmean dB			mS		
						S11	S12	S22	C1	C3	C2
.0050	.0050	.0167	.50	1.00	1.73	.0003	.0275	.0016	-.0035	.0033	-.0203
.0050	.0050	.0370	.50	1.00	1.78	.0020	.0244	.0020	-.0257	.0019	-.0257
.0050	.0050	.0926	.50	1.00	1.82	.0018	.0530	.0018	-.0233	.0013	-.0233
.0050	.0067	.0200	.50	1.00	1.74	.0023	.0017	.0002	-.0288	.0001	-.0020
.0050	.0067	.0444	.50	1.00	1.76	.0020	.0504	.0012	-.0248	-.0038	-.0148
.0050	.0100	.0444	.50	1.00	1.76	.0022	.0528	.0001	-.0283	-.0045	.0015
.0050	.0100	.0889	.50	1.00	1.80	.0023	.0041	.0001	-.0291	-.0001	.0007
.0050	.0150	.0444	.50	1.00	1.76	.0015	.0171	.0000	-.0192	-.0016	.0001
.0050	.0050	.0167	.50	3.00	1.73	.0003	.0275	.0016	-.0035	.0033	-.0203
.0050	.0050	.0370	.50	3.00	1.78	.0020	.0244	.0020	-.0257	.0019	-.0257
.0050	.0050	.0926	.50	3.00	1.82	.0018	.0530	.0018	-.0233	.0013	-.0233
.0050	.0067	.0200	.50	3.00	1.74	.0023	.0017	.0002	-.0288	.0001	-.0020
.0050	.0067	.0444	.50	3.00	1.76	.0020	.0504	.0012	-.0248	-.0038	-.0148
.0050	.0100	.0444	.50	3.00	1.76	.0022	.0528	.0001	-.0283	-.0045	.0015
.0050	.0100	.0889	.50	3.00	1.80	.0023	.0041	.0001	-.0292	-.0001	.0007
.0050	.0150	.0444	.50	3.00	1.76	.0015	.0171	.0000	-.0192	-.0016	.0001
.0050	.0150	.0429	1.00	1.00	1.76	.0016	.0521	.0000	-.0205	.0048	-.0004
.0050	.0050	.0067	1.00	3.00	1.73	.0001	.0563	.0018	-.0009	.0102	-.0229
.0050	.0150	.0429	1.00	3.00	1.76	.0016	.0521	.0000	-.0206	.0048	-.0004
.0025	.0075	.0429	.50	1.00	1.78	.0001	.0567	.0004	.0008	.0038	.0047
.0025	.0075	.0965	.50	1.00	1.82	.0020	.0122	.0001	-.0255	-.0003	.0010
.0025	.0075	.0429	.50	3.00	1.78	.0001	.0567	.0004	.0008	.0038	.0045
.0025	.0075	.0965	.50	3.00	1.82	.0020	.0122	.0001	-.0255	-.0003	.0010
.4000	.4000	.1500	2.96	1.00	1.63	.0018	.0409	.0018	.0240	.0175	.0240
.4000	.4000	.1500	2.96	3.00	1.63	.0044	.0486	.0044	.0569	-.0223	.0569
.2000	.4000	.1500	2.93	1.00	1.65	.0009	.0053	.0019	-.0121	-.0014	-.0242
.2000	.6000	.1500	3.00	1.00	1.63	.0037	.0127	.0062	-.0481	-.0036	-.0838
.2000	.2000	.1500	3.00	3.00	1.69	.0016	.0036	.0016	.0210	.0007	.0210
.1000	.1000	.1500	3.00	1.00	1.76	.0076	.0276	.0076	-.0973	-.0027	-.0973
.1000	.2000	.1500	2.97	1.00	1.73	.0005	.0418	.0016	-.0061	.0054	.0207
.1000	.3000	.1500	3.00	1.00	1.71	.0017	.0551	.0021	.0217	-.0088	-.0272
.1000	.2000	.1500	2.97	3.00	1.73	.0000	.0271	.0003	-.0003	-.0037	.0043

Table 2

W1	W2	G	WS	HH	XP	FC_N
.4000	.4000	.0500	2.000	.500	1.962	.79
.4000	.4000	.1000	2.000	1.000	2.088	1.13
.4000	.4000	.0500	2.000	1.000	2.088	.86
.1000	.1000	.1000	1.967	.500	1.962	1.15
.1000	.1000	.0500	2.000	.500	1.962	1.08
.1000	.1000	.0200	2.000	.500	1.960	.96
.1000	.2000	.1000	2.000	.500	1.962	1.48
.1000	.2000	.0500	2.000	.500	1.962	1.41
.1000	.3000	.0500	2.000	.500	1.962	1.49
.1000	.1000	.1000	2.000	1.000	2.088	1.08
.1000	.1000	.0500	2.000	1.000	2.088	1.05
.1000	.1000	.0200	2.000	1.000	2.080	.84
.1000	.2000	.0500	2.000	1.000	2.088	1.45
.1000	.3000	.1000	2.000	1.000	2.088	1.20
.1000	.3000	.0500	2.000	1.000	2.088	1.34
.0200	.0200	.0500	2.000	.500	1.962	1.12
.0200	.0200	.0200	2.000	.500	1.960	1.17
.0200	.0200	.0100	2.000	.500	1.960	1.26
.0200	.0400	.1000	2.000	.500	1.962	.71
.0200	.0400	.0500	2.000	.500	1.962	1.14
.0200	.0400	.0200	2.000	.500	1.960	1.20
.0200	.0400	.0100	2.000	.500	1.960	1.27
.0200	.0600	.1000	2.000	.500	1.962	.82
.0200	.0600	.0500	2.000	.500	1.962	1.20
.0200	.0600	.0200	2.000	.500	1.960	1.30
.0200	.0600	.0100	2.000	.500	1.960	1.29
.0200	.0200	.1000	2.000	1.000	2.088	1.04
.0200	.0200	.0500	2.000	1.000	2.088	1.15
.0200	.0200	.0200	2.000	1.000	2.080	1.04
.0200	.0200	.0100	2.000	1.000	2.080	1.07
.0200	.0400	.1000	2.000	1.000	2.088	1.17
.0200	.0400	.0500	2.000	1.000	2.088	1.34
.0200	.0400	.0200	2.000	1.000	2.080	1.41
.0200	.0400	.0100	2.000	1.000	2.080	1.43
.0200	.0600	.1000	2.000	1.000	2.088	1.32
.0200	.0600	.0500	2.000	1.000	2.088	1.44
.0100	.0100	.1000	2.000	.500	1.962	.82
.0100	.0100	.0500	2.000	.500	1.962	1.01
.0100	.0100	.0200	2.000	.500	1.960	1.12
.0100	.0100	.0100	2.000	.500	1.960	1.11
.0100	.0200	.0500	2.000	.500	1.962	1.06
.0100	.0200	.0200	2.000	.500	1.960	1.16
.0100	.0200	.0100	2.000	.500	1.960	1.16
.0100	.0100	.1000	2.000	1.000	2.088	.99
.0100	.0100	.0500	2.000	1.000	2.088	1.11
.0100	.0100	.0200	2.000	1.000	2.080	1.18
.0100	.0100	.0100	2.000	1.000	2.080	1.11
.0100	.0200	.1000	2.000	1.000	2.088	1.07
.0100	.0200	.0500	2.000	1.000	2.088	1.20
.0100	.0200	.0200	2.000	1.000	2.080	1.31
.0100	.0200	.0100	2.000	1.000	2.080	1.30
.0100	.0300	.1000	2.000	1.000	2.088	1.14
.0100	.0300	.0500	2.000	1.000	2.088	1.30
.4000	.4000	.1000	2.933	.500	1.737	.89
.4000	.4000	.0500	2.933	.500	1.737	1.20
.4000	.4000	.1000	2.933	1.000	1.825	1.04
.4000	.4000	.0500	2.933	1.000	1.825	1.19

W1	W2	G	WS	HH	XP	FC_N
.1000	.2000	.1000	3.000	.500	1.737	.62
.1000	.2000	.0500	3.000	.500	1.737	1.02
.1000	.3000	.0500	3.000	.500	1.737	.96
.1000	.1000	.1000	2.967	1.000	1.825	.96
.1000	.1000	.0500	2.967	1.000	1.825	1.19
.1000	.1000	.0200	3.000	1.000	1.820	1.14
.1000	.2000	.1000	3.000	1.000	1.825	.95
.1000	.2000	.0500	3.000	1.000	1.825	1.09
.1000	.3000	.1000	3.000	1.000	1.825	.89
.1000	.3000	.0500	3.000	1.000	1.825	1.08
.0200	.0200	.1000	3.000	.500	1.737	1.26
.0200	.0200	.0500	3.000	.500	1.737	.82
.0200	.0200	.0200	3.000	.500	1.740	.96
.0200	.0200	.0100	3.000	.500	1.740	1.04
.0200	.0400	.1000	3.000	.500	1.737	1.10
.0200	.0400	.0500	3.000	.500	1.737	.87
.0200	.0400	.0200	3.000	.500	1.740	1.01
.0200	.0400	.0100	3.000	.500	1.740	1.07
.0200	.0600	.1000	3.000	.500	1.737	1.05
.0200	.0600	.0500	3.000	.500	1.737	.74
.0200	.0600	.0200	3.000	.500	1.740	1.03
.0200	.0600	.0100	3.000	.500	1.740	1.08
.0200	.0200	.1000	3.000	1.000	1.825	.95
.0200	.0200	.0500	3.000	1.000	1.825	1.07
.0200	.0200	.0200	3.000	1.000	1.820	1.21
.0200	.0200	.0100	3.000	1.000	1.820	1.29
.0200	.0400	.1000	3.000	1.000	1.825	.85
.0200	.0400	.0500	3.000	1.000	1.825	1.06
.0200	.0400	.0200	3.000	1.000	1.820	1.02
.0200	.0400	.0100	3.000	1.000	1.820	1.29
.0200	.0600	.1000	3.000	1.000	1.825	.79
.0200	.0600	.0500	3.000	1.000	1.825	1.05
.0200	.0600	.0200	3.000	1.000	1.820	1.03
.0200	.0600	.0100	3.000	1.000	1.820	1.33
.0100	.0100	.1000	3.000	.500	1.737	1.32
.0100	.0100	.0500	3.000	.500	1.737	.77
.0100	.0100	.0200	3.000	.500	1.740	.89
.0100	.0100	.0100	3.000	.500	1.740	1.00
.0100	.0200	.1000	3.000	.500	1.737	1.27
.0100	.0200	.0200	3.000	.500	1.740	.94
.0100	.0200	.0100	3.000	.500	1.740	1.02
.0100	.0300	.1000	3.000	.500	1.737	1.14
.0100	.0300	.0500	3.000	.500	1.737	.84
.0100	.0300	.0200	3.000	.500	1.740	1.11
.0100	.0300	.0100	3.000	.500	1.740	1.25
.0100	.0100	.1000	3.000	1.000	1.825	1.08
.0100	.0100	.0500	3.000	1.000	1.825	.92
.0100	.0100	.0200	3.000	1.000	1.820	1.03
.0100	.0100	.0100	3.000	1.000	1.820	1.07
.0100	.0200	.1000	3.000	1.000	1.825	1.00
.0100	.0200	.0500	3.000	1.000	1.825	.96
.0100	.0200	.0200	3.000	1.000	1.820	1.04
.0100	.0200	.0100	3.000	1.000	1.820	1.06
.0100	.0300	.1000	3.000	1.000	1.825	.87
.0100	.0300	.0500	3.000	1.000	1.825	.93
.0100	.0300	.0200	3.000	1.000	1.820	1.03
.0100	.0300	.0100	3.000	1.000	1.820	1.09

Table 3

W1	W2	G	WS	HH	XP	FO′	F1
.0500	.0500	.0139	1.000	1.000	1.069	1.00	2.19
.0500	.0500	.0500	1.000	1.000	1.100	1.00	2.48
.0500	.0500	.1000	1.000	1.000	1.150	1.00	3.46
.0500	.0750	.0200	1.000	1.000	1.060	1.00	2.24
.0500	.0750	.0434	1.000	1.000	1.094	1.00	2.38
.0500	.0750	.0955	1.000	1.000	1.137	1.00	3.22
.0500	.1500	.0167	1.000	1.000	1.033	1.00	1.95
.0500	.1500	.0500	1.000	1.000	1.063	1.00	2.31
.0500	.1500	.1000	1.000	1.000	1.112	1.00	3.27
.0200	.0200	.0139	1.000	1.000	1.097	1.00	2.38
.0200	.0200	.0500	1.000	1.000	1.138	1.00	2.88
.0200	.0200	.1000	1.000	1.000	1.188	1.00	3.98
.0200	.0300	.0200	1.000	1.000	1.100	1.00	2.43
.0200	.0300	.0434	1.000	1.000	1.128	1.00	2.77
.0200	.0300	.0955	1.000	1.000	1.181	1.00	3.88
.0200	.0600	.0167	1.000	1.000	1.083	1.00	2.41
.0200	.0600	.0500	1.000	1.000	1.112	1.00	2.63
.0200	.0600	.1000	1.000	1.000	1.163	1.00	3.76
.0200	.0200	.0111	1.500	1.000	3.167	1.00	69.80
.0100	.0100	.0116	1.000	1.000	1.123	1.00	2.49
.0100	.0100	.0417	1.000	1.000	1.146	1.00	2.95
.0100	.0100	.0937	1.000	1.000	1.198	1.00	3.93
.0100	.0150	.0185	1.000	1.000	1.120	1.00	2.53
.0100	.0150	.0417	1.000	1.000	1.146	1.00	2.96
.0100	.0150	.0937	1.000	1.000	1.198	1.00	4.15
.0100	.0300	.0167	1.000	1.000	1.100	1.00	2.66
.0100	.0300	.0434	1.000	1.000	1.136	1.00	2.83
.0100	.0300	.0940	1.000	1.000	1.186	1.00	3.94
.4000	.4000	.0500	2.933	.800	1.663	1.00	3.99
.4000	.4000	.1000	2.933	.800	1.663	1.00	10.24
.4000	.6000	.1000	3.000	.800	1.663	1.00	11.03
.4000	.4000	.0500	2.933	1.500	1.712	1.00	2.26
.4000	.4000	.1000	2.933	1.500	1.712	1.00	5.22
.4000	.6000	.1000	3.000	1.500	1.712	1.00	4.73
.2000	.2000	.0500	2.933	.800	1.663	1.00	7.03
.2000	.2000	.1000	2.933	.800	1.663	1.00	19.29
.2000	.3000	.0500	3.000	.800	1.663	1.00	6.87
.2000	.3000	.1000	3.000	.800	1.663	1.00	19.81
.2000	.6000	.1000	3.000	.800	1.663	1.00	18.84
.2000	.2000	.0500	2.933	1.500	1.712	1.00	4.27
.2000	.2000	.1000	2.933	1.500	1.712	1.00	9.93
.2000	.3000	.0500	3.000	1.500	1.712	1.00	3.48
.2000	.3000	.1000	3.000	1.500	1.712	1.00	9.79
.2000	.6000	.1000	3.000	1.500	1.712	1.00	6.73
.1000	.1000	.0167	2.967	.800	1.667	1.00	8.82
.1000	.1000	.0500	2.967	.800	1.663	1.00	11.79
.1000	.1000	.1000	2.967	.800	1.663	1.00	47.37
.1000	.1500	.0139	3.000	.800	1.667	1.00	7.86
.1000	.1500	.0500	3.000	.800	1.663	1.00	15.48

W1	W2	G	WS	HH	XP	F0	F1
.1000	.1500	.1000	3.000	.800	1.663	1.00	64.67
.1000	.3000	.0500	3.000	.800	1.663	1.00	9.13
.1000	.3000	.1000	3.000	.800	1.663	1.00	40.06
.1000	.1000	.0167	2.967	1.500	1.717	1.00	5.31
.1000	.1000	.0500	2.967	1.500	1.712	1.00	8.02
.1000	.1000	.1000	2.967	1.500	1.712	1.00	46.69
.1000	.1500	.0139	3.000	1.500	1.722	1.00	4.48
.0500	.0750	.0200	1.500	1.000	1.500	1.00	1.82
.0500	.0750	.0500	1.500	1.000	1.500	1.00	2.04
.0500	.0750	.1000	1.500	1.000	1.487	1.00	2.64
.0500	.1500	.0200	1.500	1.000	1.500	1.00	1.71
.0500	.1500	.0417	1.500	1.000	1.500	1.00	1.73
.0500	.1500	.0937	1.500	1.000	1.500	1.00	2.35
.0200	.0200	.0200	1.500	1.000	1.500	1.00	2.13
.0200	.0200	.0500	1.500	1.000	1.500	1.00	2.54
.0200	.0200	.1000	1.500	1.000	1.487	1.00	3.42
.0200	.0300	.0200	1.500	1.000	1.500	1.00	2.06
.0200	.0300	.0500	1.500	1.000	1.500	1.00	2.36
.0200	.0300	.1000	1.500	1.000	1.487	1.00	3.17
.0200	.0600	.0200	1.500	1.000	1.500	1.00	2.03
.0200	.0600	.0417	1.500	1.000	1.500	1.00	2.09
.0200	.0600	.0937	1.500	1.000	1.500	1.00	2.88
.0100	.0100	.0167	1.500	1.000	1.500	1.00	2.06
.0100	.0100	.0469	1.500	1.000	1.500	1.00	1.53
.0100	.0300	.0200	1.500	1.000	1.500	1.00	2.19
.0100	.0300	.0417	1.500	1.000	1.500	1.00	2.31
.0100	.0300	.0937	1.500	1.000	1.500	1.00	3.32

Table 4

W1	W2	G	WS	HH	XP	Fmean	Fmax	Fmaxr
.0500	.0500	.0139	1.000	1.000	1.069	.005	.013	.013
.0500	.0500	.0500	1.000	1.000	1.100	.006	.013	.056
.0500	.0500	.1000	1.000	1.000	1.150	.023	.014	.182
.0500	.0750	.0200	1.000	1.000	1.060	.007	.018	.021
.0500	.0750	.0434	1.000	1.000	1.094	.007	.020	.020
.0500	.0750	.0955	1.000	1.000	1.137	.019	.019	.170
.0500	.1500	.0167	1.000	1.000	1.033	.009	.035	.038
.0500	.1500	.0500	1.000	1.000	1.063	.011	.039	.039
.0500	.1500	.1000	1.000	1.000	1.112	.024	.037	.148
.0200	.0200	.0139	1.000	1.000	1.097	.004	.007	.037
.0200	.0200	.0500	1.000	1.000	1.138	.007	.009	.069
.0200	.0200	.1000	1.000	1.000	1.188	.043	.010	.142
.0200	.0300	.0200	1.000	1.000	1.100	.005	.009	.024
.0200	.0300	.0434	1.000	1.000	1.128	.007	.010	.069
.0200	.0300	.0955	1.000	1.000	1.181	.032	.011	.212
.0200	.0600	.0167	1.000	1.000	1.083	.006	.016	.023
.0200	.0600	.0500	1.000	1.000	1.112	.007	.016	.039
.0200	.0600	.1000	1.000	1.000	1.163	.032	.018	.174
.0200	.0200	.0111	1.500	1.000	3.167	.031	.009	.468
.0100	.0100	.0116	1.000	1.000	1.123	.004	.006	.027
.0100	.0100	.0417	1.000	1.000	1.146	.005	.006	.040
.0100	.0100	.0937	1.000	1.000	1.198	.042	.007	.092
.0100	.0150	.0185	1.000	1.000	1.120	.004	.007	.035
.0100	.0150	.0417	1.000	1.000	1.146	.006	.007	.041
.0100	.0150	.0937	1.000	1.000	1.198	.045	.008	.127
.0100	.0300	.0167	1.000	1.000	1.100	.004	.009	.015
.0100	.0300	.0434	1.000	1.000	1.136	.007	.010	.064
.0100	.0300	.0940	1.000	1.000	1.186	.030	.011	.097
.4000	.4000	.0500	2.933	.800	1.663	.024	.048	.099

W1	W2	G	WS	HH	XP	Fmean	Fmax	Fmaxr
.4000	.4000	.1000	2.933	.800	1.663	.044	.045	.276
.4000	.6000	.1000	3.000	.800	1.663	.054	.091	.284
.4000	.4000	.0500	2.933	1.500	1.712	.022	.043	.072
.4000	.4000	.1000	2.933	1.500	1.712	.034	.046	.228
.4000	.6000	.1000	3.000	1.500	1.712	.040	.071	.207
.2000	.2000	.0500	2.933	.800	1.663	.014	.020	.107
.2000	.2000	.1000	2.933	.800	1.663	.041	.019	.289
.2000	.3000	.0500	3.000	.800	1.663	.018	.039	.100
.2000	.3000	.1000	3.000	.800	1.663	.046	.053	.299
.2000	.6000	.1000	3.000	.800	1.663	.063	.096	.339
.2000	.2000	.0500	2.933	1.500	1.712	.013	.021	.090
.2000	.2000	.1000	2.933	1.500	1.712	.028	.016	.236
.2000	.3000	.0500	3.000	1.500	1.712	.016	.033	.091
.2000	.3000	.1000	3.000	1.500	1.712	.031	.039	.242
.2000	.6000	.1000	3.000	1.500	1.712	.042	.072	.237
.1000	.1000	.0167	2.967	.800	1.667	.008	.009	.066
.1000	.1000	.0500	2.967	.800	1.663	.012	.007	.108
.1000	.1000	.1000	2.967	.800	1.663	.044	.011	.335
.1000	.1500	.0139	3.000	.800	1.667	.009	.016	.059
.1000	.1500	.0500	3.000	.800	1.663	.015	.021	.125
.1000	.1500	.1000	3.000	.800	1.663	.048	.023	.326
.1000	.3000	.0500	3.000	.800	1.663	.019	.042	.112
.1000	.3000	.1000	3.000	.800	1.663	.054	.054	.320
.1000	.1000	.0167	2.967	1.500	1.717	.007	.009	.057
.1000	.1000	.0500	2.967	1.500	1.712	.010	.008	.092
.1000	.1000	.1000	2.967	1.500	1.712	.033	.009	.288
.1000	.1500	.0139	3.000	1.500	1.722	.008	.017	.048
.0500	.0750	.0200	1.500	1.000	1.500	.012	.022	.046
.0500	.0750	.0500	1.500	1.000	1.500	.018	.022	.075
.0500	.0750	.1000	1.500	1.000	1.487	.035	.019	.174
.0500	.1500	.0200	1.500	1.000	1.500	.015	.037	.049
.0500	.1500	.0417	1.500	1.000	1.500	.020	.038	.074
.0500	.1500	.0937	1.500	1.000	1.500	.036	.039	.155
.0200	.0200	.0200	1.500	1.000	1.500	.010	.010	.044
.0200	.0200	.0500	1.500	1.000	1.500	.017	.009	.074
.0200	.0200	.1000	1.500	1.000	1.487	.043	.011	.167
.0200	.0300	.0200	1.500	1.000	1.500	.010	.012	.046
.0200	.0300	.0500	1.500	1.000	1.500	.019	.022	.075
.0200	.0300	.1000	1.500	1.000	1.487	.039	.012	.140
.0200	.0600	.0200	1.500	1.000	1.500	.011	.020	.044
.0200	.0600	.0417	1.500	1.000	1.500	.016	.019	.068
.0200	.0600	.0937	1.500	1.000	1.500	.033	.018	.177
.0100	.0100	.0167	1.500	1.000	1.500	.010	.007	.045
.0100	.0100	.0469	1.500	1.000	1.500	.027	.008	.101
.0100	.0300	.0200	1.500	1.000	1.500	.011	.010	.046
.0100	.0300	.0417	1.500	1.000	1.500	.015	.012	.084
.0100	.0300	.0937	1.500	1.000	1.500	.035	.012	.137

Table 5

W1	W2	G	WS	HH	XP	Fmean	Fmax	Fmaxr
.0500	.0500	.0139	1.000	1.000	1.069	.006	.012	.015
.0500	.0500	.0500	1.000	1.000	1.100	.013	.012	.057
.0500	.0500	.1000	1.000	1.000	1.150	.027	.014	.182
.0500	.0750	.0200	1.000	1.000	1.060	.009	.018	.021
.0500	.0750	.0434	1.000	1.000	1.094	.013	.020	.038
.0500	.0750	.0955	1.000	1.000	1.137	.025	.020	.171
.0500	.1500	.0167	1.000	1.000	1.033	.025	.045	.048
.0500	.1500	.0500	1.000	1.000	1.063	.019	.038	.054
.0500	.1500	.1000	1.000	1.000	1.112	.030	.040	.148
.0200	.0200	.0139	1.000	1.000	1.097	.004	.007	.037
.0200	.0200	.0500	1.000	1.000	1.138	.008	.009	.070
.0200	.0200	.1000	1.000	1.000	1.188	.043	.010	.144
.0200	.0300	.0200	1.000	1.000	1.100	.006	.009	.027
.0200	.0300	.0434	1.000	1.000	1.128	.007	.010	.070
.0200	.0300	.0955	1.000	1.000	1.181	.032	.011	.212
.0200	.0600	.0167	1.000	1.000	1.083	.009	.016	.022
.0200	.0600	.0500	1.000	1.000	1.112	.011	.016	.040
.0200	.0600	.1000	1.000	1.000	1.163	.033	.018	.174
.0200	.0200	.0111	1.500	1.000	3.167	.037	.011	.467
.0100	.0100	.0116	1.000	1.000	1.123	.004	.006	.026
.0100	.0100	.0417	1.000	1.000	1.146	.005	.006	.040
.0100	.0100	.0937	1.000	1.000	1.198	.042	.007	.090
.0100	.0150	.0185	1.000	1.000	1.120	.004	.007	.035
.0100	.0150	.0417	1.000	1.000	1.146	.006	.007	.041
.0100	.0150	.0937	1.000	1.000	1.198	.047	.008	.106
.0100	.0300	.0167	1.000	1.000	1.100	.004	.009	.018
.0100	.0300	.0434	1.000	1.000	1.136	.007	.010	.064
.0100	.0300	.0940	1.000	1.000	1.186	.031	.011	.090
.4000	.4000	.0500	2.933	.800	1.663	.028	.048	.099
.4000	.4000	.1000	2.933	.800	1.663	.045	.045	.276
.4000	.6000	.1000	3.000	.800	1.663	.054	.095	.284
.4000	.4000	.0500	2.933	1.500	1.712	.027	.043	.073
.4000	.4000	.1000	2.933	1.500	1.712	.039	.046	.228
.4000	.6000	.1000	3.000	1.500	1.712	.047	.087	.207
.2000	.2000	.0500	2.933	.800	1.663	.015	.020	.107
.2000	.2000	.1000	2.933	.800	1.663	.042	.018	.289
.2000	.3000	.0500	3.000	.800	1.663	.019	.046	.100
.2000	.3000	.1000	3.000	.800	1.663	.047	.051	.299
.2000	.6000	.1000	3.000	.800	1.663	.063	.095	.339
.2000	.2000	.0500	2.933	1.500	1.712	.015	.020	.089
.2000	.2000	.1000	2.933	1.500	1.712	.029	.016	.237
.2000	.3000	.0500	3.000	1.500	1.712	.019	.041	.091
.2000	.3000	.1000	3.000	1.500	1.712	.032	.042	.242
.2000	.6000	.1000	3.000	1.500	1.712	.046	.081	.237
.1000	.1000	.0167	2.967	.800	1.667	.008	.009	.066
.1000	.1000	.0500	2.967	.800	1.663	.012	.007	.108
.1000	.1000	.1000	2.967	.800	1.663	.051	.011	.335
.1000	.1500	.0139	3.000	.800	1.667	.009	.018	.058
.1000	.1500	.0500	3.000	.800	1.663	.015	.019	.125
.1000	.1500	.1000	3.000	.800	1.663	.054	.018	.326
.1000	.3000	.0500	3.000	.800	1.663	.019	.045	.112
.1000	.3000	.1000	3.000	.800	1.663	.058	.050	.320
.1000	.1000	.0167	2.967	1.500	1.717	.007	.009	.057
.1000	.1000	.0500	2.967	1.500	1.712	.011	.008	.092
.1000	.1000	.1000	2.967	1.500	1.712	.034	.008	.287
.1000	.1500	.0139	3.000	1.500	1.722	.009	.019	.049

W1	W2	G	WS	HH	XP	Fmean	Fmax	Fmaxr
.0500	.0750	.0200	1.500	1.000	1.500	.018	.022	.058
.0500	.0750	.0500	1.500	1.000	1.500	.027	.023	.107
.0500	.0750	.1000	1.500	1.000	1.487	.051	.020	.255
.0500	.1500	.0200	1.500	1.000	1.500	.032	.047	.069
.0500	.1500	.0417	1.500	1.000	1.500	.030	.042	.106
.0500	.1500	.0937	1.500	1.000	1.500	.052	.039	.232
.0200	.0200	.0200	1.500	1.000	1.500	.015	.009	.054
.0200	.0200	.0500	1.500	1.000	1.500	.025	.009	.106
.0200	.0200	.1000	1.500	1.000	1.487	.050	.010	.302
.0200	.0300	.0200	1.500	1.000	1.500	.015	.012	.062
.0200	.0300	.0500	1.500	1.000	1.500	.026	.026	.129
.0200	.0300	.1000	1.500	1.000	1.487	.054	.012	.239
.0200	.0600	.0200	1.500	1.000	1.500	.018	.020	.055
.0200	.0600	.0417	1.500	1.000	1.500	.024	.019	.098
.0200	.0600	.0937	1.500	1.000	1.500	.046	.018	.218
.0100	.0100	.0167	1.500	1.000	1.500	.015	.006	.061
.0100	.0100	.0469	1.500	1.000	1.500	.057	.008	.327
.0100	.0300	.0200	1.500	1.000	1.500	.015	.011	.059
.0100	.0300	.0417	1.500	1.000	1.500	.022	.013	.122
.0100	.0300	.0937	1.500	1.000	1.500	.043	.013	.224

11. MICROSTRIP STEP MODEL

The physical structure of the step discontinuity in a package is shown in Fig. 11.1.

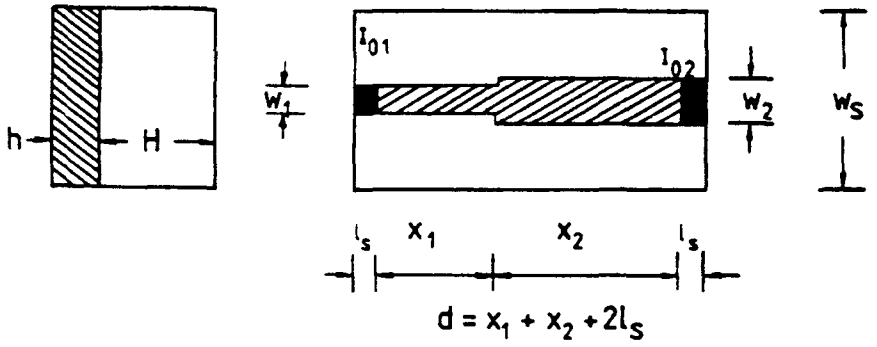


Fig. 11.1: Microstrip step discontinuity

This structure shows the feed lines and current sources used in the numerical full wave analysis. The model of the step discontinuity is the 4-port equivalent circuit shown in Figure 11.2.

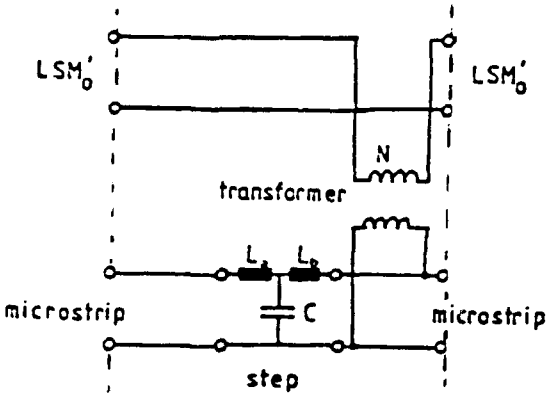


Fig. 11.2: Step discontinuity equivalent circuit

In the model the quasi-static behaviour of the discontinuity is represented by a T-equivalent circuit of inductors and a capacitor, L_a, L_b and C respectively.

The circuit model Fig. 11.3, equivalent to Fig. 11.1, used in the de-embedding of the numerical S-parameters, has transmission lines for the microstrip and LSM_0 modes together with sources and microstrip-LSM_0 mode coupling transformers N located at the wider feedstrip side and M1 and M2 and at the sources are also required added to this discontinuity model.

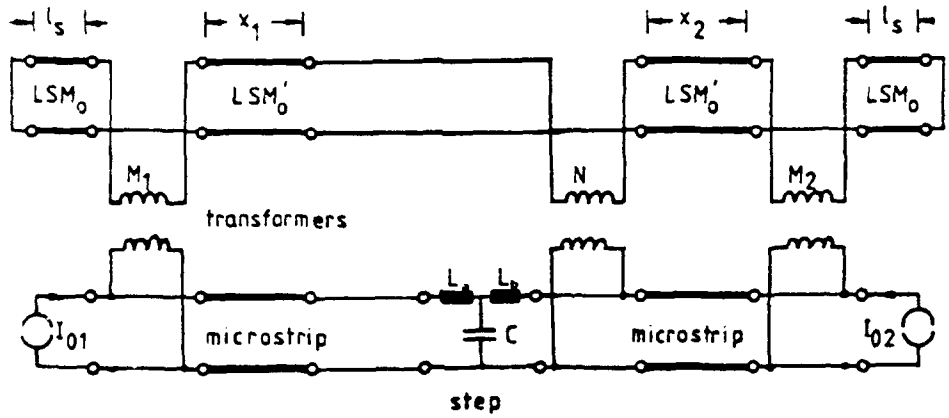


Fig. 11.3: Equivalent circuit representation of step discontinuity in a package

11.1. ANALYTIC FORMULAE FOR THE QUASI-STATIC STEP MODEL

A common quasi-static equivalent circuit used for the microstrip step is the T-equivalent circuit of Fig. 11.4.

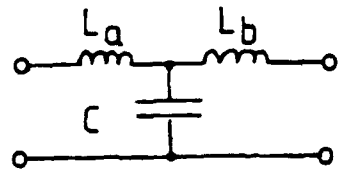


Fig. 11.4: Quasi-static equivalent circuit model for the microstrip step discontinuity

In the model the inductances L_a and L_b represent the inductive behaviour of the step discontinuity due to the disturbance of the current distribution on the feed lines. The capacitance C describes the effect of the stray field at the step in width of the wider feed line.

In order to obtain the circuit elements defining the gap discontinuity quasi-static behaviour, a data base was generated with normalization of the geometric parameters and frequency to the substrate height h=0.1 mm. The step geometries analysed were:

strip width w_1:	400μm, 200μm, 100μm, 50μm, 20μm, 10μm
strip width ratio w_2/w_1:	2, 3, 4, 5, 6, 7, 8, 9, 10
package width w_s:	0.6mm, 0.8mm, 1.0mm, 1.6mm, 3mm
cover height H:	0.5mm, 2mm
frequency:	5GHz - 30GHz

A preliminary modelling study using the full wave database was done to detect any discrepancy. Correction factors for the elements of the equivalent circuit model were introduced and the model elements modified by fitting the S-parameters to the data base results. Investigation showed that the values of the optimized correction factors differed considerably from a value of 1 for most step configurations, indicating that the basic description used was not very accurate.

Due to these deviations some additional convergence tests were performed. It was found that in certain cases results were not sufficiently convergent. For the transmission parameter S12 and for the magnitude of the reflection coefficients S11 and S22 the deviation from the numerical data was quite small (Figures 11.5-6, where x_p is the package length), large deviations occurring in the S11 and S22 phases. The discrepancies were traced to the fact that the S-parameters were normalized to 50 Ohm reference impedances. As a result at low frequencies (quasi-static range) the magnitude of the

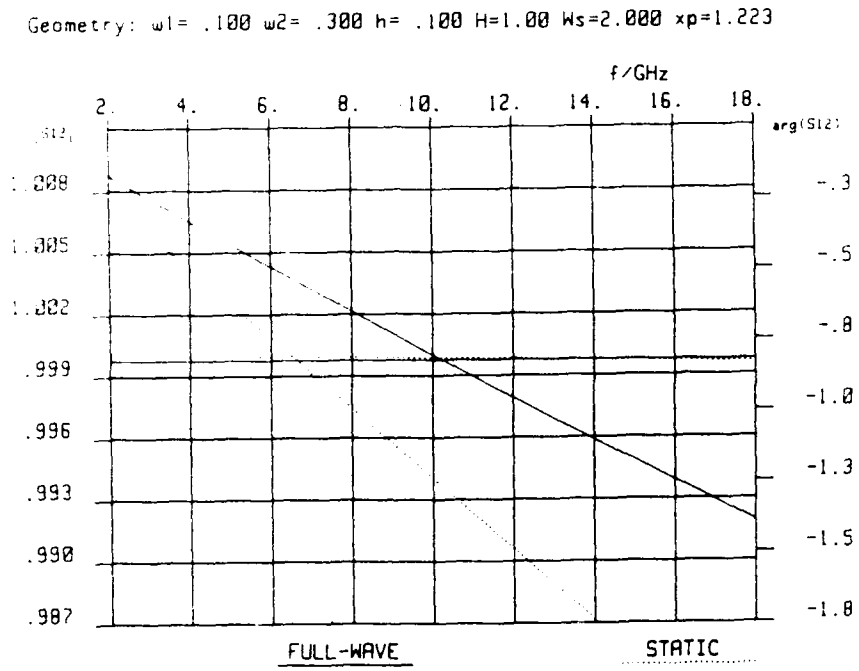
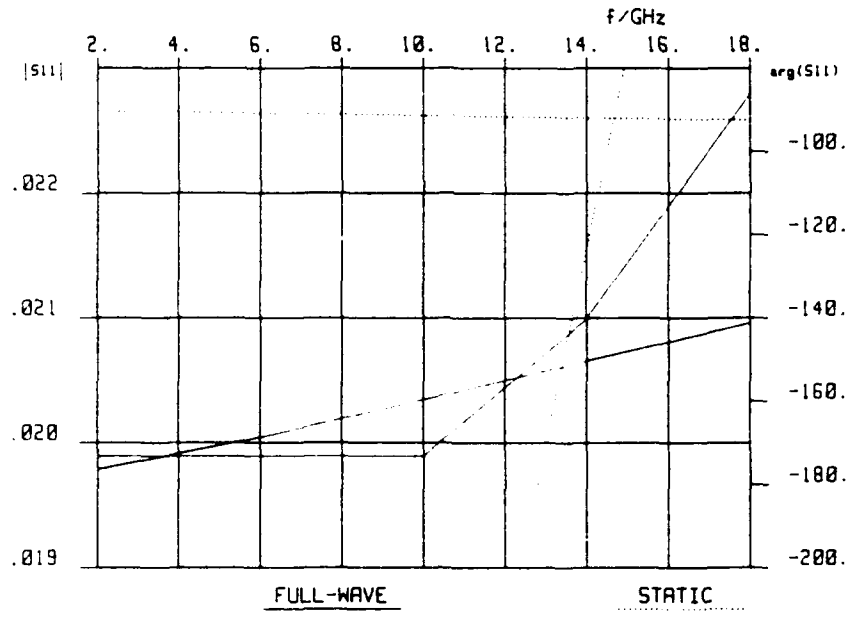


Fig. 11.5: S12 for step configuration



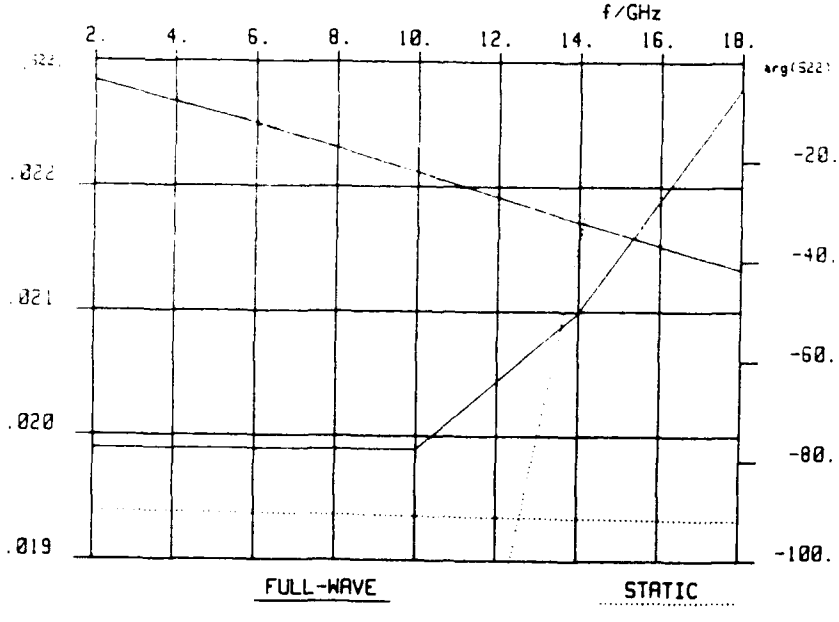


Fig. 11.6: S11 and S22 for step configuration

reflection coefficients of the step discontinuity becomes relatively small. The impedance of the elements L_a and L_b and the admittance of the element C_s of the equivalent circuit model decrease and are zero for the static case and the phase of S11 and S22 are no longer definable. These problems were overcome by using double precision accuracy in the numerical full wave analysis thus giving stable results for small steps in strip width and low frequencies (f*h>0.05 GHz mm) and changing the reference impedance from 50Ω to the individual strip impedance values at zero frequency.

A major step in the generation of the final analytic formulae for the static portion of the circuit model was to fit the S-parameters of the T-equivalent circuit to the numerical data sets. The analytic formulae structure for the elements of the circuit model were constructed to reflect the correct asymptotic behaviour of the S-parameters for the limit of low strip width ratios w_2/w_1. Analytical formulae for L_a, L_b and C developed from published expressions (1) were used as a basis for refinement. The inductances L_a and L_b were not fitted independently from each other, but were calculated from the total inductance $L_s=L_a+L_b$ and from the inductance ratio L_a/L_b. Thus L_b and L_a are given by:

$L_b=L_s / (1 + L_a/L_b)$ and
$L_a=L_s - L_b$

The total inductance L_s was fitted using the correction factor FC_ZLS, the inductance ratio L_a/L_b using the correction factor FC_ZLAB and the capacitance C using the correction factor FC_YCS, respectively. These correction factors were derived by first fitting for each data set individually the S-parameters of the T-equivalent circut model to the data base results. The correction factors obtained are listed in Table 1 (Section 11.5) for 127 data sets. As can be seen by inspection, the total inductance

L_s and the capacitance C need only small refinement. Their correction factors do not deviate significantly from the value of 1. However the L_a/L_b ratio is obviously not predicted accurately by the basic formula.

At first it was found that the de-embedding was sensitive to the step characteristic impedances. In the model the characteristic impedances are predicted by the analytic formulae developed in Section 4 and are not exactly identical to the characteristic impedances used in the 3D full-wave analysis. To overcome this sensitivity the analytic characteristic impedances were included in the fitting procedure to get high prediction accuracy for the elements of the T-equivalent circuit together with a correction factor FC_ZL ($Z_{L1}'=Z_{L1}*FC_ZL$, $Z_{L2}'=Z_{L2}*FC_ZL$ where Z_{L1} and Z_{L2} are the characteristic impedance of the feedlines of width, w_1 and w_2 respectively). The values of the correction factor FC_ZL are in the range of $1<FC\ ZL<1.031$ and reflect the high quality of the analytic formulae (Table 1).

In a second step, the correction factors were used to develop the refined *analytic formulae for the* static portion of the step equivalent circuit model. The final analytic formulae obtained were:

$$2*\pi*f*\ L_s\ /\ \Omega = 0.3774 * (f/GHz) * (h/mm) * (1 - w_{1eff}/w_{2eff})^{1.545} * (w_2/w_1)^{0.75} * (w_1/h)^{0.629}$$

$$2*\pi*f*\ C/S = dl_2 * \beta_2 / Z_{L2} * (1 - w_{1eff} / w_{2eff})^{1.5}$$

$$L_a\ /\ L_b = 0.1444 * (w_{1eff}/w_{2eff} * (1 + 2.878*w_2/w_1)$$

the units being MKS unless stated otherwise. The parameters dl_2, β_2 and Z_{L2} are the effective open end length (determined as in Section 9), the propagation constant and the characteristic impedance of the feedline of width w_2, respectively, where the effective widths are given by the formulae in Section 11.4.

In Table 2 (Section 11.5) the mean deviation F_{mean}, the maximum deviation F_{max} and the relative maximum deviation F_{maxr} for each data set are listed for parameters S11, S12 and S22. The overall data set deviations are:

S11: F_{mean}=1.63%, F_{max}=4.63%, F_{maxr}=10.3%
S12: F_{mean}=0.419%, F_{max}=1.72%, F_{maxr}=2.56%
S22: F_{mean}=1.11%, F_{max}=4.31%, F_{maxr}=9.27%

Detailed inspection shows that the larger, maximum relative deviations are related to the S-parameters for discontinuities of small ratios in strip width (w_2/w_1=2). The respective maximum absolute deviations are also quite small and the analytic formulae take the correct behaviour for small w_2/w_1 ratios into account. The reflection coefficient residual error exceeds 2% only for one input strip width (w_1=0.2h) and width ratios larger than 6. This can be attributed to accuracy limitations in the numerical data.

11.2. DESCRIPTION OF THE TRANSFORMERS IN THE DYNAMIC MODEL

Although in previous investigations on step discontinuity circuit models circuits with 2 transformers at the step were studied (Section 5), it was found that a single transformer was adequate (Fig. 11.3). From physical considerations the transformer was positioned at the wider side of the step discontinuity where the main excitation of the parasitic LSM_0' mode occurs. In this model the transformer ratio N has to reflect that when the feed lines are of nearly equal strip width, there is no excitation of the parasitic package mode and therefore the transformer ratio has to decrease with decreasing w_2-w_1 ($w_2>w_1$).

The description of N for the step discontinuity can be determined from studying the gap discontinuity in the case of small gap widths ($g\to 0$). In this case, the LSM_0 mode transmission line length g can be neglected, the

transformers N_1 and N_2 being connected in series. The package mode is then excited by the fundamental microstrip mode depending on the difference between $N_2 - N_1$. Based on these considerations the new formulae for the transformer ratio N of the step discontinuity takes the form

$$N = N_2 - N_1$$

where N_2 and N_1 are computed as for the gap discontinuity.

For fine tuning the transformer ratio description following data base was generated:

strip width w_1:	200μm, 100μm, 50μm
strip width rato w_2/w_1:	2, 3, 4, 5, 6, 7, 8, 9, 10
substrate width W_s:	1.6mm, 3.2mm
cover height H:	1mm
feed line ratio x_1/x_2:	0.6
frequency:	90GHz - 120GHz

The package length was chosen to have a package resonance frequency of about 107 GHz within the frequency range of interest.

Dynamic model 2-port S-parameters were generated and compared to the data base results. However it was found that for several data sets the resonance behaviour of the dynamic equivalent circuit model differed from the data base S-parameters. An example of this is given for S12 in Fig. 11.7. Further investigations found that the equivalent circuit model is correct, but that the S-parameters of the step discontinuity model are sensitive with respect to the propagation constants of the fundamental microstrip modes used in the de-embedding on the feed lines. A similar sensitivity was found in the previous section regarding the characteristic impedance of the fundamental

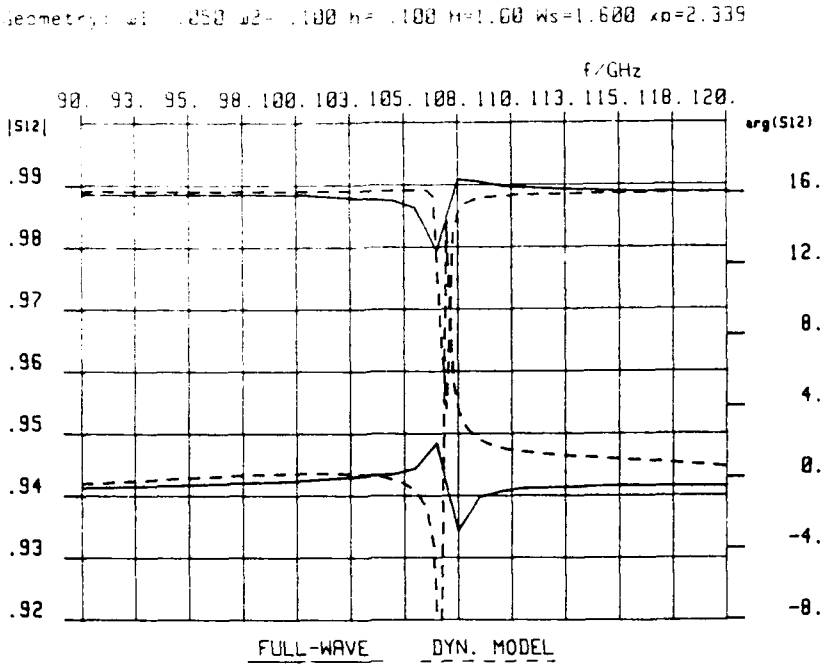


Fig. 11.7: Deviation of the dynamic model from full wave analysis

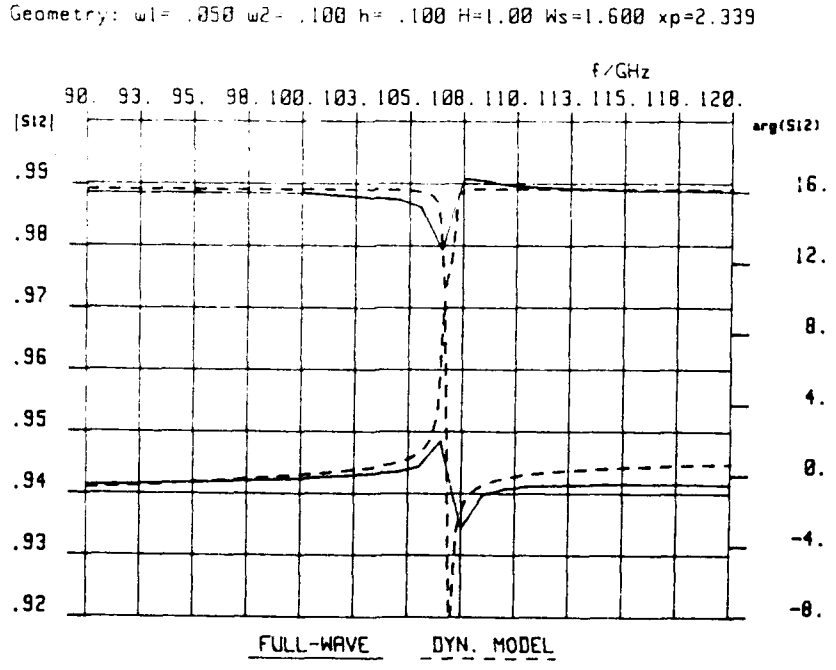


Fig. 11.8: S12 for same step with propagation constant increase

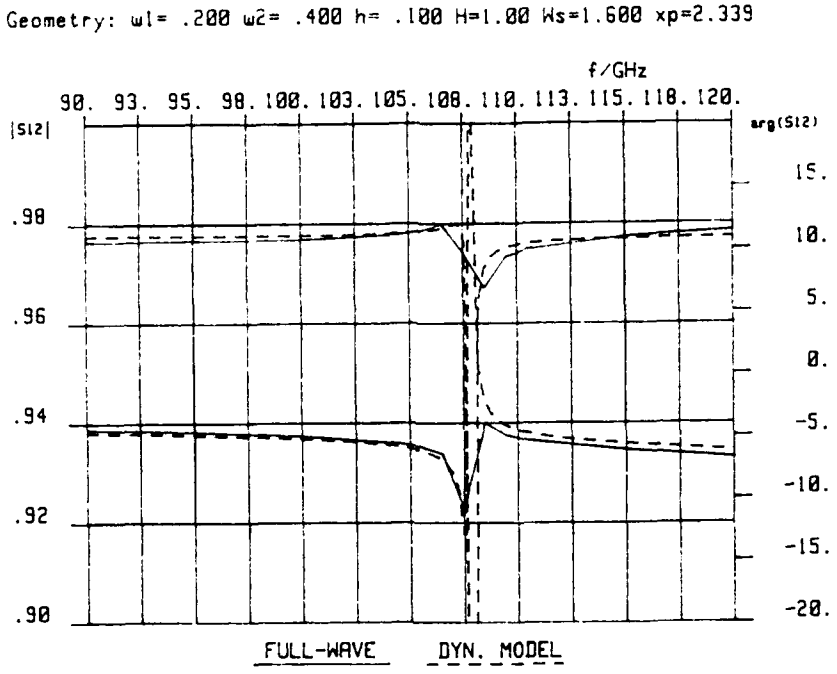


Fig. 11.9: S12 for transformer ratio verification, configuration 1

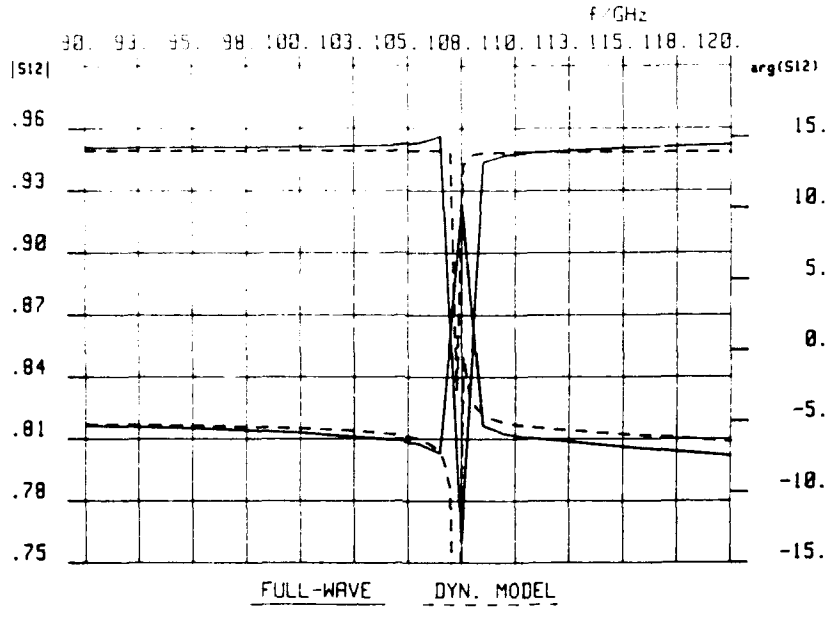


Fig. 11.10: S12 for transformer ratio verification, configuration 2

microstrip mode. The results (Fig. 11.8) show parameters S12 of the same step configuration but with the propagation constants increased slightly. As can be seen the resonance behaviour of the dynamic equivalent circuit model is in good agreement with the data base results.

In order to keep CPU times reasonable, the numerical analysis was performed using a relatively low number of expansion functions. Nevertheless, the data base generation was still time consuming. To overcome the sensitivity problems, the propagation constants were fitted by correction factors during the deembedding of the transfer ratio N.

As a result of comparing the resonance behaviour of the dynamic equivalent circuit model to the data base S-parameters it was found that the formula

$$N = N_2 - N_1$$

provides a very good prediction of the coupling between the fundamental microstrip mode and the LSM_0 package mode. Further fine tuning was found not to be necessary. Results in Figs. 11.9-11.10 show the achieved degree of accuracy.

11.3. TRANSFORMER ANALYTIC FORMULAE FOR THE FREQUENCY TRANSITION REGION

Completion of the step discontinuity model description requires an investigaton of the transition region. The transition region is defined as the frequency range beyond the validity range of the static behaviour of the step equivalent circuit model but reasonably below the package resonance frequency. A variety of step configurations were thus studied in the frequency range 0-120GHz (normalized frequency $0 < f*h < 12$GHzmm).

The close relation between the equivalent circuit model for the step and the gap discontinuity regarding the transformer ratios has been already

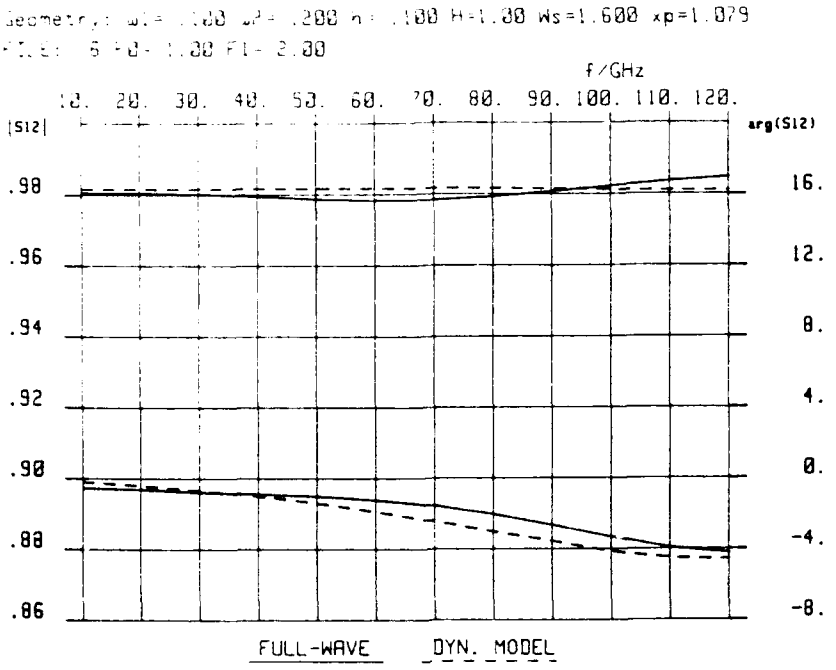


Fig. 11.11: S12 for model verification, configuration 1

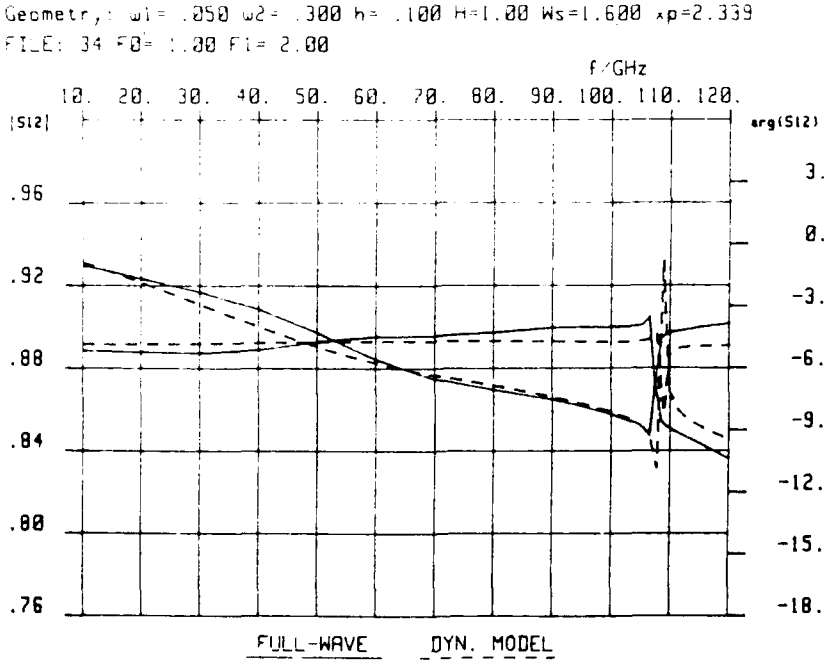


Fig. 11.12: S12 for model verification, configuration 2

explained. Based on these considerations it was expected that the analytic formulae for the dynamic transformer ratics N_{dyn} developed for the gap discontinuity can be applied successfully to the step discontinuity.

A dynamic transformer ratio description

$$N_{dyn} = N * \cos^{f_1}(0.5*\pi*(f-fo)/fo), \quad f<fo$$
$$N_{dyn} = N \qquad f>fo$$

was introduced for the step transformers M1, M2 and N, the parameters f_0 and f_1 represented by the expressions.

$$f_0 = f_c * 1.4 * f_0' * (1 + \exp(-0.638 * w_s/h * H/h)) *$$

$$(1 - 2.33 * \exp(-0.33 * w_s/h))$$

$$f_0' = 1.0$$
$$f_1 = 2$$

A specific transition region data base of 27 configurations was generated for final verification. The results (Figs. 11.11-12) show scattering parameters S12 for two different step configurations. The geometrical parameters are given in the header of the respective result figures. Fine tuning of parameters f_0' or f_1 was found not to be necessary the model fitting the data sets with sufficient accuracy.

11.4. STEP MODEL SUMMARY

A summary of the analytic formulae for the microstrip step discontinuity ($w_2>w_1$) is given in this section, where $Z_L^{microstrip}$ and $\varepsilon_{eff}^{microstrip}$ are computed according to Section 4. All units are MKS except where stated in the formulae.

Quasi-static inductances L_a, L_b and capacitance C

$$2*\pi*f * L_s / \Omega = 0.3774 * (f/GHz) * (h/mm) * (1 - w_{1eff} / w_{2eff})^{1.545} * (w_2/w_1)^{0.75} * (w_1/h)^{0.629}$$

$$2*\pi*f * C / S = dl_2 * \beta_2 / Z_{L2} * (1 - w_{1eff} / w_{2eff})^{1.5}$$

$$L_a / L_b = 0.1444 * (w_{1eff} / w_{2eff}) * (1 + 2.878*w_2/w_1)$$

$L_b = L_s / (1 + L_a/L_b)$ and

$L_a = L_s - L_b$

The parameters dl_2, β_2 and Z_{L2} are the effective open end length, the propagation constant and the characteristic impedance of the feedline of width w_2, respectively.

Transformer ratios N, M1, M2

$M1 = -N_{dyn}(w_1)$

$M2 = -N_{dyn}(w_2)$

$N = N_{dyn}(w_2) - N_{dyn}(w_1)$

$$N_{dyn}(w_i) = \begin{cases} N(w_i) * \cos^{f1} (0.5*\pi*(f-f_0)/f_0) & f<f_0 \\ N(w_i) & f>f_0 \end{cases}$$

$$N(w_i) = 1.2/\pi * \left(\cos \left(\frac{\pi}{2W_s} * (w_s - w_{eff}(w_i)) \right) - \cos \left(\frac{\pi}{2W_s} * (w_s + w_{eff}(w_i)) \right) \right)$$

$$\epsilon_{eff}(LSM_0) = \epsilon_{stat} \left(1 - \left(\frac{f_c}{f}\right)^2\right)$$

with $f_c = \frac{c_0}{2W_s \cdot \sqrt{\epsilon_{stat}}}$

and $\epsilon_{stat} = \frac{\epsilon_r (H+h)}{\epsilon_r H + h}$,

$$Z_L(LSM_0) = \frac{H+h}{W_s} \cdot \frac{Z_0}{\sqrt{\epsilon_{stat}}} \cdot \frac{1}{\sqrt{1 - (f_c/f)^2}}$$

($Z_0 = 120\pi\Omega$, $c_0 = 2.9979\ 10^8$ m/s)

$$w_{i\,eff} = Z_0 * h / Z_L^{microstrip}(w_i) / \sqrt{\varepsilon_{eff}^{microstrip}(w_i)}$$

$$f_0 = f_c * 1.4 * (1 + \exp(-0.0638 * W_s/h * H/h)) * (1 - 2.33 * \exp(-0.33 * W_s/h))$$

$$f_1 = 2$$

Range of Model Validity

The step models are valid for the following ranges (GaAs dielectric constant $\varepsilon_r = 12.9$):

quasi-static model:	50 µm	≤ h	≤	200 µm
	0.1	≤ w/h	≤	4
	2	≤ w2/w1	≤	10
	6	≤ Ws/h	≤	30
	5	≤ H/h	≤	20
dynamic model:	0.5	≤ w/h	≤	2
	2	≤ w2/w1	≤	10
	5	≤ Ws/h	≤	32
	5	≤ H/h	≤	20

where the quasi-static model is that of Fig. 11.4 and the dynamic model that of Fig. 11.2. The dynamic model range is valid for 0 ≤ f*h ≤ 12 GHz mm. Package mode coupling has little influence for 0 ≤f*h ≤ 3 GHz mm and the quasi- static formulae can be used on their own.

11.5. REFERENCES AND TABLES

1. Kirschning M.: Development of models for the computer-aided design of hybrid and monolithic microstrip circuits (in German). University of Duisburg, W. Germany, 1984.

Table 1

STEP GEOMETRY					OPTIMIZED CORRECTION FACTORS			
W1	W2	WS	HH	XP	FC_ZLS	FC_ZLAB	FC_YCS	FC_ZL
.4000	.8000	3.20	.50	3.20	1.159	1.211	.349	1.007
.4000	1.2000	3.20	.50	3.20	1.150	18.609	.490	1.008
.4000	1.6000	3.20	.50	3.20	1.193	21.390	.519	1.008
.4000	2.0000	3.20	.50	3.20	1.272	2.413	.471	1.007
.4000	2.4000	3.20	.50	3.20	1.437	.533	.494	1.003
.4000	.8000	3.20	2.00	3.20	1.429	10.277	.487	1.003
.4000	1.2000	3.20	2.00	3.20	1.257	20.761	.646	1.005
.4000	1.6000	3.20	2.00	3.20	1.278	.928	.690	1.010
.4000	2.0000	3.20	2.00	3.20	1.387	1.882	.694	1.009
.4000	2.4000	3.20	2.00	3.20	1.554	36.793	.687	1.004
.2000	.4000	3.20	.50	3.20	.603	5.307	.290	1.008
.2000	.6000	3.20	.50	3.20	.824	17.768	.489	1.011
.2000	.8000	3.20	.50	3.20	.942	25.053	.551	1.013
.2000	1.0000	3.20	.50	3.20	1.144	-.198	.825	1.027
.2000	1.2000	3.20	.50	3.20	.942	38.127	.585	1.014
.2000	1.4000	3.20	.50	3.20	1.011	35.995	.597	1.019
.2000	1.6000	3.20	.50	3.20	1.062	39.498	.593	1.017
.2000	1.8000	3.20	.50	3.20	1.113	39.830	.582	1.016
.2000	2.0000	3.20	.50	3.20	1.173	30.838	.566	1.014
.2000	.4000	3.20	2.00	3.20	1.133	-.549	.403	1.008
.2000	.6000	3.20	2.00	3.20	1.015	24.338	.601	1.008
.2000	.8000	3.20	2.00	3.20	.984	26.492	.690	1.009
.2000	1.0000	3.20	2.00	3.20	.999	15.873	.743	1.010
.2000	1.2000	3.20	2.00	3.20	1.028	44.094	.769	1.011
.2000	1.4000	3.20	2.00	3.20	1.074	.649	.786	1.016
.2000	1.6000	3.20	2.00	3.20	1.126	.457	.798	1.017
.2000	1.8000	3.20	2.00	3.20	1.178	6.691	.797	1.011
.2000	2.0000	3.20	2.00	3.20	1.241	1.037	.796	1.014
.1000	.2000	1.07	.50	1.07	.988	-.503	.318	1.007
.1000	.3000	1.07	.50	1.07	.827	12.121	.518	1.011
.1000	.4000	1.07	.50	1.07	.779	23.333	.634	1.016
.1000	.5000	1.07	.50	1.07	.764	43.490	.707	1.019
.1000	.2000	1.07	2.00	1.07	1.384	3.937	.307	1.007
.1000	.3000	1.07	2.00	1.07	.956	13.971	.519	1.012
.1000	.4000	1.07	2.00	1.07	.853	25.800	.639	1.016
.1000	.5000	1.07	2.00	1.07	.827	37.012	.711	1.021
.1000	.2000	1.60	.50	1.60	-.797	.873	.333	1.006
.1000	.3000	1.60	.50	1.60	.300	10.105	.517	1.010
.1000	.4000	1.60	.50	1.60	.471	19.790	.629	1.012
.1000	.5000	1.60	.50	1.60	.555	26.498	.695	1.015
.1000	.6000	1.60	.50	1.60	.597	44.984	.745	1 015
.1000	.7000	1.60	.50	1.60	.646	38.457	.773	1.016
.1000	.8000	1.60	.50	1.60	.676	59.403	.794	1.016
.1000	.9000	1.60	.50	1.60	.725	38.370	.808	1.017
.1000	1.0000	1.60	.50	1.60	.755	52.983	.814	1.017
.1000	.3000	1.60	2.00	1.60	.622	10.173	.525	-1.008
.1000	.4000	1.60	2.00	1.60	.655	17.043	.642	1.010
.1000	.5000	1.60	2.00	1.60	.690	28.052	.712	1.013
.1000	.6000	1.60	2.00	1.60	.702	55.286	.762	1.013
.1000	.7000	1.60	2.00	1.60	.741	53.604	.795	1.015
.1000	.8000	1.60	2.00	1.60	.767	52.050	.814	1.015
.1000	.9000	1.60	2.00	1.60	.797	58.673	.834	1.017
.1000	1.0000	1.60	2.00	1.60	.824	57.394	.840	1.018
.0500	.1000	1.07	.50	1.07	.953	1.127	.198	1.003
.0500	.1500	1.07	.50	1.07	.790	3.929	.410	1.006
.0500	.2000	1.07	.50	1.07	.595	6.665	.504	1.008

.0500	.2500	1.07	.50	1.07	.623	17.257	.597	1.011
.0500	.3000	1.07	.50	1.07	.566	17.551	.657	1.011
.0500	.3500	1.07	.50	1.07	.613	16.626	.691	1.014
.0500	.4000	1.07	.50	1.07	.605	25.822	.745	1.015
.0500	.4500	1.07	.50	1.07	.609	34.450	.773	1.016
.0500	.5000	1.07	.50	1.07	.643	22.384	.789	1.017
.0500	.1000	1.07	2.00	1.07	1.640	1.000	.207	1.004
.0500	.1500	1.07	2.00	1.07	1.008	3.427	.390	1.006
.0500	.2000	1.07	2.00	1.07	.790	9.677	.500	1.009
.0500	.2500	1.07	2.00	1.07	.699	-.130	.595	1.011
.0500	.3000	1.07	2.00	1.07	.705	22.840	.651	1.013
.0500	.3500	1.07	2.00	1.07	.690	16.126	.701	1.016
.0500	.4000	1.07	2.00	1.07	.644	35.912	.740	1.016
.0500	.4500	1.07	2.00	1.07	.632	34.988	.770	1.017
.0500	.5000	1.07	2.00	1.07	.697	31.760	.791	1.019
.0500	.1000	1.60	.50	1.60	-2.286	1.113	.218	1.004
.0500	.2000	1.60	.50	1.60	.207	17.671	.507	1.007
.0500	.2500	1.60	.50	1.60	.291	8.587	.587	1.009
.0500	.3000	1.60	.50	1.60	.412	20.185	.650	1.011
.0500	.3500	1.60	.50	1.60	.402	16.065	.696	1.012
.0500	.4000	1.60	.50	1.60	.468	22.486	.733	1.012
.0500	.4500	1.60	.50	1.60	.523	30.332	.758	1.015
.0500	.5000	1.60	.50	1.60	.529	41.339	.784	1.014
.0500	.1000	1.60	2.00	1.60	-.297	1.013	.254	1.004
.0500	.1500	1.60	2.00	1.60	.341	7.546	.393	1.005
.0500	.2000	1.60	2.00	1.60	.476	7.332	.505	1.007
.0500	.2500	1.60	2.00	1.60	.539	9.016	.597	1.008
.0500	.3000	1.60	2.00	1.60	.500	16.479	.655	1.008
.0500	.3500	1.60	2.00	1.60	.533	17.873	.702	1.010
.0500	.4000	1.60	2.00	1.60	.603	44.782	.740	1.011
.0500	.4500	1.60	2.00	1.60	.592	33.597	.768	1.012
.0500	.5000	1.60	2.00	1.60	.623	28.504	.796	1.012
.0200	.0467	.85	.50	.85	5.272	1.060	.129	1.004
.0200	.0600	.85	.50	.85	2.439	1.237	.220	1.006
.0200	.0867	.85	.50	.85	1.303	4.796	.337	1.008
.0200	.1000	.85	.50	.85	1.135	5.342	.399	1.010
.0200	.1267	.85	.50	.85	.920	8.002	.470	1.012
.0200	.1400	.85	.50	.85	.811	7.719	.509	1.012
.0200	.1667	.85	.50	.85	.883	16.944	.562	1.015
.0200	.1800	.85	.50	.85	.818	11.574	.588	1.016
.0200	.2067	.85	.50	.85	.673	17.585	.625	1.018
.0200	.0467	.85	2.00	.85	5.122	1.013	.049	1.004
.0200	.0600	.85	2.00	.85	2.873	.984	.211	1.006
.0200	.0867	.85	2.00	.85	1.435	2.103	.340	1.009
.0200	.1000	.85	2.00	.85	1.170	11.268	.388	1.011
.0200	.1267	.85	2.00	.85	.861	8.146	.470	1.013
.0200	.1400	.85	2.00	.85	.866	9.227	.501	1.013
.0200	.1667	.85	2.00	.85	.724	14.494	.563	1.016
.0200	.1800	.85	2.00	.85	.698	14.097	.592	1.017
.0200	.2067	.85	2.00	.85	.631	15.651	.621	1.018
.0100	.0300	.64	.50	.64	7.018	2.756	.012	1.014
.0100	.0400	.64	.50	.64	3.957	4.641	.149	1.017
.0100	.0500	.64	.50	.64	2.686	6.762	.220	1.020
.0100	.0600	.64	.50	.64	1.943	8.965	.298	1.02
.0100	.0700	.64	.50	.64	1.645	10.296	.335	1.024
.0100	.0800	.64	.50	.64	1.445	8.780	.391	1.026
.0100	.0900	.64	.50	.64	1.415	14.366	.413	1.028
.0100	.1000	.64	.50	.64	1.191	12.627	.460	1.030
.0100	.0200	.64	2.00	.64	28.171	1.138	-.154	1.010
.0100	.0300	.64	2.00	.64	7.404	3.232	.019	1.014
.0100	.0400	.64	2.00	.64	4.101	2.053	.158	1.018
.0100	.0500	.64	2.00	.64	2.867	6.006	.226	1.021
.0100	.0600	.64	2.00	.64	1.973	10.403	.293	1.023
.0100	.0700	.64	2.00	.64	1.589	13.498	.344	1.025
.0100	.0800	.64	2.00	.64	1.332	7.704	.394	1.027
.0100	.0900	.64	2.00	.64	1.206	6.50	.415	1.029
.0100	.1000	.64	2.00	.64	1.328	19.78	.463	1.031

Table 2

STEP GEOMETRY					S11			S12			S22		
W1	W2	WS	HH	XP	Fmean	Fmax	Fmaxr	Fmean	Fmax	Fmaxr	Fmean	Fmax	Fmaxr
.4	.8	3.2	.5	3.2	.042	.017	.062	.008	.012	.013	.028	.011	.040
.4	1.2	3.2	.5	3.2	.037	.022	.050	.010	.013	.015	.021	.014	.032
.4	1.6	3.2	.5	3.2	.043	.034	.064	.014	.017	.020	.022	.024	.045
.4	2.0	3.2	.5	3.2	.000	.000	.000	.000	.000	.000	.000	.000	.000
.4	2.4	3.2	.5	3.2	.000	.000	.000	.000	.000	.000	.000	.000	.000
.4	.8	3.2	2.0	3.2	.015	.006	.021	.002	.005	.005	.014	.006	.020
.4	1.2	3.2	2.0	3.2	.014	.011	.025	.004	.010	.012	.011	.007	.017
.4	1.6	3.2	2.0	3.2	.020	.022	.042	.005	.014	.016	.010	.008	.016
.4	2.0	3.2	2.0	3.2	.000	.000	.000	.000	.000	.000	.000	.000	.000
.4	2.4	3.2	2.0	3.2	.000	.000	.000	.000	.000	.000	.000	.000	.000
.2	.4	3.2	.5	3.2	.026	.009	.039	.006	.007	.007	.018	.006	.025
.2	.6	3.2	.5	3.2	.016	.012	.031	.003	.006	.006	.014	.010	.026
.2	.8	3.2	.5	3.2	.019	.015	.030	.004	.006	.007	.015	.014	.029
.2	1.0	3.2	.5	3.2	.000	.000	.000	.000	.000	.000	.000	.000	.000
.2	1.2	3.2	.5	3.2	.021	.018	.030	.010	.012	.015	.018	.023	.038
.2	1.4	3.2	.5	3.2	.023	.025	.038	.010	.012	.015	.019	.028	.043
.2	1.6	3.2	.5	3.2	.025	.029	.042	.012	.014	.019	.020	.033	.048
.2	1.8	3.2	.5	3.2	.029	.035	.049	.014	.016	.022	.022	.038	.053
.2	2.0	3.2	.5	3.2	.034	.046	.063	.016	.017	.026	.024	.043	.058
.2	.4	3.2	2.0	3.2	.011	.004	.017	.001	.002	.002	.010	.003	.014
.2	.6	3.2	2.0	3.2	.008	.008	.020	.004	.008	.008	.006	.003	.009
.2	.8	3.2	2.0	3.2	.009	.011	.024	.006	.010	.011	.006	.004	.009
.2	1.0	3.2	2.0	3.2	.010	.014	.026	.006	.010	.012	.006	.005	.009
.2	1.2	3.2	2.0	3.2	.011	.017	.029	.005	.010	.012	.006	.005	.009
.2	1.4	3.2	2.0	3.2	.012	.021	.032	.004	.010	.013	.006	.006	.009
.2	1.6	3.2	2.0	3.2	.015	.025	.037	.005	.011	.014	.007	.008	.011
.2	1.8	3.2	2.0	3.2	.019	.033	.047	.007	.013	.018	.007	.008	.011
.2	2.0	3.2	2.0	3.2	.025	.046	.062	.009	.016	.024	.008	.012	.016
.1	.2	1.1	.5	1.1	.009	.003	.014	.001	.002	.002	.007	.002	.010
.1	.3	1.1	.5	1.1	.008	.004	.013	.003	.004	.004	.005	.003	.008
.1	.4	1.1	.5	1.1	.008	.006	.015	.004	.005	.005	.004	.004	.009
.1	.5	1.1	.5	1.1	.007	.007	.014	.005	.005	.006	.005	.004	.009
.1	.2	1.1	2.0	1.1	.011	.003	.017	.002	.002	.003	.008	.002	.012
.1	.3	1.1	2.0	1.1	.010	.005	.015	.004	.004	.004	.003	.002	.006
.1	.4	1.1	2.0	1.1	.010	.005	.013	.006	.006	.006	.003	.003	.006
.1	.5	1.1	2.0	1.1	.011	.006	.013	.006	.006	.007	.003	.004	.008
.1	.2	1.6	.5	1.6	.030	.012	.059	.005	.010	.010	.021	.008	.040
.1	.3	1.6	.5	1.6	.019	.012	.038	.003	.007	.007	.013	.008	.023
.1	.4	1.6	.5	1.6	.016	.013	.031	.003	.006	.006	.012	.008	.019
.1	.5	1.6	.5	1.6	.016	.013	.026	.003	.005	.006	.011	.008	.016
.1	.6	1.6	.5	1.6	.013	.013	.025	.003	.005	.006	.010	.008	.014
.1	.7	1.6	.5	1.6	.013	.014	.023	.003	.006	.007	.009	.007	.012
.1	.8	1.6	.5	1.6	.014	.014	.023	.004	.006	.008	.009	.007	.011
.1	.9	1.6	.5	1.6	.015	.014	.022	.005	.007	.009	.007	.006	.009
.1	1.0	1.6	.5	1.6	.016	.015	.023	.006	.008	.011	.006	.006	.008
.1	.2	1.6	2.0	1.6	.015	.005	.028	.002	.004	.004	.011	.004	.020
.1	.3	1.6	2.0	1.6	.009	.005	.015	.001	.004	.004	.008	.004	.013
.1	.4	1.6	2.0	1.6	.007	.005	.011	.002	.004	.004	.008	.005	.013
.1	.5	1.6	2.0	1.6	.006	.005	.009	.003	.004	.005	.008	.006	.013
.1	.6	1.6	2.0	1.6	.004	.004	.007	.003	.003	.003	.009	.006	.012
.1	.7	1.6	2.0	1.6	.005	.004	.006	.003	.004	.004	.008	.006	.011
.1	.8	1.6	2.0	1.6	.006	.007	.011	.003	.005	.006	.008	.006	.010
.1	.9	1.6	2.0	1.6	.005	.004	.006	.002	.003	.004	.007	.006	.009
.1	1.0	1.6	2.0	1.6	.006	.005	.007	.001	.002	.002	.006	.005	.008
.05	.10	1.07	.5	1.1	.014	.004	.025	.002	.002	.003	.012	.003	.020
.05	.15	1.07	.5	1.1	.012	.005	.020	.002	.004	.004	.008	.003	.012
.05	.20	1.07	.5	1.1	.009	.007	.019	.002	.005	.005	.005	.003	.009

STEP GEOMETRY

W1	W2	WS	HH	XP	S11			S12			S22		
					Fmean	Fmax	Fmaxr	Fmean	Fmax	Fmaxr	Fmean	Fmax	Fmaxr
.05	.25	1.07	.5	1.1	.007	.007	.018	.003	.005	.006	.004	.003	.007
.05	.30	1.07	.5	1.1	.006	.005	.011	.002	.004	.004	.005	.004	.009
.05	.35	1.07	.5	1.1	.008	.009	.019	.004	.006	.007	.005	.005	.009
.05	.40	1.07	.5	1.1	.005	.006	.011	.003	.004	.005	.005	.005	.010
.05	.45	1.07	.5	1.1	.005	.006	.010	.003	.004	.005	.005	.006	.011
.05	.50	1.07	.5	1.1	.009	.013	.023	.005	.008	.010	.006	.006	.010
.05	.10	1.07	2.0	1.1	.016	.004	.026	.001	.002	.003	.014	.003	.021
.05	.15	1.07	2.0	1.1	.014	.006	.023	.003	.004	.004	.009	.004	.015
.05	.20	1.07	2.0	1.1	.013	.008	.025	.004	.006	.007	.007	.004	.012
.05	.25	1.07	2.0	1.1	.009	.007	.018	.004	.005	.006	.004	.003	.007
.05	.30	1.07	2.0	1.1	.011	.008	.018	.005	.006	.007	.004	.003	.006
.05	.35	1.07	2.0	1.1	.011	.010	.021	.006	.007	.008	.004	.004	.008
.05	.40	1.07	2.0	1.1	.007	.009	.017	.005	.006	.007	.005	.005	.009
.05	.45	1.07	2.0	1.1	.004	.006	.010	.004	.004	.005	.006	.005	.009
.05	.50	1.07	2.0	1.1	.009	.012	.020	.006	.007	.009	.005	.005	.009
.05	.10	1.60	.5	1.6	.028	.008	.050	.004	.007	.007	.020	.006	.036
.05	.15	1.60	.5	1.6	.017	.009	.034	.003	.006	.007	.011	.006	.021
.05	.20	1.60	.5	1.6	.014	.009	.028	.003	.005	.006	.009	.006	.017
.05	.25	1.60	.5	1.6	.013	.010	.024	.003	.005	.005	.009	.006	.014
.05	.30	1.60	.5	1.6	.012	.011	.023	.003	.005	.005	.008	.006	.013
.05	.35	1.60	.5	1.6	.015	.011	.022	.003	.005	.005	.009	.007	.013
.05	.40	1.60	.5	1.6	.012	.012	.022	.003	.005	.005	.008	.007	.013
.05	.45	1.60	.5	1.6	.013	.011	.020	.004	.007	.008	.008	.006	.011
.05	.50	1.60	.5	1.6	.011	.013	.021	.003	.005	.006	.008	.007	.012
.05	.10	1.60	2.0	1.6	.014	.003	.020	.002	.004	.004	.010	.002	.015
.05	.15	1.60	2.0	1.6	.007	.003	.013	.001	.002	.002	.005	.002	.008
.05	.20	1.60	2.0	1.6	.006	.004	.010	.001	.003	.003	.005	.003	.009
.05	.25	1.60	2.0	1.6	.007	.006	.014	.002	.005	.005	.005	.004	.009
.05	.30	1.60	2.0	1.6	.007	.004	.009	.002	.004	.004	.007	.005	.010
.05	.35	1.60	2.0	1.6	.007	.006	.012	.002	.005	.005	.007	.006	.011
.05	.40	1.60	2.0	1.6	.009	.008	.014	.004	.006	.007	.006	.006	.011
.05	.45	1.60	2.0	1.6	.007	.006	.011	.003	.006	.007	.007	.006	.011
.05	.50	1.60	2.0	1.6	.007	.006	.011	.004	.005	.006	.007	.007	.012
.02	.05	.85	.5	.9	.041	.006	.045	.003	.004	.004	.034	.005	.038
.02	.06	.85	.5	.9	.029	.006	.032	.003	.004	.004	.024	.005	.026
.02	.09	.85	.5	.9	.023	.008	.030	.003	.005	.005	.017	.006	.022
.02	.10	.85	.5	.9	.022	.009	.030	.004	.005	.005	.015	.006	.019
.02	.13	.85	.5	.9	.020	.010	.028	.004	.006	.006	.012	.006	.016
.02	.14	.85	.5	.9	.018	.008	.021	.004	.005	.005	.010	.004	.011
.02	.17	.85	.5	.9	.021	.015	.034	.006	.009	.010	.010	.006	.015
.02	.18	.85	.5	.9	.020	.011	.025	.006	.006	.007	.009	.005	.011
.02	.21	.85	.5	.9	.014	.011	.023	.004	.006	.007	.006	.004	.008
.02	.05	.85	2.0	.9	.043	.007	.047	.003	.004	.004	.036	.006	.040
.02	.06	.85	2.0	.9	.033	.008	.043	.003	.005	.005	.026	.006	.033
.02	.09	.85	2.0	.9	.025	.008	.028	.004	.005	.005	.017	.005	.019
.02	.10	.85	2.0	.9	.022	.008	.026	.004	.005	.005	.015	.005	.017
.02	.13	.85	2.0	.9	.018	.009	.024	.004	.005	.005	.011	.005	.013
.02	.14	.85	2.0	.9	.019	.009	.024	.004	.005	.006	.010	.005	.013
.02	.17	.85	2.0	.9	.015	.010	.024	.004	.006	.006	.008	.005	.011
.02	.18	.85	2.0	.9	.014	.008	.017	.004	.004	.005	.006	.003	.008
.02	.21	.85	2.0	.9	.012	.010	.022	.004	.006	.007	.005	.004	.008
.01	.02	.64	.5	.6	.000	.000	.000	.000	.000	.000	.000	.000	.000
.01	.03	.64	.5	.6	.052	.011	.067	.004	.005	.005	.044	.010	.057
.01	.04	.64	.5	.6	.044	.012	.056	.004	.005	.005	.035	.010	.046
.01	.05	.64	.5	.6	.039	.013	.049	.005	.005	.005	.030	.010	.039
.01	.06	.64	.5	.6	.033	.012	.041	.004	.005	.005	.025	.009	.031

STEP GEOMETRY

W1	W2	WS	HH	XP	S11			S12			S22		
					Fmean	Fmax	Fmaxr	Fmean	Fmax	Fmaxr	Fmean	Fmax	Fmaxr
.01	.07	.64	.5	.6	.032	.013	.041	.004	.005	.005	.023	.010	.031
.01	.08	.64	.5	.6	.030	.015	.041	.005	.006	.007	.021	.010	.028
.01	.09	.64	.5	.6	.032	.018	.047	.005	.008	.009	.021	.011	.029
.01	.10	.64	.5	.6	.028	.017	.043	.005	.008	.008	.019	.010	.026
.01	.02	.64	2.0	.6	.082	.010	.104	.005	.005	.005	.073	.009	.093
.01	.03	.64	2.0	.6	.053	.011	.069	.004	.005	.005	.044	.010	.058
.01	.04	.64	2.0	.6	.044	.012	.057	.005	.005	.005	.035	.010	.046
.01	.05	.64	2.0	.6	.040	.013	.052	.005	.006	.006	.030	.010	.040
.01	.06	.64	2.0	.6	.033	.012	.041	.004	.005	.005	.025	.009	.032
.01	.07	.64	2.0	.6	.031	.012	.037	.004	.005	.005	.022	.009	.027
.01	.08	.64	2.0	.6	.028	.012	.034	.004	.005	.005	.020	.009	.025
.01	.09	.64	2.0	.6	.028	.015	.041	.004	.007	.007	.019	.010	.026
.01	.10	.64	2.0	.6	.031	.020	.051	.006	.010	.011	.020	.012	.029

12. MICROSTRIP 90° BEND MODEL

The physical realisation of the 90° bend in a package is shown in Fig. 12.1.

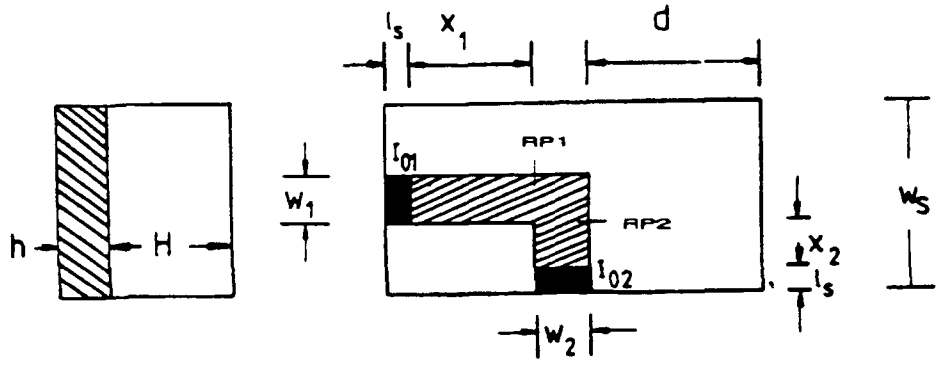


Fig. 12.1: Microstrip 90° bend structure in a package

where the package is described by its width w_s and its cover height H. The bend feedlines strip1 and strip2 are centred in the package. The figure also shows the total current sources I_{01} and I_{02} used in the full field analysis. The dynamic equivalent circuit model description of this situation is shown in Fig. 12.3.

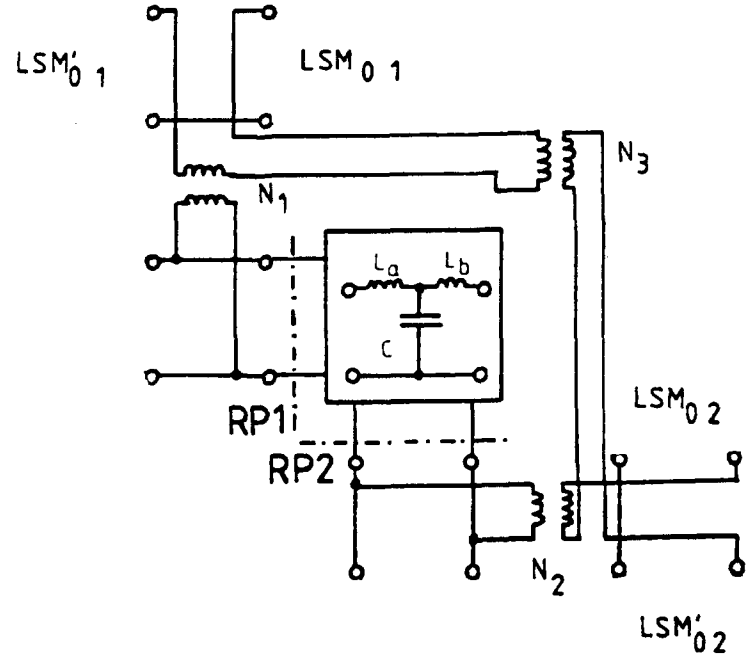


Fig. 12.2: Dynamic equivalent circuit model

The model includes a quasi-static T-equivalent circuit model described by two inductors and a capacitor, the microstrip-LSM_0 mode coupling transformers M1, M2, N1 and N2 and the bidirectional LSM_{01} - LSM_{02} coupling transformer N3.

The bend discontinuity stripped of feedlines and current sources is shown in Figure 12.2.

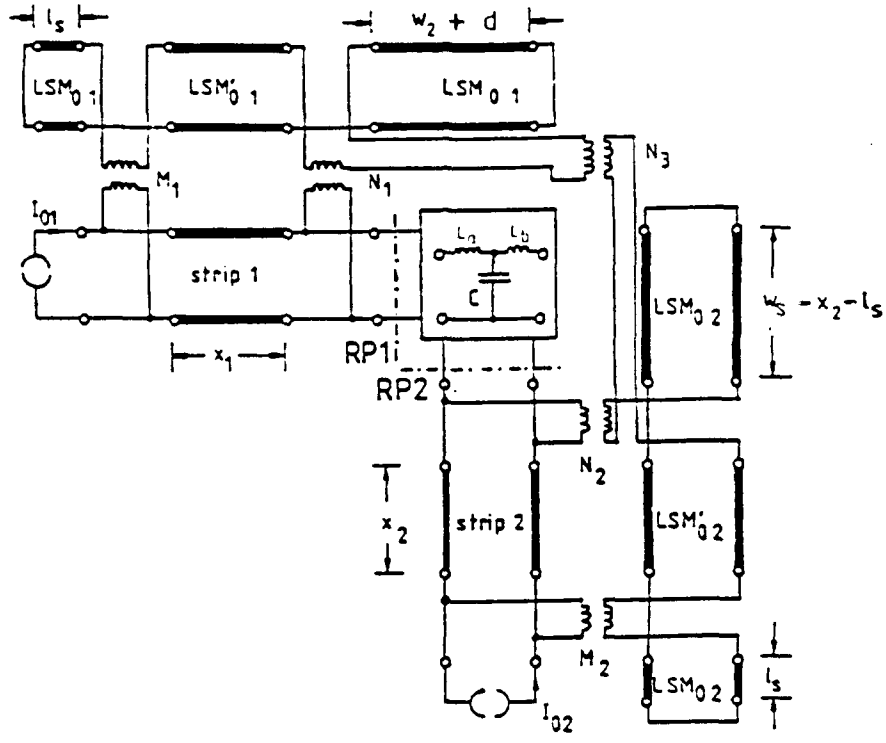


Fig. 12.3: Equivalent circuit representation of a bend discontinuity in a package

12.1. EXPRESSIONS FOR THE STATIC PART OF THE DYNAMIC BEND MODEL

The quasi-static equivalent circuit model in Figure 12.4 was used for the 90°-bend discontinuity. This equivalent circuit model has been used extensively in the technical literature (1,2), the element values being expressed by anaytical formulae.

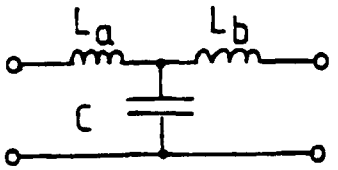


Fig 12.4. Quasi-static equivalent circuit model for the microstrip 90°-bend discontinuity.

Static Model Full Wave Database

A specific quasi-static data base for the 90°-bend was generated using the full-wave analysis program. For the database the 90°-bend configurations were analysed for frequencies of 5 GHz to 30 GHz in steps of 5 GHz, the geometrical parameters of the 90°-bend configurations being chosen for values of strip widths w_1 and w_2 and package dimensions H and W_s normalized to the substrate height h=0.1 mm as outlined in Fig. 12.1.

The cover heights used in the generation of the data base were 0.5 mm and 2 mm, with package dimension, width/lengths W_s = 3.2 mm, 2.1 mm, 1.6 mm and 1.3 mm and the position of strip1 was fixed at the centre of the package x_m = $0.5*w_s$ and that of strip2 d = $l_s + x_1$.

The feed line widths and ratios were:

w_1 = 400 μm, 200 μm, 100 μm, 50 μm, 20 μm, 10 μm, and

w_2/w_1 = 1, 1.25, 1.5, 2, 3, 4, 5.

From all possible parameter combinations a subset of 85 different bend configurations were analysed to generate the specific quasi-static data base.

Due to a high CPU time requirement, tests performed for full convergence of the numerical computations were limited. Convergence checks for bend configurations with very narrow feed lines showed an accuracy of about 5%, the accuracy being better for wide strips. Strip widths of less than 10 µm were not analysed because the numerical computations would have taken too long a time or the achievable accuracy would not have been acceptable.

Expressions for the Static Model Description

As a basis for the static modelling, analytical formulae were taken for the unsymmetric 90°-bend from the Ph.D thesis by Kirschning (2).

The S-parameters of the T-equivalent circuit model were fitted to the numerical data sets for the generation of the analytic formulae describing the static behaviour of the bend equivalent circuit model. During this process the inductances L_a and L_b were not fitted independently of each other, but were calculated from the total inductance $L_s=L_a+L_b$ and the inductance ratio L_a/L_b similar to the step discontinuity.

The total inductance L_s was fitted using the correction factor FC_ZLS; the inductance ratio, L_a/L_b using the correction factor FC_ZLAB and the capacitance C using the correction factor FC_YCS. These correction factors were derived by first fitting the S-parameters of the T-equivalent circuit model for each data set to the numerical data base results. The correction factors obtained are listed in Table 1 (Section 12.6) for 85 data sets.

A detailed look at the correction factor showed that the basic analytical expression did not reflect the correct behaviour of the bend discontinuity (correction factors far away from the value 1). Only for symmetrical bends do the expressions show a reasonable accuracy. However using these factors, a new set of analytic formulae were derived:

$$2*\pi*f * L_s / \Omega = 2*\pi* (f/GHz) * (h/mm) * 0.1865 * (L_1 + L_2)$$
$$* (w_2/w_1)^{0.558} * (1 - 0.0303*w1/h)$$
$$* \exp (-0.214*(w_2/w_1-1)^{-0.0751} * (w_1/h)^{-0.419})$$

$$L_1 = (1 - 1.667 * \exp(-0.5862*(w_1/h)^{1.066}) *$$
$$(1 + 0.691* \exp(-3.88*(w_1/h-1.2)^2))$$

$$L_2 = (1 - 1.667 * \exp(-0.5862*(w_2/h)^{1.066}) *$$
$$(1 + 0.691* \exp(-3.88*(w_2/h-1.2)^2))$$

$$2*\pi*f * C / S = 2*\pi* (f/GHz) * (h/mm) *$$
$$(104.0*(w_1/h)^{2.179} + 55.66*(w_1/h) - 10.36*\exp(-4.1*w_1/h)) *$$
$$(6.55 - 5.55*\exp(-0.2022*(w_2/w_1-1)^{0.7172})) *$$
$$(w_2/w_1)^{0.842*(1 - 0.176 * w1/h)} *$$
$$\exp(-0.0581*(w_2/w_1-1)^{1.12} * (w_1/h)^{-0.5775})$$

with $L_a = L_s - L_b$

$L_b = L_s / (1 + L_a/L_b)$

$L_a / L_b = 0.5 * (1 + (w_2/w_1)^{11.21-1.8*w1/h})$

where the units are MKS unless otherwise stated in the formulae.

In Table 2 (Section 12.6) the mean deviation F_{mean}, the maximum deviation F_{max} and the relative maximum deviation F_{max} are listed for parameters S11, S12 and S22 for each data set. The overall deviations considering all evaluated data sets are:

S11:	F_{mean}=3.38%,	F_{max}=0.0308,	F_{maxr}=47.9%
S12:	F_{mean}=0.56%,	F_{max}=0.0381,	F_{maxr}=4.02%
S22:	F_{mean}=3.00%,	F_{max}=0.0256,	F_{maxr}=47.9%

As found with the microstrip step discontinuity the larger maximum relative deviations occur for discontinuities of small strip widths (e.g. w_1=w_2=50μm, w_1=10μm/w_2=12.5μm). For these two cases the maximum absolute deviations are still quite small (F_{max}=0.004, F_{max}=0.01) and acceptable for design applications. Reasonable high accuracy was achieved for strip width ratios of up to w_2/w_1=5.

12.2. STUDY OF THE STATIC MODEL OVER THE COMPLETE FREQUENCY RANGE

In order to bring out the basic dynamic behaviour of the bend discontinuity, representative discontinuity structures were reanalysed over an increased frequency range of 120 GHz. These bends were described by the following geometry parameters; w_1 = 125μm, 62,26μm, w_2/w_1 = 1, 2, and H = 0.5mm, 1mm.

Package lengths equal to the package widths of W_s=1mm and W_s=2mm, were used, the bend position in the package being either in the centre or defined by x_1=0.7x_1 centre and x_2=0.7x_2 centre respectively.

Based on the full-wave data generated, it was identified that in order to obtain a good fit over the extended frequency range, the quasi-static portion of the circuit model should be extended to have a more frequency dependent description. The impedances and admittances of the elements L_a, L_band C of the equivalent circuit model of Fig. 12.4 were therefore defined as follows:

$$Z^{La} = j\,2\pi\,(f + F2*f^2 + F4*f^3...)\,*L_a$$
$$Z^{Lb} = j\,2\pi\,(f + F2*f^2 + F4*f^3...)\,*L_b$$

$$Y^{C} = j\,2\pi\,(f + F3*f^2 + F5*f^3...)\,*C$$

with frequency expanded correction factors.

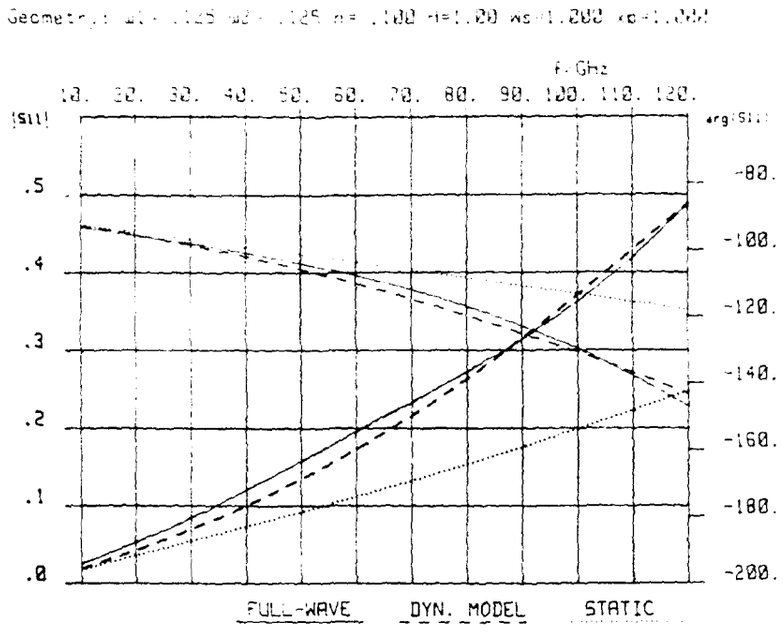


Fig. 12.5: 90° bend S11

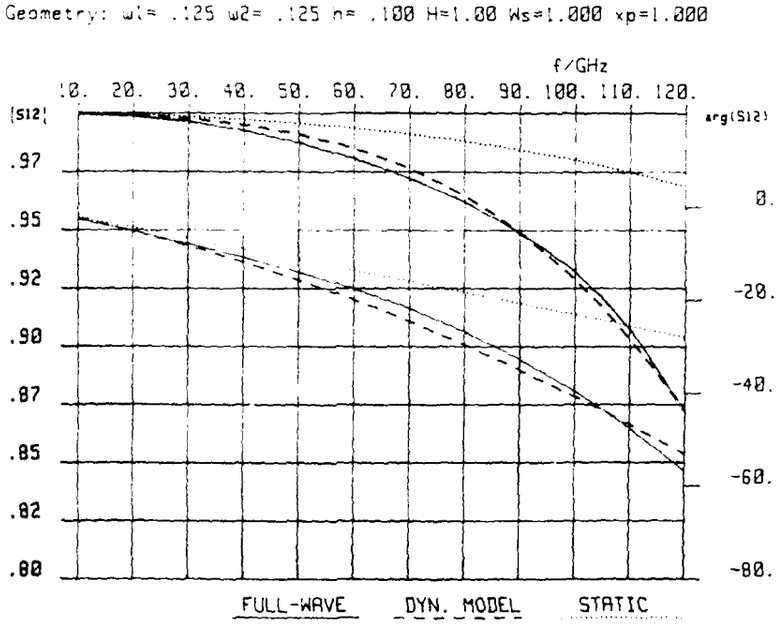


Fig. 12.6: 90° bend S12

In the preliminary investigation only the factors F2 and F3 were considered in the S-parameter fitting procedure. Their optimised values are shown in Table 3 (Section 12.6). A further round of fitting taking into account the f^3 dependent factors was done, the values of F2, F3, F4 and F5 being listed in Table 4 (Section 12.6). As can be seen only the correction factors F2 and F3 are needed to give sufficient accuracy.

In order to emphasise the need for a complex description of the static model an investigation on individual bend configurations within narrow packages was made in order to highlight package resonance effects. In Figs. 12.5 and 12.6 the S11 and S12 magnitude and phase are shown for symmetric bend configuration of strip width 125 μm. The choice of package dimensions of 1mm (length, x_p and width, w_s) ensured that the package resonance frequency was much higher than 120 GHz. In the results the scattering parameters are also shown for the modified dynamic circuit model and the static circuit model. It can be seen that the static model gives agreement up to 30-40 GHz but the modifications are important to obtain an accurate model valid through 120 GHz.

12.3. TRANSFORMER RATIO EXPRESSIONS FOR THE DYNAMIC MODEL

In order to understand the behaviour of the coupling between the microstrip and LSM_0 package modes a study was done for a few individual bend structures. These structures were situated in a wide package of width = 2 mm, length = 2 mm and cover heights 0.5 and 1.0 mm to enhance the resonance effects. Comparative full wave and modified dynamic model S11 and S12 parameters were plotted in the same figures.

The results for the bend centred in the package with strip widths of 0.125 mm can be seen in Figs. 12.7 and 12.8 for 1.00 mm cover height and Figs. 12.9 and 12.10 for 0.5 mm cover height. As can be seen the full wave and dynamic models agree well. The strength of the resonance however increases with

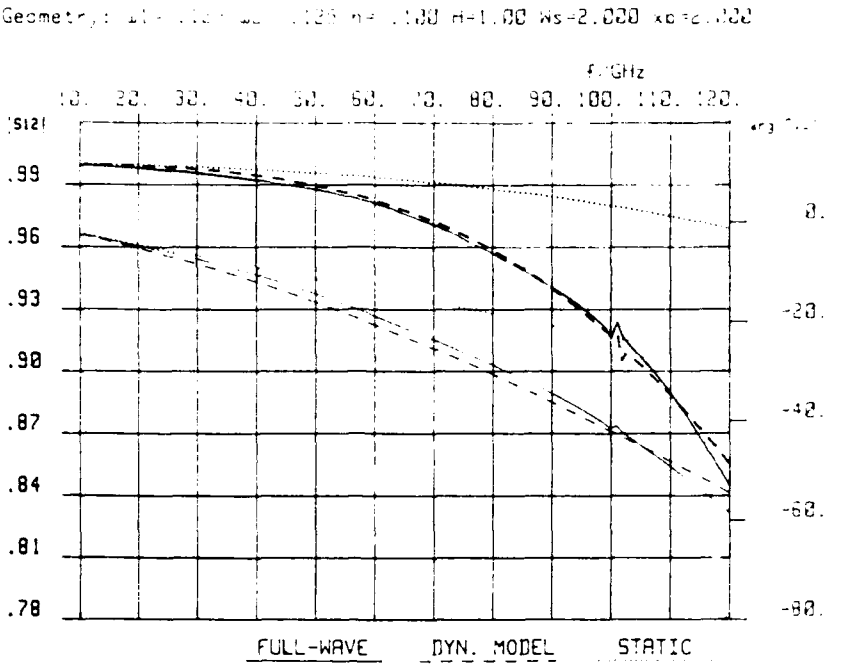


Fig. 12.7: S11 for 90° bend, cover height 1.0 mm

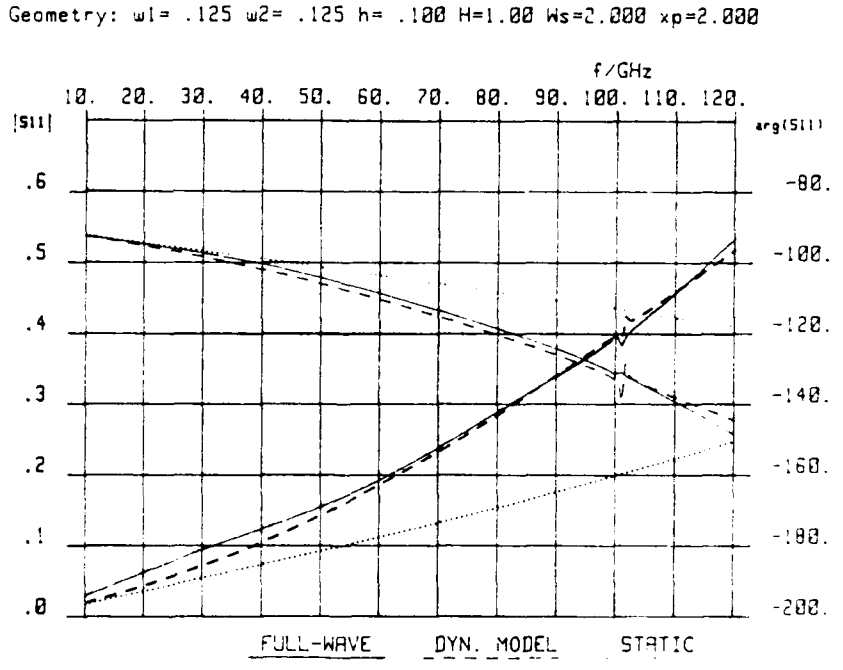


Fig. 12.8: S12 for 90° bend, cover height 1.0 mm

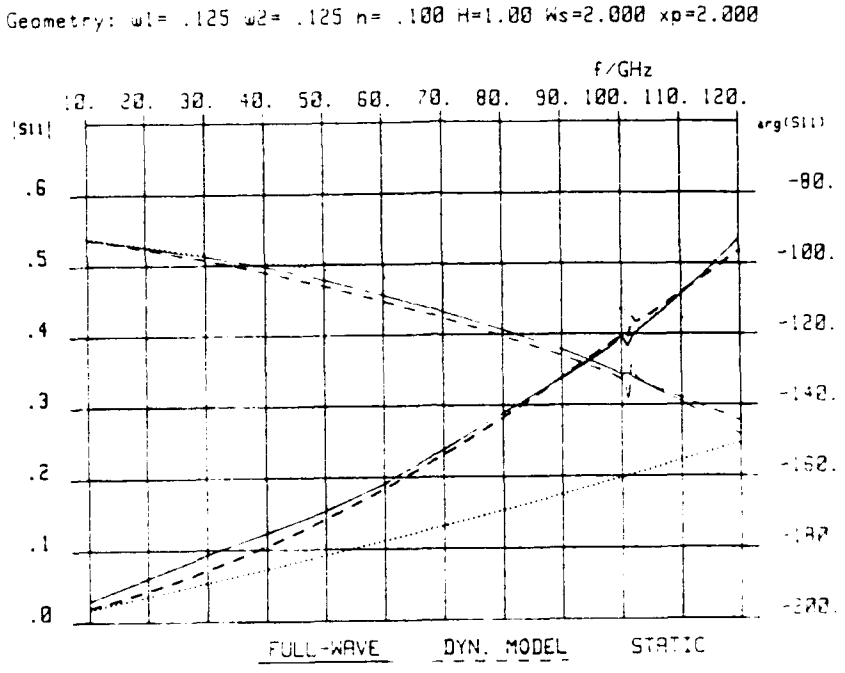


Fig. 12.11: S11 for 90° bend, discontinuity at centre

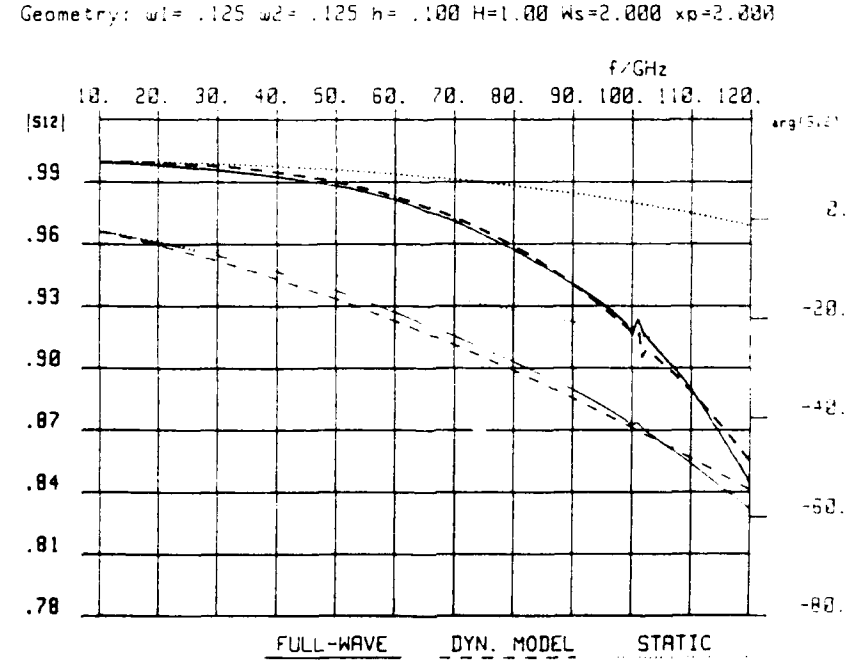


Fig. 12.12: S12 for 90° bend, discontinuity at centre

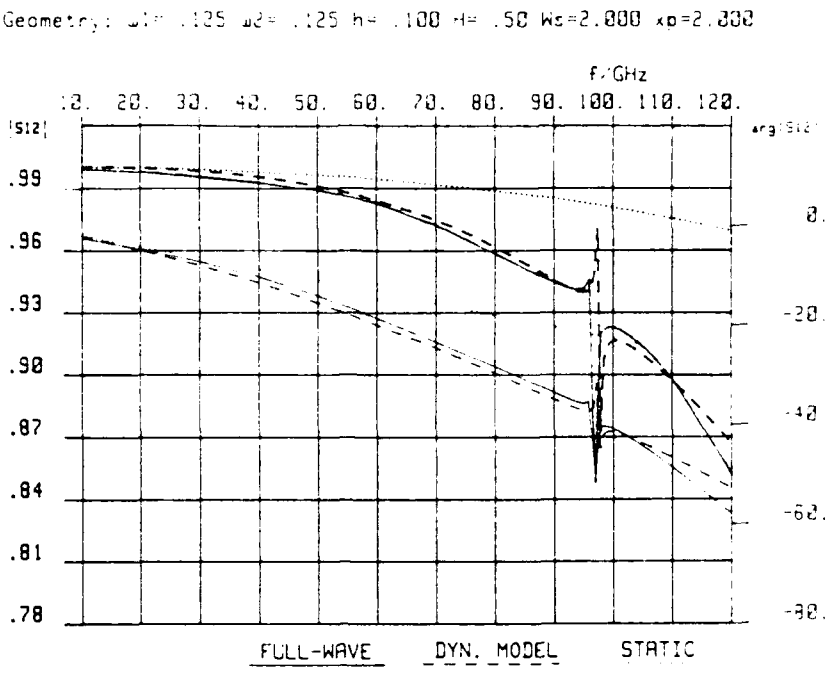


Fig. 12.9: S11 for 90° bend, cover height 0.5 mm

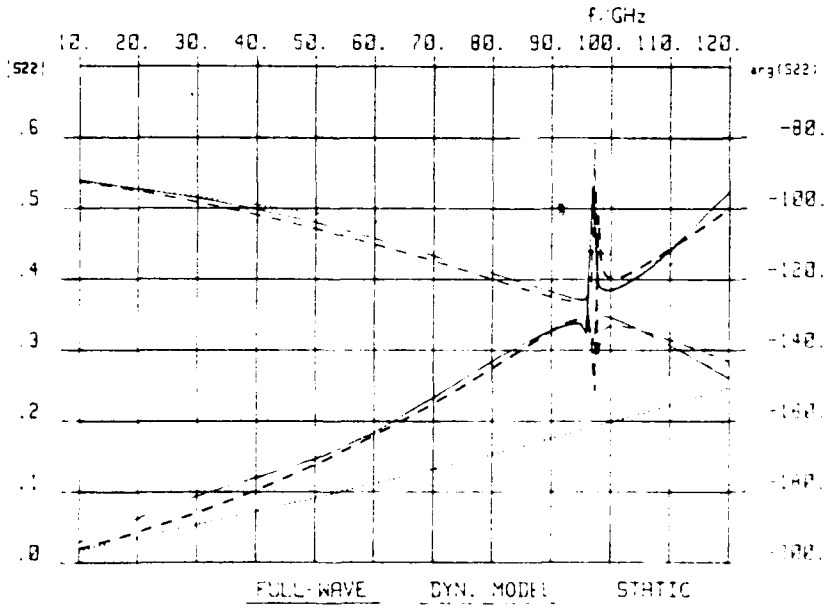


Fig. 12.10: S12 for 90° bend, cover height 0.5 mm

decreasing cover height but the influence of the coupling on the bend frequency behavour is small.

To ensure that the package effect is part of the general behaviour of the 90°-bend discontinuity and is not due to the choice of the package dimensions and to the position of the discontinuity in the package, additional bend configurations were analysed. The same discontinuity was investigated as in Figs. 12.7 and 8 for 1.00 mm cover height but with the discontinuity displaced from the package centre by 0.2 mm in the x and y directions. The results of the analysis are given in Figs. 12.11 and 12. From comparison with the original bend structure it can be concluded that the discontinuity behaviour does not depend significantly on its position in the package.

Because the quasi-static part of the bend model was developed over a frequency range of 0-120 GHz, the basic frequency behaviour of the dynamic model is already described. For frequencies below package mode cutoff this portion can be used alone to describe all effects. For frequencies beyond package mode cutoff the second part of the equivalent circuit model has an increasing influence on the bend behaviour, with the transformer ratio approaching N=1. The transition region as compared with other discontinuity models is now very small. Therefore the additional factor (not needed for the other discontinuities due to their model accuracy)

$$\exp(-f_1*(f-f_0)/f_0)$$

is introduced to ensure that for frequencies below cutoff the bend discontinuity behaviour approaches that of the quasi-static. For the transformer ratios N1, N2, M1 and M2 the improved transformer ratio is given by

$$N_{dyn} = N * \cos^{f_1}(0.5*\pi*(f-f_o)/f_o) * \exp(-f_1*(f-f_o)/f_o) \quad f<f_o$$

$$N_{dyn} = N \qquad f>f_o$$

$$M_{dyn} = -N_{dyn}$$

where the parameters f_o and f_1 have been chosen identically to those expressions developed for the microstrip gap and step discontinuity.

$$f_o = f_c * 1.4 * f_o' * (1 + \exp(0.0638 * W_s/h * H/h)) * (1 - 2.33 * \exp(-0.33 * W_s/h)$$

$$f_o' = 1.0$$

$$f_1 = 2$$

Additional unsymmetrical bend configurations were analyzed to further check the assumptions made. For two of these, the respective scattering parameters are given in Figs. 12.13-16, the cover height being 1mm.

As has been concluded from the investigations at frequencies near package resonance, the influence of the coupling between the fundamental microstrip modes on the feed lines and the LSM_0/LSM_0' package mode on the frequency dependency on the bend behaviour is again small. The resonance behaviour of the scattering parameters is predicted quite well and further fine tuning is not necessary.

In regard to the LSM_0-LSM_0' bidirectional coupling represented by the transformer N3 in the dynamic equivalent model, preliminary results indicate that the numerical values of N3 are small for frequencies below and above the first package resonance. As such, the transformer N3 is not required for the

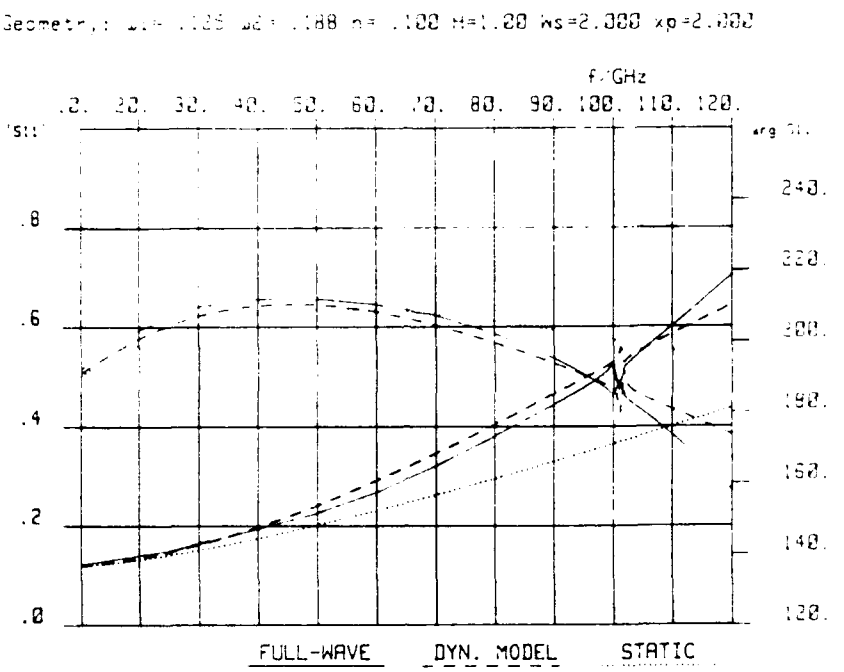


Fig. 12.13: S11 unsymmetric, 90° bend, configuration 1

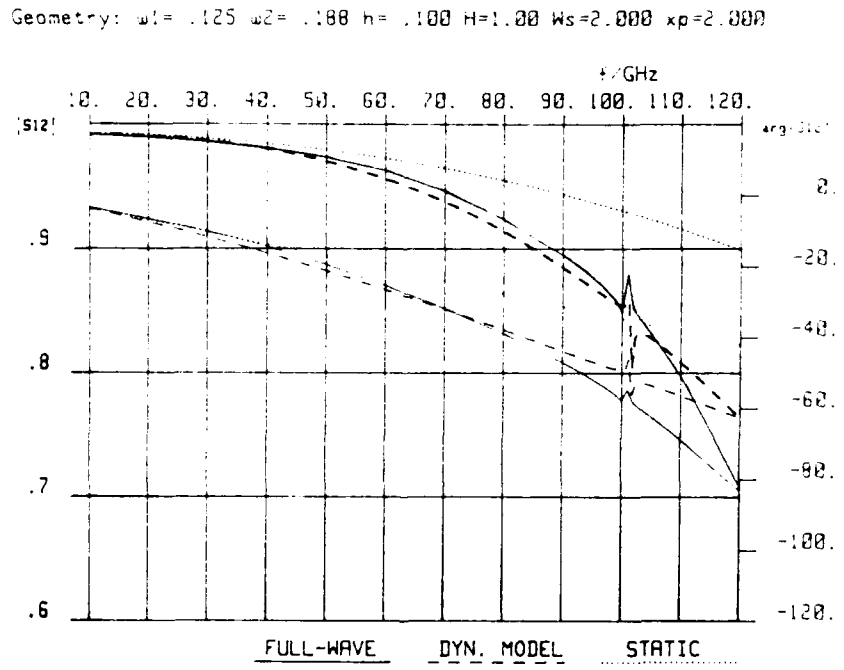


Fig. 12.14: S12 unsymmetric, 90° bend, configuration 1

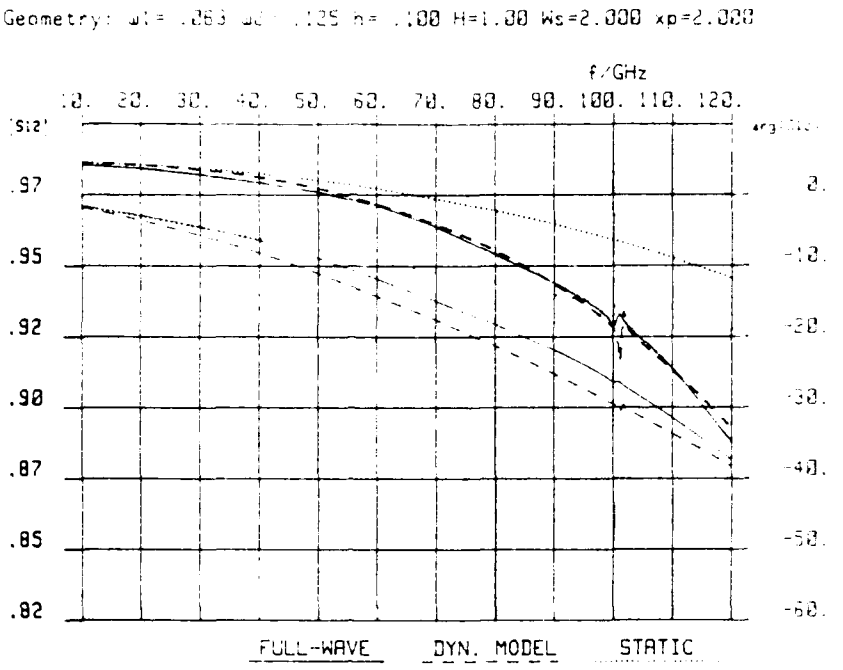


Fig. 12.15: S11 unsymmetric, 90° bend, configuration 2

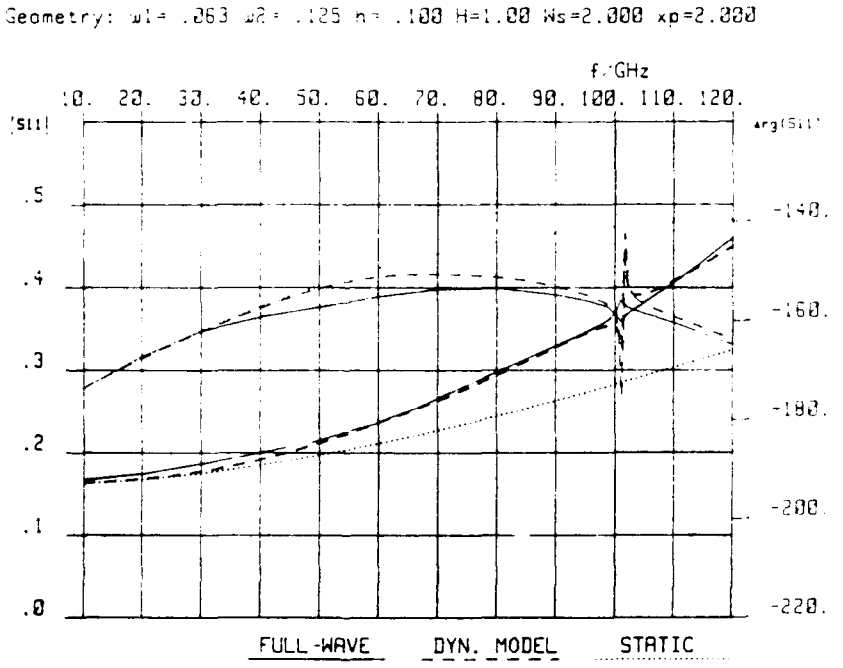


Fig. 12.16: S12 unsymmetric, 90° bend, configuration 2

bend dynamic circuit model for frequencies up to and including the first package resonance frequency and the model topology reverts to that of Fig. 5.18.

12.4. INCLUSION OF AN INCREASED FREQUENCY DEPENDENCY INTO THE STATIC CIRCUIT MODEL

The final task in the development of the analytical formulae was to extend the quasi-static portion equivalent circuit model to include analytic formulae for F2 and F3. A consistent data base was generated, the bend configurations being described by the following geometrical parameters:

h=0.1mm, H=1mm, w_1= 400μm. 200μm, 100μm, 50μm, 20μm;
w_2/w_1=1, 1.25, 1.5, 2, 4; W_s= 3.2mm, 2.0,mm, 1.6mm, 1.2mm

The maximum strip width was restricted to 400 μm and the minimum strip width to 20 μm. The data base was generated for only one cover height of H=1mm, using packages of equal widths and lengths, the discontinuities located in the centre of the package. The bend configurations were computed for the frequency range 10 GHz - 120 GHz. In the final optimization and generation of analytic formulae the frequency range was reduced for each individual configuration to approximately the package resonance frequency ($f \leq 0.9 * f_{res}$) for resonance frequencies below 120 GHz.

In order to use all degrees of freedom of the bend equivalent circuit model again, the complete set of bend configurations used previously to generate analytical formulae for L_a, L_b/L_a and C was added to this data base and the anaytical expressions for the elements of the bend equivalent circuit model were made subject to refitting. By this process, the basic physical behaviour of the model was not changed, but better modelling accuracy was obtained.

In Table 5 (Section 12.6) the mean deviation F_{mean}, the maximum deviation F_{max} and the relative maximum deviation F_{maxr} are listed for parameters S11, S12 and S22 for each data set. The larger maximum relative deviations are related to the S-parameters for discontinuities of small strip widths. The maximum absolute deviations are consequently still quite small and acceptable for design applications.

12.5. BEND MODEL SUMMARY

A summary of the bend model formulae is given below where $Z_L^{microstrip}$ and $\varepsilon_{eff}^{microstrip}$ are computed according to Section 4. All units are based on MKS except where stated in the formulae.

Quasi-static Elements

$$2*\pi*f * L_s / \Omega = 2*\pi* (f/GHz) * (h/mm) * 0.1865 * (L_1 + L_2)$$
$$* (w_2/w_1)^{0.558} * (1 - 0.0303*w1/h)$$
$$* \exp (-0.214*(w_2/w_1-1)^{-0.0751} * (w_1/h)^{-0.419})$$

$$L_1 = (1 - 1.667 * \exp(-0.5862*(w_1/h)^{1.066}) * (1 + 0.691* \exp(-3.88*(w_1/h-1.2)^2)$$

$$L_2 = (1 - 1.667 * \exp(-0.5862*(w_2/h)^{1.066}) * (1 + 0.691* \exp(-3.88*(w_2/h-1.2)^2)$$

$$2*\pi*f * C / S = 2*\pi* (f/GHz) * (h/mm) *$$
$$(104.0*(w_1/h)^{2.179} + 55.66*(w_1/h) - 10.36*\exp(-4.1*w_1/h)) *$$
$$(6.55 - 5.55*\exp(-0.2022*(w_2/w_1-1)^{0.7172})) *$$
$$(w_2/w_1)^{0.842*(1 - 0.176 * w1/h)} *$$
$$\exp(-0.0581*(w_2/w_1-1)^{1.12} * (w_1/h)^{-0.5775})$$

with $L_a = L_s - L_b$

$L_b = L_s / (1 + L_a/L_b)$

$L_a / L_b = 0.5 * (1 + (w_2/w_1)^{11.21-1.8*w1/h})$

Alternate Elements

$$L_a' = (1 + F2*(f/GHz)) * L_a \quad \text{with} \quad L_a = L_s - L_b$$

$$L_b' = (1 + F2*(f/GHz)) * L_b \quad \text{with} \quad L_b = L_s / (1 + L_a/L_b)$$

$$C' = (1 + F3*(f/GHz)) * C$$

$$2*\pi*f * L_s / \Omega = 2*\pi* (f/GHz) * (h/mm) * 0.2 * (L_1 + L_2)$$

$$* (w_2/w_1)^{0.547 * (1 + 0.034*W1/h)}$$

$$* \exp (-0.0766*(w_2/w_1-1)^{1.38} * (w_1/h)^{-1.48})$$

$$2*\pi*f * C / S = 2*\pi* (f/GHz) * (h/mm) *$$

$$(101.4*(w_1/h)^{2.066} + 95.51*(w_1/h) - 7.873*\exp(-0.638*w_1/h)) *$$

$$(2.72 - 1.72*\exp(-0.1155*(w_2/w_1-1)^{0.455})) *$$

$$(w_2/w_1)^{0.767} *$$

$$\exp(-0.0915*(w_2/w_1-1)^{0.0455} * (w_1/h)^{-0.303})$$

$$L_1 = (1 - 1.851 * \exp(-0.7677*(w_1/h)^{0.54}) *$$

$$L_2 = (1 - 1.851 * \exp(-0.7677*(w_2/h)^{0.54}) *$$

with $L_a = L_s - L_b$

$L_b = L_s / (1 + L_a/L_b)$

$L_a / L_b = 0.5 * (1 + (w_2/w_1)^{5.04-0.13*w1/h})$

and correction factors F2 and F3

$$F2 = 0.00181*\exp(0.5106*(w_1/H)^{0.7}) * 0.638*\text{atan}(0.1341*(h/w_1)*(f/Ghz)) *$$
$$(0.304*\exp(w_2/w_1*0.251*(1+0.21*w_1/h)) + 0.815*\exp(0.033*w_2/w_1*(1+4.93*w_1/h))$$

$$F3 = 0.00235 + 0.00643*(w_1/h)^2 - 0.00264*(w_1/h)^3 + 0.00450*(w_1/h)^4$$

$$* 0.638*\text{atan}(0.0617*(h/w_1)*(f/Ghz)) * (w_2/w_1)^{3.37-1.95*(w_1/h)-0.153*(h/w_1)}$$

Transformer ratios N1, N2, M1, M2

$N1 = N_{dyn}(w_1)$

$N2 = N_{dyn}(w_2)$

$M1 = -N_{dyn}(w_1)$

$M2 = -N_{dyn}(w_2)$

$$N_{dyn}(w_i) = \begin{cases} N(w_i) * \cos^{f_1}\left(0.5*\pi*(f-f_0)/f_0 \right) * \exp\left(-f_1*(f-f_0)/f_0 \right) & f<f_0 \\ N(w_i) & f>f_0 \end{cases}$$

$$N(w_i) = 1.2/\pi * \left(\cos\left(\frac{\pi}{2W_s} * (W_s - w_{eff}(w_i))\right) - \cos\left(\frac{\pi}{2W_s} * (W_s + w_{eff}(w_i))\right) \right)$$

$$w_{eff}(w_i) = Z_0 * h / Z_L^{microstrip}(w_i) / \sqrt{\varepsilon_{eff}^{microstrip}(w_i)}$$

$$f_0 = f_c * 1.4 * \left(1 + \exp(-0.0638 * W_s/h * H/h) \right) * (1 - 2.33 * \exp(-0.33 * W_s/h))$$

$f_1 = 2$

$$\varepsilon_{eff}(LSM_0) = \varepsilon_{stat}\left(1 - \left(\frac{f_c}{f}\right)^2\right)$$

with $$f_c = \frac{c_0}{2W_s \cdot \sqrt{\varepsilon_{stat}}}$$

and $$\varepsilon_{stat} = \frac{\varepsilon_r (H+h)}{\varepsilon_r H+h},$$

$$Z_L(LSM_0) = \frac{H+h}{W_s} \cdot \frac{Z_0}{\sqrt{\varepsilon_{stat}}} \cdot \frac{1}{\sqrt{1 - (f_c/f)^2}}$$

($Z_0 = 120\pi\Omega$, $c_0 = 2.9979\ 10^8$ m/s)

Range of Model Validity

The 90° bend models are valid for $\varepsilon r = 12.9$ within the following ranges:

dynamic and quasi-static model:

50µm	< h	<	200µm	
0.2	< w/h	<	4	
1	< w2/w1	<	4	
12	< Ws/h	<	32	
5	< H/h	<	20	

where the quasi-static model is that of Fig. 12.4 and the dynamic model that of Fig. 12.2. The quasi-static model is valid over the range $0 \leq f*h \leq 3$ GHz mm. The dynamic model using the alternate formulae in the quasi-static part of the model is valid over $0 \leq f*h \leq 12$ GHz mm, where La, Lb and C in Fig. 12.2 are replaced by La', Lb' and C'. For the dynamic model the transformer N3 is not needed for frequencies up to and including the first package mode.

12.6. REFERENCES AND TABLES

1. Kirschning, M., Jansen, R.H. and Koster, N.H.L.: Measurement and computer aided modelling of microstrip discontinuities by an improved resonator method, IEEE MTT-S Digest, Boston, USA, 1983 495-497.

2. Kirschning M.: Development of models for the computer-aided design of hybrid and monolithic microstrip circuits (in German). University of Duisburg, W. Germany, 1984.

Table 1

BEND GEOMETRY					OPTIMIZED CORRECTION FACTORS		
W1	W2	WS	HH	XP	FC_ZLS	FC_A/B	FC_YCS
.400	.400	3.20	.50	3.20	1.148	1.000	.805
.400	.500	3.20	.50	3.20	1.143	.820	.899
.400	.600	3.20	.50	3.20	1.179	1.151	.988
.400	.400	3.20	2.00	3.20	1.232	1.000	.817
.400	.500	3.20	2.00	3.20	1.227	.774	.910
.400	.600	3.20	2.00	3.20	1.263	1.048	.996
.200	.200	2.13	.50	2.13	2.786	1.000	.633
.200	.250	2.13	.50	2.29	1.919	.919	.811
.200	.300	2.13	.50	2.13	1.767	2.091	.888
.200	.400	2.13	.50	2.13	1.664	66.234	.959
.200	.600	2.13	.50	2.13	1.863	65.409	1.169
.200	.200	2.13	2.00	2.13	3.083	1.000	.621
.200	.250	2.13	2.00	2.29	2.070	1.093	.813
.200	.300	2.13	2.00	2.13	1.604	66.059	.799
.200	.400	2.13	2.00	2.13	1.706	66.193	.939
.200	.600	2.13	2.00	2.13	1.957	66.251	1.159
.100	.100	1.60	.50	1.60	-.731	1.000	.494
.100	.125	1.60	.50	1.60	-.916	75.157	.621
.100	.150	1.60	.50	1.60	-1.084	63.984	.615
.100	.200	1.60	.50	1.60	-59.600	1.000	.742
.100	.300	1.60	.50	1.60	3.983	63.401	.955
.100	.400	1.60	.50	1.60	3.138	64.207	1.134
.100	.500	1.60	.50	1.60	2.983	64.113	1.271
.100	.100	1.60	2.00	1.60	-.769	1.000	.499
.100	.125	1.60	2.00	1.60	-1.298	168.104	.690
.100	.150	1.60	2.00	1.60	-1.122	63.987	.614
.100	.200	1.60	2.00	1.60	-60.087	1.000	.738
.100	.300	1.60	2.00	1.60	4.100	63.404	.943
.100	.400	1.60	2.00	1.60	3.200	63.716	1.126
.100	.500	1.60	2.00	1.60	3.091	64.108	1.263
.050	.050	1.60	.50	1.60	.733	1.000	.361
.050	.063	1.60	.50	1.60	.458	-.273	.520
.050	.075	1.60	.50	1.60	.316	-.210	.595
.050	.100	1.60	.50	1.60	.068	29.325	.702
.050	.150	1.60	.50	1.60	-.631	-.251	.893
.050	.200	1.60	.50	1.60	-2.098	83.304	1.073
.050	.250	1.60	.50	1.60	-6.415	58.883	1.041
.050	.050	1.60	2.00	1.60	.713	1.000	.359
.050	.063	1.60	2.00	1.60	.409	-.168	.518
.050	.075	1.60	2.00	1.60	.303	-.275	.584
.050	.100	1.60	2.00	1.60	.103	-.519	.702
.050	.150	1.60	2.00	1.60	-.696	101.325	.901
[illegible]					-2.148	65.958	1.078
[illegible]					-6.890	58.381	1.030
[illegible]					.593	1.000	.375
[illegible]					.623	190.716	.410
.020	.030	1.28	.50	1.28	.527	.031	.506
.020	.040	1.28	.50	1.28	.452	6.359	.663
.020	.060	1.28	.50	1.28	.321	-.017	.961
.020	.080	1.28	.50	1.28	.189	.076	1.235
.020	.100	1.28	.50	1.28	.040	-.124	1.485
.020	.020	1.28	2.00	1.28	.668	1.000	.306
.020	.025	1.28	2.00	1.60	.627	121.596	.418
.020	.030	1.28	2.00	1.28	.524	-.099	.492
.020	.040	1.28	2.00	1.28	.451	4.922	.649
.020	.060	1.28	2.00	1.28	.324	-.254	.953
.020	.080	1.28	2.00	1.28	.187	-.141	1.207
.020	.100	1.28	2.00	1.28	-.014	-.124	1.498

.010	.010	1.28	.50	1.28	.580	1.000	.025
.010	.013	1.28	.50	1.60	.638	117.758	-.011
.010	.015	1.28	.50	1.28	.505	60.353	-.054
.010	.020	1.28	.50	1.28	.521	91.325	-.005
.010	.030	1.28	.50	1.28	.422	48.864	-.237
.010	.040	1.28	.50	1.28	.375	37.165	-.339
.010	.050	1.28	.50	1.28	.315	-.078	-.451
.010	.010	1.28	2.00	1.28	.596	1.000	.023
.010	.013	1.28	2.00	1.60	.639	113.492	-.017
.010	.015	1.28	2.00	1.28	.511	58.216	-.053
.010	.020	1.28	2.00	1.28	.526	78.638	-.005
.010	.030	1.28	2.00	1.28	.427	27.765	-.240
.010	.040	1.28	2.00	1.28	.380	58.452	-.345
.010	.050	1.28	2.00	1.28	.350	1.116	-.447

Table 2

					S11			S12			S22		
W1	W2	WS	HH	XP	Fmean	Fmax	Fmaxr	Fmean	Fmax	Fmaxr	Fmean	Fmax	Fmaxr
.4	.40	3.2	.5	3.2	.023	.004	.087	.008	.012	.012	.022	.004	.088
.4	.50	3.2	.5	3.2	.047	.014	.092	.011	.017	.017	.057	.012	.099
.4	.60	3.2	.5	3.2	.018	.007	.044	.011	.020	.021	.020	.008	.050
.4	.40	3.2	2.0	3.2	.026	.005	.077	.008	.021	.022	.025	.005	.077
.4	.50	3.2	2.0	3.2	.069	.018	.081	.010	.023	.024	.066	.014	.096
.4	.60	3.2	2.0	3.2	.036	.014	.048	.013	.038	.040	.036	.012	.052
.2	.20	2.1	.5	2.1	.043	.005	.146	.002	.003	.003	.042	.005	.146
.2	.25	2.1	.5	2.1	.085	.018	.135	.002	.002	.002	.084	.018	.137
.2	.30	2.1	.5	2.1	.057	.019	.097	.006	.008	.008	.048	.016	.083
.2	.40	2.1	.5	2.1	.043	.021	.072	.011	.015	.016	.027	.013	.044
.2	.60	2.1	.5	2.1	.029	.018	.042	.009	.010	.011	.026	.017	.039
.2	.20	2.1	2.0	2.1	.055	.004	.181	.001	.002	.002	.055	.004	.181
.2	.25	2.1	2.0	2.1	.059	.014	.100	.003	.008	.008	.063	.015	.111
.2	.30	2.1	2.0	2.1	.038	.013	.070	.003	.005	.005	.035	.013	.070
.2	.40	2.1	2.0	2.1	.028	.014	.046	.008	.010	.010	.019	.010	.034
.2	.60	2.1	2.0	2.1	.022	.013	.029	.006	.010	.011	.023	.014	.031
.1	.10	1.6	.5	1.6	.057	.004	.221	.002	.003	.003	.058	.004	.220
.1	.13	1.6	.5	1.6	.086	.014	.167	.004	.005	.005	.091	.015	.174
.1	.15	1.6	.5	1.6	.062	.013	.105	.001	.002	.002	.061	.013	.104
.1	.20	1.6	.5	1.6	.036	.010	.047	.002	.003	.004	.036	.010	.047
.1	.30	1.6	.5	1.6	.035	.015	.046	.006	.008	.009	.038	.017	.049
.1	.40	1.6	.5	1.6	.035	.020	.048	.008	.010	.011	.036	.021	.050
.1	.50	1.6	.5	1.6	.037	.028	.056	.011	.016	.019	.034	.025	.052
.1	.10	1.6	2.0	1.6	.034	.003	.103	.003	.005	.005	.035	.003	.103
.1	.13	1.6	2.0	1.6	.085	.012	.149	.004	.006	.006	.091	.013	.159
.1	.15	1.6	2.0	1.6	.059	.012	.093	.001	.002	.002	.059	.012	.094
.1	.20	1.6	2.0	1.6	.036	.009	.043	.002	.002	.002	.036	.009	.043
.1	.30	1.6	2.0	1.6	.037	.015	.046	.005	.006	.006	.039	.016	.049
.1	.40	1.6	2.0	1.6	.036	.022	.051	.007	.009	.010	.037	.022	.051
.1	.50	1.6	2.0	1.6	.040	.031	.063	.012	.018	.021	.035	.026	.052
.05	.050	1.6	.5	1.6	.072	.004	.480	.001	.003	.003	.072	.004	.480
.05	.063	1.6	.5	1.6	.049	.004	.091	.004	.005	.005	.046	.004	.081
.05	.075	1.6	.5	1.6	.037	.005	.063	.004	.005	.005	.030	.005	.053
.05	.100	1.6	.5	1.6	.040	.007	.048	.003	.005	.005	.034	.006	.039
.05	.150	1.6	.5	1.6	.021	.008	.030	.002	.005	.005	.018	.006	.023
.05	.200	1.6	.5	1.6	.028	.013	.037	.007	.008	.009	.016	.007	.021
.05	.250	1.6	.5	1.6	.024	.012	.029	.010	.014	.015	.011	.006	.016
.05	.050	1.6	2.0	1.6	.070	.003	.430	.001	.003	.003	.069	.003	.430
.05	.063	1.6	2.0	1.6	.041	.004	.082	.004	.005	.005	.037	.003	.074
.05	.075	1.6	2.0	1.6	.044	.005	.059	.004	.005	.005	.037	.004	.050
.05	.100	1.6	2.0	1.6	.033	.007	.044	.002	.005	.005	.029	.006	.035
.05	.150	1.6	2.0	1.6	.020	.007	.029	.002	.004	.005	.018	.005	.020
.05	.200	1.6	2.0	1.6	.027	.011	.030	.006	.008	.009	.017	.007	.020
.05	.250	1.6	2.0	1.6	.029	.016	.039	.012	.017	.018	.011	.007	.016

.02	.020	1.3	.5	1.3	.067	.002	.151	.002	.002	.002	.066	.002	.151	
.02	.025	1.3	.5	1.6	.059	.005	.131	.002	.005	.005	.055	.005	.123	
.02	.030	1.3	.5	1.3	.023	.003	.039	.001	.002	.002	.021	.002	.035	
.02	.040	1.3	.5	1.3	.023	.004	.037	.003	.004	.004	.018	.003	.029	
.02	.060	1.3	.5	1.3	.028	.007	.035	.008	.011	.011	.013	.003	.015	
.02	.080	1.3	.5	1.3	.028	.009	.035	.012	.018	.019	.007	.003	.012	
.02	.100	1.3	.5	1.3	.023	.009	.029	.016	.024	.025	.012	.008	.026	
.02	.020	1.3	2.0	1.3	.037	.001	.061	.000	.001	.001	.037	.001	.061	
.02	.025	1.3	2.0	1.6	.064	.005	.126	.002	.004	.004	.059	.005	.119	
.02	.030	1.3	2.0	1.3	.018	.002	.035	.001	.002	.002	.017	.002	.031	
.02	.040	1.3	2.0	1.3	.023	.004	.033	.003	.004	.004	.018	.003	.026	
.02	.060	1.3	2.0	1.3	.027	.007	.033	.008	.011	.011	.012	.003	.014	
.02	.080	1.3	2.0	1.3	.028	.010	.039	.012	.018	.019	.007	.003	.012	
.02	.100	1.3	2.0	1.3	.024	.011	.035	.016	.025	.026	.013	.009	.029	
.01	.010	1.3	.5	1.3	.046	.001	.173	.000	.001	.001	.045	.001	.173	
.01	.013	1.3	.5	1.6	.198	.010	.324	.005	.008	.008	.190	.010	.309	
.01	.015	1.3	.5	1.3	.163	.010	.194	.001	.004	.004	.162	.010	.190	
.01	.020	1.3	.5	1.3	.028	.008	.079	.002	.003	.003	.031	.008	.079	
.01	.030	1.3	.5	1.3	.014	.004	.026	.007	.010	.010	.021	.007	.046	
.01	.040	1.3	.5	1.3	.011	.004	.018	.011	.016	.016	.021	.009	.045	
.01	.050	1.3	.5	1.3	.016	.005	.020	.015	.021	.022	.023	.012	.050	
.01	.010	1.3	2.0	1.3	.050	.001	.270	.001	.001	.001	.050	.001	.270	
.01	.013	1.3	2.0	1.6	.216	.010	.331	.005	.007	.007	.207	.010	.318	
.01	.015	1.3	2.0	1.3	.055	.009	.142	.001	.003	.003	.054	.008	.136	
.01	.020	1.3	2.0	1.3	.029	.008	.077	.002	.003	.003	.032	.008	.078	
.01	.030	1.3	2.0	1.3	.014	.004	.026	.007	.010	.010	.021	.007	.046	
.01	.040	1.3	2.0	1.3	.010	.003	.016	.011	.016	.016	.021	.009	.045	
.01	.050	1.3	2.0	1.3	.013	.004	.018	.015	.019	.020	.023	.014	.055	

Table 3

BEND GEOMETRY					OPTIMIZED CORRECTION FACTORS			
W1	W2	WS	HH	XP	F2	F3	F4	F5
.125	.125	1.00	1.00	1.00	.0064	.0083	.0000	.0000
.125	.125	1.00	1.00	1.00	.0064	.0083	.0000	.0000
.125	.125	1.00	.50	1.00	.0064	.0080	.0000	.0000
.125	.125	1.00	.50	1.00	.0064	.0080	.0000	.0000
.125	.250	1.00	1.00	1.00	.0092	.0061	.0000	.0000
.125	.250	1.00	1.00	1.00	.0092	.0061	.0000	.0000
.125	.250	1.00	.50	1.00	.0090	.0058	.0000	.0000
.125	.250	1.00	.50	1.00	.0090	.0058	.0000	.0000
.125	.125	2.00	1.00	2.00	.0061	.0094	.0000	.0000
.125	.125	2.00	1.00	2.00	.0061	.0094	.0000	.0000
.125	.125	2.00	.50	2.00	.0062	.0089	.0000	.0000
.125	.125	2.00	.50	2.00	.0062	.0089	.0000	.0000
.125	.250	2.00	1.00	2.00	.0103	.0074	.0000	.0000
.125	.250	2.00	1.00	2.00	.0103	.0074	.0000	.0000
.125	.250	2.00	.50	2.00	.0090	.0071	.0000	.0000
.125	.250	2.00	.50	2.00	.0090	.0071	.0000	.0000
.063	.063	1.00	1.00	1.00	-.0146	.0085	.0000	.0000
.063	.063	1.00	1.00	1.00	-.0146	.0085	.0000	.0000
.063	.063	1.00	.50	1.00	-.0147	.0081	.0000	.0000
.063	.063	1.00	.50	1.00	-.0147	.0081	.0000	.0000
.063	.125	1.00	1.00	1.00	.0406	.0040	.0000	.0000
.063	.125	1.00	1.00	1.00	.0406	.0040	.0000	.0000
.063	.125	1.00	.50	1.00	.0405	.0037	.0000	.0000
.063	.125	1.00	.50	1.00	.0405	.0037	.0000	.0000
.063	.063	2.00	1.00	2.00	-.0129	.0100	.0000	.0000
.063	.063	2.00	1.00	2.00	-.0130	.0101	.0000	.0000
.063	.063	2.00	.50	2.00	-.0137	.0096	.0000	.0000
.063	.125	2.00	1.00	2.00	.0392	.0051	.0000	.0000
.063	.125	2.00	1.00	2.00	.0392	.0051	.0000	.0000

Table 4

BEND GEOMETRY					OPTIMIZED CORRECTION FACTORS			
W1	W2	WS	HH	XP	F2	F3	F4	F5
.125	.125	1.00	1.00	1.00	-.0137	.0055	.000191	.000025
.125	.125	1.00	1.00	1.00	-.0137	.0055	.000191	.000025
.125	.125	1.00	.50	1.00	-.0151	.0054	.000204	.000023
.125	.125	1.00	.50	1.00	-.0151	.0054	.000204	.000023
.125	.250	1.00	1.00	1.00	-.0174	-.0084	.000245	.000158
.125	.250	1.00	1.00	1.00	-.0174	-.0084	.000245	.000158
.125	.250	1.00	.50	1.00	-.0179	-.0086	.000250	.000155
.125	.250	1.00	.50	1.00	-.0179	-.0086	.000250	.000155
.125	.125	2.00	1.00	2.00	-.0096	.0048	.000150	.000045
.125	.125	2.00	1.00	2.00	-.0096	.0048	.000150	.000045
.125	.125	2.00	.50	2.00	-.0101	.0049	.000157	.000037
.125	.125	2.00	.50	2.00	-.0101	.0049	.000157	.000037
.125	.250	2.00	1.00	2.00	-.0072	-.0174	.000149	.000277
.125	.250	2.00	1.00	2.00	-.0072	-.0174	.000149	.000277
.125	.250	2.00	.50	2.00	-.0165	-.0124	.000248	.000211
.125	.250	2.00	.50	2.00	-.0165	-.0124	.000248	.000211
.063	.063	1.00	1.00	1.00	-.0091	.0077	-.000051	.000007
.063	.063	1.00	1.00	1.00	-.0091	.0077	-.000051	.000007
.063	.063	1.00	.50	1.00	-.0081	.0080	-.000064	.000002
.063	.063	1.00	.50	1.00	-.0081	.0080	-.000064	.000002
.063	.125	1.00	1.00	1.00	.0033	-.0011	.000329	.000046
.063	.125	1.00	1.00	1.00	.0033	-.0011	.000329	.000046
.063	.125	1.00	.50	1.00	-.0003	-.0009	.000368	.000042
.063	.125	1.00	.50	1.00	-.0003	-.0009	.000368	.000042
.063	.063	2.00	1.00	2.00	-.0016	.0042	-.000109	.000056
.063	.063	2.00	1.00	2.00	-.0104	.0078	-.000026	.000022
.063	.063	2.00	.50	2.00	-.0112	.0065	-.000024	.000029
.063	.125	2.00	1.00	2.00	.0100	.0000	.000259	.000047
.063	.125	2.00	1.00	2.00	.0100	.0000	.000259	.000047

Table 5 MICROSTRIP BEND GEOMETRY

	W1	W1	S11			S12			S22		
			Fmean	Fmax	Fmaxr	Fmean	Fmax	Fmaxr	Fmean	Fmax	Fmaxr
2	.400	.400	.0218	.0036	.0659	.0067	.0097	.0097	.0221	.0036	.0648
3	.400	.500	.0376	.0193	.0718	.0050	.0080	.0081	.0379	.0198	.0739
4	.400	.600	.0441	.0295	.0865	.0066	.0131	.0139	.0440	.0312	.0915
9	.400	.400	.0249	.0041	.0586	.0114	.0148	.0149	.0258	.0040	.0578
10	.400	.500	.0487	.0218	.0793	.0102	.0133	.0138	.0380	.0197	.0718
11	.400	.600	.0471	.0327	.0944	.0089	.0145	.0155	.0438	.0309	.0890
16	.200	.200	.0839	.0100	.0971	.0037	.0051	.0051	.0842	.0100	.0971
17	.200	.250	.0733	.0137	.0999	.0044	.0086	.0087	.0709	.0126	.0941
18	.200	.300	.0601	.0158	.0839	.0062	.0140	.0142	.0532	.0125	.0694
19	.200	.400	.0487	.0200	.0688	.0089	.0210	.0219	.0362	.0120	.0446
20	.200	.600	.0301	.0161	.0385	.0115	.0245	.0273	.0299	.0179	.0404
23	.200	.200	.0561	.0064	.0594	.0046	.0059	.0059	.0564	.0064	.0597
24	.200	.250	.0490	.0091	.0660	.0032	.0056	.0056	.0505	.0089	.0654
25	.200	.300	.0421	.0103	.0543	.0034	.0066	.0067	.0408	.0087	.0493
26	.200	.400	.0340	.0120	.0414	.0053	.0123	.0129	.0278	.0084	.0333
27	.200	.600	.0212	.0095	.0240	.0080	.0131	.0146	.0268	.0168	.0379
30	.100	.100	.0879	.0066	.1220	.0026	.0058	.0058	.0881	.0066	.1214
31	.100	.125	.0699	.0092	.1076	.0026	.0065	.0066	.0680	.0088	.1030
32	.100	.150	.0549	.0110	.0859	.0040	.0094	.0094	.0514	.0098	.0767
33	.100	.200	.0455	.0155	.0746	.0057	.0139	.0142	.0403	.0123	.0590
34	.100	.300	.0432	.0247	.0739	.0096	.0210	.0223	.0352	.0163	.0488
35	.100	.400	.0419	.0305	.0713	.0134	.0263	.0291	.0327	.0185	.0432
36	.100	.500	.0420	.0270	.0541	.0171	.0269	.0311	.0333	.0238	.0477
37	.100	.100	.0787	.0053	.0909	.0017	.0040	.0040	.0786	.0053	.0909
38	.100	.125	.0666	.0077	.0905	.0020	.0050	.0051	.0654	.0075	.0876
39	.100	.150	.0525	.0095	.0746	.0033	.0075	.0076	.0501	.0088	.0692
40	.100	.200	.0426	.0131	.0633	.0049	.0116	.0118	.0393	.0109	.0527
41	.100	.300	.0403	.0211	.0635	.0085	.0181	.0192	.0347	.0150	.0451
42	.100	.400	.0393	.0256	.0601	.0121	.0226	.0250	.0330	.0181	.0424
43	.100	.500	.0421	.0229	.0462	.0162	.0230	.0265	.0348	.0246	.0496
44	.050	.050	.1205	.0051	.4086	.0060	.0116	.0116	.1208	.0051	.4086
45	.050	.063	.0739	.0061	.1011	.0050	.0104	.0104	.0708	.0056	.0936
46	.050	.075	.0484	.0058	.0617	.0048	.0098	.0099	.0465	.0056	.0590
47	.050	.100	.0379	.0078	.0497	.0045	.0093	.0094	.0369	.0078	.0491
48	.050	.150	.0340	.0111	.0429	.0047	.0088	.0092	.0324	.0114	.0440
49	.050	.200	.0388	.0151	.0453	.0070	.0092	.0097	.0331	.0153	.0453
50	.050	.250	.0448	.0213	.0531	.0097	.0105	.0115	.0341	.0209	.0522
51	.050	.050	.1103	.0044	.3549	.0056	.0107	.0107	.1100	.0044	.3549
52	.050	.063	.0652	.0052	.0868	.0045	.0085	.0086	.0639	.0049	.0823
53	.050	.075	.0474	.0062	.0656	.0045	.0085	.0086	.0472	.0062	.0657
54	.050	.100	.0376	.0077	.0493	.0049	.0085	.0086	.0366	.0079	.0501
55	.050	.150	.0343	.0105	.0406	.0042	.0075	.0078	.0331	.0112	.0431
56	.050	.200	.0366	.0148	.0440	.0058	.0068	.0072	.0324	.0158	.0468
57	.050	.250	.0496	.0247	.0619	.0107	.0139	.0151	.0362	.0225	.0564
58	.020	.020	.0454	.0009	.0902	.0042	.0079	.0079	.0461	.0009	.0902
59	.020	.025	.0401	.0030	.0719	.0045	.0082	.0083	.0331	.0023	.0554
60	.020	.030	.1283	.0087	.1340	.0036	.0079	.0079	.1300	.0089	.1341
61	.020	.040	.0743	.0098	.0867	.0045	.0092	.0093	.0734	.0094	.0828

						.0097	.0099	.0592	.0138	.0737	
						.0071	.0074	.0509	.0151	.0611	
						.0051	.0053	.0446	.0159	.0538	
						.0078	.0078	.0316	.0006	.0581	
						.0079	.0079	.0362	.0021	.0510	
						.0065	.0065	.1322	.0091	.1368	
						.0085	.0086	.0758	.0097	.0861	
						.0095	.0097	.0593	.0126	.0676	
						.0073	.0075	.0515	.0149	.0607	
						.0055	.0057	.0469	.0172	.0585	
						.0060	.0060	.0387	.0007	.1916	
						.0097	.0097	.1213	.0052	.1615	
						.0120	.0120	.1672	.0106	.2018	
						.0172	.0173	.1116	.0161	.1769	
						.0145	.0146	.0826	.0183	.1199	
						.1004	.1030	.2710	.1243	.5545	
						.0060	.0060	.0336	.0010	.2762	
31	.010	.015	.1325	.0056	.1762	.0062	.0095	.0095	.1226	.0051	.1605
32	.010	.015	.1745	.0115	.2192	.0058	.0119	.0119	.1694	.0106	.2031
33	.010	.020	.1265	.0188	.2065	.0090	.0170	.0170	.1128	.0160	.1763
34	.010	.030	.0962	.0224	.1475	.0082	.0141	.0142	.0843	.0187	.1231
35	.010	.040	.1599	.0814	.3644	.0423	.1006	.1033	.2179	.1242	.5558
72	.400	.400	.0493	.0421	.0802	.0268	.0683	.0803	.0489	.0421	.0801
73	.200	.200	.0466	.0370	.0868	.0182	.0614	.0679	.0469	.0370	.0867
74	.200	.250	.0331	.0284	.0715	.0178	.0633	.0733	.0607	.0589	.1171
75	.200	.300	.0559	.0287	.0674	.0113	.0199	.0207	.0439	.0326	.0767
76	.200	.400	.0517	.0343	.0716	.0174	.0284	.0308	.0383	.0314	.0655
77	.100	.100	.0579	.0268	.0974	.0222	.0835	.0877	.0579	.0269	.0975
78	.100	.125	.0864	.0394	.1193	.0205	.0748	.0792	.0651	.0245	.1087
79	.100	.150	.0701	.0278	.1062	.0180	.0508	.0548	.0764	.0394	.1058
71	.100	.200	.1330	.0849	.1715	.0295	.0493	.0516	.1037	.1081	.1937
72	.100	.300	.2107	.2061	.3438	.0778	.1296	.1545	.0437	.0362	.0618
73	.100	.400	.1765	.2023	.3367	.0824	.1604	.2006	.0435	.0366	.0608
74	.050	.050	.0589	.0202	.1282	.0136	.0274	.0278	.0598	.0211	.1282
75	.050	.063	.0999	.0293	.1398	.0170	.0538	.0550	.0635	.0099	.1026
76	.050	.075	.1252	.0476	.2010	.0175	.0550	.0566	.0919	.0209	.1147
77	.050	.100	.1381	.0702	.2460	.0168	.0516	.0538	.1141	.0406	.1515
78	.050	.150	.1047	.0605	.1601	.0177	.0255	.0267	.1114	.0566	.1508
79	.050	.200	.1001	.0651	.1340	.0392	.0555	.0654	.1016	.0613	.1371
80	.050	.250	.0865	.0570	.1064	.0438	.0696	.0821	.1066	.0719	.1498
81	.020	.020	.0395	.0093	.0853	.0130	.0397	.0401	.0392	.0053	.0854
82	.020	.025	.0950	.0245	.1677	.0162	.0542	.0548	.0539	.0086	.0701
83	.020	.030	.1706	.0372	.2299	.0164	.0604	.0612	.1386	.0185	.1595
84	.020	.040	.1678	.0514	.2749	.0175	.0604	.0615	.1412	.0299	.1752
85	.020	.060	.1685	.0680	.2904	.0185	.0532	.0547	.1543	.0534	.2282
86	.020	.080	.1619	.0868	.3022	.0202	.0591	.0617	.1495	.0693	.2411
87	.020	.100	.1659	.1170	.3446	.0249	.0757	.0805	.1446	.0819	.2407
88	.025	.025	.1587	.0867	.1947	.0252	.1208	.1326	.0520	.0557	.1349
89	.025	.025	.1520	.0557	.1347	.0252	.1208	.1326	.0520	.0557	.1349
90	.025	.030	.1636	.0512	.1617	.0242	.1133	.1244	.0536	.0512	.1612
91	.025	.025	.1636	.0512	.1617	.0242	.1133	.1244	.0536	.0512	.1612
92	.025	.040	.1706	.0824	.1993	.0398	.1463	.1606	.1004	.0824	.1993
93	.025	.025	.1706	.0824	.1993	.0398	.1463	.1606	.1004	.0824	.1993
94	.025	.025	.0536	.0197	.1391	.0182	.0515	.0543	.0532	.0196	.1391
95	.025	.025	.0536	.0197	.1391	.0182	.0515	.0543	.0532	.0196	.1391
96	.063	.063	.0506	.0229	.1429	.0138	.0576	.0595	.0508	.0228	.1429
97	.063	.063	.0506	.0229	.1429	.0138	.0576	.0595	.0508	.0228	.1429
98	.063	.125	.1041	.0550	.1554	.0160	.0330	.0353	.1080	.0414	.1498
99	.063	.125	.1041	.0550	.1554	.0160	.0330	.0353	.1080	.0414	.1498
100	.063	.063	.0671	.0289	.1752	.0140	.0535	.0552	.0668	.0289	.1752
101	.063	.063	.0671	.0289	.1752	.0140	.0535	.0552	.0668	.0289	.1752

13. MICROSTRIP T-JUNCTION

The geometric position of the T-junction discontinuity in a package is shown in Fig. 13.1.

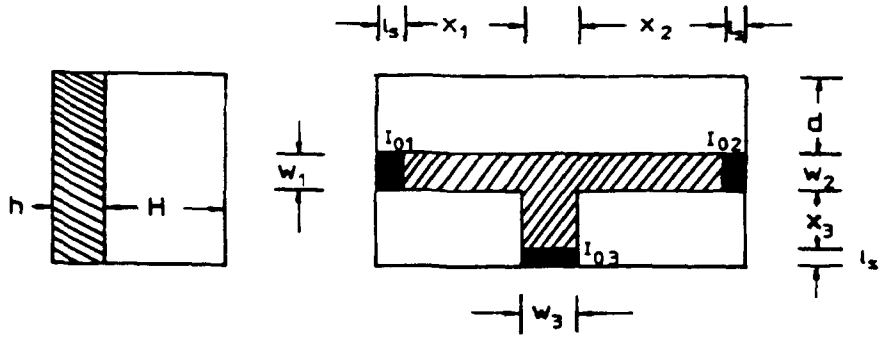


Fig. 13.1: Microstrip T-junction in a package

The discontinuity has three feed lines leading from it to the current sources I_{01}, I_{02} and I_{03} at the package edge. The package width is $w_s = d + l_s + x_3 + w_2$ and its length is $x_p = x_1 + x_2 + 2l_s$, where l_s is the source region.

The equivalent circuit model of this situation is shown in Fig. 13.2.

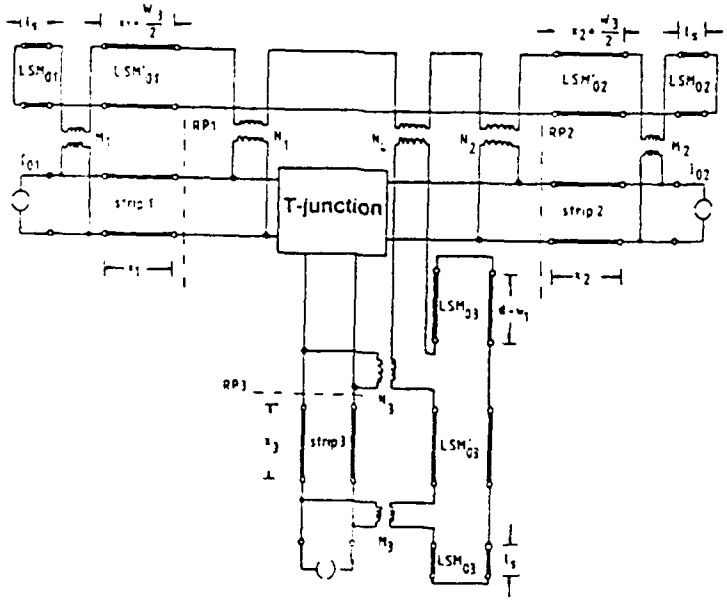


Fig. 13.2: Dynamic equivalent circuit model of T-junction in a package

As in the other discontinuities the microstrip and LSM_0 mode behaviour is represented by transmission line elements and the microstrip-LSM_0 mode coupling by the transformers M1, M2, M3, N1, N2 and N3 at the discontinuity planes as well as the sources. The transformer N4 models the bidirectional coupling between the LSM_0 and LSM_0' modes which are orthogonal to each other in the package. The 6-port T-junction discontinuity is delineated in Fig. 13.2 by the reference planes RP1, RP2 and RP3. The quasi-static model is represented in Fig. 13.2 by the 3-port blackbox.

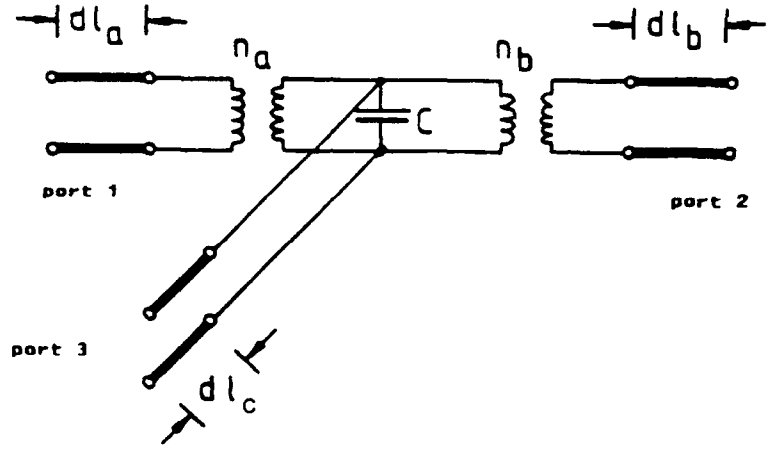


Fig. 13.3: Quasi-static circuit model for the microstrip T-junction

A commonly used quasi-static circuit model for the T-junction discontinuity is shown in Fig. 13.3. This equivalent circuit contains a capacitance C representing the excess stray field in the junction region, two transformers n_a and n_b taking the different characteristic impedances of the feed lines into account and the three transmission line sections dl_a, dl_b and dl_c for additional phase shifts.

Analytical expressions for the symmetric T-junction discontinuity ($w_1=w_2$) have been developed by Hammerstad (1), but for the non-symmetric junction

little has been published. Thus using Hammerstad's formulae a symmetric model was first developed.

13.1. DEVELOPMENT OF ANALYTIC FORMULAE FOR NORMALISED FREQUENCIES <3 GHz mm

13.1.1. Quasi-Static Database

A quasi-static data base was generated for the T-junction using the full wave analysis program. The analysis frequencies were from 5 GHz to 30 GHz in steps of 5 GHz using denormalized geometrical parameters for a substrate height of h=0.1mm.

The package dimensions were height 2 mm, width/length W_s = 3.2 mm, 2.1 mm, 1.0 mm, 1.24 mm and 0.64 mm. The positions of strip 1 and strip 2 were fixed to the centre of the package (X_m=0.5*W_s). The position of strip 3 was also fixed to the centre of the package ($d+w_2/2=l_s+W_2/2+x_3$), with respect to the other sidewall.

The widths of the feed lines of the T-junction discontinuity analyzed for the quasi-static data base were:

w_1 = 200μm, 100μm, 50μm, 20μm, 10μm
w_2/w_1 = 0.25, 0.5, 0.8, 1, 1.25, 1.5, 2, 4, (w_{max}=200μm), and
w_3/w_1 = 1, 1.5, 2, 3, 4, 5 (w_{max}=200μm).

From all three possible combinations a subset of 179 different T-junction configurations was analysed. In the analysis, strip width ratios w_2/w_1=8 and w_3/w_1 were studied only for narrow strips since for wide strips these ratios would result in absolute widths approaching the package width. Configurations having feed lines of w_2>200μm or w_3>200μm were not considered in the development, since they are rarely used in MMIC design work.

As for the bend discontinuity the high amount of CPU time that was spent for the T-junction analysis did not allow intensive convergence checks to be made. However, from working with the analysis program it can be concluded that the accuracy is in the same order of magnitude as for the other discontinuities. This means that for T-junction configurations with narrow feed lines the numerical accuracy is about 5% and better for wide strips. This data base was fitted to the above outlined equivalent circuit model. The capacitance C was fitted using the correction factor FC_BT, the transformers using the correction factors FC_TRA and FC_TRB and the transmission line sections using the correction factors FC_DLA, FC_DLB and FC_DLC for ports 1, 2 and 3, respectively. These factors were derived by first fitting the S-parameters of the circuit model to the numerical data base results. Functions were then derived to fit these factors.

13.1.2. Analytic Formulae for the Symmetric T-junction

A subset of the total quasi-static data base was used to create a reduced symmetric T-junction data base. The above procedure was used to derive analytic formulae for the symmetric T-junction. These formulae are:

$$2*\pi*f * C / S = BT * 2.606 * (1 + BT) * DL / n_a^2 / Z_L^c * \frac{w^a_{eff} * \beta^a}{w^c_{eff}}$$

$$n_a = \sqrt{1 - \tan(\pi * FC * (-0.0523*(Z_L^a/Z_L^c)^2 + (0.8932 - dl_c/w^a_{eff})^2))}$$

$$dl_c = (0.521 - 1.075 * \tan(RZ) * dl_c') * w^a_{eff}$$

$$dl_c' = 0.0598 + 0.780 * \exp(-1.742*\tan(RZ)) - 3.143 * FC * \tan(RZ) - 0.3874*\ln(1.075*\tan(RZ))$$

$$dl_a = 0.0446 * Z_L^a / Z_L^c * (1 - 2 * Z_L^a / Z_L^c * FC) * w^c_{eff}$$

with

$$BT = (0.301*\ln(RZ) + 13.81*RZ*FC - 4.784*\exp(-1.710*RZ) - 11.498*(Z_L^c/Z_0)^2)$$

$$DL = 0.0494*RZ*(1-2*RZ*FC) * w^{c}_{eff}$$

$$RZ = Z_L^a / Z_L^c$$

$$FC = \text{atan}\left(\left(2.375 * h/mm * f/GHz / (Z_L^a/\Omega) \right)^2 \right.$$

where Z_L^a and Z_L^c are the characteristic impedances, β^a is the propagation constant, w^a_{eff} and w^c_{eff} are the effective widths of the feed lines. a is related to ports 1 and 2 and c to port 3. The units are MKS except where stated in the formulae.

The mean deviation F_{mean}, the maximum deviation F_{max} and the relative maximum deviation F_{maxr} are listed in Table 1 (Section 13.6) for each data set for parameters S11, S13, S33 and S12. The overall deviations of all evaluated data are:

S11=S22:	F_{mean} = 2.22%,	F_{max} = 0.065,	F_{maxr} = 15.2%
S13=S23:	F_{mean} = 0.93%,	F_{max} = 0.039,	F_{maxr} = 5.81%
S33:	F_{mean} = 2.96%,	F_{max} = 0.042,	F_{maxr} = 30.5%
S12:	F_{mean} = 1.24%,	F_{max} = 0.064,	F_{maxr} = 11.1%

The values of F_{maxr} are listed for completeness. They refer to reasonably small F_{max} giving an indication of the approximation quality.

13.1.3. Analytic Formulae for the General T-Junction

The data base was used again to fit the numerical data sets to the equivalent circuit model using modified transformer ratios for the non symmetric case.

From the base expressions used for the symmetrical T-junction configurations, the correction factors for the transformer ratios were found to be nearly equal to the value of 1, but the other correction factors showed that the start expressions do not provide a good representation for the general T-junction discontinuity. The first modification of the expressions developed for the symmetrical T-junction, therefore, was to multiply each of the formulae with correction expressions that take the dependency on the difference in the widths of the feed lines into account. However, the accuracy achieved by these expressions was still not sufficient. Therefore in subsequent steps each expression in total was optimised by using the same mathematically structured formulae but fitting the parameters of the formulae in an optimisation. The final analytic formulae for the general T-junction are:

$$2*\pi*f * C / S = BT * 1.778 * (1 + BT) * DL / n_a / n_b / Z_L^c * \frac{\beta^a + \beta^b}{2} * \frac{w^a_{eff} + w^b_{eff}}{2*w^c_{eff}} * (1 + 0.106 * (w_2/w_1-1)^{(-0.274*(1+0.11*(w_3/w_1)^{0.901})})$$

$$n_a = \sqrt{1 - \operatorname{atan}(\pi * FCA * (0.404*(Z_L^a/Z_L^c)^2 + (1.257 - dl_c/w^a_{eff})^2))}$$

$$n_b = \sqrt{1 - \operatorname{atan}(\pi * FCB * (0.404*(Z_L^b/Z_L^c)^2 + (1.257 - dl_c/w^b_{eff})^2))}$$

$$dl_c = (0.453 - 1.17 * \operatorname{atan}(RZ) * dl_c') * \frac{w^a_{eff} + w^b_{eff}}{2} * (1 + 0.0131 * (w_2/w_1-1)^{(1.5885*(1+0.07152*(w_1/h)^{1.139})})$$

$$dl_c' = -0.03147 + 0.578 * \exp(-1.05*\operatorname{atan}(RZ)) - 13.63*FC*\operatorname{atan}(RZ) - 0.2041*\ln(1.17*\operatorname{atan}(RZ))$$

$$dl_a = 0.024 * Z_L^a / Z_L^c * (1 - 2 * Z_L^a / Z_L^c * FCA) * w^c_{eff} *$$

$$(1 - 0.298 * (w_2/w_1-1)^{(2.376*(1-0.191*(w_3/w_1)^{1.3875})})$$

$$dl_b = 0.024 * Z_L^b / Z_L^c * (1 - 2 * Z_L^b / Z_L^c * FCB) * w^c_{eff} *$$
$$(1 - 2.587 * (1-w_1/w_2)^{(2.603*(1+0.2484*(w_3/w_2)^{1.678})})$$

with

$$BT = (5.091*\ln(RZ) + 22.22*RZ*FC + 19.23*\exp(-7.938*RZ) - 15.22*(Z_L^s/Z_0)^2)$$

$$DL = 0.01844*RZ*(1-2*RZ*FC) * w^c_{eff}$$

$$RZ = \sqrt{Z_L^a * Z_L^b} / Z_L^c$$

$$FC = \sqrt{FCA * FCB}$$

$$FCA = \text{atan}((0.9941 * h/mm * f/GHz / (Z_L^a/\Omega))^2)$$

$$FCB = \text{atan}((0.9941 * h/mm * f/GHz / (Z_L^b/\Omega))^2)$$

where Z_L^a, Z_L^b and Z_L^c are the characteristic impedances of the feed lines β^a and β^b are the propagation constants of the feed lines, w^a_{eff}, w^b_{eff} and w^c_{eff} are the effective widths of the feed lines for ports 1, 2 and 3 respectively. The units are MKS except where stated. These expressions have been generated for $w_2 > w_1$.

In Table 2 (Section 13.6) for each data set the mean deviation F_{mean}, the maximum deviation F_{max} and the relative maximum deviation F_{maxr} are listed for parameters S1, S22, S33, S12, S13 and S23. The overall deviations are:

S11:	F_{mean} = 2.65%,	F_{max} = 0.065,	F_{maxr} = 16.7%
S22:	F_{mean} = 3.53%,	F_{max} = 0.064,	F_{maxr} = 24.7%
S33:	F_{mean} = 2.25%,	F_{max} = 0.053,	F_{maxr} = 15.8%

S12: F_{mean} = 0.87%, F_{max} = 0.061, F_{maxr} = 10.7%
S13: F_{mean} = 1.10%, F_{max} = 0.038, F_{maxr} = 5.82%
S23: F_{mean} = 1.14%, F_{max} = 0.034, F_{maxr} = 5.00%

Again, the remark on F_{maxr} and F_{max} applies as for the symmetric T-junction.

13.2. DEVELOPMENT OF ANALYTIC FORMULAE FOR NORMALISED FREQUENCIES <12GHzmm

As in the investigations on the microstrip 90°-bend discontinuity a dynamic correction in addition to parasitic package effects was found to be useful in obtaining a good model accuracy for high frequencies. Therefore, configurations were analysed for frequencies up to 120 GHz, chosen to ensure that within the frequency range all package modes were below cut-off.

The results in Figs. 13.4 and 5 show the magnitude and phase of parameter S12 for two analysed configurations. The numerically computed full-wave data are shown together with the results of two different discontinuity descriptions. For both, Fig. 13.2 represents the applied equivalent circuit model. The dotted curves marked 'LOW FREQ' use the analytic expressions for frequencies up to 30 GHz. The dashed curves show scattering parameter S12 using a computation based on the same equivalent circuit model but using optimised correction factors FC_BT, FC_TRA FC_TRB, FC_DLA, FC_DLS and FC_DLB for the model elements. From these results it can be concluded that the equivalent circuit model topology is also suitable for predicting the frequency dependent T-junction discontinuity behaviour for the higher frequency.

13.2.1. Study of T-junction Package Dynamic Behaviour

The numerical analysis of T-junction configurations requires relatively large CPU times. Therefore, before starting the generation of a supplementary data base for the frequency range up to 120 GHz with packages all below cut-off,

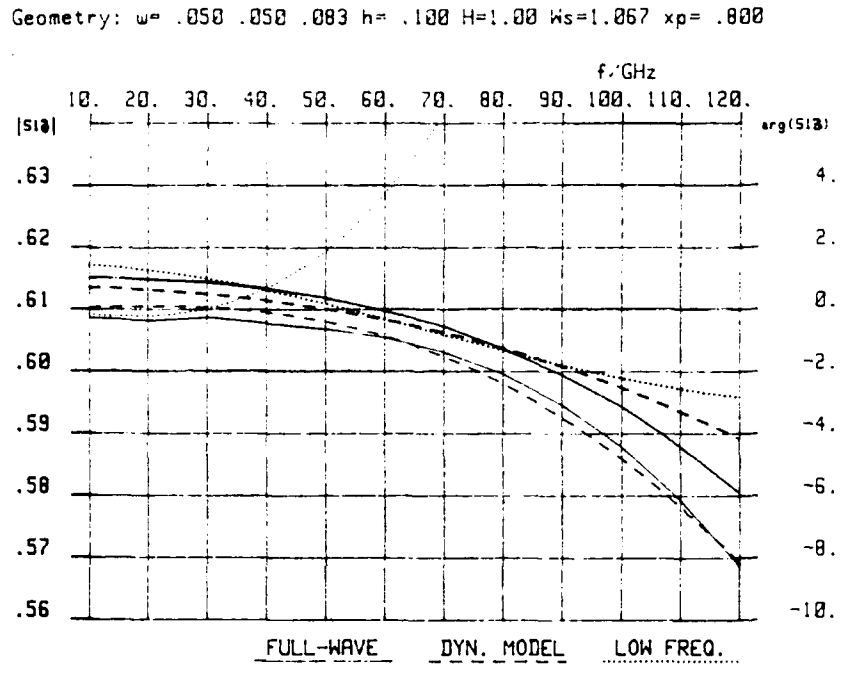


Fig. 13.4: S12 for T-junction model, configuration 1

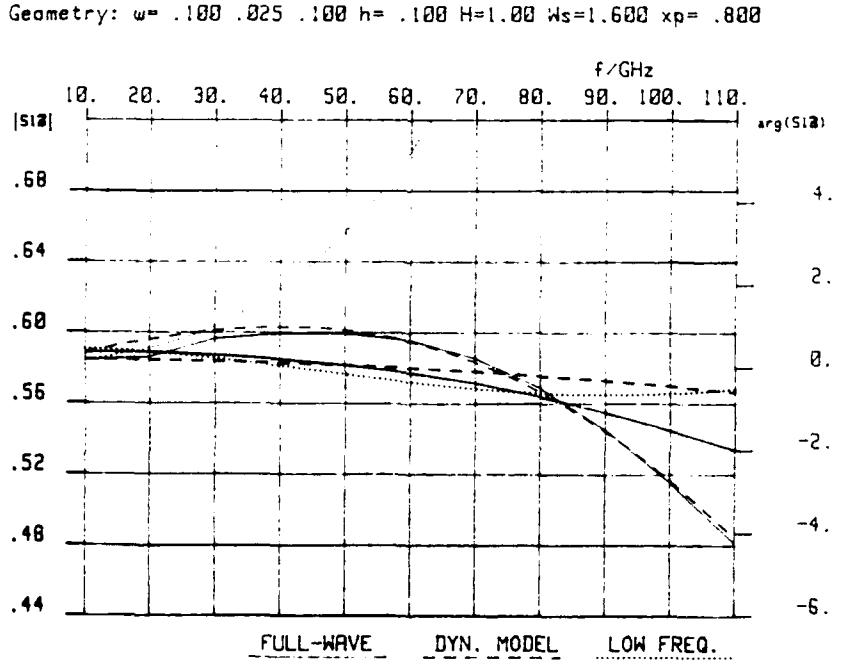


Fig. 13.5: S12 for T-junction model, configuration 2

some useful precomputations were done with the aim of restricting the size of this data base.

The data bases for the generation of equivalent circuit models for the open end, gap and step discontinuities contain discontinuity configurations of different cover heights. The investigation of the 90°-bend discontinuity showed that for this discontinuity the cover height has only a minor influence on the frequency dependent behaviour, for heights in the range of technical interest. The results of Figs. 13.6-9 show the magnitude and phase of scattering parameters S13 and S11 of a T-junction configuration for two different cover heights of H = 0.5 mm and H = 1 mm. The two sets of scattering parameters give similar frequency dependent behaviour. For large cover heights, the influence of the cover plate decreases further and for smaller cover heights are not of technical interest for circuit development. Therefore it can be concluded that the inclusion of different cover heights in the supplementary data base does not strongly affect the analytic expressions for frequencies below the package mode cut-off.

In general, the frequency dependent dynamic behaviour of the T-junction discontinuity depends on package effects and/or less pronounced dynamic effects related to the discontinuities themselves. Package effects are considerable only near or above the cut-off of the dominant parasitic package mode. To demonstrate this a symmetric T-junction configuration of strip width $w_1 = w_2 = 50\mu m$, $w_3 = 25\mu m$ was analysed for different positions in the package. The results for parameter S12 are shown for the following positions: $x_1 = 0.5*xp$, $x_3 = 0.5*W_s$; $x_1 = 0.5*xp$, $x_3 = 0.65*W_s$; $x_1 = 0.65*xp$, $x_3 = 0.5*W_s$; and $x_1 = 0.65*xp$, $x_3 = 0.65*W_s$ in Figs. 13.10-13 respectively.

The maximum deviation as a function of the discontinuity position in the package is less than 0.01 for the magnitude of parameter S12 and less than 1°

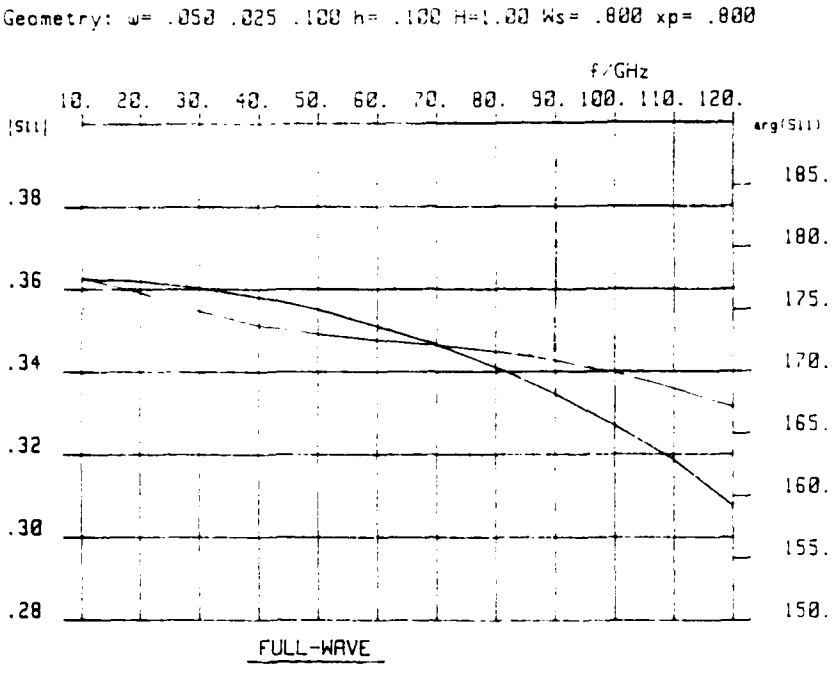


Fig. 13.6: S13 for T-junction: cover height 0.5 mm

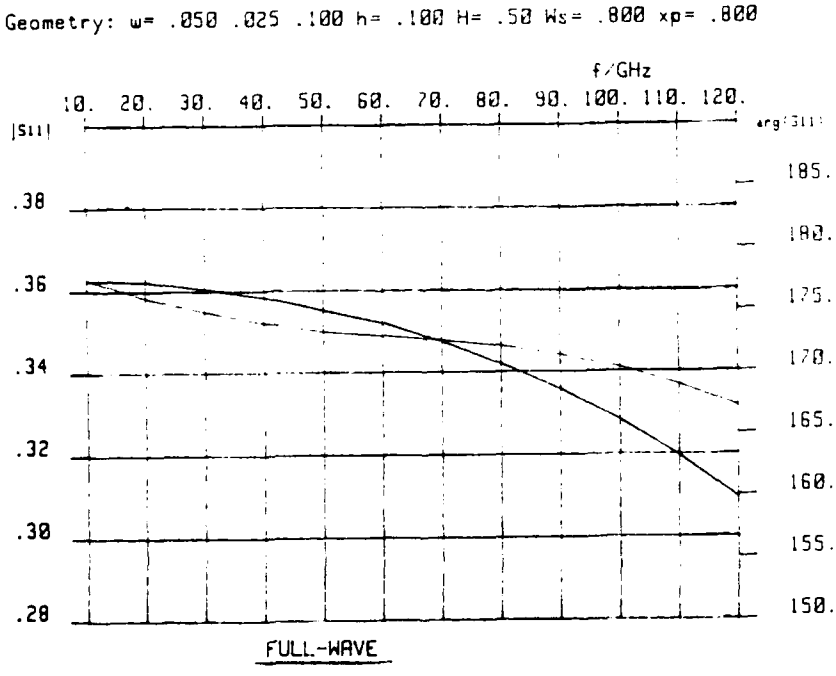


Fig. 13.7: S11 for T-junction: cover height 0.5 mm

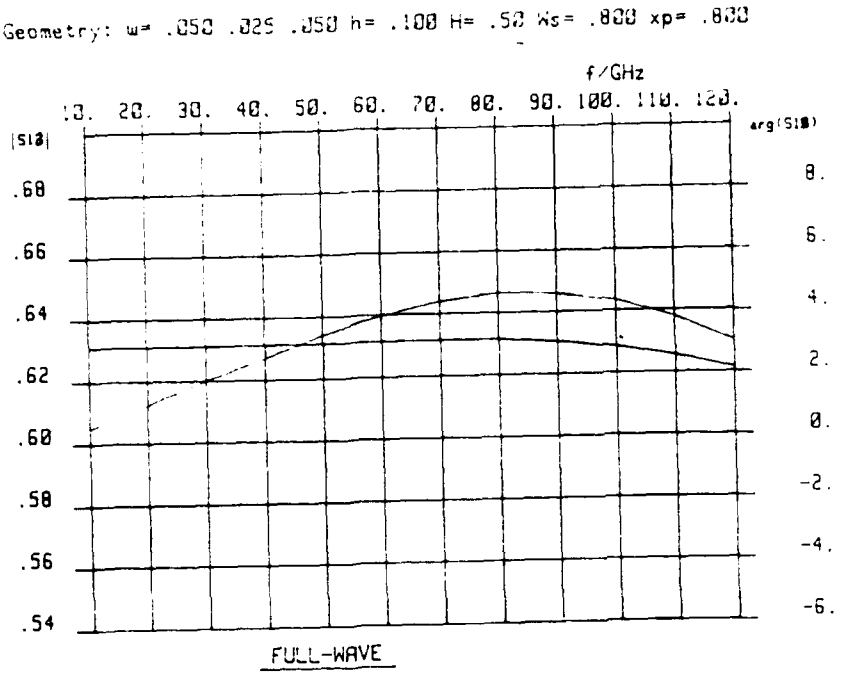


Fig. 13.8: S13 for T-junction: cover height 1.0 mm

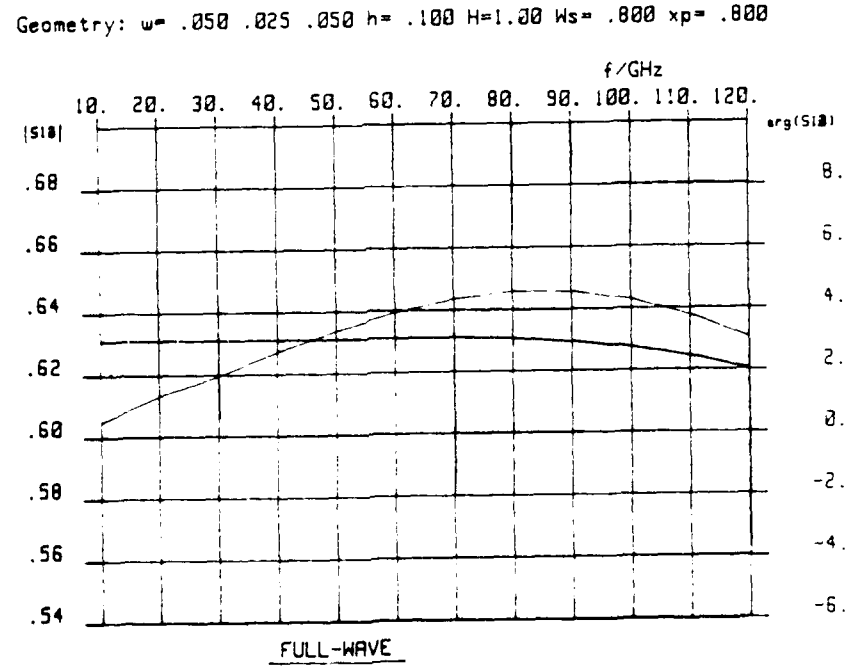


Fig. 13.9: S11 for T-junction: cover height 1.0 mm

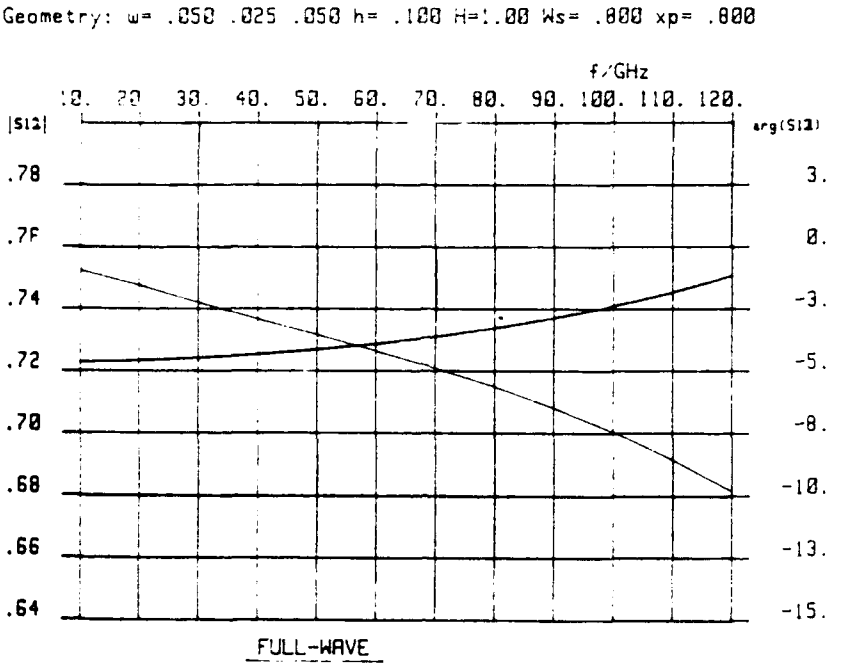


Fig. 13.10: S12 for T-junction, first position

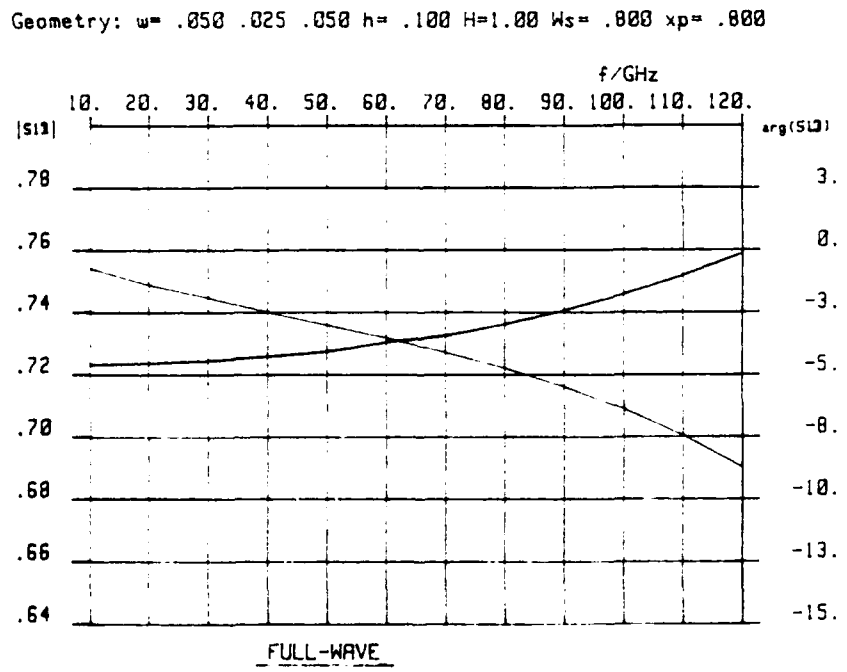


Fig. 13.11: S12 for T-junction, second position

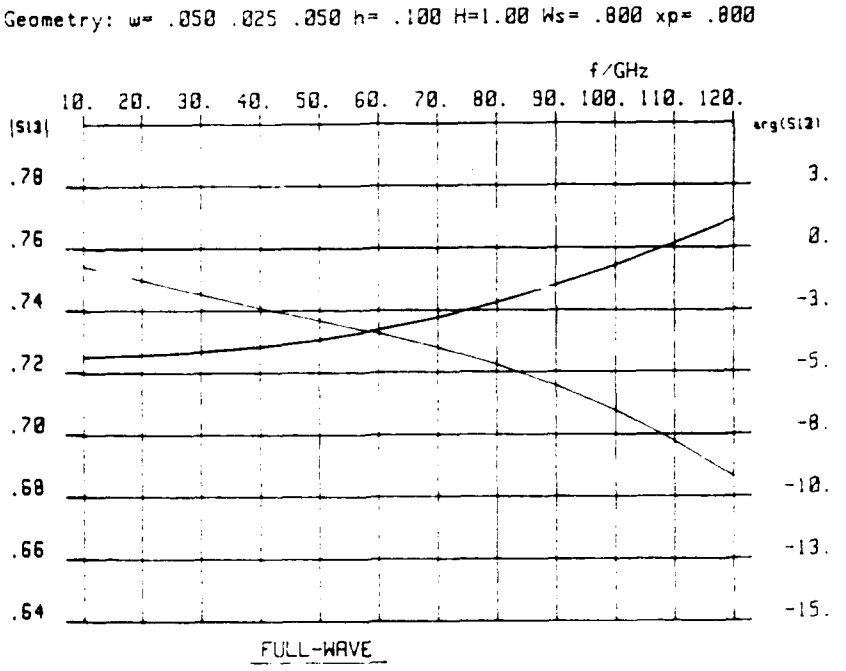


Fig. 13.12: S12 for T-junction, third position

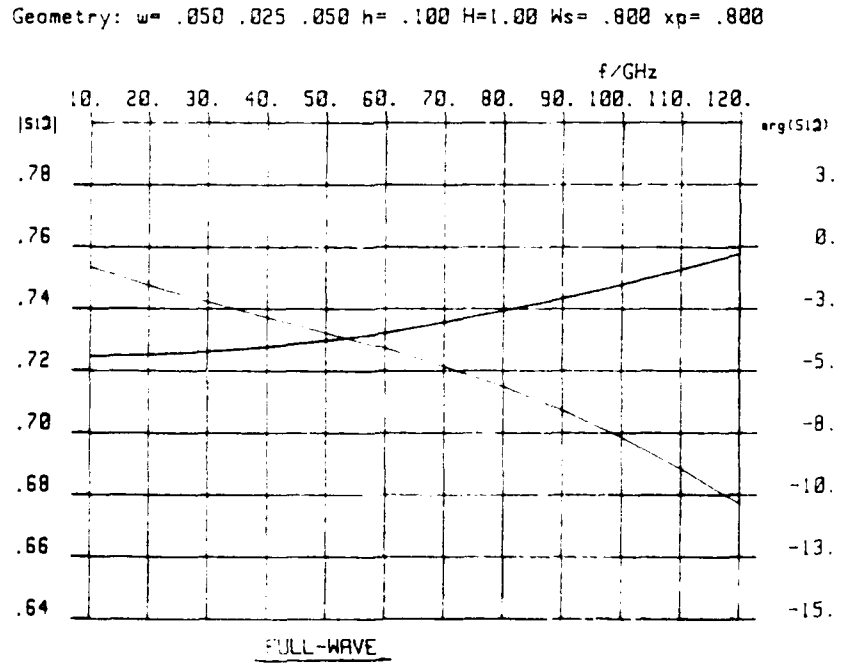


Fig. 13.13: S12 for T-junction, fourth position

for the phase. This deviation may also be caused by different degrees of convergence in the numerical analysis due to different lengths of the feed lines. As a result of this investigation, it can be concluded that the dynamic behaviour of the T-junction discontinuity is related to the discontinuity structure itself and not to the package, as long as the package dimensions are not too close to the T-junction and the frequency is far enough below the package mode cut-off frequency.

13.2.2. Analytic formulae for the symmetric T-junction

As for the quasi-static expressions for the T-junction equivalent circuit model, a first set of analytic formulae was developed to describe the symmetric T-junction discontinuity. A subset of 17 discontinuity configurations was chosen in addition and based on this supplementary data base the following expressions were obtained on fitting the 3-port scattering parameters of the equivalent circuit model to the full-wave data base results. The following formulae were obtained:

$$2*\pi*f * C / S = BT * 0.186 * (1 + BT) * DL / n_a'^2 / Z_L^c * \frac{w^a_{eff} * \beta^a}{w^c_{eff}}$$

$$n_a' = \sqrt{1 - \operatorname{atan}(\pi * FC * (0.093*(Z_L^a/Z_L^c)^2 + (0.5 - dl_c/w^a_{eff})^2))}$$

$$n_a = n_a' - 0.00027*(w_2/h)^{1.2} * f/GHz$$

$$dl_c = (0.479 - 1.029 * \operatorname{atan}(RZ) * dl_c') * w^a_{eff} * \exp(0.1105*w_3/h) * \exp(0.1111*w_1/h)$$

$$dl_c' = 0.00759 + 0.8294 * \exp(-1.698*\operatorname{atan}(RZ)) + 0.0884 * FC * \operatorname{atan}(RZ) - 0.360*\ln(1.029*\operatorname{atan}(RZ))$$

$$dl_a = 0.0292 * Z_L^a / Z_L^c * (1 - 2 * Z_L^a / Z_L^c * FC) * w^c_{eff} * (1 - \exp(-6.264*w_1/h)) * \exp(0.3136*w_3/h)$$

with

$$BT = (32.309*\ln(RZ) + 44.323*RZ*FC - 12.130*\exp(-1.169*RZ) - 98.448*(Z_L^c/Z_0)^2)$$

$$DL = 0.0399*RZ*(1-2*RZ*FC) * w^c_{eff}$$

$$RZ = Z_L^a / Z_L^c$$

$$FC = \text{atan} ((3.167 * h/mm * f/GHz / (Z_L^a/\Omega))^2)$$

where Z_L^a and Z_L^c are the characteristic impedances, β^a is the propagation constant and w^a_{eff} and w^c_{eff} are the effective widths of the feed lines. Note that ports 1 and 2 are related to a and port 3 to c, the units being MKS except where stated in the formulae.

In Table 3 (Section 13.6) for each data set the mean deviation F_{mean}, the maximum deviation F_{max} and the relative maximum deviation F_{maxr} are listed for parameters S11, S13, S33, S12, S23 and S22. The overall deviations considering all data sets are:

S11=S22:	F_{mean} = 2.77%,	F_{max} = 0.047,	F_{maxr} = 13.6%
S13=S23:	F_{mean} = 1.38%,	F_{max} = 0.068,	F_{maxr} = 10.3%
S33:	F_{mean} = 3.72%,	F_{max} = 0.080,	F_{maxr} = 23.2%
S12:	F_{mean} = 1.11%,	F_{max} = 0.027,	F_{maxr} = 4.81%

Again the relatively large F_{maxr} values are not meaningful for considering design accuracy, because they are associated with small F_{max} values.

13.2.3. Analytic formulae for the general T-junction

A subset of 46 discontinuity configurations was chosen from all possible combinations of geometry parameter sets and used to generate the following

expressions by fitting the scattering parameters of the equivalent circuit model to the full wave data base results;

$$2*\pi*f * C / S = BT * 0.202 * (1 + BT) * DL / n_a' / n_b' / Z_L^c * \frac{\beta^a + \beta^b}{2} * \frac{w^a_{eff} + w^b_{eff}}{2*w^c_{eff}}$$

$$n_a' = \sqrt{1 - \operatorname{atan}(\pi * FCA * (0.112*(Z_L^a/Z_L^c)^2 + (0.5 - dl_c/w^a_{eff})^2))}$$

$$n_a = n_a' - 0.00063*(w_2/h)^{1.02} * f/GHz$$

$$n_b' = \sqrt{1 - \operatorname{atan}(\pi * FCB * (0.112*(Z_L^b/Z_L^c)^2 + (0.5 - dl_c/w^b_{eff})^2))}$$

$$n_b = n_b' - 0.00063*(w_2/h)^{1.02} * f/GHz * (w_1/w_2)^{2.3}$$

$$dl_c = (0.477 - 0.9985 * \operatorname{atan}(RZ) * dl_c') * \frac{w^a_{eff} + w^b_{eff}}{2} * \exp(0.0360*w_3/h) * \exp(0.1475*w_1/h)$$

$$dl_c' = 0.00567 + 0.8159 * \exp(-1.696*\operatorname{atan}(RZ)) + 0.0908 * FC * \operatorname{atan}(RZ) - 0.342*\ln(0.9985*\operatorname{atan}(RZ))$$

$$dl_a = 0.0185 * Z_L^a / Z_L^c * (1 - 2 * Z_L^a / Z_L^c * FCA) * w^c_{eff} * (1 - \exp(-10.15*w_1/h)) * \exp(0.4830*w_3/h)$$

$$dl_b = 0.0185 * Z_L^b / Z_L^c * (1 - 2 * Z_L^b / Z_L^c * FCB) * w^c_{eff} * (1 - \exp(-10.15*w_2/h)) * \exp(0.4830*w_3/h)$$

with

$$BT = (26.021*\ln(RZ) + 54.639*RZ*FC - 6.856*\exp(-1.333*RZ) - 98.143*(Z_L^c/Z_0)^2)$$

$$DL = 0.0401*RZ*(1-2*RZ*FC) * w^c_{eff}$$

$$RZ = \sqrt{Z_L^a * Z_L^b} / Z_L^c$$

$$FC = \sqrt{FCA * FCB}$$

$$FCA = \operatorname{atan} ((2.711 * h/mm * f/GHz / (Z_L^a/\Omega))^2)$$

$$FCB = \operatorname{atan} ((2.711 * h/mm * f/GHz / (Z_L^b/\Omega))^2)$$

where $Z_L{}^a$, $Z_L{}^b$ and $Z_L{}^c$ are the characteristic impedances, β^a and β^b are the propagation constants, and w^a_{eff}, w^b_{eff} and w^c_{eff} are the effective widths of the feed lines. Note that ports 1, 2 and 3 are again related to the feed lines a, b and c, the units being MKS except where stated. Again the formulae have been generated for $w_2 \geq w_1$.

In Table 4 (Section 13.6) for each data set the mean deviation F_{mean}, the maximum deviation F_{max} and the relative maximum deviation F_{maxr} are listed for parameters S11, S13, S33, S12, S23 and S22. The overall deviations considering all evaluated data sets are:

S11:	F_{mean} = 3.51%,	F_{max} = 0.077,	F_{maxr} = 18.6%
S22:	F_{mean} = 4.26%,	F_{max} = 0.033,	F_{maxr} = 38.9%
S33:	F_{mean} = 3.94%,	F_{max} = 0.083,	F_{maxr} = 18.8%
S12:	F_{mean} = 1.23%,	F_{max} = 0.047,	F_{maxr} = 6.58%
S13:	F_{mean} = 1.55%,	F_{max} = 0.059,	F_{maxr} = 9.66%
S23:	F_{mean} = 1.70%,	F_{max} = 0.065,	F_{maxr} = 9.51%

The application of the final analytic formulae shows relatively large F_{maxr} deviations for some discontinuity configurations. However the respective absolute deviations listed in Tables 3 and 4 are at the same time sufficiently small. Considering the wide range of validity of the analytic formulae ($0 < f*h < 12$ GHz*mm) the final expressions above provide a great improvement on other published T-junction equivalent circuit models.

13.3. DEVELOPMENT OF THE TRANSFORMER RATIO EXPRESSIONS

To check the package resonance effect dependency on the choice of the package dimensions and on the position of the discontinuity in a package, several T-junction configurations were analysed. For simplicity cases with the same feed line widths but different discontinuity positions in the package and different package dimensions were used. The results show parameters S11, S12

and S13 for the following T-junction positions and package dimensions; package width: 1.54mm; package length: 1.92mm, x1 = 0.93mm, x2 = 0.98mm, x3 = 0.93mm (Figs. 13.14-16); package width: 1.92mm; package length: 1.92mm x1 = 0.93mm, x2 = 0.99mm, x3 = 0.93mm (Figs. 13.17-19). These results were computed using the correction factors given in the title of the respective resultant plots. As can be seen the resonance behaviour was found to be well predicted.

The dynamic transformer ratio

$$N_{dyn} = \begin{cases} N * \cos^{f1}(0.5*\pi*(f-f_0)/f_0) * \exp(-f_1*(-f_0)/f_0) & f<f_0 \\ N & f>f_0 \end{cases}$$

$$M_{dyn} = -N_{dyn}$$

were introduced into the T-junction model (Fig. 13.2) for the transformers N1, N2, N3, M1, M2 and M3. f_0 and f_1 are described identically by those expressions developed for the other discontinuities.

$$f_0 = f_c * 1.4 * f_0' * (1 + \exp(-0.0638 * W_s/h * H/h)) * (1 - 2.33 * \exp(-0.33 * W_s/h))$$

$$f_0' = 1.0$$

$$f_1 = 2$$

Refinement of the transformer ratio expressions were done by analysing T-junction configurations situated with in packages having dimensions that cause a package resonance at frequencies below 120 GHz. The formulae accuracy is shown by the results given in Figs. 13.14-19.

In the T-junction equivalent circuit model, the transformer N4 describes the LSM_0/LSM_0' mode orthogonal excitation similar to transformer N3 in

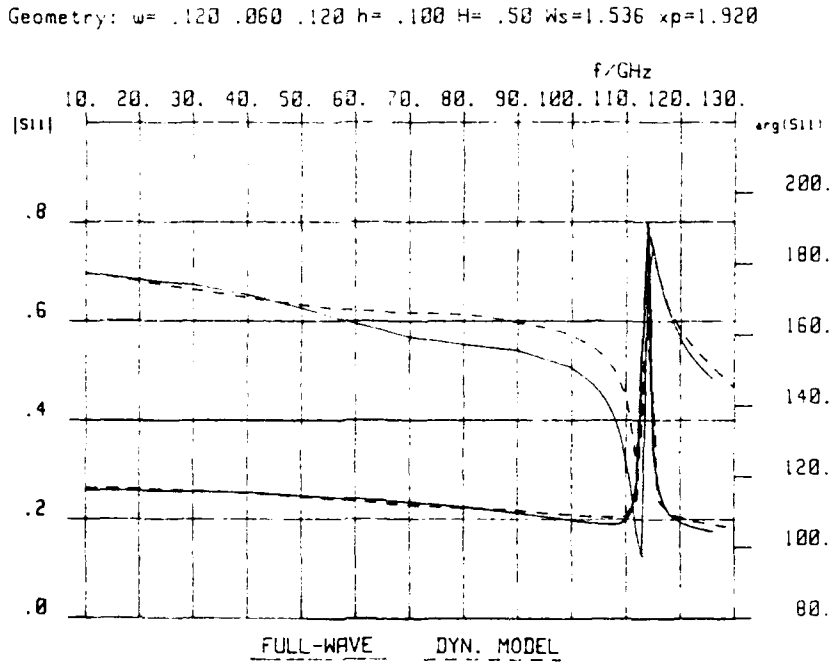


Fig. 13.14: S11 for T-junction, first position

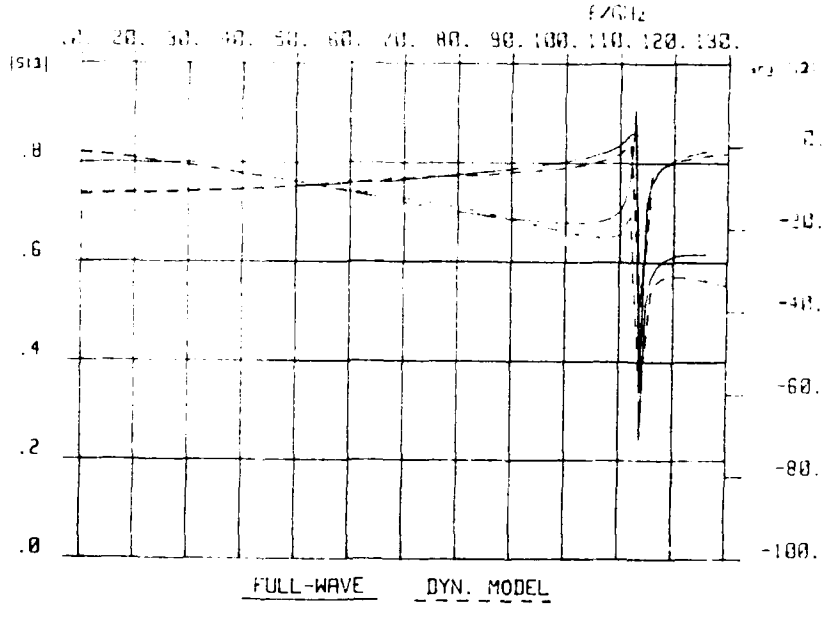


Fig. 13.15: S12 for T-junction, first position

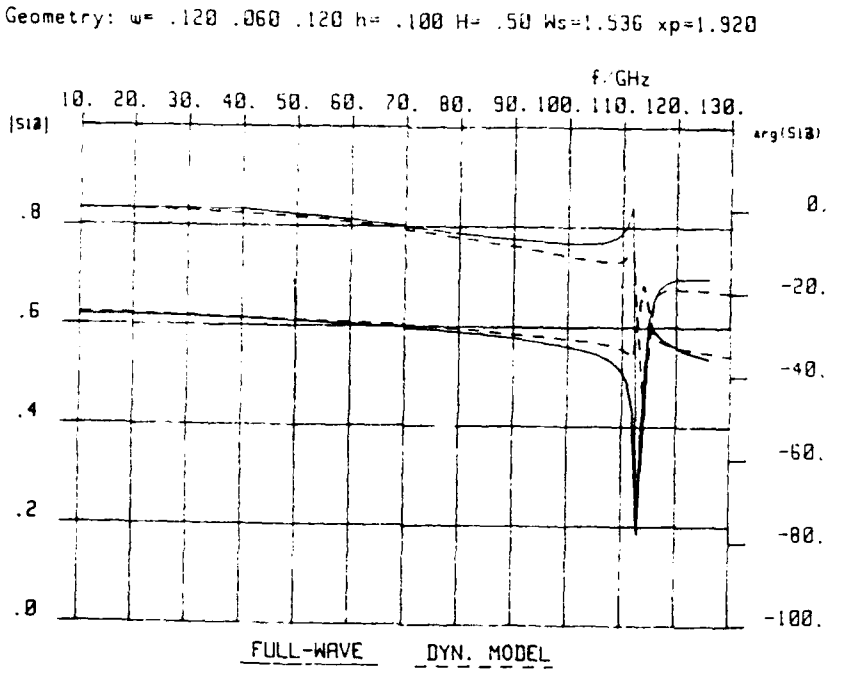


Fig. 13.16: S13 for T-junction, first position

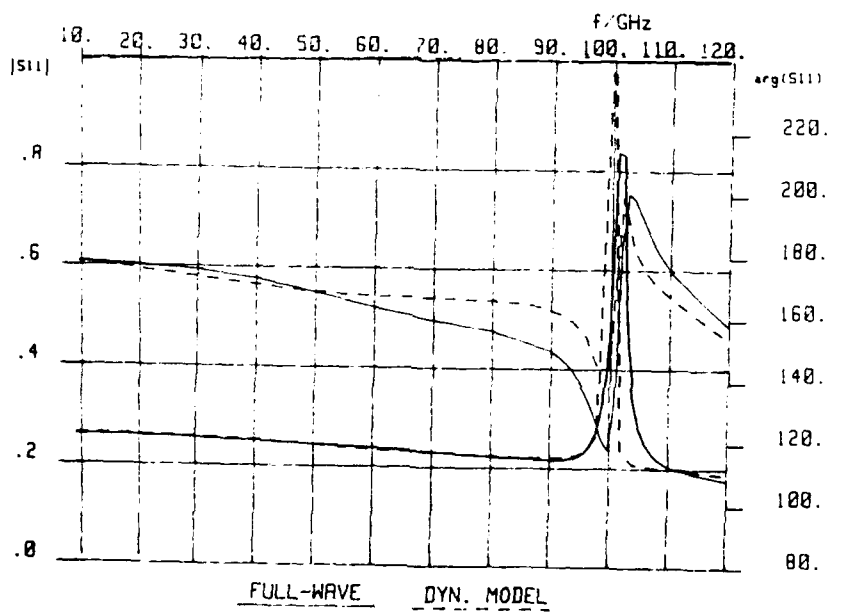


Fig. 13.17: S11 for T-junction, second position

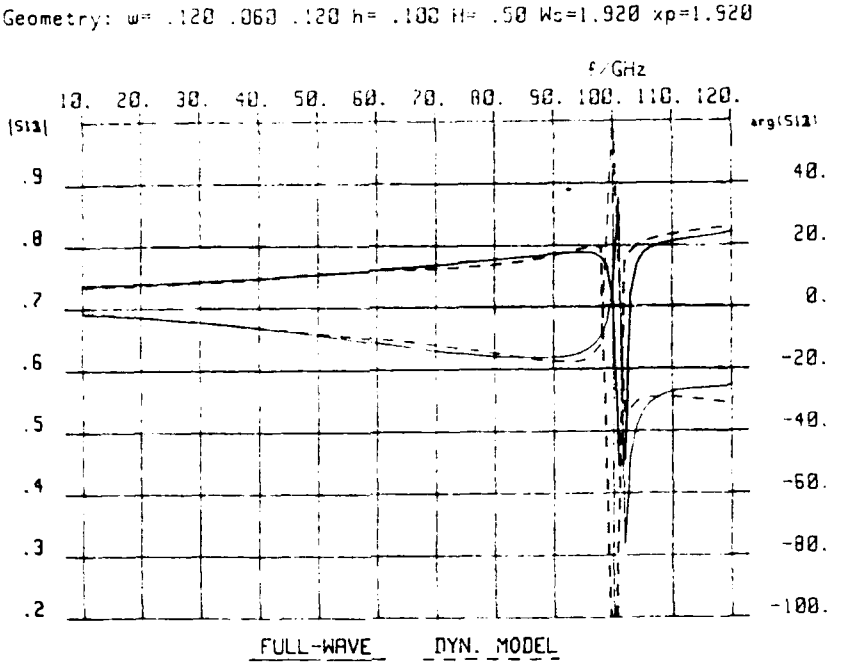


Fig. 13.18: S12 for T-junction, second position

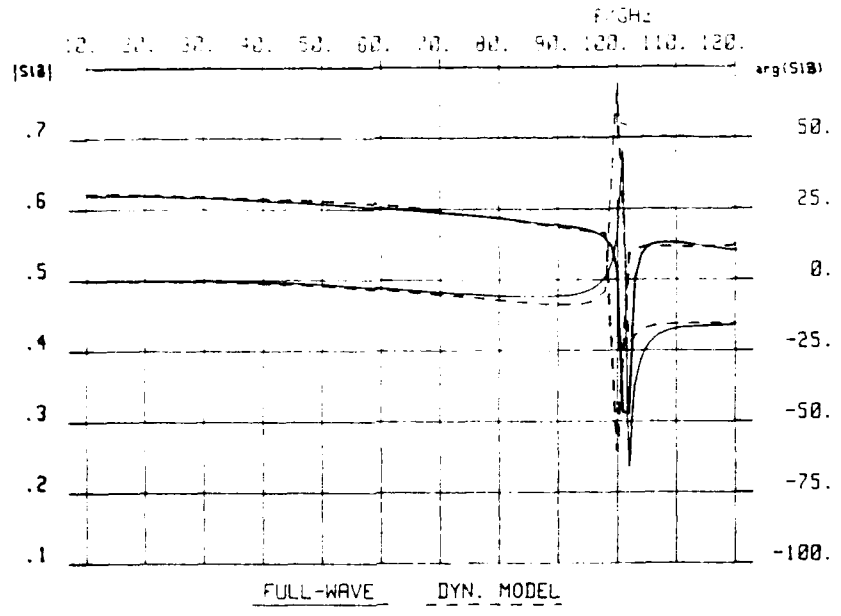


Fig. 13.19: S13 for T-junction, second position

the 90°-bend discontinuity model. Preliminary investigations on the transformer N4 for the T-junction showed that the numerical value was again very small (N4 = 0.001 for all computations). However it could not be neglected as in the 90° bend, because it was found that a small non-zero transformer ratio was necessary to match the two slightly different resonance frequencies of both orthogonal LSM_0/LSM_0' package modes into a single resonance.

13.4. VERIFICATION OF THE T-JUNCTION ANALYTIC FORMULAE

The refined model expressions for the T-junction discontinuity are given in the summary. These formulae were used also to analyse some additional T-junction configurations for final model verification. Due to the amount of CPU time necessary for accurate numerical computations this was done for only a small data base of 15 different T-junction configurations. For a high number of frequencies (up to 40) the respective configurations were computed to show clearly the resonance behaviour. For an example T-junction configuration, the S11, S12 and S13 magnitude and phase generated by the dynamic equivalent circuit model are plotted in Figs. 13.20-22 together with the data base results. As can be seen the results show good agreement between the predicted discontinuity behaviour and the numerically computed full-wave results.

13.5. T-JUNCTION MODEL SUMMARY

In this section, the microstrip T-junction formulae are summarised, where $Z_L^{microstrip}$ and $\varepsilon_{eff}^{microstrip}$ are computed according to procedures in Section 4. For the unsymmetric T-junction the formulae have been derived for $w_2 > w_1$. All units are MKS except where stated otherwise in the formulae.

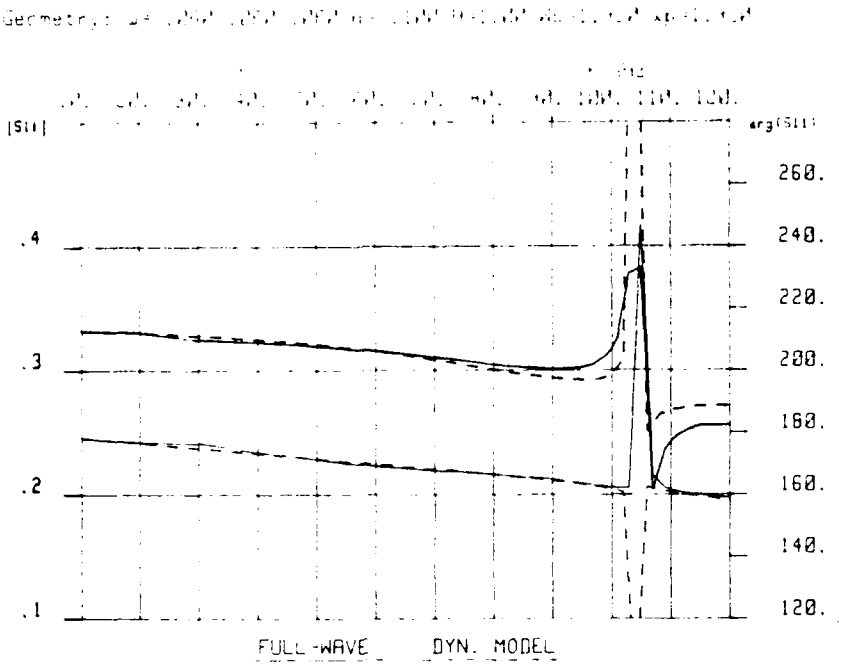


Fig. 13.20: S11 for T-junction, model verification

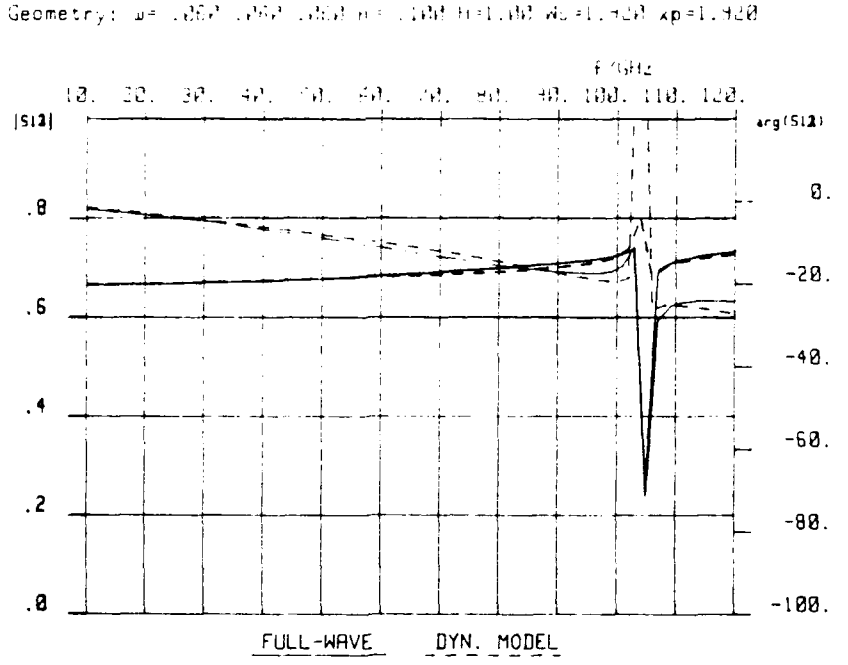


Fig. 13.21: S12 for T-junction, model verification

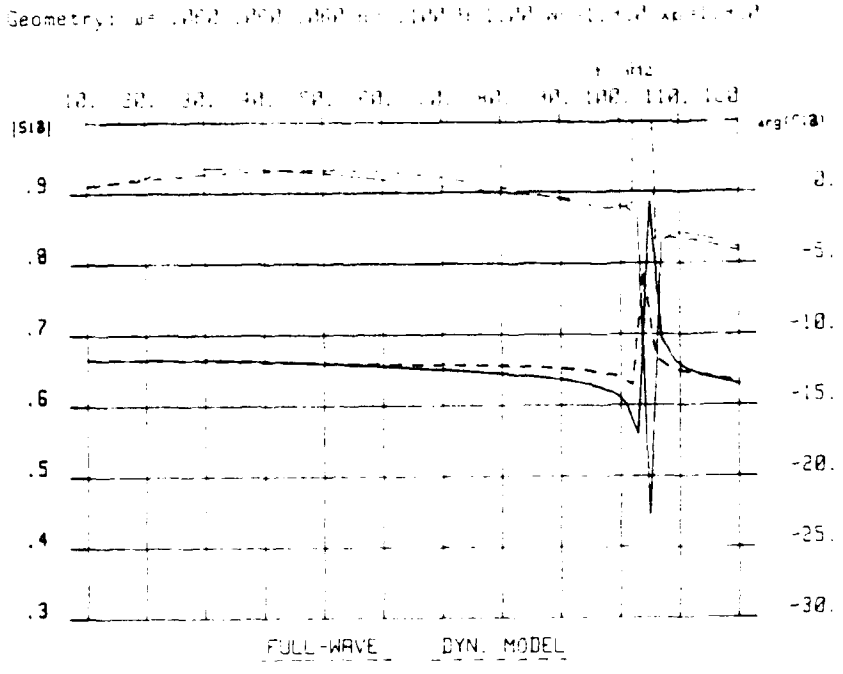


Fig. 13.22: S13 for T-junction, model verification

Quasi-static formulae for the symmetric T-junction

$$2*\pi*f * C / S = BT * 2.606 * (1 + BT) * DL / n_a^2 / Z_L^c * \frac{w^a_{eff} * \beta^a}{w^c_{eff}}$$

$$n_a = \sqrt{1 - \operatorname{atan}(\pi * FC * (-0.0523*(Z_L^a/Z_L^c)^2 + (0.8932 - dl_c/w^a_{eff})^2))}$$

$$dl_c = (0.521 - 1.075 * \operatorname{atan}(RZ) * dl_c') * w^a_{eff}$$

$$dl_c' = 0.0598 + 0.780 * \exp(-1.742*\operatorname{atan}(RZ)) - 3.143 * FC * \operatorname{atan}(RZ) - 0.3874*\ln(1.075*\operatorname{atan}(RZ))$$

$$dl_a = 0.0446 * Z_L^a / Z_L^c * (1 - 2 * Z_L^a / Z_L^c * FC) * w^c_{eff}$$

with

$$BT = (0.301*\ln(RZ) + 13.81*RZ*FC - 4.784*\exp(-1.710*RZ) - 11.498*(Z_L^c/Z_0)^2)$$

$$DL = 0.0494*RZ*(1-2*RZ*FC) * w^c_{eff}$$

$$RZ = Z_L^a / Z_L^c$$

$$FC = \operatorname{atan} ((2.375 * h/mm * f/GHz / (Z_L^a/\Omega))^2$$

Quasi-static formulae for the general T-junction

$$2\pi f \cdot C / S = BT \cdot 1.778 \cdot (1 + BT) \cdot DL / n_a / n_b / Z_L^c \cdot \frac{\beta^a + \beta^b}{2} \cdot \frac{w^a_{eff} + w^b_{eff}}{2 w^c_{eff}} \cdot \left(1 + 0.106 \cdot (w_2/w_1 - 1)^{(-0.274 \cdot (1 + 0.11 \cdot (w_3/w_1)^{0.901}))}\right)$$

$$n_a = \sqrt{1 - \operatorname{atan}\left(\pi \cdot FCA \cdot \left(0.404 \cdot (Z_L^a/Z_L^c)^2 + (1.257 - dl_c/w^a_{eff})^2\right)\right)}$$

$$n_b = \sqrt{1 - \operatorname{atan}\left(\pi \cdot FCB \cdot \left(0.404 \cdot (Z_L^b/Z_L^c)^2 + (1.257 - dl_c/w^b_{eff})^2\right)\right)}$$

$$dl_c = (0.453 - 1.17 \cdot \operatorname{atan}(RZ) \cdot dl_c') \cdot \frac{w^a_{eff} + w^b_{eff}}{2} \cdot \left(1 + 0.0131 \cdot (w_2/w_1 - 1)^{(1.5885 \cdot (1 + 0.07152 \cdot (w_1/h)^{1.139}))}\right)$$

$$dl_c' = -0.03147 + 0.578 \cdot \exp(-1.05 \cdot \operatorname{atan}(RZ)) - 13.63 \cdot FC \cdot \operatorname{atan}(RZ) - 0.2041 \cdot \ln(1.17 \cdot \operatorname{atan}(RZ))$$

$$dl_a = 0.024 \cdot Z_L^a / Z_L^c \cdot (1 - 2 \cdot Z_L^a / Z_L^c \cdot FCA) \cdot w^c_{eff} \cdot \left(1 - 0.298 \cdot (w_2/w_1 - 1)^{(2.376 \cdot (1 - 0.191 \cdot (w_3/w_1)^{1.3875}))}\right)$$

$$dl_b = 0.024 \cdot Z_L^b / Z_L^c \cdot (1 - 2 \cdot Z_L^b / Z_L^c \cdot FCB) \cdot w^c_{eff} \cdot \left(1 - 2.587 \cdot (1 - w_1/w_2)^{(2.603 \cdot (1 + 0.2484 \cdot (w_3/w_2)^{1.678}))}\right)$$

with

$$BT = 5.091 \cdot \ln(RZ) + 22.22 \cdot RZ \cdot FC + 19.23 \cdot \exp(-7.938 \cdot RZ) - 15.22 \cdot (Z_L^c/Z_0)^2$$

$$DL = 0.01844 \cdot RZ \cdot (1 - 2 \cdot RZ \cdot FC) \cdot w^c_{eff}$$

$$RZ = \sqrt{Z_L^a \cdot Z_L^b} / Z_L^c$$

$$FC = \sqrt{FCA \cdot FCB}$$

$$FCA = \operatorname{atan}\left(\left(0.9941 \cdot h/mm \cdot f/GHz / (Z_L^a/\Omega)\right)^2\right)$$

$$FCB = \operatorname{atan}\left(\left(0.9941 \cdot h/mm \cdot f/GHz / (Z_L^b/\Omega)\right)^2\right)$$

Alternate formulae for the symmetric T-junction

$$2*\pi*f * C / S = BT * 0.186 * (1 + BT) * DL / n_a'^2 / Z_L^c * \frac{w^a_{eff} * \beta^a}{w^c_{eff}}$$

$$n_a' = \sqrt{1 - \operatorname{atan}(\pi * FC * (0.093*(Z_L^a/Z_L^c)^2 + (0.5 - dl_c/w^a_{eff})^2))}$$

$$n_a = n_a' - 0.00027*(w_2/h)^{1.2} * f/GHz$$

$$dl_c = (0.479 - 1.029 * \operatorname{atan}(RZ) * dl_c') * w^a_{eff} * \exp(0.1105*w_3/h) * \exp(0.1181*w_1/h)$$

$$dl_c' = 0.00759 + 0.8294 * \exp(-1.698*\operatorname{atan}(RZ)) + 0.0884 * FC * \operatorname{atan}(RZ) - 0.360*\ln(1.029*\operatorname{atan}(RZ))$$

$$dl_a = 0.0292 * Z_L^a / Z_L^c * (1 - 2 * Z_L^a / Z_L^c * FC) * w^c_{eff} * (1 - \exp(-6.264*w_1/h)) * \exp(0.3136*w_3/h)$$

with

$$BT = (32.309*\ln(RZ) + 44.323*RZ*FC - 12.130*\exp(-1.169*RZ) - 98.448*(Z_L^c/Z_0)^2)$$

$$DL = 0.0399*RZ*(1-2*RZ*FC) * w^c_{eff}$$

$$RZ = Z_L^a / Z_L^c$$

$$FC = \operatorname{atan} ((3.167 * h/mm * f/GHz / (Z_L^a/\Omega))^2)$$

Alternate formulae for the general T-junction

$$2*\pi*f * C / S = BT * 0.202 * (1 + BT) * DL / n_a' / n_b' / Z_L^c * \frac{\beta^a + \beta^b}{2} * \frac{w^a_{eff} + w^b_{eff}}{2*w^c_{eff}}$$

$$n_a' = \sqrt{1 - \text{atan}(\pi * FCA * (0.112*(Z_L^a/Z_L^c)^2 + (0.5 - dl_c/w^a_{eff})^2))}$$

$$n_a = n_a' - 0.00063*(w_2/h)^{1.02} * f/GHz$$

$$n_b' = \sqrt{1 - \text{atan}(\pi * FCB * (0.112*(Z_L^b/Z_L^c)^2 + (0.5 - dl_c/w^b_{eff})^2))}$$

$$n_b = n_b' - 0.00063*(w_2/h)^{1.02} * f/GHz * (w_1/w_2)^{2.3}$$

$$dl_c = (0.477 - 0.9985 * \text{atan}(RZ) * dl_c') * \frac{w^a_{eff} + w^b_{eff}}{2} * \exp(0.0360*w_3/h) * \exp(0.1475*w_1/h)$$

$$dl_c' = 0.00567 + 0.8159 * \exp(-1.696*\text{atan}(RZ)) + 0.0908 * FC * \text{atan}(RZ) - 0.342*\ln(0.9985*\text{atan}(RZ))$$

$$dl_a = 0.0185 * Z_L^a / Z_L^c * (1 - 2 * Z_L^a / Z_L^c * FCA) * w^c_{eff} * (1 - \exp(-10.15*w_1/h)) * \exp(0.4830*w_3/h)$$

$$dl_b = 0.0185 * Z_L^b / Z_L^c * (1 - 2 * Z_L^b / Z_L^c * FCB) * w^c_{eff} * (1 - \exp(-10.15*w_2/h)) * \exp(0.4830*w_3/h)$$

with

$$BT = (26.021*\ln(RZ) + 54.639*RZ*FC - 6.856*\exp(-1.333*RZ) - 98.143*(Z_L^c/Z_0)^2)$$

$$DL = 0.0401*RZ*(1-2*RZ*FC) * w^c_{eff}$$

$$RZ = \sqrt{Z_L^a * Z_L^b} / Z_L^c$$

$$FC = \sqrt{FCA * FCB}$$

$$FCA = \text{atan} ((2.711 * h/mm * f/GHz / (Z_L^a/\Omega))^2)$$

$$FCB = \text{atan} ((2.711 * h/mm * f/GHz / (Z_L^b/\Omega))^2)$$

where Z_L^s, Z_L^a and Z_L^b are the characteristic impedances lines, and β^a and β^b are the propagation constants, w^s_{eff}, w^a_{eff} and w^b_{eff} are the effective widths of the feed lines. Note that ports 1, 2 and 3 are related to the feed lines a, b and c.

Transformer ratios N1, N2, N3, N4, M1, M2, M3

$N1 = N_{dyn}(w_1)$

$N2 = N_{dyn}(w_2)$

$N3 = N_{dyn}(w_3)$

$N4 = 0.001$

$M1 = -N_{dyn}(w_1)$

$M2 = -N_{dyn}(w_2)$

$M3 = -N_{dyn}(w_3)$

$$N_{dyn}(w_i) = \begin{cases} N(w_i) * \cos^{f_1}\left(0.5*\pi*(f-f_0)/f_0 \right) * \exp\left(-f_1*(f-f_0)/f_0 \right) & f<f_0 \\ N(w_i) & f>f_0 \end{cases}$$

$$N(w_i) = 4.8/\pi * \left(\cos\left(\frac{\pi}{2w_s} * (w_s - w_{eff}(w_i)) \right) - \cos\left(\frac{\pi}{2w_s} * (w_s + w_{eff}(w_i)) \right) \right)$$

$$w_{eff}(w_i) = w^k_{eff} = Z_0 * h / Z_L^k(w_i) / \sqrt{\varepsilon_{eff}^k(w_i)}$$

$$f_0 = f_c * 1.4 * \left(1 + \exp(-0.0638 * W_s/h * H/h) \right) * (1 - 2.33 * \exp(-0.33 * W_s/h))$$

$$f_1 = 2$$

$$\varepsilon_{eff}(LSM_0) = \varepsilon_{stat}\left(1 - \left(\frac{f_c}{f}\right)^2\right)$$

with $$f_c = \frac{c_0}{2W_s \cdot \sqrt{\varepsilon_{stat}}}$$

and $$\varepsilon_{stat} = \frac{\varepsilon_r (H+h)}{\varepsilon_r H + h},$$

$$Z_L(LSM_0) = \frac{H+h}{W_s} \cdot \frac{Z_0}{\sqrt{\varepsilon_{stat}}} \cdot \frac{1}{\sqrt{1 - (f_c/f)^2}}$$

$(Z_0 = 120\pi\Omega,\ c_0 = 2.9979\ 10^8\ m/s)$

Transmission lines LSM_{03}, LMS'_{03}

In the above formulae the LSM_{03}, LSM'_{03} characteristics should be derived with the package length x_p instead of the width W_s.

Range of Model Validity

The validity range of the T-junction models for a GaAs dielectric constant = 12.9, is:

quasi-static model:	50μm	≤ h	≤	200μm	
	0.1	≤ w/h	≤	2	
	0.25	≤ w2/w1	≤	4	(w2/h max = 2)
	1	≤ w3/w1	≤	5	(w3/h max = 2)
	6.4	≤ Ws/h	≤	32	
	5	≤ H/h	≤	20	
dynamic model:	0.1	≤ w/h	≤	2	
	0.25	≤ w2/w1	≤	4	(w2/h max = 2)
	1	≤ w3/w1	≤	4	(w3/h max = 2)
	6.4	≤ Ws/h	≤	32	
	5	≤ H/h	≤	20	

where the quasi-static model is described by Fig. 13.3 and the dynamic model by Fig. 13.2 between the reference planes RP1, RP2 and RP3. The quasi-static model is valid for the range 0 ≤ f*h ≤ 3 GHz mm. The dynamic model using the alternate expressions in the quasi-static part of the model is valid for the range 0 ≤ f*h ≤ 12 GHz.

13.6. REFERENCES AND TABLES

1. Hammerstad, E.O., IEEE MTT-S Digest, Los Angeles, 1981, 54-55.

Table 1

W1	W2	W3	S11 Fmean	S11 Fmax	S11 Fmaxr	S13	S13	S13	S33 Fmean	S33 Fmax	S33 Fmaxr
.20	.025	.200	.014	.004	.026	.010	.007	.014	.022	.022	.032
.20	.050	.200	.011	.003	.016	.014	.009	.017	.033	.026	.043
.20	.100	.200	.015	.004	.017	.013	.011	.019	.037	.025	.050
.20	.160	.200	.005	.003	.009	.007	.010	.015	.023	.018	.044
.20	.200	.200	.008	.006	.020	.018	.033	.049	.046	.043	.120
.20	.250	.200	.010	.006	.015	.011	.009	.013	.042	.014	.049
.20	.400	.200	.028	.019	.042	.012	.016	.023	.158	.033	.236
.10	.013	.100	.031	.007	.037	.003	.002	.004	.004	.004	.006
.10	.025	.100	.031	.009	.041	.002	.002	.003	.005	.004	.007
.10	.050	.100	.016	.005	.018	.005	.004	.006	.018	.009	.019
.10	.080	.100	.018	.006	.019	.002	.002	.003	.010	.005	.012
.10	.100	.100	.011	.004	.011	.002	.002	.003	.005	.004	.011
.10	.125	.100	.011	.005	.013	.002	.003	.005	.009	.003	.011
.10	.200	.100	.007	.005	.012	.002	.003	.004	.030	.006	.042
.10	.400	.100	.023	.024	.043	.025	.030	.043	.134	.021	.152
.05	.013	.050	.035	.011	.044	.008	.006	.010	.019	.010	.019
.05	.025	.050	.037	.014	.049	.010	.009	.014	.029	.014	.032
.05	.040	.050	.026	.010	.031	.007	.007	.010	.030	.012	.032
.05	.050	.050	.031	.016	.047	.009	.010	.016	.023	.012	.037
.05	.063	.050	.027	.013	.037	.008	.009	.013	.021	.009	.030
.05	.100	.050	.024	.013	.033	.009	.010	.014	.031	.008	.039
.05	.200	.050	.021	.012	.024	.000	.001	.001	.133	.008	.306
.05	.400	.050	.023	.016	.026	.033	.040	.058	.101	.031	.141
.02	.010	.020	.033	.014	.049	.008	.009	.014	.018	.012	.029
.02	.016	.020	.020	.008	.024	.005	.005	.008	.008	.004	.011
.02	.020	.020	.017	.008	.024	.004	.003	.005	.009	.006	.018
.02	.025	.020	.017	.008	.022	.004	.004	.007	.021	.007	.025
.02	.040	.020	.016	.008	.022	.005	.005	.007	.024	.007	.028
.02	.080	.020	.019	.009	.020	.004	.003	.004	.114	.012	.118
.02	.160	.020	.007	.004	.008	.004	.005	.007	.090	.011	.108
.01	.010	.010	.027	.014	.041	.014	.014	.021	.036	.019	.058
.01	.013	.010	.031	.015	.043	.015	.015	.022	.048	.018	.059
.01	.020	.010	.032	.019	.052	.016	.018	.026	.054	.018	.071
.01	.040	.010	.087	.065	.152	.018	.020	.028	.108	.018	.126

			S12 Fmean	S12 Fmax	S12 Fmaxr	S23	S23	S23	S22 Fmean	S22 Fmax	S22 Fmaxr
.20	.025	.200	.003	.003	.003	.010	.007	.014	.014	.004	.026
.20	.050	.200	.005	.005	.006	.014	.009	.017	.011	.003	.016
.20	.100	.200	.007	.006	.008	.013	.011	.019	.015	.004	.017
.20	.160	.200	.003	.003	.005	.007	.010	.015	.005	.003	.009
.20	.200	.200	.004	.004	.006	.018	.033	.049	.008	.006	.020
.20	.250	.200	.007	.008	.012	.011	.009	.013	.010	.006	.015
.20	.400	.200	.019	.024	.044	.012	.016	.023	.028	.019	.042
.10	.013	.100	.008	.008	.010	.003	.002	.004	.031	.007	.037
.10	.025	.100	.010	.011	.014	.002	.002	.003	.031	.009	.041
.10	.050	.100	.007	.006	.008	.005	.004	.006	.016	.005	.018
.10	.080	.100	.009	.008	.011	.002	.002	.003	.018	.006	.019
.10	.100	.100	.007	.006	.009	.002	.002	.003	.011	.004	.011
.10	.125	.100	.007	.005	.008	.002	.003	.005	.011	.005	.013
.10	.200	.100	.007	.005	.009	.002	.003	.004	.007	.005	.012
.10	.400	.100	.021	.014	.031	.025	.030	.043	.023	.024	.043
.05	.013	.050	.011	.011	.015	.008	.006	.010	.035	.011	.044
.05	.025	.050	.014	.013	.019	.010	.009	.014	.037	.014	.049
.05	.040	.050	.012	.010	.014	.007	.007	.010	.026	.010	.031
.05	.050	.050	.013	.014	.021	.009	.010	.016	.031	.016	.047
.05	.063	.050	.013	.012	.019	.008	.009	.013	.027	.013	.037
.05	.100	.050	.013	.011	.019	.009	.010	.014	.024	.013	.033
.05	.200	.050	.024	.014	.028	.000	.001	.001	.021	.012	.024
.05	.400	.050	.047	.023	.059	.033	.040	.058	.023	.016	.026

.02	.010	.020	.013	.015	.021	.008	.009	.014	.033	.014	.049
.02	.016	.020	.011	.009	.014	.005	.005	.008	.020	.008	.024
.02	.020	.020	.009	.010	.015	.004	.003	.005	.017	.008	.024
.02	.025	.020	.011	.010	.016	.004	.004	.007	.017	.008	.022
.02	.040	.020	.012	.011	.018	.005	.005	.007	.016	.008	.022
.02	.080	.020	.019	.012	.023	.004	.003	.004	.019	.009	.020
.02	.160	.020	.021	.017	.036	.004	.005	.007	.007	.004	.008
.01	.010	.010	.010	.011	.017	.014	.014	.021	.027	.014	.041
.01	.013	.010	.013	.013	.020	.015	.015	.022	.031	.015	.043
.01	.020	.010	.015	.016	.026	.016	.018	.026	.032	.019	.052
.01	.040	.010	.058	.064	.117	.018	.020	.028	.087	.065	.152

Table 2

W1	W2	W3	S11			S13			S33		
			Fmean,	Fmax,	Fmaxr				Fmean,	Fmax,	Fmaxr
.20	.025	.200	.023	.004	.025	.006	.004	.007	.009	.010	.015
.20	.025	.300	.000	.000	.000	.000	.000	.000	.000	.000	.000
.20	.050	.200	.021	.005	.023	.010	.008	.013	.013	.010	.017
.20	.050	.300	.030	.011	.039	.006	.006	.013	.016	.015	.023
.20	.100	.200	.024	.008	.031	.016	.013	.022	.032	.019	.039
.20	.100	.300	.020	.008	.026	.008	.008	.015	.029	.024	.043
.20	.200	.200	.158	.065	.168	.029	.021	.032	.110	.042	.130
.20	.200	.300	.027	.018	.045	.018	.017	.029	.030	.023	.055
.20	.250	.200	.033	.019	.054	.020	.022	.033	.042	.019	.068
.20	.250	.300	.028	.019	.046	.018	.020	.032	.034	.021	.060
.10	.013	.100	.045	.012	.060	.005	.004	.008	.021	.021	.035
.10	.025	.100	.040	.013	.056	.003	.002	.003	.016	.014	.025
.10	.025	.150	.042	.015	.053	.006	.005	.009	.011	.012	.019
.10	.050	.100	.021	.006	.023	.008	.007	.011	.019	.010	.022
.10	.050	.150	.017	.006	.017	.004	.004	.007	.007	.005	.010
.10	.050	.200	.020	.009	.023	.003	.002	.004	.013	.010	.018
.10	.080	.100	.014	.006	.018	.007	.007	.010	.006	.004	.010
.10	.080	.150	.015	.007	.021	.006	.006	.010	.008	.005	.011
.10	.080	.200	.017	.008	.020	.005	.005	.009	.011	.008	.017
.10	.100	.100	.007	.003	.009	.011	.010	.015	.011	.005	.016
.10	.100	.150	.008	.005	.014	.012	.009	.014	.013	.006	.017
.10	.100	.200	.015	.009	.021	.009	.007	.012	.014	.009	.021
.10	.125	.100	.006	.003	.009	.012	.011	.017	.014	.005	.018
.10	.125	.150	.007	.004	.010	.012	.010	.015	.010	.005	.015
.10	.125	.200	.009	.006	.013	.011	.009	.016	.015	.009	.023
.10	.200	.100	.023	.017	.040	.023	.023	.033	.062	.013	.078
.10	.200	.150	.022	.018	.040	.025	.022	.033	.030	.008	.038
.10	.200	.200	.025	.022	.044	.023	.018	.030	.023	.009	.034
.05	.013	.050	.043	.014	.057	.007	.005	.009	.029	.019	.038
.05	.013	.083	.044	.016	.054	.009	.007	.012	.019	.017	.031
.05	.013	.250	.037	.023	.047	.030	.014	.036	.012	.012	.018
.05	.025	.050	.040	.015	.054	.007	.005	.008	.035	.019	.044
.05	.025	.083	.038	.015	.046	.008	.005	.009	.021	.015	.031
.05	.025	.250	.034	.022	.044	.016	.009	.020	.009	.007	.011
.05	.040	.050	.026	.010	.030	.005	.004	.006	.033	.014	.038
.05	.040	.083	.016	.007	.020	.002	.002	.003	.011	.008	.019
.05	.040	.150	.026	.014	.031	.007	.005	.009	.005	.003	.006
.05	.040	.250	.025	.015	.028	.009	.007	.014	.008	.008	.013
.05	.050	.050	.028	.014	.041	.002	.003	.004	.025	.013	.039
.05	.050	.083	.032	.014	.036	.003	.003	.004	.023	.012	.032
.05	.050	.150	.024	.013	.027	.005	.004	.008	.015	.011	.023
.05	.050	.250	.014	.013	.023	.009	.006	.012	.012	.012	.023
.05	.063	.050	.021	.009	.025	.003	.003	.004	.016	.006	.021
.05	.063	.083	.017	.008	.021	.004	.004	.006	.014	.008	.021
.05	.063	.150	.016	.009	.020	.005	.004	.007	.010	.005	.012
.05	.063	.250	.019	.013	.024	.006	.004	.008	.010	.006	.011
.05	.100	.083	.006	.005	.012	.009	.009	.014	.017	.005	.019
.05	.100	.150	.010	.008	.015	.009	.006	.011	.013	.006	.017
.05	.200	.083	.024	.026	.049	.037	.039	.058	.085	.007	.110
.05	.200	.150	.021	.020	.035	.023	.020	.034	.027	.005	.034
.05	.200	.250	.016	.017	.027	.012	.009	.017	.027	.012	.045

.02	.010	.020	.036	.016	.054	.004	.004	.006	.023	.015	.036
.02	.010	.040	.058	.021	.063	.011	.008	.014	.023	.017	.036
.02	.016	.020	.021	.008	.024	.002	.002	.003	.010	.006	.015
.02	.016	.040	.036	.014	.039	.008	.007	.012	.015	.009	.021
.02	.016	.080	.028	.014	.033	.007	.004	.007	.016	.009	.018
.02	.020	.020	.015	.008	.024	.009	.008	.011	.012	.007	.020
.02	.020	.040	.030	.024	.063	.013	.017	.029	.008	.004	.010
.02	.020	.080	.013	.010	.023	.013	.012	.023	.015	.008	.018
.02	.025	.020	.015	.007	.019	.005	.006	.008	.024	.009	.029
.02	.025	.040	.024	.017	.042	.013	.014	.023	.010	.007	.020
.02	.025	.080	.015	.009	.019	.011	.008	.015	.007	.005	.011
.02	.040	.020	.011	.005	.012	.007	.008	.011	.025	.006	.028
.02	.040	.040	.020	.009	.020	.010	.008	.012	.011	.004	.014
.02	.040	.080	.016	.011	.023	.010	.008	.014	.013	.005	.014
.02	.080	.020	.013	.006	.014	.014	.014	.020	.122	.012	.123
.02	.080	.040	.016	.009	.018	.017	.017	.026	.035	.006	.041
.02	.080	.080	.014	.009	.016	.008	.007	.012	.021	.007	.031
.01	.010	.010	.034	.012	.036	.019	.028	.041	.077	.053	.159
.01	.010	.020	.064	.055	.146	.026	.034	.054	.042	.021	.055
.01	.010	.040	.024	.015	.035	.020	.017	.030	.049	.029	.067
.01	.013	.010	.030	.014	042	.008	.007	.010	.049	.019	.062
.01	.013	.020	.045	.026	.070	.019	.021	.033	.037	.019	.052
.01	.013	.040	.035	.016	.037	.010	.008	.013	.036	.024	.056
.01	.020	.010	.029	.017	.046	.008	.007	.011	.053	.018	.069
.01	.020	.020	.036	.019	.047	.011	.008	.013	.046	.020	.068
.01	.020	.040	.041	.020	.044	.012	.008	.014	.049	.028	.076
.01	.040	.010	.079	.064	.150	.005	.005	.007	.109	.018	.126
.01	.040	.020	.035	.020	.044	.007	.005	.007	.068	.019	.097
.01	.040	.040	.040	.022	.045	.018	.012	.020	.070	.025	.097
.01	.040	.080	.000	.000	.000	.000	.000	.000	.000	.000	.000

			S12			S23			S22		
			Fmean,	Fmax,	Fmaxr				Fmean,	Fmax,	Fmaxr
.20	.025	.200	.006	.009	.011	.006	.004	.007	.023	.004	.025
.20	.025	.300	.000	.000	.000	.000	.000	.000	.000	.000	.000
.20	.050	.200	.006	.009	.011	.010	.008	.013	.021	.005	.023
.20	.050	.300	.003	.004	.005	.022	.017	.029	.071	.008	.162
.20	.100	.200	.010	.010	.014	.016	.013	.022	.024	.008	.031
.20	.100	.300	.004	.004	.005	.024	.019	.031	.037	.005	.038
.20	.200	.200	.030	.023	.035	.047	.035	.050	.099	.030	.101
.20	.200	.300	.012	.013	.019	.022	.023	.034	.054	.013	.073
.20	.250	.200	.019	.020	.031	.020	.022	.033	.033	.019	.054
.20	.250	.300	.019	.020	.030	.019	.024	.034	.034	.013	.058
.10	.013	.100	.003	.003	.004	.005	.004	.008	.045	.012	.060
.10	.025	.100	.003	.003	.004	.003	.002	.003	.040	.013	.056
.10	.025	.150	.004	.004	.005	.007	.004	.007	.070	.009	.076
.10	.050	.100	.007	.007	.010	.008	.007	.011	.021	.006	.023
.10	.050	.150	.003	.004	.006	.011	.010	.015	.018	.003	.020
.10	.050	.200	.003	.004	.005	.016	.015	.024	.046	.005	.084
.10	.080	.100	.004	.005	.007	.007	.007	.010	.014	.006	.018
.10	.080	.150	.005	.005	.006	.011	.010	.014	.018	.005	.024
.10	.080	.200	.004	.005	.007	.014	.014	.020	.034	.006	.054
.10	.100	.100	.005	.007	.010	.011	.010	.015	.007	.003	.009
.10	.100	.150	.006	.008	.011	.013	.012	.017	.011	.003	.014
.10	.100	.200	.006	.009	.012	.016	.015	.022	.031	.007	.051
.10	.125	.100	.008	.008	.013	.012	.011	.017	.006	.003	.009
.10	.125	.150	.007	.009	.014	.013	.012	.018	.010	.004	.016
.10	.125	.200	.009	.011	.016	.015	.014	.019	.020	.005	.032
.10	.200	.100	.016	.015	.026	.023	.023	.033	.023	.017	.040
.10	.200	.150	.017	.018	.030	.021	.020	.028	.015	.009	.029
.10	.200	.200	.019	.021	.033	.019	.019	.026	.020	.008	.034

.05	.013	.050	.006	.005	.006	.007	.005	.009	.043	.014	.057
.05	.013	.083	.005	.004	.005	.004	.003	.004	.071	.012	.086
.05	.013	.250	.010	.009	.012	.017	.014	.024	.085	.020	.122
.05	.025	.050	.008	.006	.008	.007	.005	.008	.040	.015	.054
.05	.025	.083	.003	.003	.004	.005	.004	.005	.062	.013	.072
.05	.025	.250	.014	.011	.014	.014	.012	.018	.106	.020	.161
.05	.040	.050	.009	.006	.009	.005	.004	.006	.026	.010	.030
.05	.040	.083	.003	.003	.005	.003	.002	.004	.027	.006	.030
.05	.040	.150	.007	.008	.011	.011	.010	.015	.184	.010	.247
.05	.040	.250	.015	.017	.023	.014	.012	.018	.104	.014	.149
.05	.050	.050	.003	.003	.005	.002	.003	.004	.028	.014	.041
.05	.050	.083	.004	.004	.005	.001	.001	.001	.043	.012	.052
.05	.050	.150	.003	.003	.004	.005	.005	.008	.100	.010	.136
.05	.050	.250	.013	.016	.023	.007	.006	.009	.071	.011	.113
.05	.063	.050	.002	.002	.003	.003	.003	.004	.021	.009	.025
.05	.063	.083	.003	.003	.004	.004	.004	.005	.028	.007	.030
.05	.063	.150	.006	.007	.010	.008	.007	.010	.056	.007	.063
.05	.063	.250	.016	.017	.025	.011	.009	.013	.087	.007	.130
.05	.100	.050	.004	.003	.005	.007	.008	.012	.011	.005	.013
.05	.100	.083	.007	.007	.011	.007	.008	.011	.018	.006	.019
.05	.100	.150	.010	.012	.018	.009	.008	.011	.035	.008	.048
.05	.200	.083	.024	.022	.042	.027	.031	.042	.016	.007	.018
.05	.200	.150	.023	.022	.039	.020	.022	.028	.010	.004	.014
.05	.200	.250	.021	.021	.036	.010	.013	.016	.046	.008	.066
.02	.010	.020	.006	.006	.009	.004	.004	.006	.036	.016	.054
.02	.010	.040	.008	.006	.008	.012	.010	.015	.074	.017	.089
.02	.016	.020	.003	.004	.006	.002	.002	.003	.021	.008	.024
.02	.016	.040	.003	.002	.003	.007	.005	.008	.044	.011	.049
.02	.016	.080	.011	.011	.015	.009	.006	.009	.105	.009	.118
.02	.020	.020	.004	.006	.010	.009	.008	.011	.015	.008	.024
.02	.020	.040	.006	.009	.013	.009	.011	.016	.024	.006	.026
.02	.020	.080	.010	.012	.018	.004	.006	.008	.067	.007	.075
.02	.025	.020	.006	.004	.007	.005	.006	.008	.015	.007	.019
.02	.025	.040	.005	.005	.007	.008	.007	.010	.018	.005	.020
.02	.025	.080	.011	.011	.016	.008	.008	.011	.038	.005	.049
.02	.040	.020	.005	.004	.006	.007	.008	.011	.011	.005	.012
.02	.040	.040	.005	.003	.005	.010	.010	.013	.023	.007	.024
.02	.040	.080	.010	.009	.014	.008	.008	.011	.034	.006	.040
.02	.080	.020	.011	.006	.011	.014	.014	.020	.013	.006	.014
.02	.080	.040	.008	.006	.011	.013	.015	.020	.012	.005	.014
.02	.080	.080	.012	.009	.015	.012	.014	.018	.018	.006	.027
.01	.010	.010	.012	.014	.021	.019	.028	.041	.034	.012	.036
.01	.010	.020	.016	.021	.031	.022	.025	.036	.064	.019	.078
.01	.010	.040	.007	.006	.008	.010	.011	.015	.135	.020	.145
.01	.013	.010	.008	.006	.009	.008	.007	.010	.030	.014	.042
.01	.013	.020	.004	.005	.008	.012	.008	.012	.060	.018	.068
.01	.013	.040	.009	.007	.010	.013	.011	.015	.077	.014	.094
.01	.020	.010	.009	.007	.012	.008	.007	.011	.029	.017	.046
.01	.020	.020	.005	.004	.006	.012	.010	.014	.051	.019	.065
.01	.020	.040	.010	.007	.010	.016	.014	.019	.079	.018	.097
.01	.040	.010	.047	.062	.108	.005	.005	.007	.079	.064	.150
.01	.040	.020	.008	.005	.009	.009	.007	.010	.042	.020	.056
.01	.040	.040	.008	.006	.009	.012	.010	.013	.058	.016	.063

Table 3

MICROSTRIP T-JUNCTION GEOMETRY

W1	W2	W3	S11 Fmean	S11 Fmax	S11 Fmaxr	S13 Fmean	S13 Fmax	S13 Fmaxr	S33 Fmean	S33 Fmax	S33 Fmaxr
.20	.100	.200	.022	.008	.036	.004	.003	.005	.015	.013	.025
.20	.200	.200	.013	.005	.016	.037	.034	.053	.064	.053	.128
.20	.250	.200	.026	.018	.055	.071	.069	.103	.138	.080	.233
.10	.025	.100	.023	.008	.044	.014	.012	.023	.027	.025	.038
.10	.050	.100	.032	.021	.094	.011	.011	.018	.023	.019	.039
.10	.100	.100	.010	.006	.019	.004	.007	.011	.031	.033	.074
.05	.013	.050	.027	.009	.038	.007	.008	.014	.017	.016	.028
.05	.025	.050	.021	.010	.034	.005	.005	.008	.012	.009	.019
.05	.050	.050	.025	.012	.038	.009	.009	.013	.026	.011	.029
.05	.100	.050	.044	.047	.136	.011	.022	.033	.034	.019	.061
.02	.010	.020	.034	.013	.044	.011	.017	.026	.020	.013	.030
.02	.020	.020	.021	.016	.052	.009	.011	.017	.039	.025	.066
.02	.040	.020	.016	.012	.032	.009	.013	.020	.056	.024	.087
.02	.080	.020	.037	.040	.095	.015	.019	.027	.133	.034	.185
.01	.010	.010	.027	.015	.045	.020	.018	.028	.048	.023	.066
.01	.020	.010	.028	.017	.045	.021	.017	.025	.063	.028	.110
.01	.040	.010	.039	.033	.077	.009	.009	.013	.085	.019	.133

W1	W2	W3	S12 Fmean	S12 Fmax	S12 Fmaxr	S23 Fmean	S23 Fmax	S23 Fmaxr	S22 Fmean	S22 Fmax	S22 Fmaxr
.20	.100	.200	.004	.006	.008	.004	.003	.005	.022	.008	.036
.20	.200	.200	.016	.014	.019	.037	.034	.053	.013	.005	.016
.20	.250	.200	.026	.021	.031	.071	.069	.103	.026	.018	.055
.10	.025	.100	.007	.008	.010	.014	.012	.023	.023	.008	.044
.10	.050	.100	.005	.005	.007	.011	.011	.018	.032	.021	.094
.10	.100	.100	.012	.023	.032	.004	.007	.011	.010	.006	.019
.05	.013	.050	.008	.010	.012	.007	.008	.014	.027	.009	.038
.05	.025	.050	.007	.009	.012	.005	.005	.008	.021	.010	.034
.05	.050	.050	.012	.012	.018	.009	.009	.013	.025	.012	.038
.05	.100	.050	.016	.020	.031	.011	.022	.033	.044	.047	.136
.02	.010	.020	.016	.016	.022	.011	.017	.026	.034	.013	.044
.02	.020	.020	.013	.021	.030	.009	.011	.017	.021	.016	.052
.02	.040	.020	.011	.015	.023	.009	.013	.020	.016	.012	.032
.02	.080	.020	.013	.013	.023	.015	.019	.027	.037	.040	.095
.01	.010	.010	.009	.009	.013	.020	.018	.028	.027	.015	.045
.01	.020	.010	.007	.007	.011	.021	.017	.025	.028	.017	.045
.01	.040	.010	.017	.027	.048	.009	.009	.013	.039	.033	.077

Table 4

W1	W2	W3	S11 Fmean	S11 Fmax	S11 Fmaxr	S13	S13	S13	S33 Fmean	S33 Fmax	S33 Fmaxr
.20	.100	.200	.030	.012	.056	.011	.014	.024	.033	.041	.071
.20	.100	.300	.045	.025	.089	.017	.017	.033	.020	.016	.026
.20	.200	.200	.031	.012	.042	.039	.040	.063	.091	.069	.160
.20	.200	.300	.065	.031	.096	.034	.032	.054	.068	.065	.130
.20	.250	.200	.030	.013	.040	.059	.060	.092	.115	.072	.187
.20	.250	.300	.029	.016	.046	.053	.048	.081	.097	.081	.182
.10	.025	.100	.028	.008	.037	.009	.013	.025	.026	.034	.052
.10	.025	.150	.051	.024	.097	.016	.023	.048	.017	.020	.029
.10	.025	.200	.080	.050	.158	.041	.043	.099	.033	.036	.053
.10	.050	.100	.035	.023	.104	.006	.006	.009	.025	.038	.068
.10	.050	.150	.043	.033	.119	.007	.005	.010	.023	.021	.039
.10	.050	.200	.067	.054	.157	.013	.017	.037	.034	.036	.062
.10	.100	.100	.026	.012	.043	.008	.013	.021	.055	.054	.118
.10	.100	.150	.044	.019	.062	.007	.008	.015	.043	.050	.098
.10	.100	.200	.052	.024	.068	.010	.010	.018	.038	.044	.077
.10	.200	.150	.028	.021	.054	.012	.010	.016	.039	.025	.075
.10	.200	.200	.021	.015	.036	.011	.008	.013	.039	.033	.087
.05	.013	.050	.025	.009	.038	.010	.014	.025	.029	.029	.050
.05	.013	.083	.032	.013	.048	.014	.017	.033	.017	.021	.034
.05	.025	.050	.023	.010	.035	.008	.010	.016	.030	.025	.048
.05	.025	.083	.031	.013	.041	.007	.010	.017	.014	.015	.026
.05	.050	.050	.026	.012	.036	.009	.009	.015	.045	.025	.060
.05	.050	.083	.041	.018	.050	.006	.007	.012	.029	.019	.040
.05	.050	.150	.046	.027	.063	.010	.010	.019	.038	.035	.064
.05	.100	.050	.026	.019	.054	.009	.011	.016	.029	.015	.048
.05	.100	.083	.025	.019	.051	.010	.012	.019	.029	.029	.077
.05	.100	.150	.026	.025	.059	.011	.014	.025	.036	.043	.088
.05	.200	.083	.039	.038	.079	.019	.029	.044	.120	.030	.159
.05	.200	.150	.036	.034	.066	.018	.022	.037	.044	.017	.063
.02	.010	.020	.035	.014	.046	.013	.021	.033	.033	.023	.052
.02	.010	.040	.041	.017	.048	.015	.021	.036	.026	.022	.043
.02	.010	.080	.044	.025	.059	.024	.022	.043	.031	.027	.047
.02	.020	.020	.020	.017	.053	.010	.012	.019	.035	.026	.070
.02	.020	.040	.022	.019	.053	.014	.017	.028	.034	.033	.076
.02	.020	.080	.031	.028	.065	.017	.014	.028	.039	.028	.057
.02	.040	.020	.016	.013	.035	.010	.010	.015	.051	.024	.087
.02	.040	.040	.018	.018	.046	.008	.011	.017	.038	.030	.088
.02	.040	.080	.037	.038	.080	.012	.012	.023	.035	.024	.056
.02	.080	.020	.032	.026	.061	.024	.027	.039	.118	.024	.140
.02	.080	.040	.030	.028	.061	.018	.021	.032	.067	.022	.089
.02	.080	.080	.036	.039	.077	.020	.019	.032	.057	.028	.084
.01	.010	.010	.028	.015	.046	.021	.020	.031	.055	.026	.075
.01	.010	.020	.035	.023	.062	.027	.021	.034	.061	.030	.077
.01	.010	.040	.056	.077	.186	.029	.023	.040	.075	.087	.189
.01	.020	.010	.027	.016	.042	.019	.015	.022	.062	.023	.087
.01	.040	.010	.037	.033	.076	.006	.008	.011	.077	.017	.121

			S12 Fmean	S12 Fmax	S12 Fmaxr	S23	S23	S23	S22 Fmean	S22 Fmax	S22 Fmaxr
.20	.100	.200	.007	.009	.011	.011	.014	.024	.030	.012	.056
.20	.100	.300	.006	.007	.009	.017	.014	.024	.054	.007	.062
.20	.200	.200	.016	.015	.021	.039	.040	.063	.031	.012	.042
.20	.200	.300	.015	.014	.019	.029	.028	.044	.059	.016	.087
.20	.250	.200	.021	.020	.031	.059	.060	.092	.030	.013	.040
.20	.250	.300	.016	.018	.026	.046	.049	.074	.036	.010	.049

.10	.025	.100	.008	.010	.013	.009	.013	.025	.028	.008	.037
.10	.025	.150	.007	.013	.016	.025	.020	.035	.068	.009	.138
.10	.025	.200	.015	.030	.036	.044	.034	.062	.683	.0291	.255
.10	.050	.100	.005	.006	.008	.006	.006	.009	.035	.023	.104
.10	.050	.150	.004	.004	.005	.022	.019	.031	.065	.019	.170
.10	.050	.200	.010	.016	.020	.036	.031	.052	.346	.0283	.891
.10	.100	.100	.016	.024	.033	.008	.013	.021	.026	.012	.043
.10	.100	.150	.014	.021	.028	.013	.013	.020	.051	.020	.109
.10	.100	.200	.010	.012	.015	.019	.023	.034	.110	.021	.222
.10	.200	.150	.020	.026	.039	.015	.018	.026	.024	.013	.044
.10	.200	.200	.017	.022	.032	.013	.019	.028	.027	.007	.030
.05	.013	.050	.006	.008	.010	.010	.014	.025	.025	.009	.038
.05	.013	.083	.007	.012	.015	.013	.014	.024	.058	.012	.115
.05	.025	.050	.006	.006	.008	.008	.010	.016	.023	.010	.035
.05	.025	.083	.006	.007	.009	.011	.012	.019	.030	.008	.045
.05	.050	.050	.014	.015	.020	.009	.009	.015	.026	.012	.036
.05	.050	.083	.013	.013	.018	.012	.012	.018	.032	.010	.052
.05	.050	.150	.013	.013	.018	.027	.030	.046	.169	.012	.426
.05	.100	.050	.019	.024	.036	.009	.011	.016	.026	.019	.054
.05	.100	.083	.019	.024	.035	.011	.015	.021	.021	.008	.032
.05	.100	.150	.014	.015	.021	.019	.033	.048	.056	.011	.125
.05	.200	.083	.023	.020	.034	.017	.029	.039	.035	.032	.083
.05	.200	.150	.021	.019	.031	.012	.016	.021	.035	.017	.069
.02	.010	.020	.012	.012	.017	.013	.021	.033	.035	.014	.046
.02	.010	.040	.014	.016	.021	.010	.018	.028	.049	.013	.074
.02	.010	.080	.023	.031	.041	.012	.011	.018	.377	.021	.913
.02	.020	.020	.010	.017	.025	.010	.012	.019	.020	.017	.053
.02	.020	.040	.010	.020	.028	.010	.016	.024	.067	.024	.116
.02	.020	.080	.016	.031	.042	.015	.015	.022	.183	.021	.261
.02	.040	.020	.008	.013	.020	.010	.010	.015	.016	.013	.035
.02	.040	.040	.008	.013	.020	.011	.020	.029	.023	.015	.060
.02	.040	.080	.015	.023	.034	.016	.024	.034	.086	.018	.202
.02	.080	.020	.015	.017	.029	.024	.027	.039	.032	.026	.061
.02	.080	.040	.012	.015	.025	.012	.015	.020	.016	.008	.023
.02	.080	.080	.013	.017	.027	.017	.027	.037	.029	.010	.059
.01	.010	.010	.007	.007	.010	.021	.020	.031	.028	.015	.046
.01	.010	.020	.011	.009	.013	.026	.021	.032	.063	.019	.076
.01	.010	.040	.022	.047	.066	.033	.065	.095	.150	.026	.205
.01	.020	.010	.007	.006	.010	.019	.015	.022	.027	.016	.042
.01	.040	.010	.017	.027	.048	.006	.008	.011	.037	.033	.076

14. COMPARISON OF THE 3-D ANALYSIS APPROACH USED BY SFPMIC AND THE SOE DISCONTINUITY ANALYSIS PROGRAM

14.1. VERIFICATION OF THE DATABASES USED IN MODELLING WITH THE SOE DISCONTINUITY ANALYSIS

To check the SFPMIC generated S-parameter databases a variety of representative configurations were simulated using the SOE based analysis software (see Appendix). Below are the results of example discontinuities.

Open End

A comparison plot was generated for a microstrip open end simulated on a 100μm thick GaAs substrate situated non-symmetrically in a 1.28 mm square package. As can be seen in Fig. 14.1 the S-parameters generated show good agreement, the deviations found are small.

Gap

For the gap example a microstrip gap discontinuity in a 1 mm square package on the same substrate with a 50μm gap and strip widths 100μm was analysed by the two full-wave analysis programs. The results are shown in Fig. 14.2. Again the comparison shows the deviation is of the same order as the errors achieved in the discontinuity model.

Step

A symmetric microstrip step discontinuity was investigated with the line width changing from 100 microns to 300 microns. The structure is embedded symmetrically into the package of 1 mm x 1 mm. The frequency range of the simulation was again 10 GHz to 100 GHz. The comparison is shown in Fig. 14.3 where the transmission phases are plotted. The agreement between the compared data sets are good.

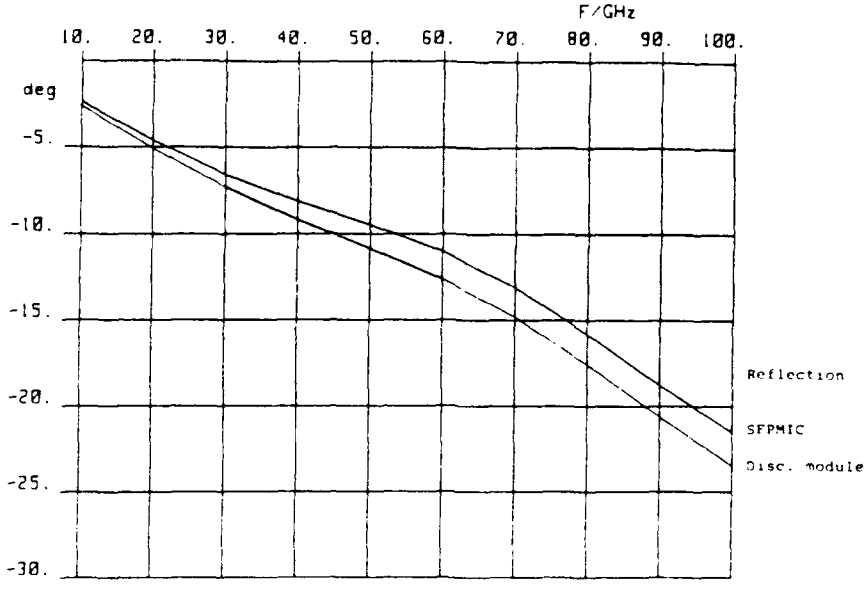


Fig. 14.1: Open end SFPMIC, SOE analysis comparison

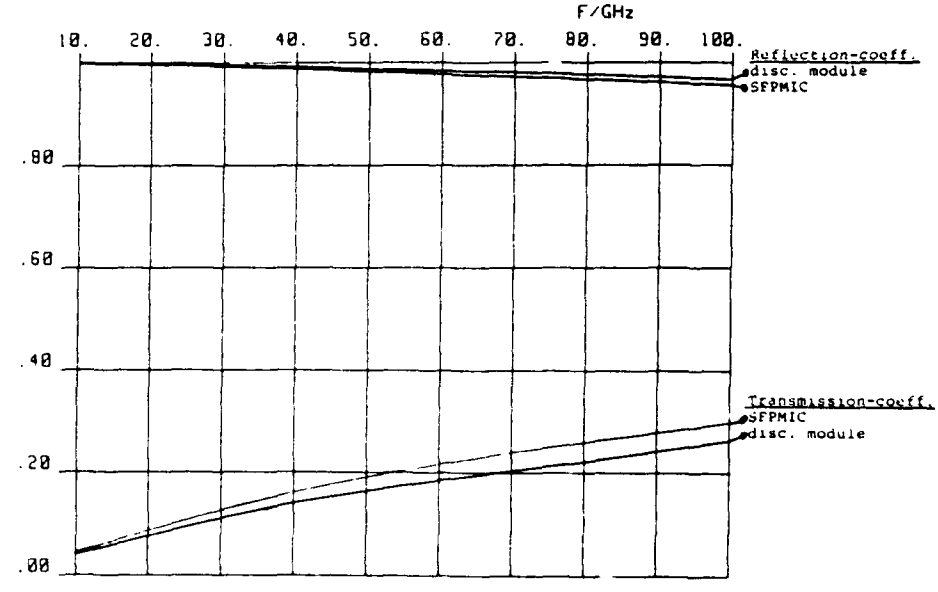


Fig. 14.2: Gap SFPMIC, SOE analysis comparison

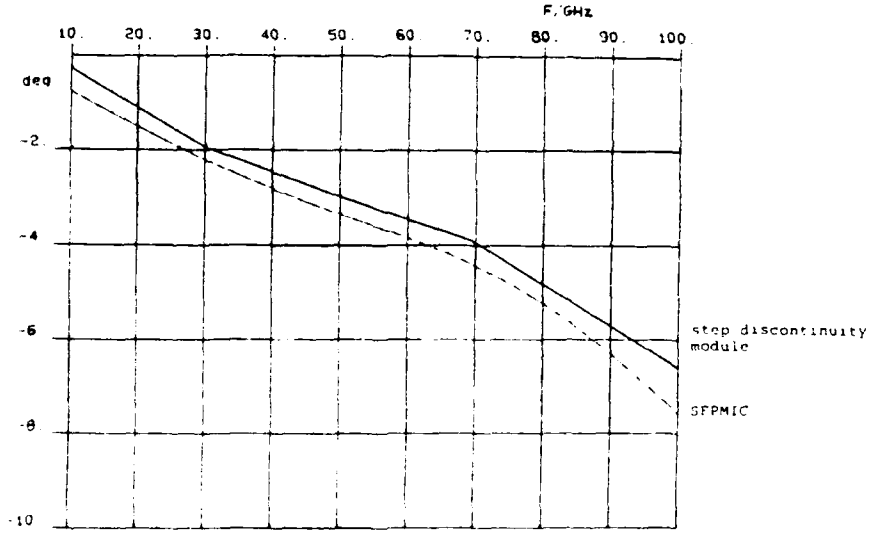


Fig. 14.3: Step SFPMIC, SOE analysis comparison

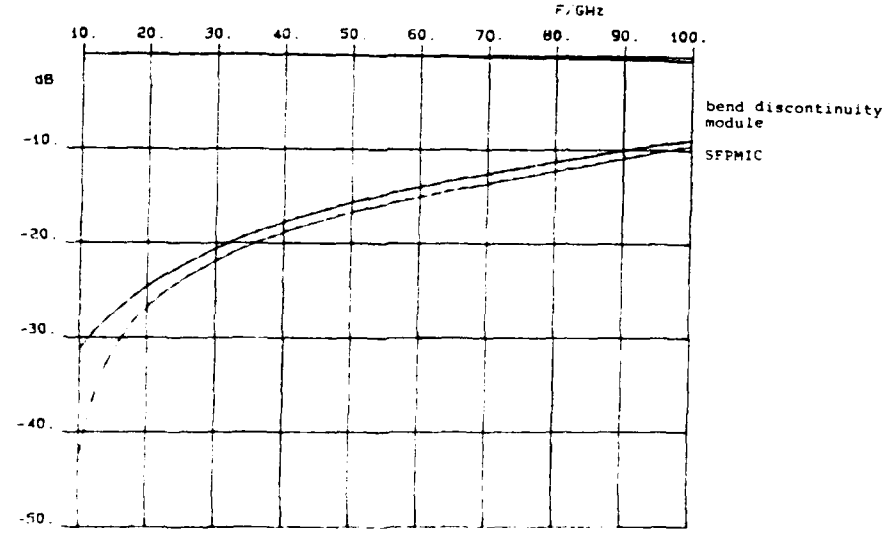


Fig. 14.4: 90° bend SFPMIC, SOE analysis comparison

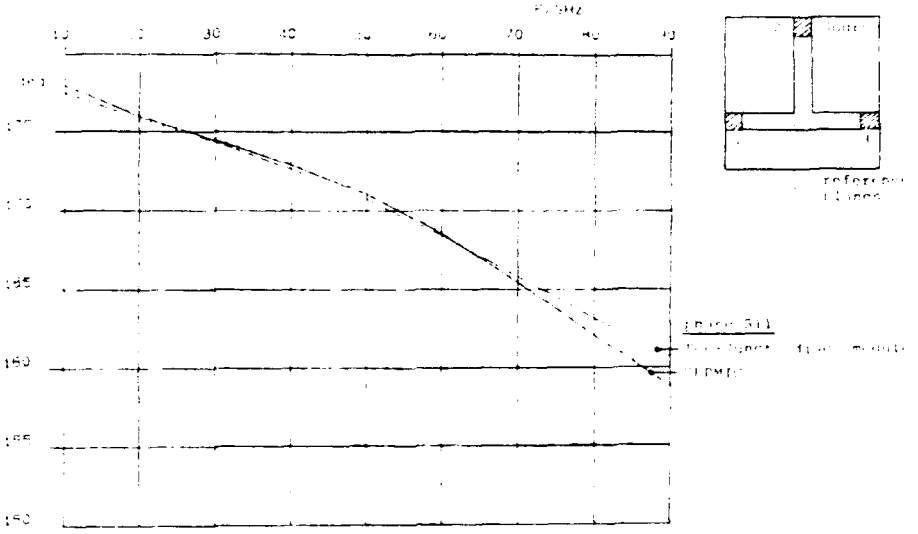


Fig. 14.5: T-junction SFPMIC, SOE analysis comparison for S11

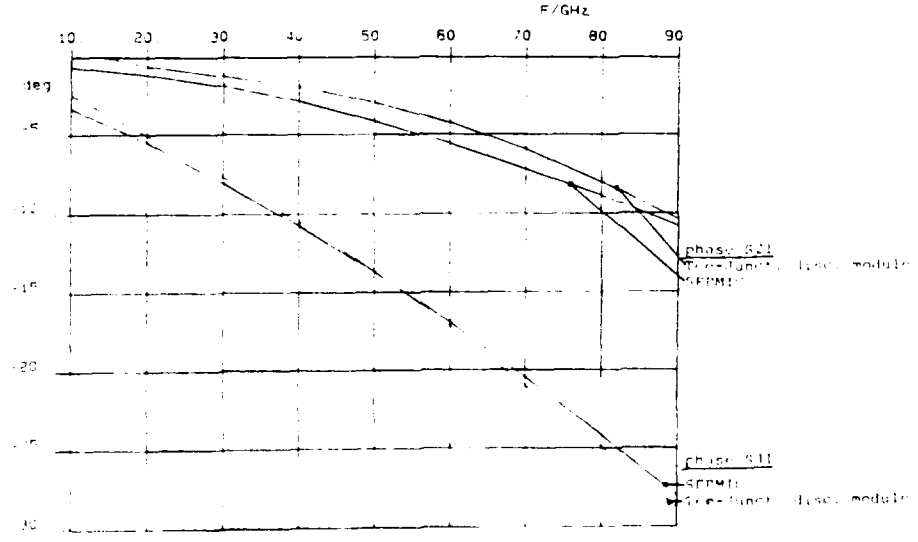


Fig. 14.6: T-junction SFPMIC, SOE analysis comparison for S21 and S31

90° bend

As an example structure, a rectangular microstrip bend of line width 100 microns was simulated for a GaAs-substrate of thickness 100 microns embedded in a package of 1mm x 1mm. The simulated frequency range was 10 GHz to 100 GHz. Comparison results for the two methods are given in Fig. 14.4 where the reflection and the transmission coefficients have been plotted. The results show very good agreement.

T-junction

To compare the two analysis methods a symmetric microstrip T-junction with all line widths of 100 microns was studied. The T-junction was simulated on a GaAs-substrate of thickness 100 microns in a package of 1.4 mm x 1 mm.

The simulated frequency range was 10 GHz to 90 GHz. The phases computed by the different approaches are shown. The reflection phases of port one (first port of the through-line) are plotted in Fig. 14.5. In Fig. 14.6, the transmission phases between port one and the two other ports two and three (second port of the through-line and port of the stub-line) are plotted. Both the computed reflection and transmission phases show good agreement and confirm the validity of the numerical results except for relatively small discrepancies probably due to different convergence behaviour.

14.2. THE STRENGTHS AND WEAKNESSES OF THE SFPMIC PROGRAM AND THE SOE BASED SOFTWARE

The program SFPMIC and the new SOE based software have been written independently. Some of the algorithms and methods which the programs are based on are different. Therefore, the two approaches have different properties in some respects. Investigations have revealed the strong and

weak points of both approaches. This is important in judging the consistency and quality of the data bases generated and used for the development of analytical models.

The main advantage of the discontinuity modules is the application of the SOE (spectral operator expansion) method. The SOE-method allows substantial speed-up in frequency-dependent, broad band, discontinuity computations. Comparisons have shown that the SOE-initialisation takes about 3 times the CPU time taken in the computation of a single frequency point using the technique of SFPMIC. However, this initialisation has to be performed only once per structure. Following frequency points can be computed then within 1/1000 to 1/100 of the CPU time required for the computation of the first frequency point. This advantage of the SOE method becomes apparent if an analysis is required for more than 4 frequency points.

The main advantage of the program SFPMIC lies in the application of the local function method. This method is based on the pre-computation of the feed-strip modes and the consecutive use in their 3-dimensional analysis as a part of the system of expansion functions. This results in a comparatively low number of unknowns for which the system matrix has to be generated. This keeps the amount of CPU time required also reasonably low. However, it is not possible to apply the SOE method to such a system of expansion functions in order to combine the advantages of the two concepts. As to the numerical stability of the discontinuity SOE software as compared tc the SFPMIC program, the following has been found.

Whilst the numerical stability of the new modules in total is better than that of SFPMIC, it was found to be certainly lower in the vicinity of package resonances. This is a consequence of the local function method and the associated relatively low number of expansion functions used in SFPMIC. On the other hand, the system of functions chosen in the SOE approach and the different method of S-parameter extraction applied along with this, provides

improved stability (as originally expected) in the quasi-static and intermediate region below resonances. In the frequency range near resonances, SFPMIC still gives good results when the discontinuity modules suffer from ill-conditioning of the discretised (matrix) operator.

As a conclusion, to cover the full range of frequencies of interest, it is an advantage to have both approaches available for data base generation.

15. CONCLUSION

This work has shown that systematic models can be developed to describe the electrical behaviour of GaAs discontinuities up to 60 GHz. The physics related modelling approach can be used to describe the microstrip and first package LSM mode and their interaction at the discontinuity.

APPENDIX

CONTENTS

		Page No.
1.	SPECTRAL OPERATOR EXPANSION APPROACH TO DISCONTINUITY ANALYSIS	276
	1.1. Theoretical and analytical considerations in the development of the improved full-wave approach	
	1.1.1. Continuous spectrum formulation	
	1.1.2. Discrete spectrum formulation	
	1.2. Brief description of the mathematical algorithm and its associated characteristics	
	1.3. References	
2.	STUDY OF THE CURRENT DENSITY EXPANSION FUNCTIONS	287
	2.1. Current density boundary expansion functions	
	2.2. Inner current density expansion functions	
	2.2.1. Investigation of the piece wise expansion functions	
	2.2.2. Expansion function grid pattern tests	
	2.2.3. Expansion function study of the microstrip open end	
	2.2.4. Expansion function study of the microstrip gap	
	2.3. Source representations for improved 3-D solution quality	
	2.4. Expansion function scheme for the microstrip step	
	2.5. Expansion function scheme for the microstrip 90° bend	
	2.6. Expansion function scheme for the T-junction	
3.	DEVELOPMENT OF THE SOE PROGRAMME	308
	3.1. Structure of the programme	
	3.2. Summary of the 3-D full wave SOE approach	
	3.3. Outline of the system matrix software	
	3.4. Testing of the system matrix generation and the linear system of equations	
	3.5. Treatment of the Greens function spectral expansion	
	3.6. Verification of the tangential electric field density computation	
	3.7. Numerical accuracy of the spectral operator expansion Greens function terms	

Page No.

4. COMPUTATION OF THE SCATTERING PARAMETERS 327

4.1. S-parameter computation method
4.2. Verification of the open end S-parameter computation
4.3. 3-D electromagnetic field solution accuracy requirements for S-parameter evaluation

1. SPECTRAL OPERATOR EXPANSION APPROACH TO DISCONTINUITY ANALYSIS

1.1 THEORETICAL AND ANALYTICAL CONSIDERATIONS IN THE DEVELOPMENT OF THE IMPROVED FULL-WAVE APPROACH

Although the fundamental mathematical problems have been solved in SFPMIC, in order to generate quickly step, bend and T-junction data a more efficient approach was needed. For this reason, theoretical investigations were carried out to apply the SOE (spectral operator expansion) method. This approach should increase the computational speed of 20...50 as compared to SFPMIC. Fig. A1.1 shows the current state for the analysis of step structures.

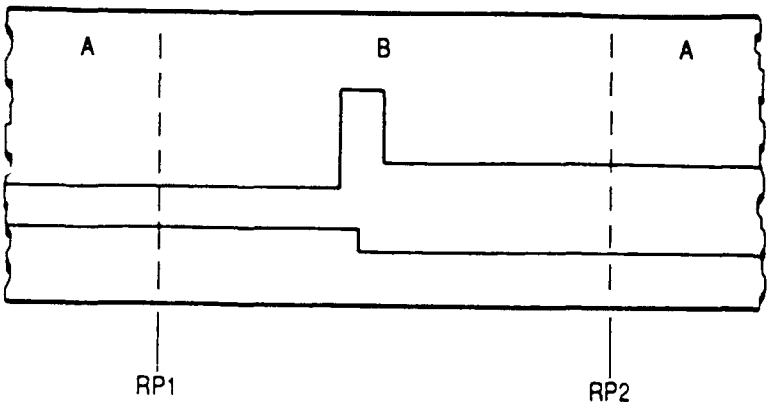


Fig. A1.1: Schematic of T-junction structure

Compared to the present SFPMIC approach, a wider region B around the discontinuity needs to be described by nonmodal expansion functions, i.e. the method no longer contains the precomputed TL elements. The reason for this is that the transmission line elements depend directly on β_i, the modal propagation constants associated with the fundamental modes on the feed strips complicating the usage of the SOE by their direct frequency

dependence. Precomputed transmission line functions are now used only in the A regions where a modal representation of the field is applied. The respective transmission line data can be generated by a transmission line package which is already available and needs only to be modified and updated.

The SOE method as applied to the hybrid-mode problem of multiply coupled-MIC transmission lines provides the possibility of enhancing the computational speed and accuracy of 3D-discontinuity problems. Application of the SOE, however, requires that the expansion functions in a wider region near the discontinuity of interest do not depend on the operating frequency thus forbidding the use of precomputed transmission line distributions. This dictates that the discontinuity region (Figure A1.1) has to be restricted in size as much as possible in order not to end up with a very high number of expansion functions. The consequence is that the modal wave amplitudes cannot be extracted from the field in region B, but only from the modal solution obtained for region A. In addition, the source formulation has to be placed into region A and has to be chosen in such a way that it does not introduce a disturbance of the boundary conditions required to be satisfied by each transmission line mode. Such a disturbance is a disadvantage of the present SFPMIC approach in which a sufficiently long transmission line section has to be placed between the planar sources (impressed current density distributions) and the discontinuity region. The only way to avoid such disturbances, but nevertheless to obtain a source formulated solution, is to use precomputed modes coming from infinity to excite tne structure of interest. The price paid for such use of source functions (having infinite support) is the high testing time. As a result one of the main requirements was to study the possibility of, and develop, the mathematical methods which form a best compromise between or satisfy all of the aspects mentioned above. Two possible methods were developed and studied, one of which was in terms of a discrete and the other in terms of a continuous spectrum of the electromagnetic field.

1.1.1. Continuous Spectrum Formulation

The geometry of a discontinuity in a package is shown below in Fig. A1.2.

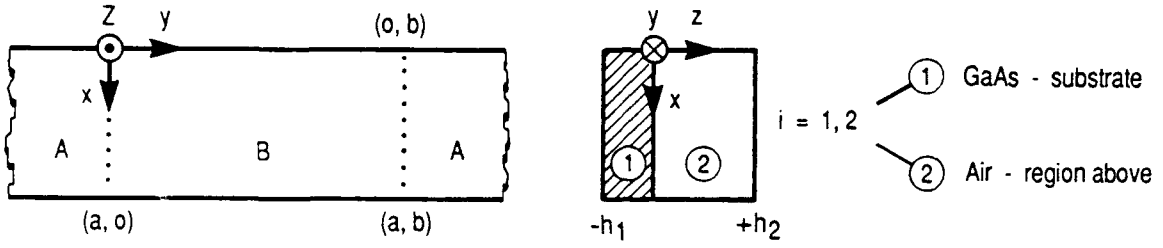


Fig. A1.2:

within which the electromagnetic field can be described by

$$\psi_i = \sum_m \sin(k_{xm}x) \int_{-\infty}^{\infty} \tilde{b}_{im}(k_y) e^{jk_y y} f(k_{zm}^i z)\, dk_y,$$

$$\phi_i = \sum_m \cos(k_{xm}x) \int_{-\infty}^{\infty} \tilde{c}_{im}(k_y) e^{jk_y y} g(k_{zm}^i z)\, dk_y.$$

where ψ, ϕ are wave potentials.

The continuous version was studied in detail taking into account all necessary steps to arrive at a final set of equations which can be solved numerically. Due to the properties of the Fourier transforms with respect to the y-direction the field quantities can be processed elegantly to yield a spectral relation between the electric flux density in the plane of the strip conductors and the associated surface current density. This is equivalent to an integral operator equation in the space domain, mapping the surface current density J_s into the electric field E_s tangential to the metallisation

pattern. One of the advantages of this formulation is that the current density can be defined piecewise in the space domain without violating continuity conditions. This prevails because J_s is not used in the analytical process of setting up the equations, but $\mathfrak{J}_s$, its Fourier transform. Accordingly, the introduction of discrete mode functions (precomputed) in the space regions A outside of the discontinuity region B is possible in a straightforward manner.

In view to applying the SOE technique, nevertheless, it is a problem that the prevailing operator is of infinite range, i.e. it encounters all current density contributions in the range $-\infty<y<\infty$. Though any test functions used in the numerical evaluation of the problem may be restricted to the discontinuity region B, $o<y<b$ (chosen large enough) the expansion in terms of modes in B introduces spectral contributions of the form

$$\tilde{t}(k_y) = 1/(j(k_y-\beta_i)) = 1/(j(k_y k_o \sqrt{\varepsilon_{effi}})),$$

where j is the imaginary unit and β_i the propagation constant of the ith discrete mode encountered at one of the reference planes y = 0 or y = b (Fig. A1.2). This is a relatively simple mathematical form and can be expanded in principle, in terms of frequency. However, it complicates the application of SOE. The SOE can be applied efficiently if only the operator depends on frequency and the expansion functions and the test functions used do not.

The alternative of splitting off the associated discrete mode poles $k_{ypi} = \beta_i$ from the integral operator has also been studied. This leaves the problem of subtracting the associated residues from the integrand and results in a form where the β_i-dependence is still not removed from the analytical formulation (numerically it is). For that reason, SOE in conjunction with the continuous spectrum version is possible in principle but requires a relatively high amount of analytical manipulation and preparation of the numerical algorithm

without achieving its full efficiency. A comparison between the individual steps to be performed for the continuous spectral formulation and for the discrete spectral version exhibits an advantage of the latter as far as application of the SOE is concerned. This is because in the discrete formulation the operator is defined with finite support, i.e. over the range $0<y<b$ only, for which the construction of frequency-independent expansion functions is found to be easier.

1.1.2. Discrete Spectrum Formulation

For the discrete spectrum formulation the electromagnetic field can be represented by

$$\psi_i = \sum_m \sum_n \sin(k_{xm}x)\,[b_{1mn}\sin(k_{ym}y) + b^1_{1mn}\cos(k_{yn}y)\,].f(k^i_{zmn}z)$$

$$\phi_i = \sum_m \sum_n \cos(k_{xm}x)\,[c_{1mn}\cos(k_{yn}y) + c^1_{1mn}\sin(k_{yn}y)\,].g(k^i_{zmn}z)$$

where ψ, ϕ = wave potentials.

The discrete method was followed through all its structural mathematical details to arrive at a solution required to formulate a computer program. The way followed in order to satisfy all of the outlined requirements, is a modified mode matching technique applied to the planes $y = 0$ and $y = b$ using precomputed transmission line solutions. The continuity conditions arising can be fitted into the system of equations for region B's boundary conditions by implementing a special, additional set of expansion functions. The structure of a computer program based on this formulation is very similar to that of the existing SFPMIC program. The main difficulty is to obtain an em field expansion having completeness in the closed interval $0<y<b$ instead of the open interval $0<y<b$ and which simultaneously satisfies orthogonality in order to efficiently process the start equations. The closed interval

properties are required for mode matching at $y = 0$, $y = b$. Some computer tests have been made to study the required completeness properties using elementary examples. The closedness problem can be avoided by the use of the continuous spectrum formulation shown above, the price being a higher analytical complexity in evaluating and processing the start equations. Two possible ways of introducing the discrete exciting (or reflected and transmitted) modes have been investigated for this method: subdivision of the spatial counterparts of the spectral functions $\tilde{b}_{im}$, $\tilde{c}_{im}$ and splitting of associated discrete mode poles from the integral representations in terms of k_y.

The problem of achieving completeness for the closed interval $0 \leq y \leq b$ in case of the discrete formulation has been overcome by redefining the region B as a subregion of this interval. The reference planes, say RP1 and RP2, now are not allowed to coincide with $y = 0$ or $y = b$, the boundaries of the interval. RP1 and RP2 are chosen near $y = 0$, $y = b$ in the interior of the interval, sufficiently distant from its boundaries in accordance with numerical considerations and the specified spatial resolution. The discrete formulation can even be simplified with that choice as compared to the original description (i denotes the dielectric layer, i = 1 or i = 2 here):

$$\Psi_i = \sum_m \sum_n \sin(k_{xm}x) \begin{bmatrix} \cos(k_{yn}y) \\ \sin(k_{yn}y) \end{bmatrix} \cdot b_{imn} f_i(k^i_{zmn}z),$$

$$\Phi_i = \sum_m \sum_n \cos(k_{xm}x) \begin{bmatrix} \sin(k_{yn}y) \\ \cos(k_{yn}y) \end{bmatrix} \cdot c_{imn} g_i(k^i_{zmn}z).$$

A continuation of the current density expansion beyond RP1 and RP2 can be constructed in the subintevals $0 \leq y \leq y(RP1)$ and $y(RP2) \leq y \leq b$ which has some modal

character, but does not depend on frequency, at least not in its y-dependent factor. The description of the algorithm developed follows, the expansion function continuation playing a role similar to the source distributions in the SFPMIC program used for discontinuity analyses.

1.2. BRIEF DESCRIPTION OF THE MATHEMATICAL ALGORITHM AND ITS ASSOCIATED CHARACTERISTICS

From the discrete spectrum description for the LSM and LSE wave potentials the associated electric and magnetic field components have been derived analytically also the continuity of the tangential electric field E_s at the substrate surface has been introduced as an analytical expression. The surface current density distribution J_s representing the strip conductor pattern has then been introduced as the discontinuity of the tangential magnetic field at the dielectric interface. In symbolic form this results in the operator equation,

$$E_s = L_{xy} \cdot J_s = 0, \quad \text{for x, y on conductors} \qquad (1)$$

The subscript xy indicates that the respective operation is in the plane of the substrate. J_s is expanded over the range $y(RP1) < y < y(RP2)$ using frequency-independent expansion functions (the frequency-dependence is in the weighting coefficients). A continuation of J_s was formulated into the complementary subintervals $0 < y < y(RP1)$ and $y(RP2) < y < b$. This is described in its simplest form as a constant for the longitudinal current density component and a linear function of y for the transverse component. Its choice is not critical. In its x-dependency it may be chosen as a normalised precomputed mode distribution, however, from an investigation, this does not seem to be a necessary choice (expansion function elements $\phi(x)$ as used for mode computations should be sufficient as well, which eases the SOE procedure).

Because of the SOE requirements, the wave amplitudes at the chosen reference planes can no longer be extracted directly from the expansion (does not contain 'modes'). Instead, they are derived from transverse testing, i.e. via the continuity conditions enforced at the reference planes RP1 and RP2 for the electric field E_t and the magnetic field H_t in the xz-plane (transverse to the feed lines). The respective continuity equations are of the form

$$E_t = \sum_k E_{tk}, \; H_t = \sum_k H_{tk} \quad \text{at RP1, RP2} \tag{2}$$

with the subscript k specifying relationship of the kth mode propagating through RP1 and RP2 (precomputed). In symbolic operator notation this reads as

$$L_{xz} \cdot J_s = T^a_{xz} \cdot a, \; M_{xz} \cdot J_s = T^b_{xz} \cdot b \tag{3}$$

where a, comprises a set of mode excitation amplitudes and b, is the associated set of scattered mode amplitudes. L_{xz} and M_{xz} are linear operators mapping the total current density expansion J_s, existing in the xy-plane into the field components in the transverse xz-plane. The dimension of a and b is the same and corresponds to the number of modes incident/reflected from the considered discontinuity. An equal number of continuation functions is contained in the expansion J_s leading to a consistent deterministic system when eq. (1) and (2) are combined. The structure of the final system of equations is

$$\begin{bmatrix} [L_{xy}] & \text{cont.} & 0 \\ [L_{xz}] & & 0 \\ [M_{xz}] & & -T^{b}_{xz} \end{bmatrix} \cdot \begin{bmatrix} J_s \\ \text{cont.} \\ b \end{bmatrix} = \begin{bmatrix} 0 \\ T^{a}_{xz}a \\ 0 \end{bmatrix} \qquad (4)$$

The [] brackets indicate the operation of testing with suitable test functions. From a and b the scattering matrix can be constructed. L_{xy} is SOE compatible without restriction. By suitable normalisation T^{a}_{xz} and T^{b}_{xz} become unit matrices. The term 'cont.' in eq. (4) denotes the position o f the continuation terms in the system matrix. The only difficulty for the SOE technique is that L_{xz} and M_{xz} exhibit a <u>weak</u> frequency-dependence stemming from the testing of eq. (2) with normalised modal field distributions in the transverse xz-plane. This cannot be avoided whatever the formulation since it is a consequence of the mode amplitude exaction process. The next step of the investigation is, therefore, to consider a suitable SOE scheme for this situation. A not very restrictive alternative is to constrain the SOE to the y-dependent portion of the respective operations.

The problem of applying the spectral operator expansion technique to the portions $[L_{xz}]$ and $[M_{xz}]$ of the system matix is still open. Because the operators L_{xz} and M_{xz} are related to the transverse field distributions of modes on the feed line(s) of a discontinuity, they are frequency dependent in a form which makes application of the SOE difficult. This problem has been overcome now in the following way:

$$E_t = \sum_k E_{tk} = \sum_k a_k e_{tk} = \sum_k a_k . L(\beta_k) . J'_{sk} \quad \text{in A,}$$

$$H_t = \sum_k H_{tk} = \sum_k b_k h_{tk} = \sum_k b_k . M(\beta_k) . J'_{sk} \quad \text{in A,}$$

$$\text{with } J'_{sk} = \sum_i \alpha_{ik} j'_{si},$$

$$E_t = L_{xz} . J_s \quad \text{and} \quad H_t = M_{xz} . J_s \quad \text{in B,}$$

where A and B denote the field regions adjacent to RP1, RP2. J'_{sk} is the transverse current distribution of mode k, with expansion functions j'_{si}. The requirement of continuity through the reference planes and the associated procedure of testing with the transverse mode distributions e_{tk} and h_{tk}, respectively, leads to:

$$a_k \, [e_{tk}, h_{tk}] = \sum_i \alpha_{ik} \, [L_{xz} . J_s, \, M(\beta_k) . j'_{si}] \, ,$$

$$b_k \, [h_{tk}, e_{tk}] = \sum_i \alpha_{ik} \, \frac{[M_{xz} . J, \, L(\beta_k) . j'_{si}]}{[L_{xz}]_i, \, [M_{xz}]_i}$$

Here, the orthogonality of the modes has been used and the linear property of the operators. The system matrix elements $[L_{xz}]_i$ and $[M_{xz}]_i$ from which the final scalar products [L] and [M], can be constructed by a summation over a small number i of terms are suited for application of the SOE. The original frequency dependence of the applied modes is now essentially in the mode-related weighting coefficients α_{ik} which are precomputed as a 2D solution previous to the 3D discontinuity treatment and stored in a look-up table. This is achieved by the software MSMODES not developed under this contract, which performs a modal analysis for the feed lines including higher order modes needed to describe 1D radiation effects. This software uses a 2D SOE technique and allows stable mode computations with high spectral resolution.

1.3. REFERENCES

1. Jansen, R.H., Recent advances in the full wave analysis of transmission lines for application in MIC and MMIC design, Int. Microwave Symp., Rio de Janiero July 1987, pp.467-475.

2. STUDY OF THE CURRENT DENSITY EXPANSION FUNCTIONS

In order to satisfy the strip boundary and current continuity conditions, such as in the step and T-junction discontinuities, two types of functions were studied and used. All of these functions are separable with respect to the x- and y-directions and are formulated as products.

$$e(x).f(y)$$

to form current density expansion functions. These two function types are used in different situations, the first whenever a tangential or normal current behaviour is required at a boundary, the second piecewise defined representing the current in the metallisation inner regions.

2.1. CURRENT DENSITY BOUNDARY EXPANSION FUNCTIONS

A pictorial representation of the basic function elements used in setting up the 2D expansion function sets is given below in Fig. A2.1.

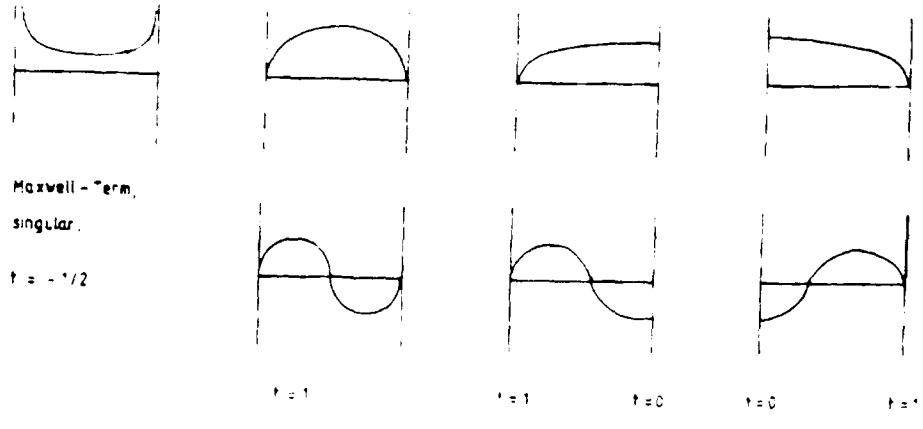


Fig. A2.1: Maxwell term expansion functions

Such function elements are defined over subregions of the total field region. Depending on whether the boundaries of these subregions are interior (artificial) or actual conductor boundaries and where the current density component described is tangential or normal to the respective boundary, the proper boundary behaviour can be realised by suitable combinations of the shown elements. The order of behaviour τ describing the vanishing or singularity at the subregion boundaries are chosen by $\tau = -1/2, 0, 1/2, 1 \ldots$ by multiplication of elements (up to 3 factors). While the outlined principle of construction applies only to one of the co-ordinates x,y the 2D expansion functions result again from multiplication of the x and y dependent terms. All spectral domain coefficients can be evaluated analytically, resulting in high numerical stability (avoiding FFT algorithms). The advantage of the piecewise modified harmonic scheme compared to a regular grid type expansion is a low number of expansion terms even in cases of large conductor width ratios and for small coupling gaps.

2.2. INNER CURRENT DENSITIES EXPANSION FUNCTIONS

Three types of piecewise expansion functions were put forward to describe the inner regions of the surface current density on the conductor metallisation. These were bell, triangle-shaped and sinus functions. Their properties are given below.

(a) Bell-shaped expansion functions

The bell-shaped expansion functions are constructed using a square cosine-function. Fig. A2.2 shows the graphical representation of the 1D bell-shaped expansion function element. The 2D form follows by element combination.

These bell-shape expansion functions are combined using an overlapping scheme where the bell-shapes overlap with a length of half the subregion. At the ends of each subregion both the function value and the first derivative of

the bell-function vanishes. In the middle of the subregion the function value reaches its maximum, the first derivative vanishing at this point.

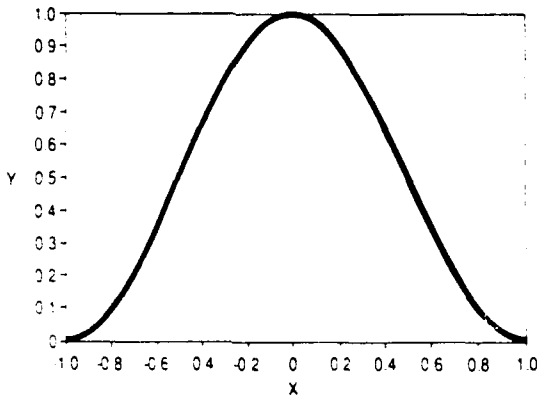


Fig. A2.2: Bell shaped expansion finder

Using the above combination scheme, such a set of expansion functions is capable of generating a straight line. However, the first derivative will always vanish at the interface of the two expansion areas due to the overlapping scheme. Therefore, a smooth linearly increasing function cannot be represented without showing ripple taking the form of a smoothed staircase function.

(b) Triangle-shaped expansion functions

The triangle-shaped expansion functions are constructed by 2 straight lines. Fig. A2.3 shows the graphical representation of the 1D triangle-shaped expansion function. The 2D form is a bilinear (pyramidal) element the surfaces of which, however, are not true planes.

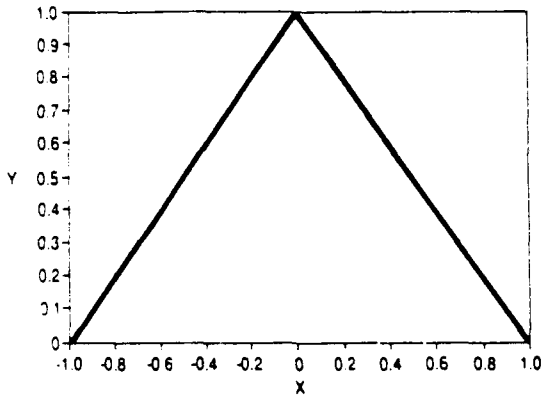


Fig. A2.3: Triangle shaped expansion function

These triangle-shape expansion functions are again combined using an overlap (overlap of a length of half the subregion). At the ends of the sub-sections the function value vanishes but not the first derivative. In the middle of the subsection the function value reaches its maximum. A first derivative does not exist at this point (but it can exist for the overlapping elements). However, because this type of piecewise defined function is capable of approximating continuous functions in a piecewise linear manner, convergence for an increasing number of elements can be obtained together with a well-behaved derivative. (Note that these functions are not used directly but only their truncated spectral representations are used.)

(c) Piecewise sinusoidal expansion functions

Such sinus-shaped expansion functions are constructed using the half of a period of a sine-wave. Fig. A2.4 shows the graphical representation of the 1D sinus-shaped expansion function. The 2D form follows by the usual combination of 1D elements.

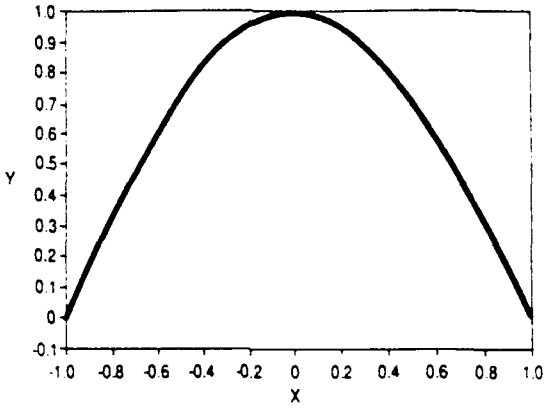


Fig. A2.4: Sinus expansion function

Two different overlapping schemes were used for the combination of the sinus-shaped expansion functions (overlap of a length of half and of a third of the subsections). At the expansion sub-sections' ends the function value of the sinus-shape vanishes but not the first derivative (as in the case of the triangles). In the middle of each subsection the function value reaches it maximum and the first derivative vanishes.

2.2.1. Investigation of the Piece-Wise Expansion Functions

These three piece-wise functions were studied for their capabilities to form continuous modal current density distributions. The functions defined over certain subregions of the conductor metallisation in conjunction with those satisfying the boundary conditions were mutually overlapped to constitute the larger subregions chosen for harmonic functions behaviour.

2.2.2. Expansion Function Grid Pattern Tests

A variety of tests were made in which a comparison between piece-wise defined functions in a quadratic grid and a rectangular grid was carried out, to see the effect of a non-equal discretisation with respect to the two co-ordinates x, y. From theory and from past investigations with spectral domain

solutions, equal maximum spatial resolution (k_{xm}, k_{yn}) was found to be particularly important, if conductor corners occur in the discontinuity geometry. The reason for this is that the singular field near a 90° corner acts as the source of a local radial wave. This wave can be described by cartesian constituents if certain point symmetry conditions are satisfied (suitable pairs of k_{xm}, k_{yn} exist). Test computations revealed that this condition is satisfied for an applied quadratic grid.

2.2.3. Expansion Function Study of the Microstrip Open End

As a test case to determine the quality and suitability of the expansion functions a near full wavelength open end resonator was simulated. The simulated structure was a rectangular conductor shape (length=1.8mm, width=0.2mm) on 100μm GaAs symmetrically embedded into a package (length=1.95mm, width=0.5mm). The analysis was done at 50 GHz. The solutions of the 3-D electromagnetic simulations were computed with a spectral resolution which was high enough to represent the expansion functions accurately. Eight expansion functions were chosen over the length of the resonator and two over the width in the inner conductor regions. A microstrip mode related source distribution previously described was used, and also the same conductor boundary terms.

The longitudinal current distribution was computed and plotted in the metallisation plane. These plots allowed the advantages and weaknesses of the expansion functions and the general mathematical behaviour of the expansion functions to be considered.

Fig. A2.5 shows the longitudinal current distribution using the bell-shaped expansion functions. The obvious ripple visible on the edge of the expansion areas is a characteristic of this type of expansion function.

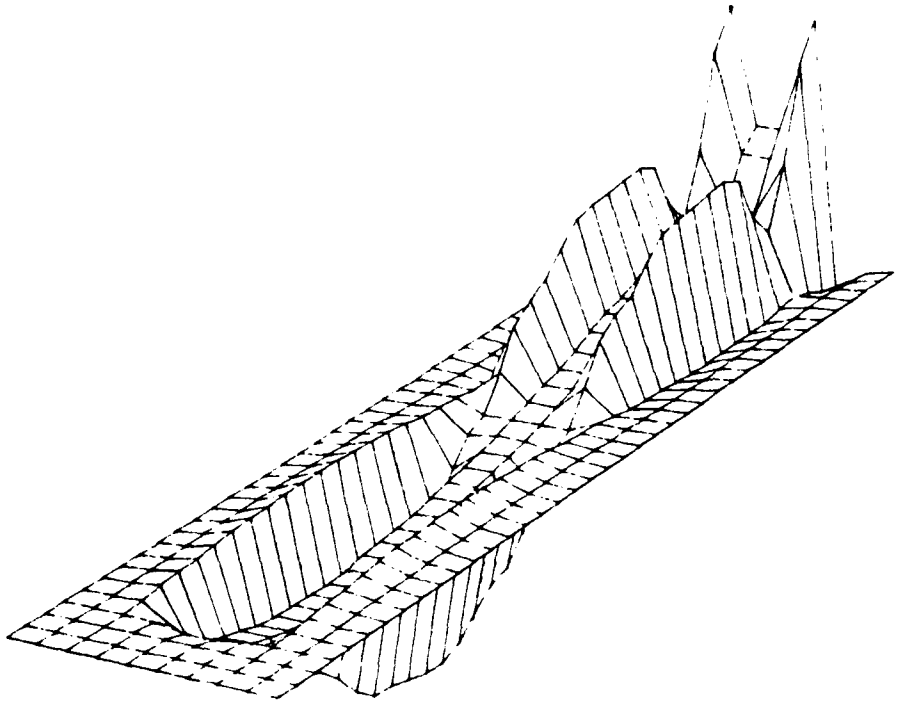


Fig. A2.5: Open end longitudinal current distribution: bell shaped functions

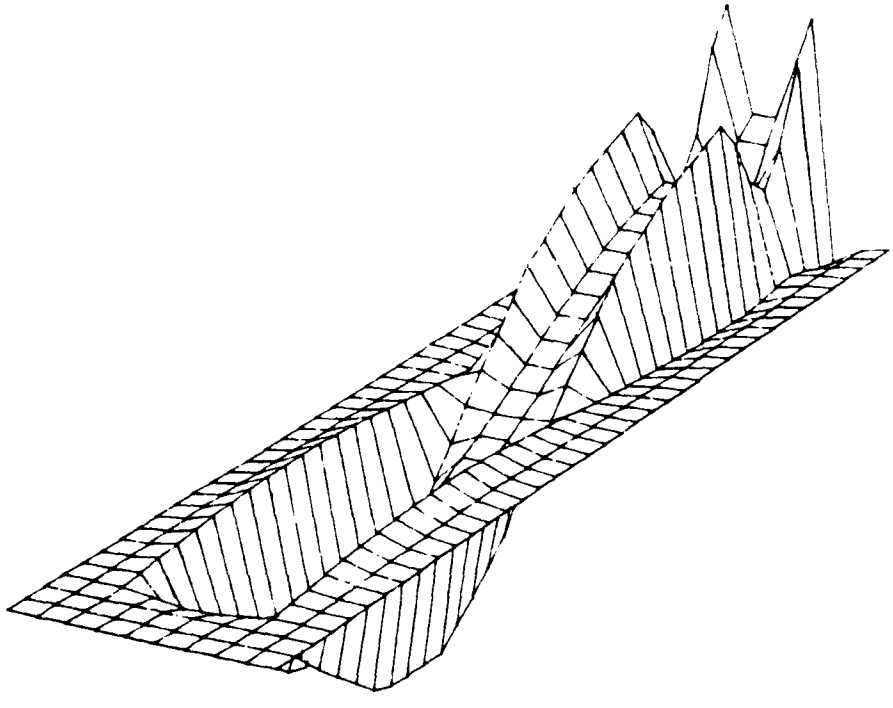


Fig. A2.6: Open end longitudinal current distribution: triangle shaped functions

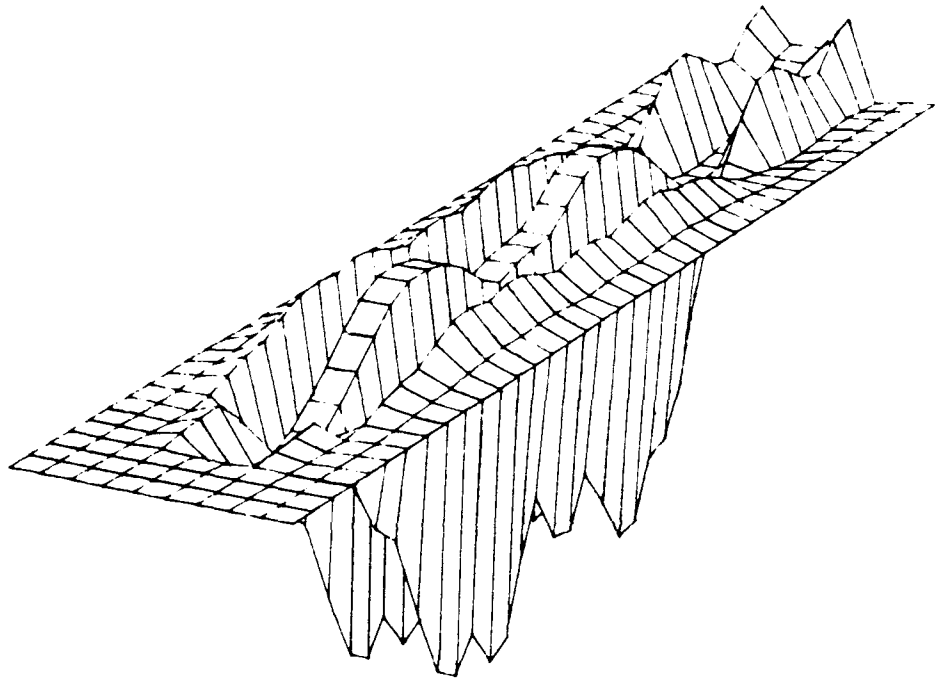


Fig. A2.7: Open end longitudinal current distribution: sinus shaped functions

The same current distribution using the triangle-type expansion functions is shown in Fig. A2.6. The piecewise linear behaviour, characteristic for this type of expansion functions is clearly visible.

On testing both overlapping schemes, the set of sinus-shaped expansion functions was found incapable of generating a straight line. In both cases only lines with ripple can be generated. The first derivative was not continuous at the interface points. Detailed study showed that a smooth function representation can be obtained only in problems for which the operator is sufficiently well behaved.

Fig. A2.7 shows the longitudinal current distribution using the sinus-type expansion functions (using the half-length overlapping scheme). Obviously the solution is not comparable in quality to the previous two cases. Several other tests showed that the sinus-type expansion functions are not well suited for the type of current expansion needed.

As a result of this study only the triangle- and the bell-shaped expansion functions were found to be well suited for the discontinuity TL feed regions. The triangle-type expansion functions were chosen for further use in the 3-D electromagnetic field discontinuity modules, because the triangle-type expansion functions do not have the first derivative fixed at zero at the common point between two sub-sections.

2.2.4. Expansion Function Study of the Microstrip Gap

Having completed the examination of the 3-D electromagnetic analysis for the open-end discontinuity the gap discontinuity was then studied. The main difference between these two discontinuities is that the microstrip-gap is a two-port device which needs independent source excitation states for its complete characterisation. The source open-end discontinuity expansion functions were also used for the gap.

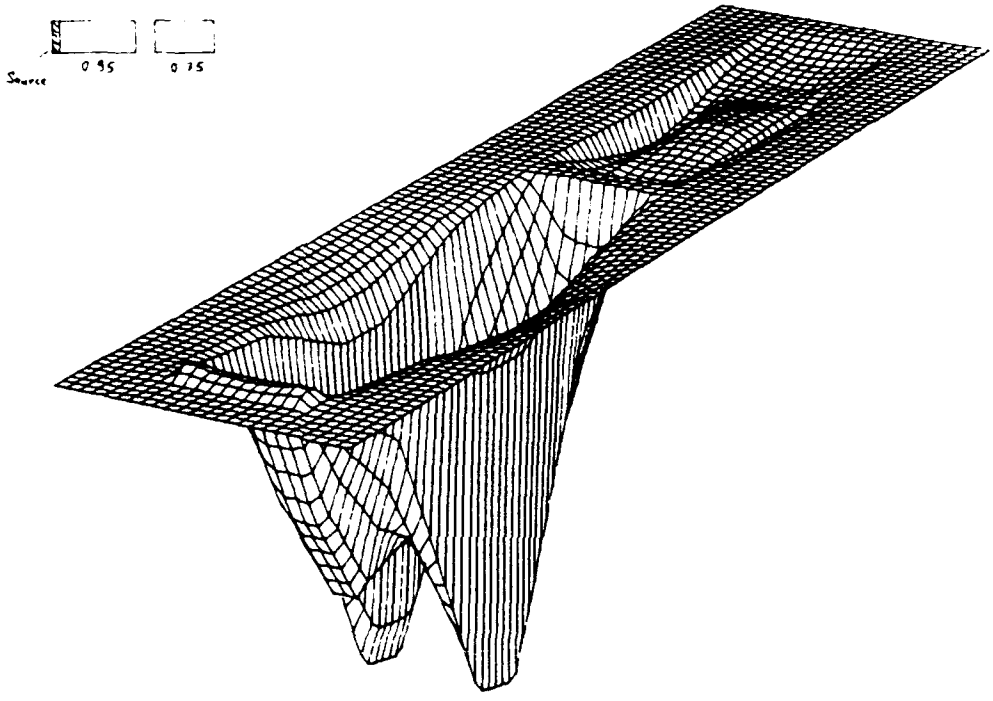


Fig. A2.8: Gap longitudinal current distribution: left hand source

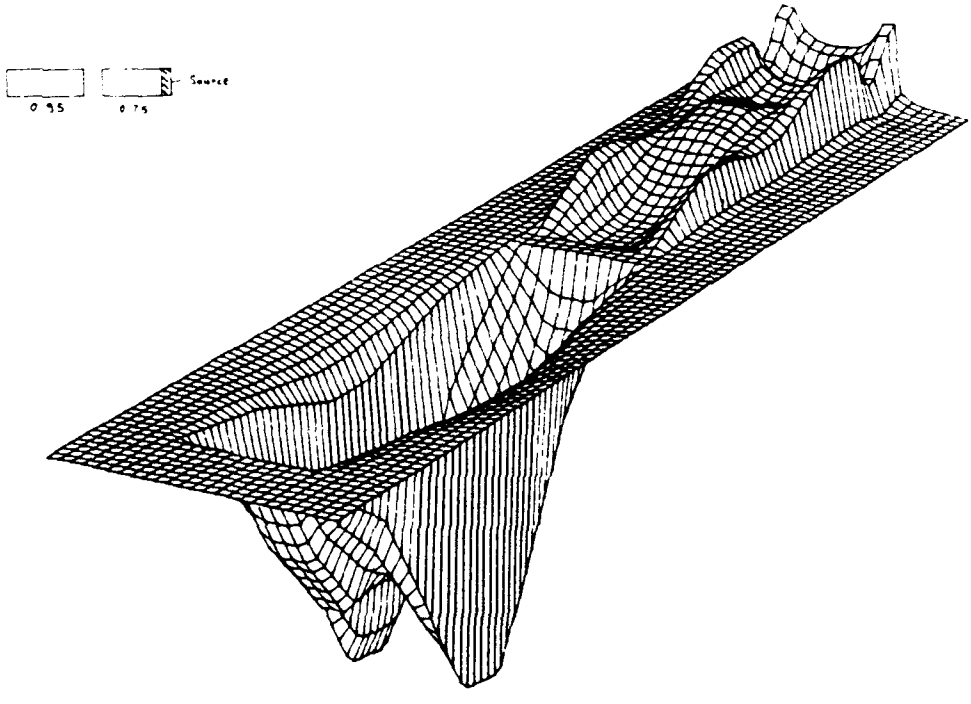


Fig. A2.9: Gap longitudinal current distribution: right hand source

The structure simulated as an example, consists of two microstrip lines (0.2mm wide) on a 100μm thick GaAs-substrate. The spacing of the coupling gap between the two lines is 50μm. The line lengths are 0.95mm (corresponding to half the wavelength) and 0.75mm. The two independent excitation states of the two sources used in the analysis were chosen such that one source is switched on, the other switched off and vice versa.

Fig. A2.8 shows the longitudinal current distribution of the simulated gap-structure. Note that this particular plot shows the excitation state in which the source on the right hand microstrip line is switched off and the left hand source on the line switched on. From the results it is obvious that there is strong coupling from the excited strip to the other. The large amplitude on the non-excited strips is due to the fact that its length is about a half-wavelength.

Fig. A2.9 shows the longitudinal current distribution of the second excitation state where the right hand source on the microstrip line is switched on and the left hand source on the line is switched off. The amplitude on the non excited line in this case is much smaller than in the first case, since the strips length, 0.75mm, is far away from a resonance condition.

2.3. SOURCE REPRESENTATIONS FOR IMPROVED 3-D SOLUTION QUALITY

During investigations on the quality of the 3-D solutions different types and systems of expansion functions were studied. It has become obvious that the link between different types of expansion functions and/or between different subregions is an important factor. The most important points in this context are the values of the expansion functions on their subregion boundaries and their respective derivatives. The influence of the first derivative especially has been investigated and was found to be very important for the quality of the solution.

Investigations have been made in order to achieve a smooth transition between the source region and the metallisation area. The current distribution is impressed over the source region and expansion functions suitable for the representation of the current density are defined over the metallisation area. The amplitudes of these expansion functions are determined during the solution of the 3-D electromagnetic field problem.

To obtain the smooth transition into the feed strip(s), different types of source functions were considered, the type of source function used being compatible with the type of expansion functions in order to avoid discontinuities in the solutions. The transverse behaviour of the source expansion functions was chosen to be the Maxwell-term which gives a good representation of the fundamental microstrip mode.

The first source tapering function investigated was a squared cosine-function. Fig. A2.10 shows the longitudinal dependency of this source function.

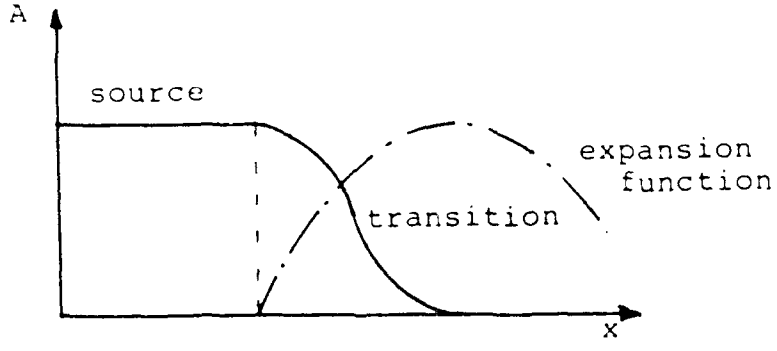


Fig. A2.10: Square cosine shaped source function

At the boundary to the feed strip both the function value and the first derivative vanish. Because the expansion functions used first were harmonic functions, the transition function appears to be compatible. However, as has been shown such a system of pure harmonic expansion functions is not a suitable choice to describe the standing wave pattern of the microstrip mode on the feedlines.

During the development of the software for the open end, a system of triangular expansion functions were found to be better suited. However, the source functions are not strictly compatible with this system of expansion functions since the first derivatives of the expansion functions do not vanish on the subregion boundaries. Depending on the overlap between the source function and the adjacent expansion function this results in a discontinuity of the solution in the vicinity of the source. This can be avoided using a longitudinal transition function with a linear dependency. The schematic (Fig. A2.11) shows the modified source and transition function in combination with the next triangular expansion function element.

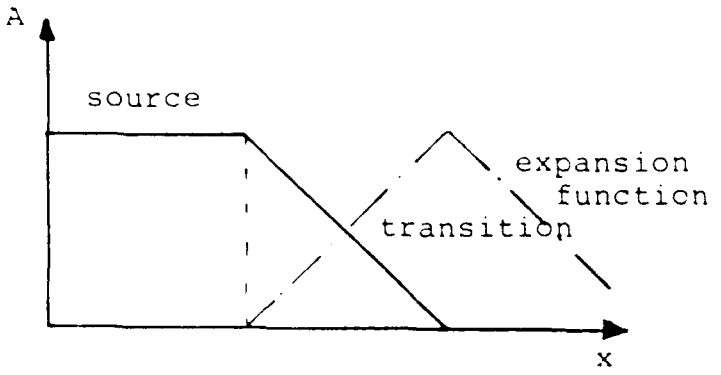


Fig. A2.11: Linear ramp source function

As can be seen, the source function is a constant combined with the linear function of the transition. At the boundary, the function value vanishes but the first derivative does not. The overlap between the source function and

the triangular expansion functions are always chosen as shown above, since this combination results in a destructive combination of the unwanted effects of the derivatives of the two elements at the overlap point. Fig. A2.12 shows an open end 3D-solution (longitudinal strip current density) taking into account the improvement described here (see Fig. A2.7 comparison).

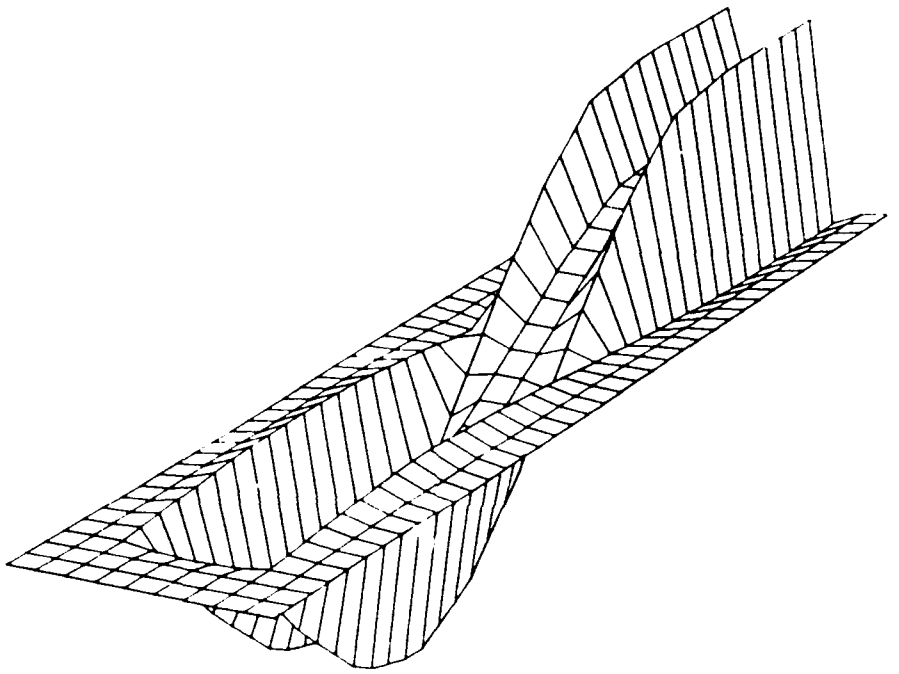


Fig. A2.12: Open end longitudinal current distribution: linear source function

2.4. EXPANSION FUNCTION SCHEME FOR THE MICROSTRIP STEP

A system of suitable subsections and expansion functions for the step discontinuity has been set up and tested for numerical data. In the case of the step, the discontinuity has been divided into seven different metallisation sections (Fig. A2.13).

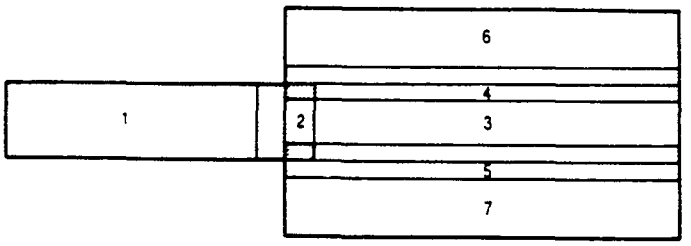


Fig. A2.13: Step subsection plan

Section 1 is the feedline section of the narrower line. Section 2 is the interconnecting section between the two feedlines. The width of section 3 is equal to the width of section 1 (narrower feedline). Sections 6 and 7 are upper and lower boundary sections of the second feedline (larger linewidth). sections 4 and 5 are interconnecting sections between the boundary sections and the internal section 3.

All of the subsections use the same types of expansion functions. Sections 1, 6 and 7 consist of both internal expansion functions (bilinear type) and boundary expansion functions (including Maxwell-terms). The other sections consist only of internal expansion functions. 2, 4 and 5 are interconnecting sections which overlap between the different expansion areas.

As a representative example, a symmetric microstrip step was analysed. The structure was simulated on 100μm GaAs embedded with a slight asymmetry in a package of 0.5mm x 1.0mm. The simulation frequency was 40 GHz.

Fig. A2.14 shows the resultant longitudinal current distribution on the metallisation area. Here the source function is connected to the narrow feedline. It is obvious that the fundamental microstrip mode which is

approximately impressed by the source, becomes distorted in the vicinity of the abrupt change of the line width. The current distribution on the wider feedline is somewhat different from the fundamental microstrip mode. This is thought to be due to the relatively small length of the wide section and the

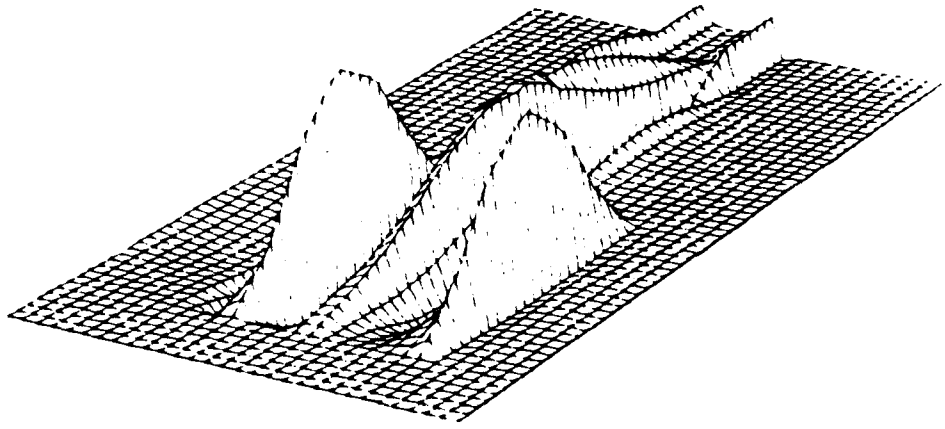


Fig. A2.14: Step longitudinal current distribution

fact that the disturbance caused by the narrow feed strip has not yet decayed sufficiently. For the evaluation of S-parameters the feedlines must have a length long enough to have two regions within which the fundamental microstrip mode can propagate.

2.5. EXPANSION FUNCTION SCHEME FOR THE MICROSTRIP 90° BEND

The expansion function scheme for the microstrip bend discontinuity was implemented in terms of 5 different subsections. Fig. A2.15 shows the layout of this scheme.

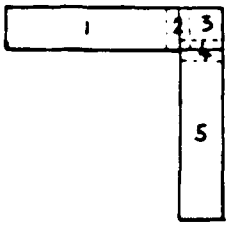


Fig. A2.15: Bend subsection plan

In the figure, section 1 is the first feedline section, section 2 the interconnecting section between the feedline and the corner segment, section 3 the bend section, section 4 denotes the interconnecting section between the bend section and the second feedline section, section 5.

All of the subsections use the same scheme and expansion functions and consist of both internal expansion functions (bilinear type) and boundary expansion functions (including Maxwell-terms). 2 and 4 are interconnection sections which overlap between the different expansion areas to obtain continuity of the current distribution.

A representative example, a symmetric microstrip bend discontinuity was analysed. The structure was simulated for a 100μm GaAs substrate embedded in a package of 0.8 mm x 0.8 mm. The simulation frequency was 40 GHz.

Fig. A2.16 shows the longitudinal (x-directed) current distribution on the metallisation area. Only one source function is switched on in this excitation state. The source is excited into the positive x-direction. As can be seen the fundamental microstrip mode which is approximately impressed by the source becomes distorted in the vicinity of the bend. The plotted x-directed current is rather small on the second line. This is due to the

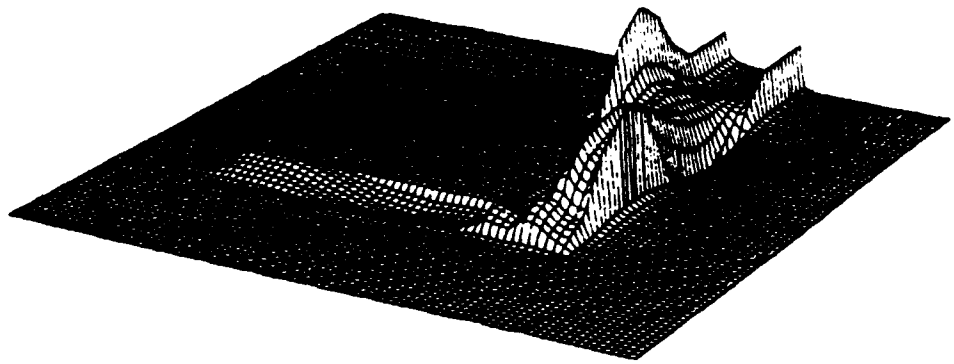


Fig. A2.16: 90° bend longitudinal current distribution: x-directed

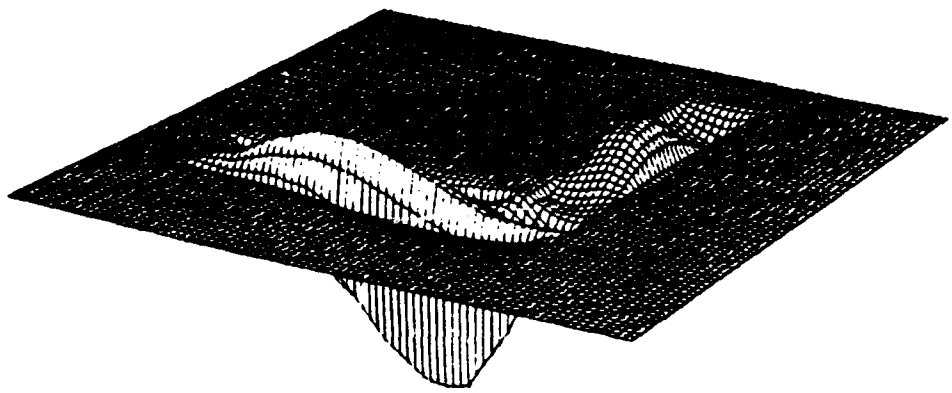


Fig. A2.17: 90° bend longitudinal current distribution: y-directed

fact that the x-directed longitudinal current on the first line represents the transverse current on the second line and as such should be much smaller, if the configuration still behaves similar to a TEM transmission line.

Fig. A2.17 shows the y-directed current distribution on the metallisation area for the same excitation state. On the second feed-line the y-directed current is the longitudinal component which now has a larger amplitude than the transverse component on the first feed-line.

2.6. EXPANSION FUNCTION SCHEME FOR THE T-JUNCTION

A system of suitable subsections and expansion functions for the symmetric T-junction discontinuity, is shown in Fig. A2.18.

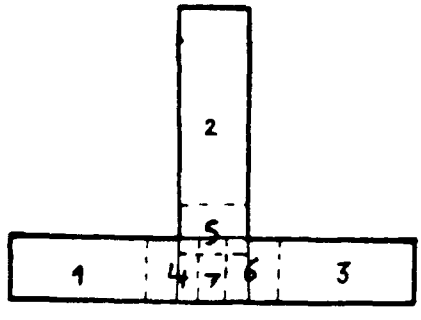


Fig. A2.18: T-junction subsection plan

In the figure sections 1 and 3 are feedline sections of the through-lines, and section 2 the respective feedline section of the stub-line. Section 7 is defined over the area between the feedline-section 3 and sections 4, 5 and 6 are interconnecting sections between the three feedlines and the interior expansion area, used to ensure continuity of the current distribution.

All subsections use the same scheme and types of expansion functions. Sections 1 to 6 consist both of internal expansion functions (bilinear type) and boundary expansion functions (including Maxwell-terms). Section 7 consists only of internal expansion functions.

As an example, a symmetric microstrip T-junction (i.e. the line width of the through-line does not change) was analysed. All line widths were chosen to be 0.1 mm. The structure was simulated on 100μm GaAs embedded in a package of 1.2 mm x 1.0 mm (cover height is 1.0 mm). The simulation frequency was 40GHz.

Fig. A2.19 shows the x-directed current distribution on the metallisation area. This current component is longitudinal on the through-feedlines. The source function is connected to one of the two ports of the through-feedline. As can be seen the fundamental microstrip mode which is approximately impressed by the source becomes distorted in the vicinity of the stub-line connection. The x-directed current plotted here is the transverse current on the stub-line and is small compared to the longitudinal current component on the feedline. Only the transition region into the stub shows noticeable values of the current density x-component.

Fig. A2.20 shows the y-directed current distribution on the metallisation area. This component is the longitudinal current on the stub-line and the transverse current on the through-feedlines (opposite to the x-directed current).

These current distributions show the correct and expected behaviour. The longitudinal current distributions, outside of the direct vicinity of the junction area, are reasonably close to the fundamental microstrip mode, one of the conditions for stable S-parameters extraction.

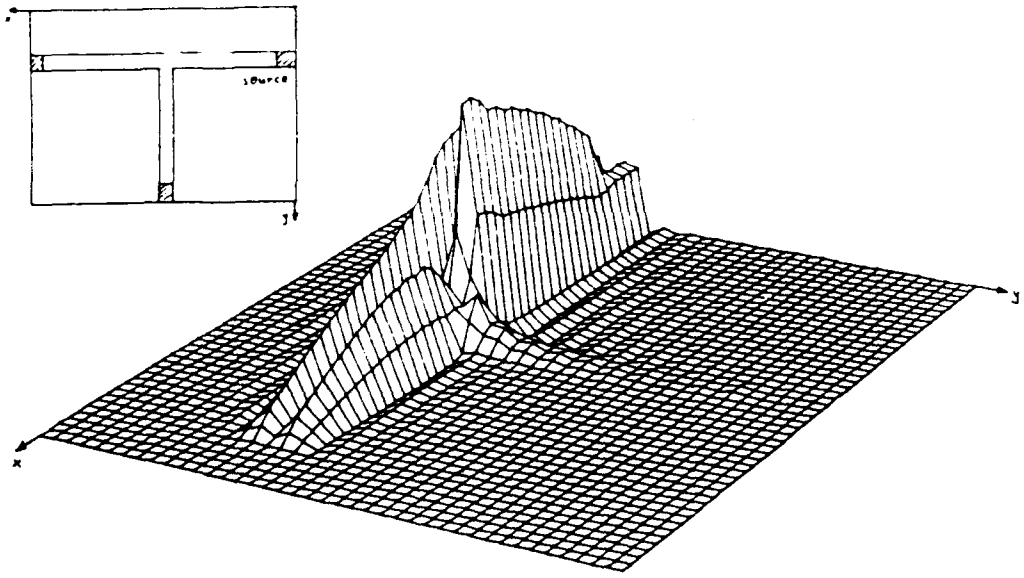


Fig. A2.19: T-junction longitudinal current distribution: x-directed

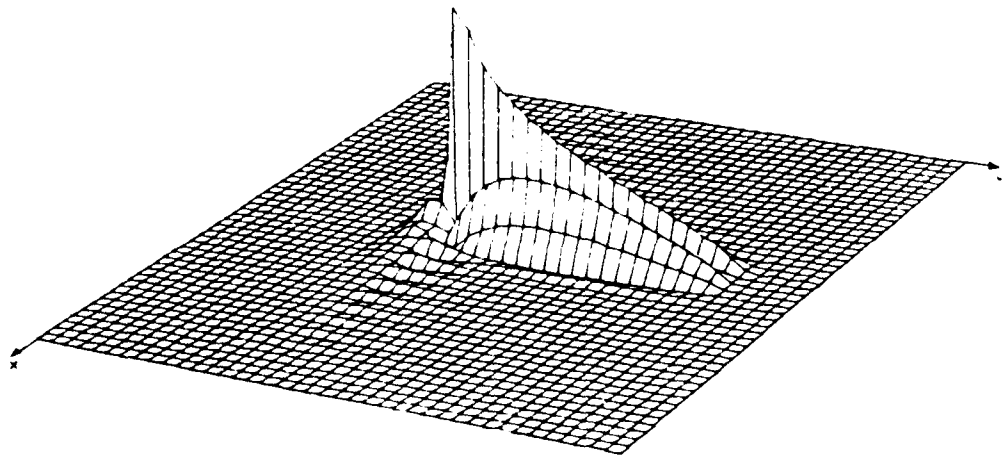


Fig. A2.20: T-junction longitudinal current distribution: y-directed

3. DEVELOPMENT OF THE SOE PROGRAMME

3.1. STRUCTURE OF THE PROGRAMME

A brief outline of the internal programme organisation in the new discontinuity programme modules is shown in Fig. A3.1:

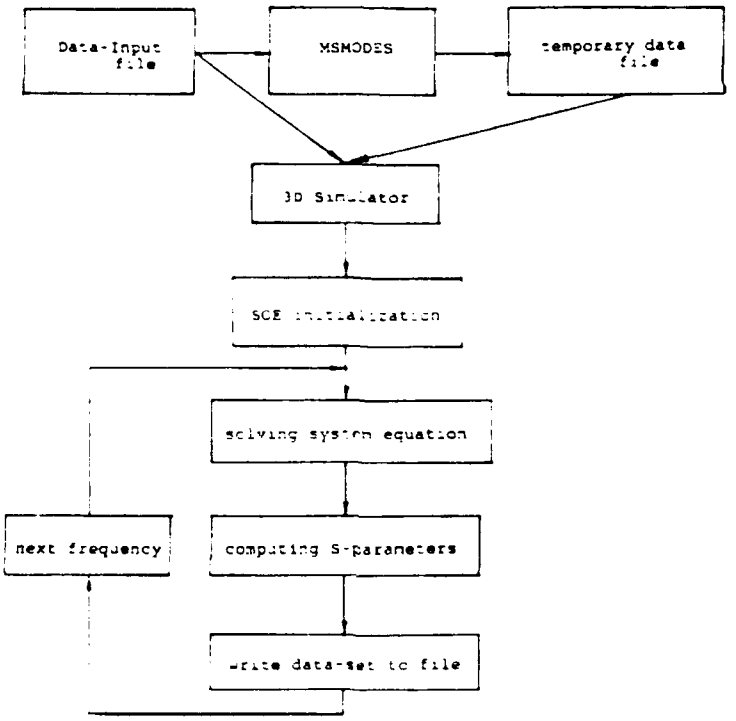


Fig. A3.1: Block diagram of SOE programme

In the programme mode field analysis software reads the input data file, computes the microstrip mode characteristics of the feed lines and writes them to a data base file. The SOE programme modules read this file and an input data file.

At the first frequency an operator initialisation for the SOE-method is performed. After this, the system matrix is generated and solved. Using the precomputed microstrip modes the S-parameters are calculated. This process is then repeated for each subsequent frequency.

3.2. SUMMARY OF THE 3D FULL-WAVE SOE APPROACH

As discussed in Section 1, the discontinuity structures are simulated in a finite field region (package). The medium considered is a single layer GaAs-substrate. Fig. A3.2 shows the cross-section and sub-division of the field region (EW = electric wall, SP = symmetry plane).

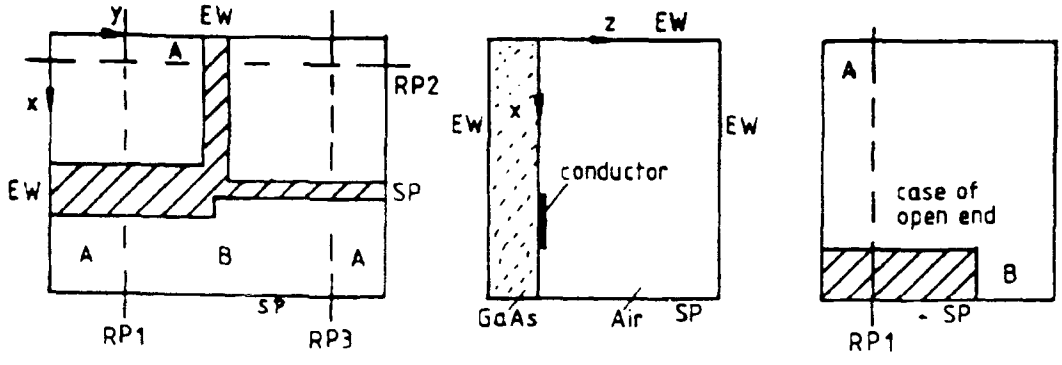


Fig. A3.2: T-junction discontinuity cross-section

The discontinuities are located in the x-y plane. In order to keep the computational expense low, two side walls in the x-y plane are software-switchable. This gives the choice of having both an electric or magnetic wall for each of the two side walls denoted SP. The figure also shows the x-y plane which contains an open-end discontinuity. Note that in this case the microstrip line with the open-end is located in the switchable wall (SP then denotes a magnetic wall, even symmetry).

The electromagnetic wave potentials for the LSM and LSE waves are described using a discrete series expansion (i denotes the dielectric layers, i = 1 for GaAs and i = 2 for air).

$$\psi = \sum_m \sum_n \sin(k_{am}X)\, \sin(k_{ym}Y)\, b_{imn}\, fi(k^1_{zmn}X)$$

$$\Phi = \sum_m \sum_n \cos(k_{xm}X)\, \cos(k_{ym}Y)\, C_{imn}\, gi(k^1_{zmn}X)$$

The electromagnetic potentials contain the z-dependency as well as the continuity of the tangential electric field at the substrate surface. From the electromagnetic potentials the resulting equations

$$E_s = L_{xy}\, J_s = 0 \text{ on conductors}$$

and

$$E_t = \sum_k E_{tk}, \quad H_t = \sum_k H_{tk} \text{ at the reference planes RP 1,2,3}$$

with $L_{xz}\, J_s = T^a{}_{xz} a$ and $M_{xz}\, J_s = T^b{}_{xz} b$

can be derived, where E_t is the tangential electric field at the conductors in region B. J_s is the surface current density and L_{xy} the 2-dimensional operator in the x-y plane. The operator L_{xy} is a linear integral dyadic and results from the dyadic Green's function in the spectral domain. The operators L_{xz} and M_{xz} result in a similar way from mapping the surface current density J_s into the transverse (x-z plane) electric and magnetic field. The modal representations of the transverse field (E_t, H_t) in the reference planes are generated by a modal analysis program and written into a suitable input file for the range of parameters of interest. T^a_{xz} and T^b_{xz} are transformation operators describing the transverse field in terms of vector wave amplitudes a and b, all operators being expandable in terms of frequency.

The operator equations given above can be solved in one or two steps. The two-step solution has been chosen for reasons of reduced organisational program complexity. To achieve this, the surface current density is split into two portions:

$$J_S = J_{SA} + J_{SB}$$

in which J_{SA} acts as an impressed source distribution. This sets up a deterministic first step problem solution which in the second step is then related to the modal data in the input file using the operators L_{xz}, M_{xz}, T^a_{xz} and T^b_{xz}, resulting in wave amplitudes or scattering parameters. The finite region chosen does not imply that energy transport phenomena are not included in the discontinuity characterisation. By the testing procedure implicit in the second step of the solution, the result is stripped down to the reference planes RP. In case of multimode analysis, this allows the incorporation of parasitic wave radiation phenomena.

3.3. OUTLINE OF THE SYSTEM MATRIX SOFTWARE

The system matrix is given by:

$$\sum_v \begin{bmatrix} g_{xv}{}^i g_{xv}{}^k (k^2_{xm} Z_{ev} + q\, k^2_{yn} Z_{hv}) & g_{xv}{}^i g_{yv}{}^k (k_{xm} k_{yn} (Z_{ev} - q Z_{hv}) \\ g_{xv}{}^i g_{xv}{}^k (k_{xm} k_{yn} Z_{ev} - q\, Z_{hv}) & g_{yv}{}^i g_{yv}{}^k (k^2_{xm} Z_{ev} + q\, k^2_{xm}\, Z_{hv}) \end{bmatrix} = 0$$

with $v = (m,n)$ being the combined index for the x and y direction, $q = k_o{}^2$ (representing the frequency parameter), Z_{ev}, Z_{hv} being the spectral

impedances and $g_{xv,yv}^{i,k}$ 2D-expansion functions, where the indices i and k determine the element number of the generated matrix element.

As mentioned in Section 2 the resulting 2-dimensional expansion functions are all of the kind

$$g_x = e_x(x)\ f_x(y)$$

$$g_y = e_y(x)\ f_y(y)$$

i.e. they are separable in the x- and y-direction. The Fourier transforms of these 1-dimensional expansion functions are evaluated in detail. Their transforms are discrete and are defined with dimensions of the x co-ordinate of the package ranging from 0 to a and the y co-ordinate from 0 to b. The spectral variables k_{xm} and k_{yn} are the new spectral variables in the Fourier domain.

As outlined the 1D-expansion functions are usually defined only over a certain package subregion in x or y direction. A very important point in the proper choice of the 1D-expansion functions is the ability to compute the Fourier-transforms for maximum CPU-time saving. In the optimum case each Fourier-transform can be precalculated analytically avoiding any kind of series expansion.

The 1D-expansion functions consist of piecewise combination harmonic terms of (sin, cos) i.e. multiplied with Maxwell terms to satisfy the correct edge behaviour. The resulting Fourier-transforms therefore consist only of harmonic function combinations with the zero-order Bessel function J_0. Since the harmonic functions are always implemented in standard compilers and Bessel functions J_0 can be calculated rather efficiently using a polynomial approximation all the requirements of the 1D-expansion functions are satisfied.

In the expansion function routines of the 3D-SOE solver only the Fourier-transforms of the 1-dimensional expansion functions are computed. This is done by using the control and geometric input data defining the actual expansion regions and expansion orders. The resulting 2D-expansion functions are generated separately by a suitable selection and combination scheme as described below. The advantage of this procedure is the very efficient computation obtained. Elements in the resulting system matrix contain constituents of the form

$$G_{xx}(k_{xm},k_{yn})^{i,k} = g_x(k_{xm},k_{yn})^i \; g_x(k_{xm},k_{yn})^k$$

$$G_{yy}(k_{xm},k_{yn})^{i,k} = g_y(k_{xm},k_{yn})^i \; g_y(k_{xm},k_{yn})^k$$

and mixed terms where (m,n) is the combined index for the spectral variable in x- and y-direction, i and k are the superscripts for the actual number (type) of expansion function and $g_{x,y}(k_{xm},k_{yn})^i$, $g_{x,y}(k_{xm},k_{yn})^k$ are the Fourier-transforms of the 2D-expansion functions of type i -or k. The two superscripts i and k result from the utilised moment method (Garlerkin) where the testing functions are equal to the expansion functions.

Since the number of spectral contributions for accurate MMIC structure analysis is rather high (usually from 100 to several 1000) due to the fact that the number of terms corresponds directly to the spatial resolution, the combined index (m,n) can easily reach several millions. The constituents $g_{x,y}(k_{xm},k_{yn})^{i,k}$ are computed, however, using the precomputed Fourier-transforms of the 1D-expansion functions. This reduces the actual computation of the 2D-expansion functions to the combination, i.e. multiplication of the 1D-expansion function which can then be made CPU-time efficient.

In order to verify the correct spatial dependencies, test software was written. This software performed the following tasks:

- computes the respective expansion function components (i.e. x- and y-components in the spectral domain).
- transforms the expansion functions generated in the spectral domain back into the space-domain.
- represents graphically the back-transformed expansion functions in the space-domain.

The final 2-D expansion function components generated are each a product of 2 different 1-D expansion functions. Two different test-programs were written to apply the outlined test-procedure both for the 1-D expansion function factors and for the 2-D combined expansion functions.

An example of the graphical representation of a 1-D expansion function is shown in Fig. A3.3. Another example shows the graphical representation of a 2-D function used as the source term for the open-end discontinuity analysis (Fig. A3.4).

During tests it became obvious that there was still an organisational problem in combinating the 1-D expansion functions into the 2-D expansion functions. So a reorganisation of the combination scheme of expansion functions became necessary. During the generation of the final matrix (linear system of equations) combinations of the 1-D expansion functions were computed in the spectral domain in a consistent manner regarding completeness and symmetry aspects. In order to avoid time-consuming control computations the complete information concerning all necessary combinations was generated once and stored. In this way the actual generation of the system matrix is done very efficiently.

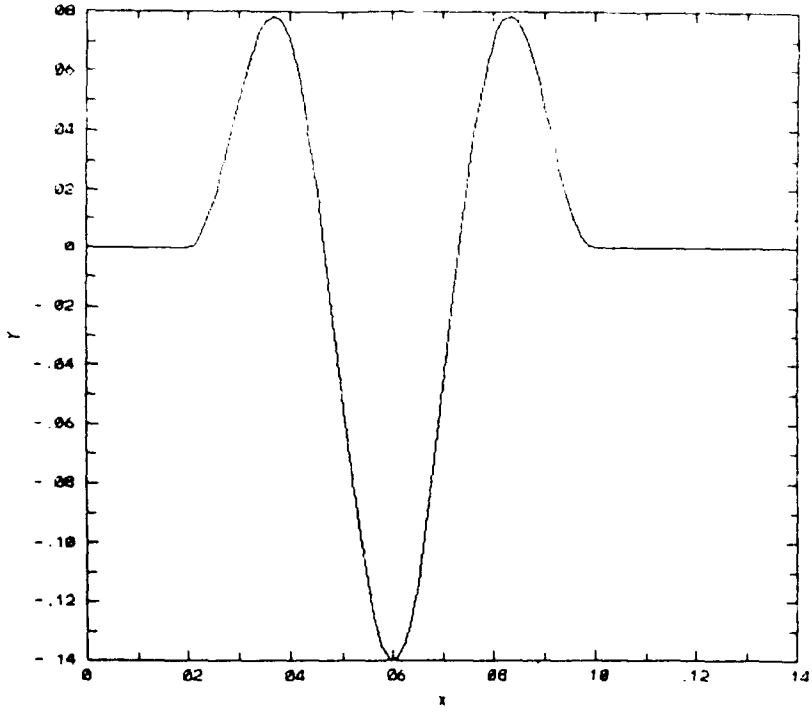


Fig. A3.3: 1-D expansion function

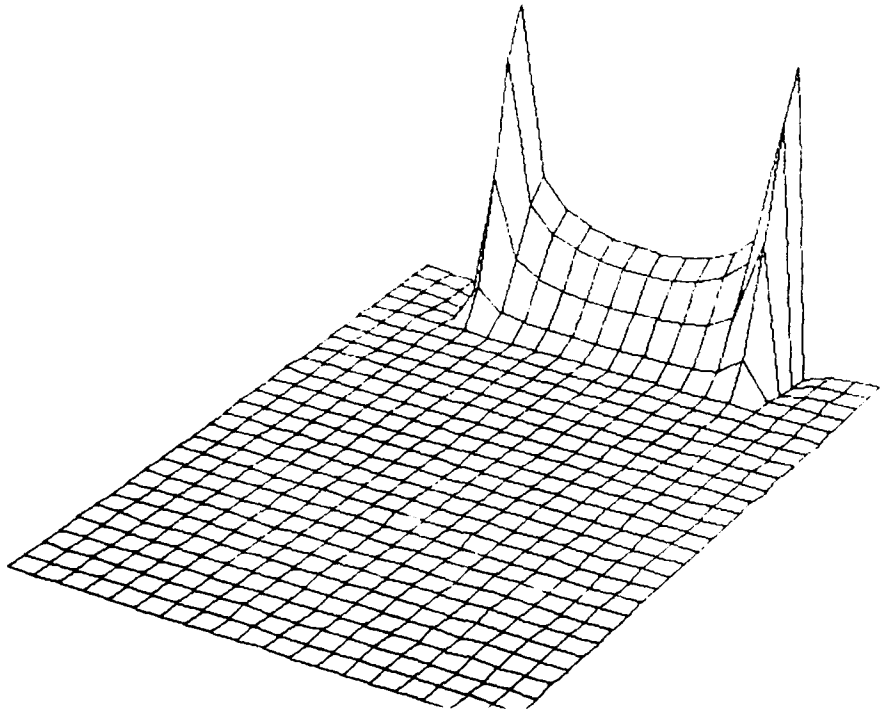


Fig. A3.4: 2-D source function

3.4. TESTING OF THE SYSTEM MATRIX GENERATION AND THE LINEAR SYSTEM OF EQUATIONS SOFTWARE

As a test of the software the current distribution on the metallic surface of the open end microstrip line was computed (Fig. A3.5). In this example a 60μm wide microstrip line (length is 100μm) was simulated on 100μm GaAs in a 100μm x 140μm package for f = 50 GHz.

As can be seen the electrical current density vanishes outside the metallisation as required. The source distribution and the edge currents (Maxwell terms) also can be seen.

In a general example a 0.2 mm wide microstrip line (length is 0.8 mm) was simulated on 100μm GaAs in a 0.8 mm x 1.0 mm package for f = 100 GHz which corresponds to about a full wavelength open end resonator. The expansion functions were chosen such that they give the correct singular behaviour at the 3 strip boundaries (Maxwell-Terms). Additional harmonic expansion functions of order 4 were chosen to account for the current expansion over the internal conductor area (transmission line type). The length of the source region was 0.2 mm and overlapped by the current expansion area. For this example the longitudinal current density, the transverse current density and the norm of the electric field density (all in the metallisation plane) were computed and plotted.

The longitudinal current, the dominant current component in the direction of wave propagation, shows the expected basic behaviour due to a physical length of about one wavelength of the resonator, i.e. one complete sine-wave on the line. However, on studying the longitudinal current (Fig. A3.6) it should be expected that the edge (Maxwell)-terms to have comparatively larger amplitudes compared to the amplitudes of the internal (harmonic) expansion areas than shown. Also, the expansion function choice did not result in

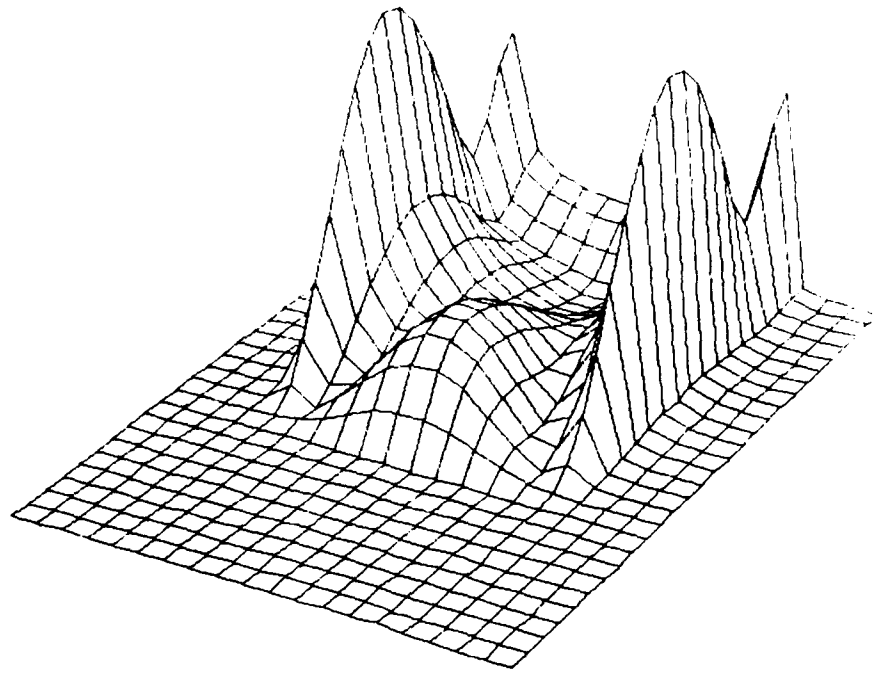


Fig. A3.5: Open end, longitudinal current distribution

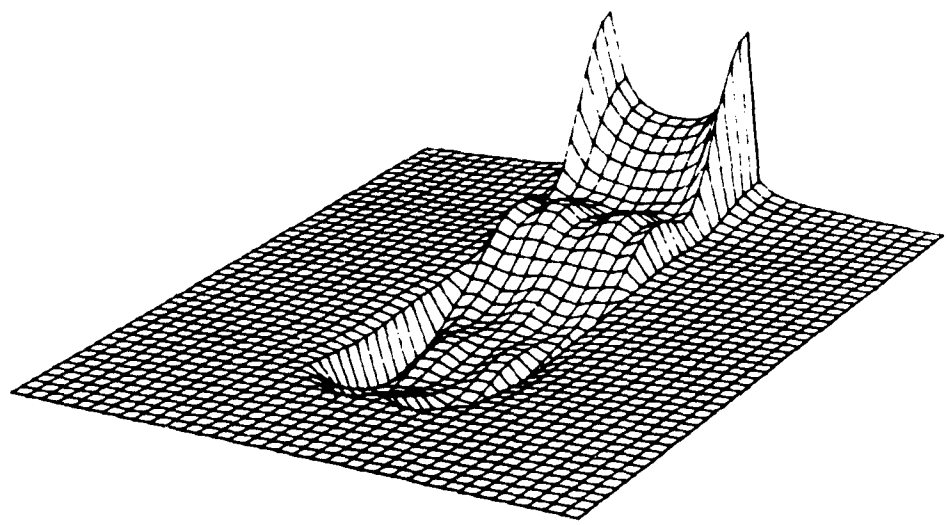


Fig. A3.6: Open end, longitudinal current distribution

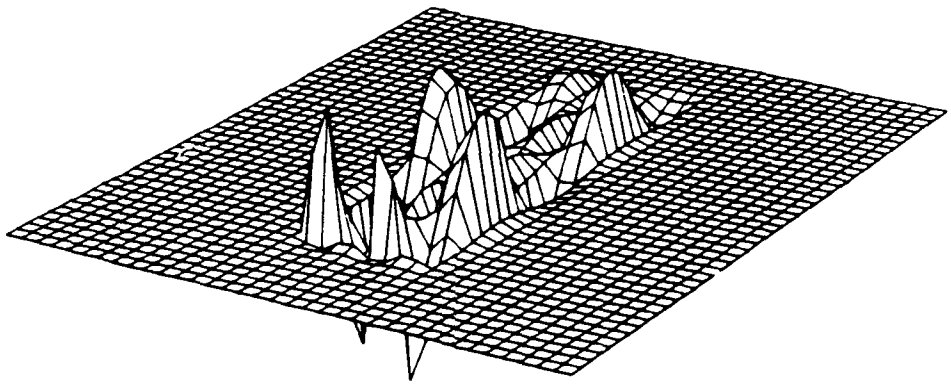


Fig. A3.7: Open end transverse current distribution

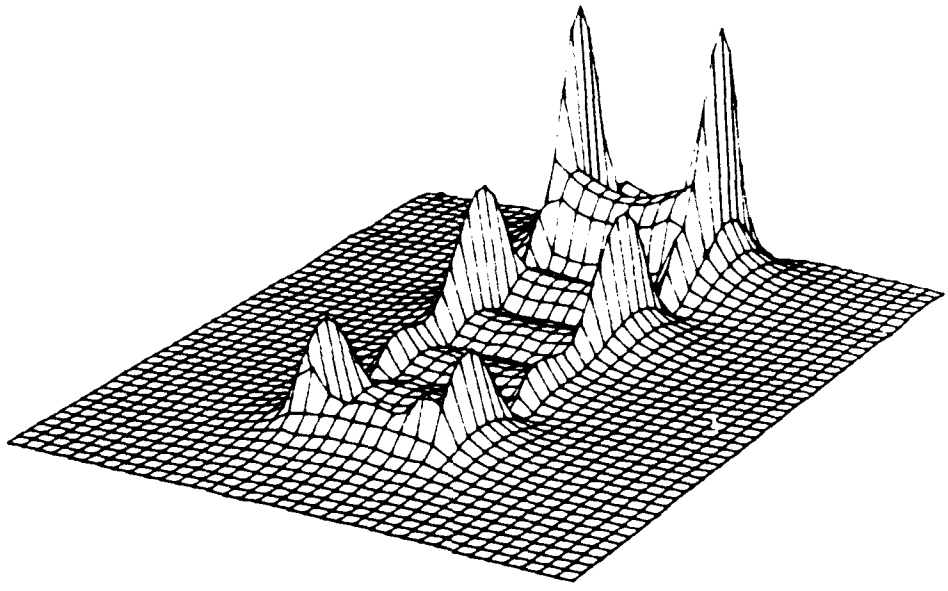


Fig. A3.8: Open end normal electric field

sufficiently smooth current behaviour. This is partially due to the order of the harmonic expansion being low (only 4).

Fig. A3.7 shows the transverse current on a different scale than that for the longitudinal current. As a result, a direct comparison between the amplitudes of the two current components is not possible. However, the odd symmetry of the transverse current component is as expected.

In Fig. A3.8 the norm of the electric field in the metallisation plane is shown. It can be seen that the electric field vanishes approximately on the metallisation except on the area where the source current is impressed and as expected outside the metallisation, the tangential electric field is relatively strong in the vicinity of the edges.

3.5. TREATMENT OF THE GREENS FUNCTION SPECTRAL EXPANSION

As to the spectral expansion of the Green's function terms with respect to frequency, this is performed similar to the method outlined in a recent paper ([1], Section 1.3). The spectral interface impedance linking the spectral representations of electric field and current density can be written according to this in the form:

$$Z_v\,(q) = \begin{bmatrix} (k^2_{xm}\, Z_{ev} + q\, K^2_{ym}\, Z_{hv}) & k_{xm}\, k_{ym}\, (Z_{ev} - q\, Z_{hv}) \\ k_{xm}\, k_{ym}\, (Z_{ev} - q\, Z_{hv}) & (k^2_{ym}\, Z_{ev} + q\, k^2_{xm}\, Z_{hv}) \end{bmatrix}$$

with $v = (m,n)$ and $q = k_0^2$ (representing the frequency parameter).

The LSM and LSE spectral impedances are Z_{ev} and Z_{hv} in this expression. With the explicit factors of q split off as shown above, these can efficiently be expanded in terms of q for values of v beyond a precomputed threshold value v_0. This takes the form of a Taylor expansion and together with the choice of frequency independent expansion functions results in the expansion of the operator L_{xy}. These respective sub-operators related to the expansion are set up during the initialisation of the programme, when the analysis for the first frequency point is invoked.

The idea of the spectral operator expansion method is that both the expansion functions have no dependency and the spectral impedance terms have only a very weak dependency on the frequency. This is valid in the above equation beyond a certain subscript v (m,n). So the above equation can be written as a sum of a Taylor series expansion in terms of frequency which can be truncated after the third element and for matrix terms computed up to a low order v (m,n).

Those parts of the equations which can be expanded can be written as

$$\text{Matrix operator}\Big|_{v_{expanded}} + \text{Source operator}\Big|_{v_{expanded}}$$

$$= M(q_0) + M'(q_0)\,(q-q_0) + M''(q_0)\,(q-q_0)^2$$

$$+ S(q_0) + S'(q_0)\,(q-q_0) + S(q_0)(\,(q-q_0)^2$$

where q_0 is the frequency parameter around which the Taylor series is expanded, q is the actual frequency, the $M(q_0)$ and $S(q_0)$ terms stand for the matrices at the expansion frequency, $M'(q_0)$, $S'(q_0)$ for the first and $M''(q_0)$, $S''(q_0)$ for the second derivative of the matrices at the expansion frequency.

All the M-terms consist of 6 different submatrices (S-terms of 4) so that the complete number of necessary submatrices adds up to 18 (12). These matrices M,S,M',S',M'' and S'' have to be generated only once (at the expansion frequency q_0). Their multiplication with the $(q-q_0)$ and $(q-q_0)^2$ terms can be done efficiently, so that the full summation for the system generation needs only to be performed once for a given expansion frequency.

In summary, the matrix generation is done in the following steps:

- generation of the Fourier-transformed 1D-expansion functions.
- combination to the actual 2D-expansion functions.
- computation of the spectral impedances Z_{ev} and Z_{hv}.
- combination to the resulting matrix operations M ... and S ...

Because the spectral impedances Z_{ev} and Z_{hv} depend only upon the term $k_r^2 = k_x^2 + k_y^2$ a very efficient computation of these values is possible by first generating linear vectors $Z_{ev}(k_r^2)$, $Z_{hv}(k_r^2)$ and then utilising a fast interpolation concept, used successfully in the SFPMIC program.

The final resulting linear equation

$$\begin{bmatrix} M_{xx} & M_{xy} \\ M_{xy} & M_{yy} \end{bmatrix} \cdot \begin{bmatrix} v_x \\ v_y \end{bmatrix} = \begin{bmatrix} S_{xx} \\ S_{yy} \end{bmatrix}$$

having the submatrices M and the subvectors S (source) consisting of real coefficient, submatrices being symmetric. Due to the characteristics of the Fourier coefficients (different types) of the expansion functions, the submatrices and subvectors can again be split up (e.g. M_{xx}) as

$$M_{xx} = \begin{bmatrix} M^{a}_{xx} & M^{b}_{xx} \\ M^{b}_{xx} & M^{c}_{xx} \end{bmatrix}$$

the submatrices having different summation properties (decay of residual error). So it is possible to compute for each of the blocks of the optimum spectral threshold for which the spectral operator expansion can be performed. For simplicity at present they are treated with constant thresholds in order to avoid unnecessary complications. An advantage is that the necessary matrix inversion can be done in a very stable way utilising the special block structure of the submatrices.

3.6. VERIFICATION OF THE TANGENTIAL ELECTRIC FIELD DENSITY COMPUTATION

The 3-dimensional electromagnetic field problem is solved utilising the condition that the tangential electric field must vanish on the metallisation. This is formulated using a Galerkin procedure. The essential criterion is the computation of the electric field in the metallisation plane from the numerical solution and the check for the tangential electric field being zero on the conductor.

The spectral electric field components can be written in matrix form:

$$\begin{bmatrix} e_x\ (k_x,k_y) \\ e_y\ (k_x,k_y) \end{bmatrix} = \begin{bmatrix} Za\ (k_x,k_y) & Zb\ (k_x,k_y) \\ Zb\ (k_x,k_y) & Zc\ (k_x,k_y) \end{bmatrix} \begin{bmatrix} I_x\ (k_x,k_y) \\ I_y\ (k_x,k_y) \end{bmatrix}$$

where the elements Za,b,c (k_x,k_y) are the Green's functions in the spectral domain, $e_{x,y}\ (k_x,k_y)$ the spectral electric field components and $I_{x,y}\ (k_x,k_y)$ the spectral current density components.

The electric field components at an arbitrary location (x_0,y_0) in the metallisation plane can be computed in the approach using the Fourier series

$$E_x\ (x_0,y_0) \quad \sum_m \cos(k_x.x_0) \quad \sum_n e_x\ (k_x,k_y)\ \sin(k_y.y_0)$$

$$E_y\ (x_0,y_0) = \sum_m \sin(k_x.x_0) \quad \sum_n e_y\ (k_x,k_y)\ \cos(k_y.y_0)$$

With the electric field components computed in this manner for a grid of points the electric field norm can be computed at several locations in the metallisation plane and plotted.

3.7. NUMERICAL ACCURACY OF THE SPECTRAL OPERATOR EXPANSION GREEN'S FUNCTION TERMS

As has already been mentioned the SOE-method is based on the fact that the contributions to the generated system matrices have only weak dependencies on the frequency if the element spectral order is high enough. As such the SOE-approach utilizes a Taylor-series in which the elements can be truncated after the second derivative. In the program the SOE implementation of these

spectral matrix elements derivatives are computed using finite difference approximations.

During testing, it became obvious that the generation of the second derivative could become numerically unstable, when its value is very small. Due to roundoff error, the instability increases if the differences of the frequencies, which are used for the computation of the derivatives is small. On the other hand, the accuracy of the derivatives is lower if the larger differences are taken. As a result a suitable compromise for the difference-values of the frequency had to be found by empirical investigations/trial computations. A reasonable practical value of f for the difference approximations was found to be about 1% of the highest frequency chosen in wide band frequency analyses.

Another aspect which had to be considered in more detail was the truncation of the spectral series, i.e. the number of spectral terms used. As already outlined, the elements of the generated system matrices consist of a SOE-expanded part and the direct spectral contribution. The threshold between the direct contribution and the SOE-part is computed using the requirement that

$$K_z^2 = K_{omax}^2 \cdot \varepsilon_{rmax} - K_{rT}^2 \qquad (\text{with } K_{rT}^2 = K_{xT}^2 + K_{yT}^2)$$

has only a very weak dependency on the frequency, where the subscript T indicates the threshold value. This situation occurs if the value of K_{rT}^2 is much larger than the maximum frequency dependent term. Accordingly, a suitable threshold/function criterion

$$K_{rT}^2 = C_T \; K_{omax}^2 \quad \varepsilon_{rmax}$$

was chosen, where K_{rT}^2 is the threshold-value, C_T a constant interchange 10 ... 100 determining the actual ratio between the direct and the

SOE-contribution and ε_{rmax} the maximum relative dielectric constant of the media associated with a configuration.

Graphically seen in the v-plane (v=(m,n), spectral index) the direct and the SOE-part of the matrix-elements generated to describe a discontinuity can be represented in Fig. A3.9.

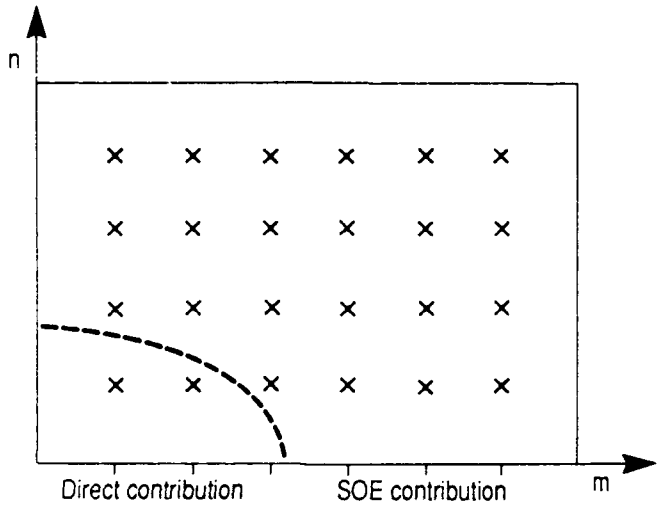


Fig. A3.9: Spectral index

The SOE-contributions of the system matrices have to be generated only once at the initialization frequency (K^2_{omax}). At subsequent frequencies only the direct contribution has to be computed. The amount of time spent for the computation of the matrix is proportional to the area in the v-plane. Typically the truncation subscript (m,n) are in the order of 10 .. 20 corresponding roughly to 100 ... 400 direct spectral terms for the substrates, frequency range and package sizes investigated.

Depending on the structure and the package of the simulated discontinuity the truncation indices (m,n) of the SOE-expandable part of the matrices can easily reach 100 ... 2000 corresponding to 10,000 ... 4,000,000 spectral

terms. This results in a speed-up factor of between 100 ... 1000 from the SOE-initialization to the frequency-dependent solution of the discontinuity. A representative CPU-time performance curve for an open stub example, time consumption on a MicroVAX (resolution m=49, n=22) versus the number of frequency points analysed is shown in Fig. A3.10.

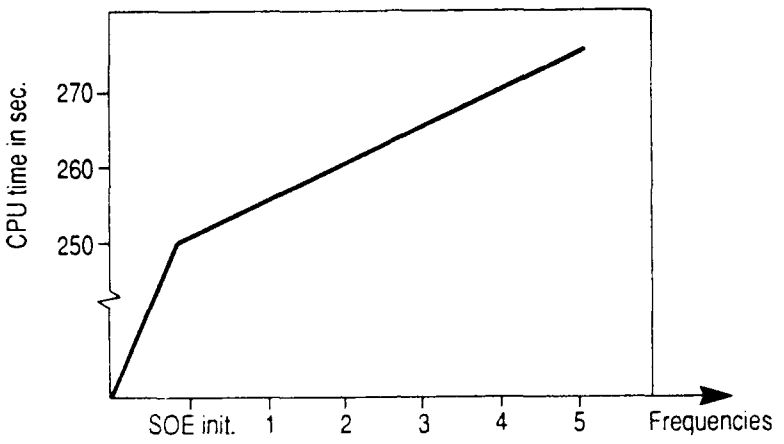


Fig. A3.10: Computation performance

4. COMPUTATION OF THE SCATTERING PARAMETERS

4.1. S-PARAMETER COMPUTATION METHOD

The method of S-parameter computation chosen is based on the projection of the 3-D solution of the discontinuity electromagnetic field in the reference plane of interest onto the vector space of precomputed microstrip-feedline modes where the hybrid microstrip modes are used together with their orthogonality properties. Figure A4.1 shows a general, representative scheme for the extraction of S-parameters following this method,

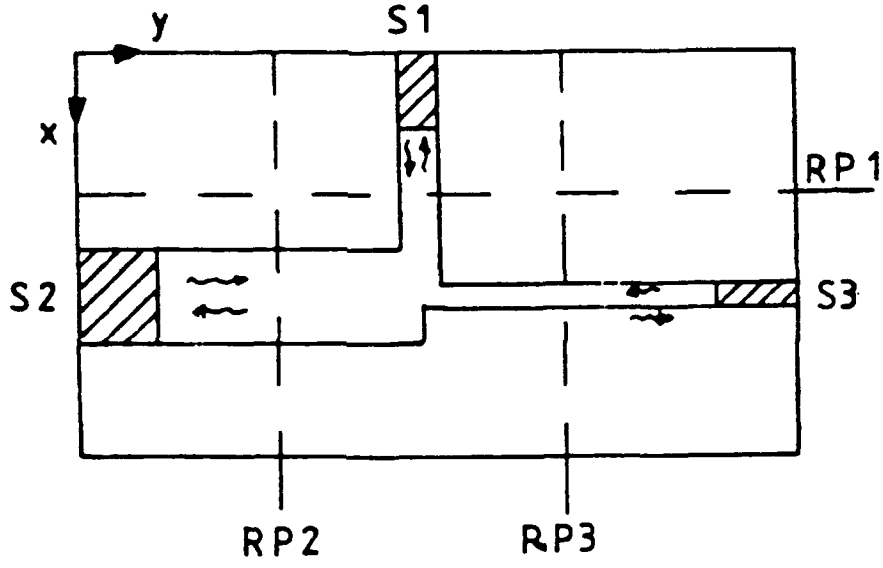


Fig. A4.1: T-junction discontinuity S-parameter extraction scheme

where the elements S1,2,3 are the 3 necessary sources for the discontinuity considered (a 3-port T-junction), the S-parameters being computed in the reference planes (RP1,2,3).

The mathematical formulation of the method is

$$E_t^{3Dp} = \sum_q (a_{q+} + a_{q-})\, E_t^{TLq+} \rightarrow \int_{RP_i} X\, E^*_t{}^{TLq+}\, dA_i$$

$$H_t^{3Dp} = \sum_q (a^*_{q+} - a^*_{q-})\, H^*_t{}^{TLq+} \rightarrow \int_{RP_i} X\, E_t^{TLq+}\, dA_i$$

which leads to a linear system of equations. The elements of this linear system consist of integrals which have to be computed over the reference planes of interest. The analytical and the numerical evaluation of these integrals needs to be quite sophisticated in order to exploit the advantages of the SOE.

A significant advantage of this S-parameter extraction method as compared to methods used previously is the available accurate description of radiation effects (LSM-modes). This is due to considerable improvement in distinguishing between the LSM_0-mode and the lowest microstrip mode propagating on the feed-line. Experience has shown that due to the similarity of these two modes in the cross-section of the microstrip feed-line, their separation has been rather difficult in using SFPMIC in which the local function method for S-parameter extraction is used.

4.2. VERIFICATION OF THE OPEN END S-PARAMETER COMPUTATION

In order to get results quickly on the reflection coefficient of the open end effect a simple verification method was chosen for the computation of the S-parameters. This was not a substitute for the method of S-parameter extraction as already described. The rigorous extraction method is rather complicated. Therefore it was helpful to have a simple approximate S-parameter extraction procedure for debugging and verification purposes.

These are the assumptions made in the simplified S-parameter extraction procedure:

- only the dominant microstrip-mode is propagating on the feed line
- the feed line must be sufficiently long (at least about half a wavelength
- no package modes are present in considerable strength.

Under these assumptions, the longitudinal current on the feed line is a pure standing microstrip type wave pattern and can be written as

$$I_{long}(x) = a0.\cos(\beta(x-d)) + b0.\sin(\beta(x-d))$$

assuming a propagation in the x-direction. The a0 and b0 are unknown real coefficients, β is the propagation constant and d is the location where the reflection coefficient is computed (location of the reference plane).

The quantities a0 and b0 are computed using the longitudinal strip current from the 3-D electromagnetic discontinuity module output by calculating the inner products,

$$a0 = < I_x(x,y_0), \cos(\beta(d-x)) >$$

$$b0 = < I_x(x,y_0), \sin(\beta(x-d)) >$$

y_0 being in the y-plane where the longitudinal strip current is computed. The testing area (x-coordinate) is at least about half of a wavelength to give reasonable accuracy.

The following complex power related wave amplitudes

$$A = Z_0/2 \cdot (a0 + j\ b0) \cdot \exp(+j\ \beta d)$$

$$B = Z_0/2 \cdot (a0 - j\ b0) \cdot \exp(-j\ \beta d)$$

can be computed with Z_0 being the strip characteristic impedance of the fundamental mode (quasi TEM). Using these quantities the complex reflection coefficient r can then be calculated as

$$r = B/A$$

On implementation of this method shortcoming identified is due to the fact that the mode field analysis program applied to generate the numerical values of β, uses expansion functions differing from those used in the 3-D electromagnetic open end module. Two possible solutions to the problem were considered.

The first solution was to use exactly the same expansion function in the precomputation of the strip-type solution (β) as in the 3D discontinuity module.

The second was to compute the required value of β from the 3D solution which eliminates the error introduced by an external (non-compatible) β value. This can be done via the use of the error function:

$$E_{LSQ} = \left[\sum_{i=1}^{1} \frac{\left(1^{cs}_{long}(x_i) - 1^{3D}_{long}(x_i)\right)^2}{1^{3D}_{long}(x_i)^2} - \right]^{\frac{1}{2}}$$

with $1^{cs}_{long}(x)$ being the appropriate cosine and sine approximation of the longitudinal current and $1^{3D}_{long}(x)$ the longitudinal current computed in the 3D electromagnetic field solution for the feed region x1 ... x2, the error being minimised to determine the unknown parameter β. The actual S-parameter phase on the feed strip as computed by the 3D electromagnetic discontinuity program is thus determined. First tests of this approach giving satisfying results.

Fig. A4.2 shows a schematic representation of the S-parameter extraction and error computation in the case of the open-end discontinuity.

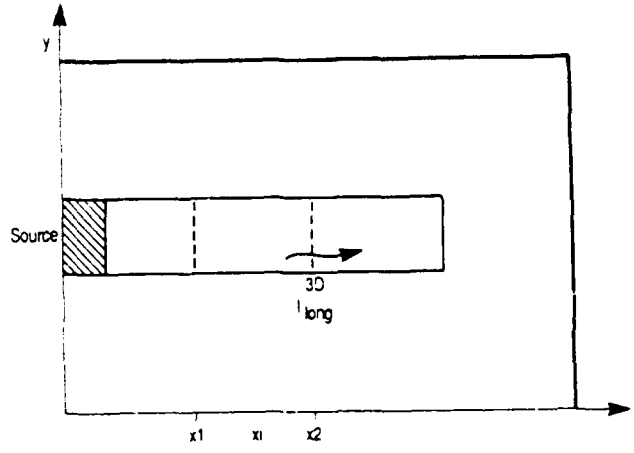


Fig. A4.2: Open end S-parameter extraction scheme

The range chosen for S-parameter extraction on the feed line and for error computation is between x1 and x2. The x_i in this picture corresponds to the x_i-values noted above. *The errors defined by this error-function are* usually found to be below one percent. An open-end discontinuity on 100μm GaAs line-width 100μm, resonator length 0.80mm, package dimensions 0.5mm x 1.00mm and simulation frequency 50 GHz was chosen as an example.

Table 1 shows the values of the currents of the 3D-solution, the cosine-sine approximation and the difference between these values in percent (error) at specific points over the range x1 and x2. The overall-error (LSQ) is 0.807 percent indicating a very good agreement with the current computed from the 3-D electromagnetic field with the cosine-sine standing wave representation assumed in the S-parameter evaluation process.

Further investigations on the error behaviour clearly showed that the error minimisation as described in the above definition was a good accuracy criterion. However, it does not provide a stable and accurate way to determine the "best possible" phase constant β for S-parameter evaluation since the minimum is very flat as a function of β. Such can be concluded from the Table 2 (an open end example).

```
* FREQUENCY =   50.000 GHZ
*-------------------------------------------------------------------

X=0.300, VAL=   0.81603   0.79851, ERR (PERCENT):      2.21
X=0.311, VAL=   0.81264   0.80143, ERR (PERCENT):      1.41
X=0.321, VAL=   0.80986   0.80353, ERR (PERCENT):      0.80
X=0.332, VAL=   0.80728   0.80480, ERR (PERCENT):      0.32
X=0.342, VAL=   0.80406   0.80525, ERR (PERCENT):      0.14
X=0.353, VAL=   0.80132   0.80488, ERR (PERCENT):      0.43
X=0.363, VAL=   0.79870   0.80367, ERR (PERCENT):      0.61
X=0.374, VAL=   0.79551   0.80165, ERR (PERCENT):      0.76
X=0.384, VAL=   0.79185   0.79880, ERR (PERCENT):      0.86
X=0.395, VAL=   0.78733   0.79513, ERR (PERCENT):      0.97
X=0.405, VAL=   0.78247   0.79064, ERR (PERCENT):      1.02
X=0.416, VAL=   0.77814   0.78535, ERR (PERCENT):      0.91
X=0.426, VAL=   0.77359   0.77935, ERR (PERCENT):      0.72
X=0.437, VAL=   0.76870   0.77235, ERR (PERCENT):      0.46
X=0.447, VAL=   0.76446   0.76465, ERR (PERCENT):      0.03
X=0.458, VAL=   0.75968   0.75618, ERR (PERCENT):      0.47
X=0.468, VAL=   0.75242   0.74693, ERR (PERCENT):      0.74
X=0.479, VAL=   0.74316   0.73691, ERR (PERCENT):      0.86
X=0.489, VAL=   0.73364   0.72613, ERR (PERCENT):      1.04
X=0.500, VAL=   0.72452   0.71461, ERR (PERCENT):      1.39
```

Table 1:

LAMBDA IN MM	D LAMBDA IN PER CENT	PHI IN DEG.	D PHI IN PER CENT	ERR IN PER CENT
2.0444	-1.0	-19.0	-5.9	0.834
2.0547	-0.5	-19.9	-2.9	0.820
2.0650	0.0	-20.5	0.0	0.807
2.0753	+0.5	-21.1	+2.9	0.794
2.0857	+1.0	-21.7	+5.2	0.781
2.0959	+1.5	-22.3	+8.8	0.768
2.2063	+2.0	-22.9	+11.7	0.756
2.1683	+5.0	-26.2	+27.8	0.687
2.2715	+10.0	-31.2	+52.2	0.585

Table 2: Phase Error

In this table the influence of the precomputed phase constant β (or equivalently λ, the wavelength) on the reflection coefficient of the open end effect and the computed error is listed. Since there are no losses, the magnitude of the reflection coefficient is always 1.0, it is therefore sufficient to list only the phase angle. Also, the deviation of the computed phase angle from the phase angle computed for the nominal reference input value of the wavelength is listed. The nominal input value of the precomputed wavelength of the feed strip mode is 2.065mm. The value of this precomputed wavelength has changed between -1 percent and +10 percent of the nominal value.

The above discussion shows clearly that the defined error function is unsuitable for the computation of the actual phase constant on the feed lines by the minimisation procedure. On the other hand it can be concluded that the error in the precomputed phase constants does not result in unacceptable errors of the reflection coefficient (seen in the example of the open end discontinuity) since the precomputed values have an accuracy of better than 1%. At the same time, E_{LSQ} was found to result in a quite stable S-parameter evaluation if its value is below 0.2 percent.

4.3. 3-D ELECTROMAGNETIC FIELD SOLUTION ACCURACY REQUIREMENTS FOR S-PARAMETER EVALUATION

The method of S-parameter extraction consists essentially in the mapping of the longitudinal current on the feedline section (computed from the 3-D electromagnetic field) on suitable cosine-sine functions. Because the method uses precomputed feedline data, an error function was defined which corresponds to the approximation quality of this mapping procedure.

However, it became obvious for short evaluation sections that a measure of the 3-D electromagnetic field solution quality is required, because it is only reasonable to extract S-parameters from stable and convergent electromagnetic field solutions. Therefore, a second error function was defined which makes use of the electric field values computed in the region for S-parameter extraction. The quality of the 3-D electromagnetic field solution is considered sufficiently good if the tangential electric field vanishes with good accuracy on the metallization. The normal electric field component directly under the metallization (in the GaAs layer) is bounded and is used for normalization of the tangential electric field.

The electric field error function

$$ERR_{E\text{-}LSQ} = \sum_{i=1}^{N} \left(E_{tan}(x_i) \,/\, E_{nor}(x_i) \right)^2$$

was defined with x_i representing the sampling points where the electric field is computed and N denoting the total number of sampling points, the x_i chosen in exactly the same region where the S-parameter extraction is performed.

An open-end structure was chosen here as a representative example for the introduced residual electric field error. The tangential and normal electric field components, as outlined before, have been computed in the longitudinal direction of the microstrip-line.

Fig. A4.3 shows the computed tangential and normal electric field components along the coordinate $y=y_0$. It can be seen that the tangential part vanishes approximately on the metallization area except near the end of the strip where it rises sharply in the vicinity of the open end. The normal electric field is plotted on the same scale. The oscillatory behaviour is due to the relatively low resolution applied in the computation. In this example the least squares electric field error is 2.03% which indicates a 3-D electromagnetic solution of good quality.

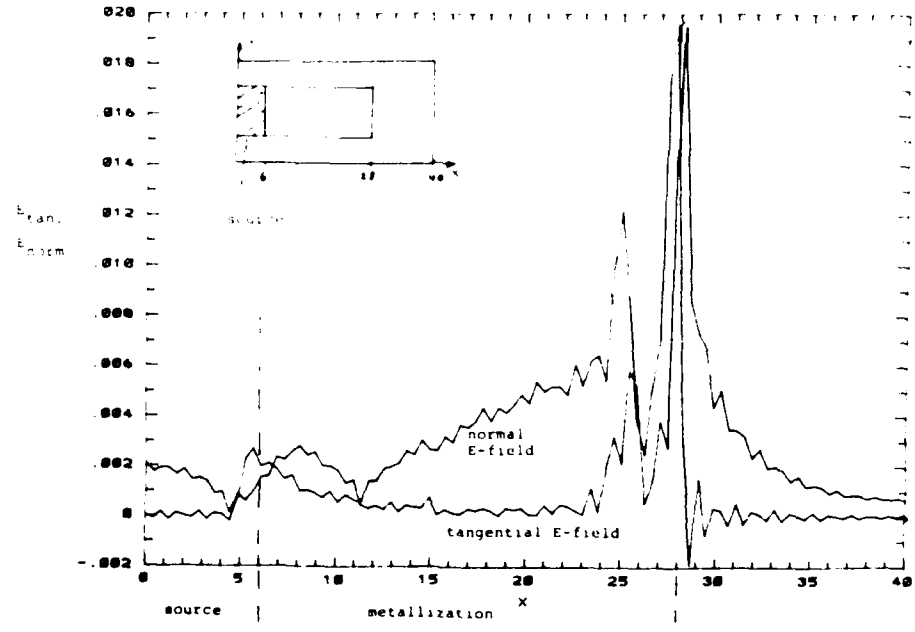


Fig. A4.3: Tangential and normal electric field

MISSION

OF

ROME LABORATORY

Rome Laboratory plans and executes an interdisciplinary program in research, development, test, and technology transition in support of Air Force Command, Control, Communications and Intelligence (C^3I) activities for all Air Force platforms. It also executes selected acquisition programs in several areas of expertise. Technical and engineering support within areas of competence is provided to ESD Program Offices (POs) and other ESD elements to perform effective acquisition of C^3I systems. In addition, Rome Laboratory's technology supports other AFSC Product Divisions, the Air Force user community, and other DOD and non-DOD agencies. Rome Laboratory maintains technical competence and research programs in areas including, but not limited to, communications, command and control, battle management, intelligence information processing, computational sciences and software producibility, wide area surveillance/sensors, signal processing, solid state sciences, photonics, electromagnetic technology, superconductivity, and electronic reliability/maintainability and testability.